CHARACTERIZATION OF TERFENADINE AS A MODEL OF A HYDROPHOBIC AMORPHOUS FORM OF A DRUG AND PREPARATION AND CHARACTERIZATION OF SOME OF ITS DERIVATIVES

By

Raya M. Samra

Thesis presented for the degree of Doctor of Philosophy in the Faculty of Medicine

University of London/ School Of Pharmacy

Department of Pharmaceutics

29-39 Brunswick square, London WC1N 1AX

September 2002

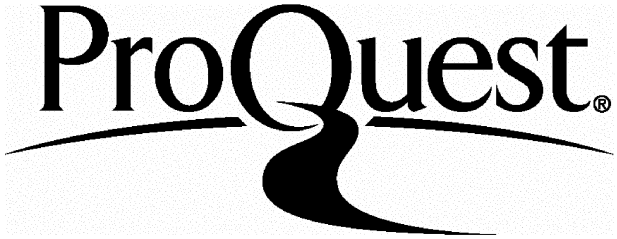

ABSTRACT:

Terfenadine was used as a model hydrophobic drug from which an amorphous form was prepared by melting followed by slow or quench- cooling. It was not possible to crystallize amorphous terfenadine at elevated RH either in the isothermal microcalorimeter or the Dynamic Vapour Sorption apparatus. Amorphous terfenadine samples crystallized completely in 95 % ethanol in the DVS. SEM showed crystallization to start at pores and/or cracks on the surface of the amorphous beads with enlargement of the pores during crystallization resulting in diffusion of more organic vapours and complete crystallization. Long term storage at elevated RH (up to 2 years) resulted in slow crystallization. This was followed by crystallization of the remainder amorphous content by use of a mixture of organic liquids in the isothermal microcalorimeter. Crystallization rates over these storage periods were slow with linear regression analysis showing that very long time is needed for complete crystallization. SEM showed that crystallization starts at cracks and/or pores on the surface of the beads while sealing the pores with crystalline material once crystallization started. This limited the access of water and prevented further crystallization of the samples.

Homologous salts of terfenadine were prepared by reacting terfenadine (basic drug) with a series of dicarboxylic acids. The salts were proven to be ammonium salts of terfenadine reacting in equimolar ratio (1 mole of terfenadine: 1 mole of dicarboxylic acid). Terfenadine oxalate, succinate and glutarate were found to be hydrates. These hydrates collapsed into their amorphous forms after prolonged drying under vacuum. Amorphous forms of the terfenadine salts were prepared by melting and slow cooling. The amorphous forms showed a decrease in Tg going from the oxalate to the adipate salt. Amorphous terfenadine glutarate did not crystallize in the presence of either humidity or ethanol while terfenadine adipate crystallized in the presence of ethanol in the DVS. The results show an agreement with Tm/Tg ratios where lower Tm/Tg ratios suggest lower crystallization potential. Solubility of amorphous and crystalline forms of terfenadine and its salts at pH 2 and pH 6 was investigated. The amorphous forms showed higher apparent solubility than their crystalline counterparts. The interesting thing was that an increase in solubility accompanied an increase in physical stability of the amorphous forms. This observation indicated the possibility of enhancing the physical stability of a compound while at the same time enhancing the rate and/or extent of solution through the preparation of salts with the correct Tm/Tg ratio.

Acknowledgement:

Along the passage of my Ph.D journey, I was blessed with many people who paved the way and provided me with either direct help or psychological support in order to achieve my ambition and fulfil my dream of having a Ph.D as a seed to start an academic career. First of all, I would like to thank my supervisor professor Graham Buckton for providing all sorts of support whether by enhancing my knowledge, putting me on the right track whenever I was confused or by being there asking about me when I was (as I put it) hiding in a cave writing. I am thankful for my husband Hassan who supported and encouraged me in pursuing a Ph.D degree and took on lots of responsibility with the kids during the times when I was away. I extend my thanks to him for the whole lot he tolerated all along and for the time and effort he dedicated to proof read this manuscript. Many thanks to my daughter Lulwa and my son Said who continuously supported me and constantly showed their pride in what I was doing while tolerating a lot with me going through this experience. My father Mahmud and my mother Siham who pampered me with their love, support and encouragement and in the eyes of whom I remained that little girl whom they needed to take care of. Mum and dad, I will remain endlessly indebted to you both. My brother Raed and my sister May who did their best to encourage me, show their pride in me and to keep the jokes and laughs going even in stressful days. I am grateful for the University of Petra for their financial support and trust by providing me with a scholarship. Professor Tawfiq Arafat, the dean of the school of pharmacy at the university of Petra for his support and for his guidance on the HPLC and Differential Scanning Calorimeter. I am thankful for Dr. Adnan Badwan who provided me with advice during the first year of my research while I was in Jordan and who helped in directing me towards this line of research. I would like to extend my thanks to many people who performed some specialized tests in this thesis; Dr. Mire Zloh for carrying out the NMR experiments and explaining the NMR data, Dr. Lily Randall for carrying out the elemental analysis, Dr. Ghazzi Saffarini for running part of the powder X-ray diffraction tests and Dave McCarthy for performing the SEM experiments. I am grateful to Dr. Patricia Darcey for the time and effort she dedicated in teaching me the use of the DSC, TGA and DVS when I first started my work in London, to Hashim Salman for all his support and for the help he provided me with on the use of the DVS and to Roy Lane for helping me in the use of the isothermal microcalorimetry. Many thanks To Professor Nizar Alrayyes (professor of chemistry and vice president at the University of Petra) for his help in explaining the possible

chemical reactions between terfenadine and the dicarboxylic acids. My friend Basma for her help and for keeping me company in the lab until late hours of the night while I was working on the HPLC. My friend Kholoud, for being there and for sharing all the stressful moments during research as well as the joyful ones. Kholoud, thanks for your help in the last minute scare and running around during the print out. Last but not least, I am thankful to all my friends who kept in touch with me while I was in London, who broke the silence and the loneliness and made those rough days seem brighter; Sana, Christine, Manal, Mervat, Alia, Abir, Dana, Hanan, Kevin, Letithia and Ajay. Thanks for being there.

Dad, this is to you hoping I can follow your footsteps
Mum, Hassan, Lulwa and Said this is to you hoping it
will make you as proud as you thought you will be
My students who had faith I can do it, This is to you

TABLE OF CONTENTS: page

LIST OF TABLES: **page**

LIST OF FIGURES:

CHAPTER ONE

INTRODUCTION

1 INTRODUCTION:

Solids can either be in amorphous or crystalline form:

1.1 CRYSTALLINE SOLIDS:

A solid crystal is a mass of ions, atoms or molecules, which are packed in a neat, fixed, rigid and orderly fashion called a crystal lattice; having both short and long range order. The basic unit of a crystal is called the unit cell and repetitions of this unit cell in three dimensions give rise to the crystal. In three dimensional crystalline structures, there are seven possible crystal systems (forms) resulting in seven independent, different unit cell shapes as seen in Figure 1.1; these are cubic, tetragonal, orthorhombic, hexagonal, trigonal, monoclinic and triclinic (Florence and Attwood, 1998, Mullin, 1993, Carstensen, 1993)

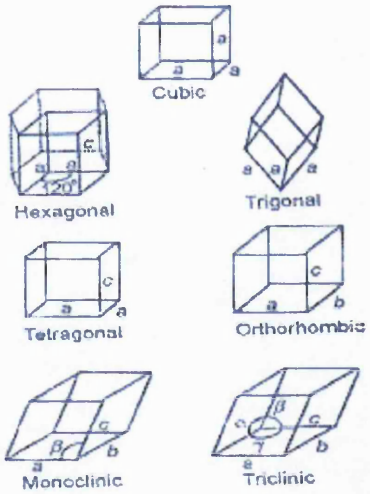

Figure 1.1 *Diagram of the seven possible unit cell shapes in crystals. (Adapted from Florence and Attwood, 1998).*

As the crystal grows, the high degree of internal order results in the crystal having an external characteristic shape; with smooth surfaces or faces developing as the crystal is growing. The planes of these faces are parallel to atomic planes in the lattice (Mullin, 1993). This external shape of the grown crystal; which reflects the overall shape of the

crystal is termed a crystal habit and there are different crystal habits such as needle (acicular), tabular, and prismatic shaped crystals (Figure 1.2).

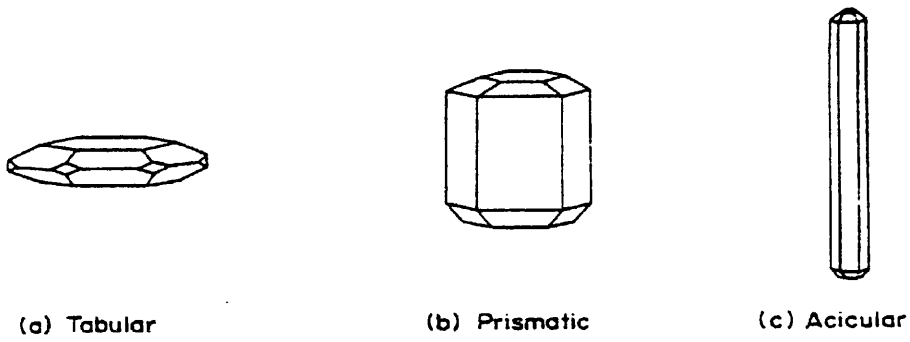

Figure 1.2 *Examples of crystal habits illustrated on a hexagonal crystal. (Adapted from Mullin, 1993).*

It is not surprising that crystals from different chemical entities can show different crystal habits, however it has to be noted that very rarely can any two crystals of a given substance look identical; in fact they usually look quite different in both size and external shape. Different habits of the same substance are generally due to the crystal growing in a strained environment resulting in a stunted or inhibited growth in one direction and an exaggerated growth in another direction. This observation is quite common in nature as few natural crystals are left to grow free; most of those natural crystals grow in an environment with some sort of restraint such as in the case of natural minerals (Mullin, 1993). The type of habit formed is affected by crystallization conditions such as cooling rate. Rapid crystallization achieved through sudden cooling or seeding of a supersaturated solution can for example result in the elongated growth of the crystal in a vertical direction resulting in the formation of needle shaped crystals. Presence of impurities in the crystallizing solution on the other hand can inhibit growth of the crystal in a certain direction resulting for example in tabular shaped or the more excessively flattened plate shaped crystals (Mullin, 1993). Change in solvent of crystallization can give rise to different crystal habits as the different surface energy of each face will interact differently with liquids of different polarity (Buckton, 1995a). Crystals may vary in the development of various faces (crystal habit) and in size, but the angle between two adjacent faces (interfacial angles) is a constant value; it is characteristic of the substance. This is termed as the law of constant interfacial angles proposed by Hauy in 1784 (Mullin, 1993). The importance of knowing the crystal habit at hand from a pharmaceutical point of view

stems from the effect that the habit has on some pharmaceutical characteristics. Though different crystal habits of the same substance might not show a significant difference in their bioavailability they might show other types of variability. An injectable suspension of a crystalline drug for example can be injected more easily through a fine needle if the crystals were plate-like than if they were needle-shaped crystals (Byrn, 1982). The crystal habit can also affect the flow properties of a powder through the hopper as well as the ease of compression in a tablet machine. Cubic shaped crystals flow better in a powder hopper than needle shaped crystals (Carstensen, 1993). In the case of tolbutamide for example, the plate-like crystals cause powder bridging in the hopper of the tablet machine as well as capping problems during tableting. Neither of these problems is seen with tolbutamide in other crystal habits (Florence and Attwood, 1998).

Crystalline solids undergo melting; a first order phase transition. Upon heating a crystalline solid its temperature will start rising up to the melting point. Due to the latent heat of fusion, the temperature will stop rising until all the solid mass melts. Once all the mass has melted, the temperature resumes its rise while heating continues but with a change in slope indicating a change in the heat capacity of the material (Figure 1.3). Hence a first order transition involves both a change in latent heat and in heat capacity.

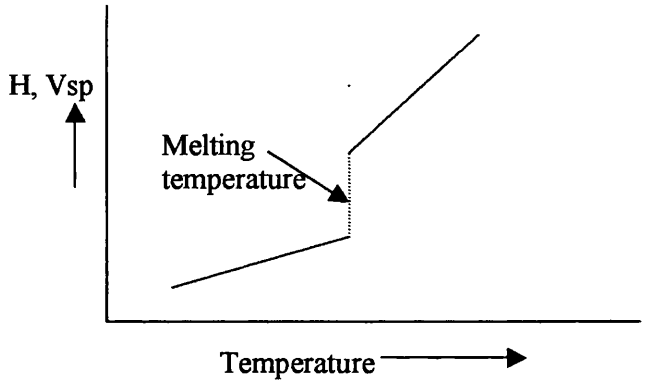

Figure 1.3 *Schematic representation of change in heat or specific volume with temperature in a crystalline solid.*

Where H: enthalpy, Vsp: specific volume.

1.1.1 POLYMORPHISM:

Polymorphism in crystalline substances is the presence of the same chemical entity in different crystal forms resulting from a different arrangement of ions, atoms or molecules in the crystal lattice. Thus polymorphism involves a change at the inner structural level of the crystal. A chemical substance can have two or more polymorphs having different crystal habits with different physical and chemical properties triggered by variation in their crystal structures. One of the polymorphs will be the most stable form with the lowest free energy while the rest of the polymorphs will be metastable forms with higher free energy levels and thus tend to convert to the most stable polymorph at different rates depending on the free energy difference between the metastable and the stable polymorphs. Martin (1993) explains that in thermodynamic laws, a system always proceeds in a direction where minimum free energy (Gibb's free energy, ΔG) is attained, thus a spontaneous process at certain constant temperature (T) and pressure is accompanied by a loss in free energy. At the same time according to the second law of thermodynamics, a system proceeds in a direction of increased randomness, disorder or entropy (ΔS). This indicates that sufficient loss of enthalpy (ΔH) should be taking place to counteract the loss in entropy associated with a change from a less stable to a more stable polymorph so that there is a net loss in free energy when going from the less stable to the more stable polymorph as indicated by equation 1.1

$$\Delta G = \Delta H - T\,\Delta S \qquad \text{.....Equation 1.1}$$

Having the least free energy level, the most stable polymorph usually has higher melting point, lower solubility, higher physical stability and lower chemical reactivity than the other metastable forms. This is critical in pharmaceutical formulation as differences in apparent solubility (solubility that is achieved experimentally) can lead to variable dissolution rates, which in turn can lead to different bioavailability levels among the different polymorphs. Higher solubility of the less stable polymorph was concluded in the work of Lin (1972) and Moustafa et al. (1971). Changes in crystal size of pharmaceutical suspensions leading to their detrimental eventual caking, grittiness in creams brought about by crystal growth as well as inadequate melting characteristics of suppositories when using theobroma oil as the vehicle can all take place due to transformation from one polymorphic form to another. Different polymorphs exhibit different X-ray diffraction

patterns and this technique is one of the main methods used for detecting the presence of polymorphs. Polymorphism is quite common in the pharmaceutical area with many examples being mentioned in the literature. Aulton (1988) reported that some of the most famous drugs to exhibit polymorphism were studied by Kuhnert-Brandstatter (1965) and included the sulfonamides with 40% of them showing polymorphism, barbiturates (63%) and steroids (67%). Polymorphism can be caused by differences in the crystallization process such as the use of a different solvent, changes in cooling rate and temperature of crystallization.

1.1.2 PSEUDOPOLYMORPHISM:

Pseudopolymorphism is a term used sometimes to refer to the formation of solvates and hydrates (Aulton, 1988). A solvate is formed when the solvent of crystallization gets trapped in the crystalline lattice. When the solvent is water it is called a hydrate. Anhydrous forms on the other hand reflect the absence of such solvent of crystallization in the crystal lattice (Florence and Attwood, 1998, Carstensen, 1993). The investigation of the presence or absence of solvates or hydrates is as important as investigating the presence of different polymorphs of the same substance. Solvates tend to exhibit different apparent solubilities and melting points when compared with the anhydrous form (as will be explained later).

1.1.3 CRYSTALLIZATION:

The process of crystallization is one of ordering during which, randomly organized molecules in a solution, a melt, or the vapour phase take up regular positions in the solid (Byrn, 1982). Crystallization is a method that can be used to purify drug substances in pharmaceutical industry. In the recrystallization process a drug is usually dissolved to its saturation concentration at a certain temperature, then the temperature is reduced to induce the formation of a supersaturated system. An example from the literature showing crystallization to be used in order to purify a solid material is the crystallization of sulfanilamide (Carstensen, 1993). The solubilities of sulfanilamide in water are 4 % and 0.75 % w/w at 60 °C and 25 °C respectively. A solution of the drug with a concentration equivalent to the drug solubility is prepared at 60 °C. The solution is then filtered and allowed to cool to 25 °C, hence the solubility falls to a value of 0.75 %w/w with most of

the drug precipitating out of solution. The solubility of the impurities (present in small amounts) would most often not be superseded, so that the sulfanilamide crystals obtained would be fairly pure. Sometimes successive crystallizations are necessary to obtain a high purity level of the crystalline solid material. If the cooling is slow, then the crystals will be fairly large since sufficient time is provided for more crystal growth to take place, whereas if it is fast, the crystals obtained will be fairly small. Determination of the size of the crystals to be achieved should be weighed in terms of a favoured dissolution which can sometimes be obtained from smaller crystals versus a poor flow of powder and capping tendencies (in the case of tablets) which might be encountered in those smaller crystals. Thus a controlled particle size with optimum overall properties is what is usually required.

Crystallization can be considered to pass through three successive phases.

a. Supersaturation of a solution: This can be achieved in different ways such as solvent evaporation; cooling, or by addition of a precipitant.

b. Nucleation (formation of crystal nuclei): Takes place in both crystallization from a solution and crystallization from a liquid melt. For crystallization to be triggered, the formation of a supersaturated or supercooled system is not sufficient on its own. There is a need for the formation of the so-called seeds or nuclei on the surface of which the material can be deposited and crystallized.

Mullin (1993) explains that there are two types of nucleation processes depending on whether nucleation was self initiated or artificially triggered through deliberately adding seeds (ready crystals added to crystallizing medium) for crystallization and these are primary and secondary nucleation methods.

Primary nucleation: Refers to either a spontaneously crystallizing system (homogenous) in which case collisions between molecules of the solute take place in solution resulting in a sequential addition of molecules leading eventually to nuclei formation, or a system containing particles of non crystalline nature which are not deliberately added to the system such as dust particles, impurities or even container particles such as glass residues. These particles can act as seeds that enhance deposition of crystals from solution on their surfaces (heterogeneous).

Secondary nucleation: Results when crystals of the solute are already present or deliberately added to the system. A supersaturated solution nucleates much more readily,

i.e. at a lower supersaturation in such a situation. Deliberate seeding is frequently employed in industrial crystallization to better control crystal size and size distribution.

c. Crystal Growth:

Once formed, the nuclei grow into crystals by deposition of molecules on the crystal faces. This is an equilibrium process, with the molecules in equilibrium between the solution and the solid, with dissolution taking place from solid surface to bulk liquid as reverse to crystallization (Byrn, 1982). Many models are suggested to explain crystal growth (Mullin, 1993) but Buckton (1995a) simplified the matter by stating that crystal growth is related to surface roughness at the molecular level, with growth occurring most rapidly in cases where the surface is sufficiently rough for molecules to be able to attach and in all cases the end crystal habit will be such that the growth will have minimised interfacial free energy with the solvent used. It is explained by Buckton (1995a) that in energetic terms, the system will deposit more material onto surfaces that will liberate the most energy. These surfaces will grow fastest and eventually will become the smallest faces in the final crystal as they eventually grow out of existence as seen in Figure 1.4

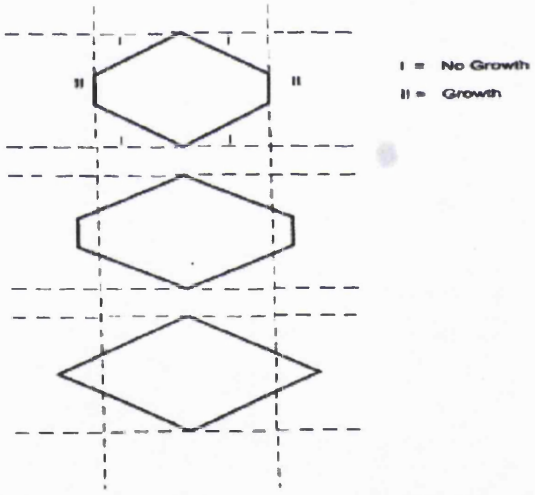

Figure 1.4 *Diagram showing how faster growing faces of a crystal grow out of existence. (Adapted from Buckton, 1995a).*

1.2 AMORPHOUS SOLIDS:

Unlike crystalline solids, amorphous solids lack the presence of three dimensional long range order and can only have short range order resembling a liquid and not exceeding a

few angstroms (Slade and Levine, 1996). The word amorphous is taken from the Greek amorphos where a = without and morphe = shape so it basically means without shape (Elias, 1997). Amorphous solids have no crystal shape and cannot be identified as either habits or polymorphs (Byrn, 1982). A random or irregular arrangement of molecules is seen in the case of amorphous solids resulting in larger spacing between molecules in comparison with that of crystalline solids. Figure 1.5 shows a microcrystalline polymer where both crystalline and amorphous domains can be seen and thus visually compared. This random or irregular arrangement of molecules in the case of amorphous solids leads to larger specific volume and lower density, and we can say that there is a greater free volume (Hancock et al., 1997, Ediger et al., 1996).

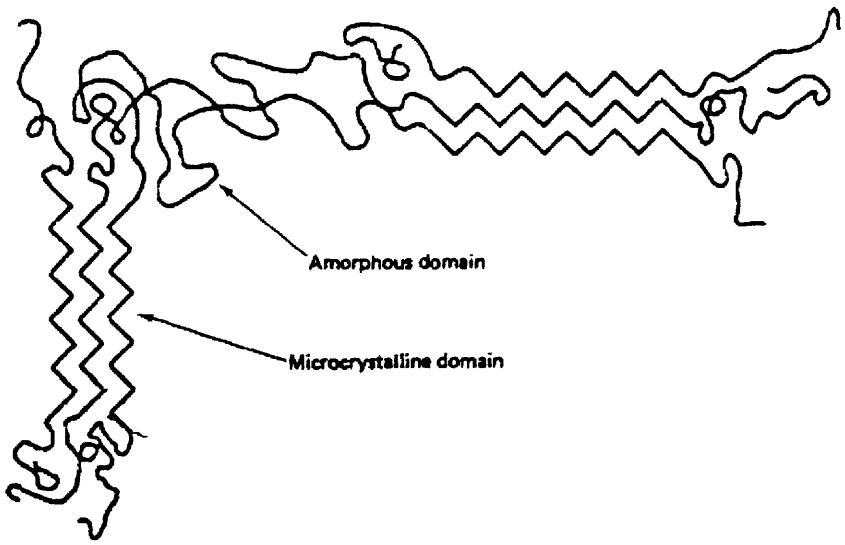

Figure 1.5 *Diagram showing both amorphous and microcrystalline domains in a microcrystalline polymer. (Adapted from Allcock and Lampe, 1990).*

Three basic expressions must be discussed when talking about amorphous solids and these are: **Glass transition temperature (T_g), Glassy state and Rubbery state.**
Amorphous solids exist in either the glassy state or the rubbery (supercooled liquid) state. Below a certain temperature specific to the material but affected by different factors (mentioned later) an amorphous solid exists in the glassy state. As this glassy mass is heated the temperature rises continuously with no break indicating the absence of a latent heat seen in crystalline materials. A point is reached where a change in slope is seen suggesting a change in heat capacity (Figure 1.6) at this point the material changes from a glassy state with less free volume and higher density to a rubbery state with higher free

volume and less density. The point at which the alteration between the glassy and the rubbery states takes place is known as the glass transition temperature (Tg).

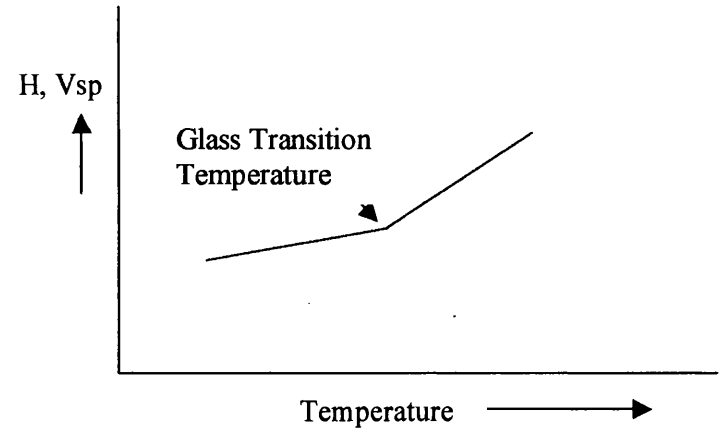

Figure 1.6 *Schematic representation of change in heat or specific volume with temperature in an amorphous solid.*

The dependence of the glass transition temperature on heating/cooling rates is widely reported in the literature and examples of which include (Andronis and Zografi, 1998, Hancock et al., 1997, Ediger et al., 1996, Slade and Levine, 1996, Moynihan et al., 1974). A smaller cooling rate gives the sample a chance to stay in equilibrium (or more accurately an apparent but not true equilibrium state which is the supercooled liquid state) until lower temperatures. The lower change in temperature with time allows for more molecular rearrangements resulting in a more dense glass and the sample will become frozen in the glassy state at a lower temperature (Figure 1.7). Composition and purity of the sample have an effect on its glass transition temperature. Her et al (1995) showed that the addition of sodium chloride to aqueous solutions of sucrose, lactose, dextran and poly (vinyl) pyrrolidone results in a decrease in the Tg values of their quenched solutions by 14 to 18 °C. Hofer et al. (1991) studied the effect of incorporating different monovalent and divalent salts such as sodium chloride and magnesium chloride respectively as well as polyhydric alcohols such as propylene glycol on the Tg of their hyperquenched aqueous solutions. They noted a reduction in Tg of dilute aqueous solutions relative to that of water alone and they explained this as being due to break-up of the hydrogen bonded tetrahedral network structure of frozen water by the added solute. However a minimum Tg value is followed by an increase in Tg upon further addition of the salt or the polyhydric alcohol as new bonds are formed with the solute. Gordon and Taylor

(1952) proposed a simple mixing rule to describe the variation in the glass transition temperature with blend composition when no specific interactions are involved between the components of the blend (as will be explained later). A perfectly miscible system will show a single distinct glass transition temperature. However the effects of nonidealities (e.g., immiscibility or certain specific interactions) can result in deviation from this theory (Hancock et al., 1997).

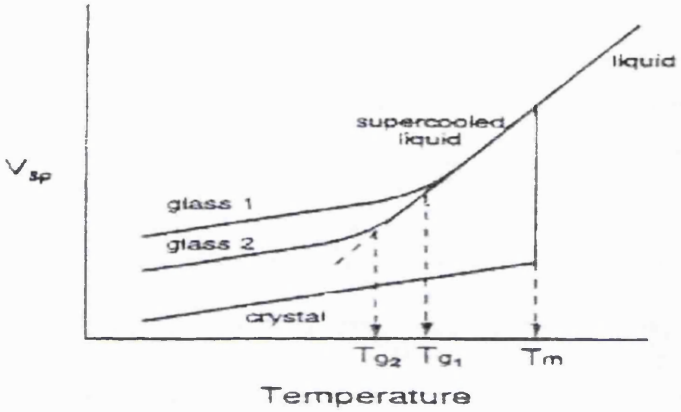

Figure 1.7 *Schematic representation showing the specific volume as varied with temperature in a sample that can either crystallize or form glass. Glass 2 is formed at a slower cooling rate than glass 1. (Adapted from Ediger et al, 1996).*

1.2.1 SUPERCOOLED LIQUID (RUBBERY) STATE:

Liquids that are cooled below their crystalline melting points (Tm) and manage to do so without crystallizing or glasses that are heated above their glass transition temperatures are called supercooled liquids as shown in Figure 1.7 (Ediger et al., 1996). Rapid cooling from the liquid state or melt is usually used in order to escape crystallization of the supercooled liquid. This is an amorphous state with the structural characteristics of a liquid but with a much greater viscosity. The enthalpy and volume changes immediately below Tm show no discontinuity with those seen above it. In fact specific volume and other thermodynamic properties of a supercooled liquid can be obtained by extrapolating the properties of the liquid above Tm to a lower temperature as seen in Figure 1.7. That is why this amorphous state is considered to be a supercooled liquid in an equilibrium state (Ediger et al., 1996, Hancock et al., 1997).

Supercooled liquids can be classified as either strong or fragile amorphous materials depending on the magnitude and temperature dependence of the apparent activation

energy for molecular motions (Hancock and Zografi, 1997). Strong liquids typically show Arrhenius like changes in molecular mobility with temperature with a comparatively small change in heat capacity at Tg. Proteins and SiO_2 are examples of strong glass formers (Ediger et al, 1996, Hancock et al, 1997). Fragile supercooled liquids have much stronger temperature dependence of molecular mobility near Tg with a relatively large change in heat capacity. Ethanol and o-terphenyl are examples of fragile glass formers (Ediger et al., 1996, Hancock et al., 1997).

The average time scale of molecular motions within a supercooled liquid is usually less than 100 s, the viscosity is typically between 10^{-3} and 10^{12} Pa.s (Hancock et al, 1997).

The supercooled liquid state is sometimes referred to as the rubbery state due to its macroscopic properties. A rubber can be stretched to many times its original length and can later bounce back into its original shape upon removal of the applied force without permanent deformation. According to Elias (1997) amorphous substances convert at the glass transition temperature (Tg) from a glassy state to a liquid state (low molar mass compounds) or a rubbery state (high molar mass chains). Flink (1983) stated that in the supercooled liquid state, the molecular motions overlap and free volume exists throughout the system with the molecules being able to change structure and molecular associations leading to crystal formation are possible. Free volume is explained by Flink (1983) as the volume unoccupied by solid matter of the molecules and represents the volume available for free movements of the molecules.

1.2.2 GLASSY STATE:

Cooling a supercooled liquid further results in an additional decrease in molecular mobility. A point is reached where the material is kinetically unable to attain equilibrium in the time scale of the experiment resulting in a change in temperature dependence of the enthalpy and volume indicated by a change in slope (Figure 1.7). This change in slope marks the glass transition temperature and a state, which is kinetically frozen (due to the high viscosity and restricted molecular motions) and is thermodynamically unstable (since the Gibb's free energy is not at the minimum value) is reached. This is termed as the glassy state. Flink (1983) stated that at the point that the free volume no longer extends throughout the system, the system that exists at the moment is frozen in and the glassy state is established. Molecular relaxations towards a local energy minimum are taking place in the glassy state though might be at too slow a rate to be measured within

the time scale of practical experiments. Slade and Levine (1996) reported the viscosity of the glass to be in the range of 10^{10} - 10^{14} Pa.s. Hancock et al (1997) pointed that the viscosity of a glass is usually greater than 10^{12} Pa.s and that molecular motions in glasses typically occur over a period in excess of 100 s.

Glass transition temperature/ thermodynamic versus kinetic event:

Ediger et al (1996), Hancock et al (1997) showed that Tg is considered by some to be a thermodynamic event. The presence of Tg is a thermodynamic necessity since if the change in slope did not take place (Figure 1.7) this would mean that upon further cooling of a glass, the enthalpy will keep on dropping until reaching that of a crystalline material and this extrapolated point is the Kauzmann temperature (Tk). As cooling continues a value will be reached where the enthalpy or entropy of the amorphous glass falls below that of the crystalline one which is counterintuitive. Eventually a negative value will be obtained which is thermodynamically unacceptable. Hence the glassy material is behaving in such a way as would be expected and considered thermodynamically acceptable. Based on the above, Tk is considered to mark the lower limit of the glass transition temperature. This idea of Tk being a thermodynamic event was debated by some researchers as mentioned by Ediger et al (1996), Hancock et al (1997), Slade and Levine (1996). Those debating this idea argue that Tg is not a true thermodynamic value as different heating/cooling rates will result in different Tg values (Figure 1.7) and based on this it is merely a kinetic event related to an increase in viscosity as cooling proceeds which impedes molecular motions and the point at which the amorphous material becomes a frozen in liquid is hence related to the heating/cooling rate.

1.2.3 MOLECULAR RELAXATION KINETICS IN THE AMORPHOUS STATE AND THEIR TEMPERATURE DEPENDENCY:

Depending on whether the amorphous solid is in the rubbery or glassy state different relaxation kinetics can be observed.

Hancock et al (1995) stated that the glass transition event is usually considered to reflect co-operative type translational molecular motions whether by segments of a polymer molecule or substituent groups of smaller glass forming species. Hancock et al (1995) also pointed out that below Tg translational molecular motions in the amorphous material still take place, but over longer time periods (hours and days). Slade and Levine (1996) explained that the most important distinction between dimensionally extended (α)

relaxations which give rise to the glass transition as translational motions become constrained at Tg and small scale (β and γ) relaxations, for which small-scale rotational motions do not become constrained as T falls below Tg is the cooperative nature of α relaxations.

Relaxations follow the typical, linear, Arrhenius kinetics at temperature (T) below Tg and again at T above Tm (Figure 1.8). The difference in average relaxation times between these two Arrhenius regions is typically more than 14 orders of magnitude with the rates of all diffusion limited relaxations being much lower in the region of high viscosity (T < Tg) Slade and Levine (1996).

Based on Arrhenius kinetics

$\eta = A.e^{E/RT}$ ..... Equation. 1.2

Where:

η = Viscosity and is related to molecular relaxation time.

A = Constant value related to frequency of collisions between molecules (referred to as frequency or collision number).

E = Activation energy for viscous flow.

T = Temperature.

R = gas constant

A plot of log η versus 1/T gives a straight line in the regions where Arrhenius kinetics applies, with the activation energy being a constant value, which is the slope (Figure 1.8).

Relaxations tend to deviate from Arrhenius type of kinetics at temperatures between Tg and Tm and a completely different non-linear type of kinetics apply (Figure 1.8). Their behaviour in this case follows Williams, Landel and Ferry (WLF) whereby a change in temperature results in an exponential change in relaxation times as explained by Slade and Levine (1996).

$\eta = \eta_g e [c_1 (T-T_g / c_{2+} (T-T_g)]$ ..... Equation. 1.3

Where:

η_g = Mean viscosity at T_g

c_1 and c_2 = Constants

Slade and Levine (1996) reported that relaxation times for WLF behaviour near Tg would change by a factor of 10 for every 3 °C change in temperature.

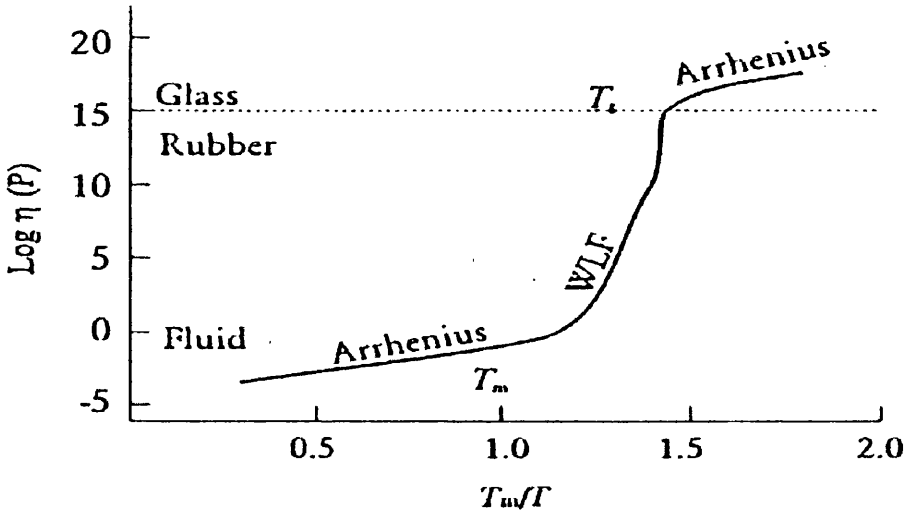

Figure 1.8 *Diagram showing temperature dependency of molecular relaxation kinetics in the amorphous state and regions following Arrhenius type kinetics and those following WLF kinetics. (Adapted from Slade and Levine, 1996).*

1.2.4 EFFECTS OF STRUCTURAL CHANGES ON Tg:

Seymour and Carraher (1996), Allcock and Lampe (1990) related a number of structural modifications to changes in mobility of the resulting molecule and consequently to changes in the glass transition temperature of amorphous or partially amorphous polymers. In general, anything that increases the flexibility of the molecule will result in enhanced mobility, which will end up with a lower Tg value. In contrast, anything that increases the stiffness of the molecule will result in reduced molecular mobility leading to a higher Tg value. Forces can either be primary or secondary forces. Primary binding forces include ionic bonds, metallic or covalent bonds, and these are the most prevalent in polymers. Secondary forces are commonly called Van der Waals forces. The flexibility of the molecule is dependent on rotation or torsion of the skeletal bonds rather than changes in bond angles or lengths.

Several factors can lead to a reduced molecular mobility resulting in increased Tg value, examples of which include:

1. Presence of charged side groups: These can either repel or attract one another restricting free motion.
2. Presence of bulky pendent groups: Being bulky can result in steric hindrance and restricting mobility of the molecule.

3. Polymer chain symmetry: Better molecular packing can be achieved in this case resulting in less available free volume and more restricted mobility.
4. Polar side groups: These groups form hydrogen bonds resulting in a restricted mobility.
5. Presence of stiffening groups: These are groups, which restrict mobility and increase Tg value. Examples of which are the sulfone, carbonyl, p-phenylene

Other factors can result in increased molecular flexibility and mobility leading to a decreased Tg value, examples of which include:

1. Presence of many methylene groups or oxygen atoms between stiffening groups in the polymer chain will result in enhanced molecular mobility relative to the parent compound.
2. Presence of nonpolar groups: In contrast to polar groups which reduce mobility as they restrict motion, nonpolar groups which lack hydrogen bonding and are basically accompanied by weaker Van der Waals forces will enhance mobility and reduce Tg.
3. Dissymmetry of polymer chains: In the case of polymers poorer ability of the molecular chains to pack well results in larger molecular voids and larger molecular free volume. This leads to higher flexibility of the molecule.

1.3 WATER AND PHARMACEUTICAL SOLIDS:

Presence of residual water in solids can lead to a variety of problems such as, increase in chemical reactivity; decrease in physical stability; changes in post compaction hardness of tablets as well as aggregation and poor flow of powder beds. There are a number of sources for residual water in pharmaceutical solids and these include procedures involved in pharmaceutical processing such as, lyophilization; spray drying; crystallization; wet granulation and aqueous film coating. Other sources of residual water include uncontrolled humidity of the environment leading to water uptake by the solid (Zografi and Hancock, 1994, Ahlneck and Zografi, 1990).

1.3.1 WATER AND CRYSTALLINE SOLIDS:

Water can interact with crystalline solids in a variety of mechanisms:

1.3.1.1 ADSORPTION:

Water will hydrogen bond to the surface of the crystalline solid under ambient conditions of temperature and pressure. Adsorption rarely involves more than 2-3 layers of water (multilayered adsorption) and depends on surface area of solid particles. Ahlneck and Zografi (1990) stated that water molecules adsorbed to the surface of the solid generally exist, as expected for physically adsorbed monolayers, with a first layer hydrogen bonded to the solid, and at most 2-3 additional molecular layers formed at the higher relative humidity values. Such adsorption generally is readily reversed by small increases in temperature or by small decreases in relative humidity. Adsorption takes place if the strength of the hydrogen bond formed between water and the solid is involved in high negative enthalpy of interaction, high enough to overcome the significant loss of entropy experienced by condensation of water on the surface of the solid (Zografi and Hancock, 1994). It has to be mentioned though that water at room temperature shows little tendency to adsorb to nonpolar surfaces or relatively hydrophobic organic solids and much more so to polar solids, such as alkali halides and sugars (Zografi, 1988). The simplest model to describe such adsorption was the 2-state BET equation (Hancock and Zografi, 1993):

$$W = \frac{W_m C_b (P/P_o)}{\{1-(P/P_o)\}\{(1-(P/P_o)+C_b(P/P_o)\}} \quad \text{.....Equation. 1.4}$$

Where:

W: weight of water adsorbed per unit weight of dry solid at a relative vapour pressure of P/P_o.

W_m: weight of water adsorbed corresponding to monolayer coverage.

C_b: constant related to the equilibrium constant of the process.

This equation assumes that the influence of the adsorbed solid on the enthalpy and entropy extends only to the first layer and that the rest of the molecules making the multiplayer have properties, which are the same as water in the bulk state. Zografi (1988) explains that BET equation was found to fit data well only at P/P_o below 0.35 suggesting more than two thermodynamic states exist. The BET equation was thus extended to the so

called GAB equation, which basically includes a second equilibrium constant and which though still simplified but fits almost entire adsorption isotherm data (Zografi, 1988). Whereas the BET isotherm considers the presence of two water states, a preliminary monolayer, which is involved in direct interaction with the solid and subsequent water layers adsorbed with no interaction with the solid, which is the state of the condensed adsorbate, the GAB isotherm assumes the presence of three water states. The previously mentioned two states in the BET isotherm as well as a third intermediate water state in which the adsorbent still has some influence due to the effect it exerts on the bound molecules of adsorbate (Buckton, 1995a). The BET isotherm was originally developed to fit those situations, which follow type II isotherm (Figure 1.9). This might be the most commonly encountered practically determined type of isotherm (Buckton, 1995a). From Figure 1.9, it can be seen that monolayer coverage of the surface starts to take place as marked by W_m. This monolayer coverage is followed by additional layers being adsorbed at higher vapour pressures with extensive adsorption occurring in the form of multilayers. This extensive adsorption is due to strong interactions present between the molecules of the adsorbate. W_f in Figure 1.9, marks the point where water molecules begin to associate with themselves and hence water beyond this point behaves as free water or water in the bulk state. Water associated with solids is often described as either being free or bound. Bound water is that water which is tightly bound and is not free to move within the solid. This restricted movement of water means that it will not be available to trigger processes such as chemical degradation and microbial spoilage (Buckton, 1995a). Free water on the other hand, is water that is associated with the solid but is free to move as it is not fixed by any strong bonding and so it is this type of water that is considered available and is frequently associated with either chemical degradation or microbial spoilage. Oksanen and Zografi (1993), however showed that even lowest fractions (0.015) of water taken up by PVP still possess a high degree of translational mobility and are not tightly bound or immobilized in the glassy polymer structure. In contrast, the highest water levels studied in excess of W_g (in amorphous solids and is equivalent to W_f in crystalline solids) show that water molecules are somewhat restricted by the polymeric structure and are not entirely free.

It is usually assumed that molecular water is the adsorbing species, though this is true in most cases, sometimes water dissociates into H and OH radicals which are even more reactive than molecular water itself and hence tend to be more problematic than molecular water (Zografi, 1988).

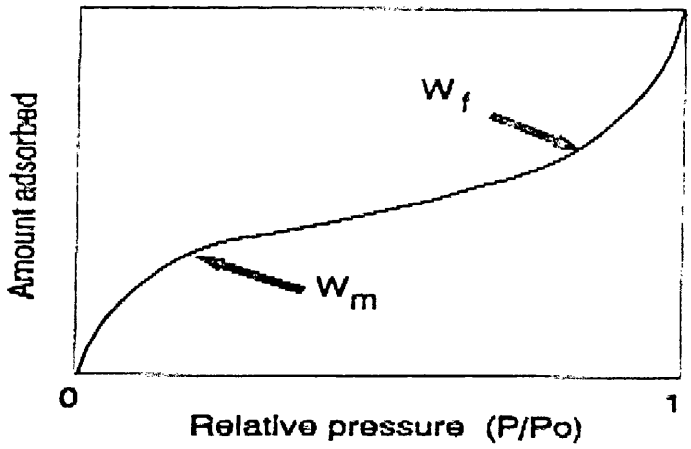

Figure 1.9 *Diagram showing water adsorption typical of type II adsorption isotherm where Wm is the point where monolayer coverage has occurred and Wf is the point beyond which water is regarded as free. (Adapted from Buckton, 1995a).*

1.3.1.2 CAPILLARY CODENSATION AND DELIQUESCENCE:

Condensation of water in microporous solid structures can take place at fairly low relative humidity values leading to occluded water (Ahlneck and Zografi, 1990). This condensation can occur with any solid possessing a highly porous structure with very small pores. Most pharmaceutical solids do not have such small pores in any significant amount. Thus, capillary condensation is not considered a major factor of water uptake under ambient conditions and is only an important factor in the case of silica gel and other microporous high surface area solids used as desiccants in pharmaceutical systems (Zografi and Hancock, 1994). Deliquescence occurs with water-soluble crystalline solids when the atmospheric relative humidity (RH) exceeds the relative humidity of the solid (RH_O) (RH produced by a saturated aqueous solution of the solid) thus allowing dissolution of the solid to take place. As long as $RH \leq RH_O$ deliquescence will not take place and the properties of the solid will not be altered (Zografi and Hancock, 1994).
Both capillary condensation and deliquescence result in the formation of condensed or bulk water, able of dissolving water-soluble components (Ahlneck and Zografi, 1990).

1.3.1.3 CRYSTAL HYDRATES:

Crystal hydrates are characterized by the penetration of water molecules into the crystal lattice, most often, but not always, in a well-defined molecular position within the unit cell, and hydrogen bonded to certain groups with a specific geometry. The nature of stoichiometry, position of the water molecules and the strength of the interaction determine the extent to which such water can enter or leave the crystal unit cell under a given set of conditions (Ahlneck and Zografi, 1990). It is stated that upon crystallization, drugs sometimes entrap solvent in the crystal and that this solvent can either be in stoichiometric or nonstoichiometric amounts (Byrn, 1982). Comparisons of the aqueous solubilities of the anhydrous and the hydrated forms of the drug are widely reported in literature. Aulton (1988), Florence and Attwood (1998) explained that generally speaking the aqueous solubility of the hydrate form is lower than that of the anhydrous one. Examples include, glutethimide, caffeine, theophylline and cholesterol (Florence and Attwood, 1998). This is expected since in the case of the hydrated crystal form, the drug has already interacted intimately with water and so the amount of energy liberated when the hydrate dissolves in water is reduced. According to Zografi and Hancock (1994), two broad categories of crystal hydrates may be considered when the evaluation is based on the way they respond when water is removed from the hydrate. In the first type of hydrates, their water of hydration is lost at temperatures well above 100 °C showing the stability of these hydrates. Removal of this water is accompanied by a distinct transformation into another crystalline form, the anhydrate. An example on this type of hydrates is lactose monohydrate, which loses its water of hydration well above 100 °C and converts to the anhydrous form (Zografi and Hancock, 1994). In the second type of hydrates, their water of hydration is lost well below 100 °C while either retaining their original crystalline structure or collapsing into an amorphous form. Whenever collapse of the existing crystal hydrate structure takes place, it indicates that water in this case, is involved in the crystalline structure in such a way that its presence is essential to hold the crystal together, hence, once water is removed the crystal collapses into the anhydrous or the amorphous form. It is explained by Byrn (1982) that formation of hydrogen-bonding network that includes the solvent in the crystal is quite common in this type. The new forms of the solid, whether the anhydrous crystalline or the amorphous form show different x-ray powder diffraction pattern from that of the original hydrate (Florence and Attwood, 1998, Zografi and Hancock, 1994). If the original crystal hydrate structure is

retained, it is assumed that water in this case is contained in distinct tunnels or channels that span the entire unit cell (Zografi and Hancock, 1994) or that water does not comprise part of the crystal bonding but rather it just acts, as a filler of voids in the crystal and desolvation does not destroy the crystal as explained by Byrn (1982). In this case, a network of hydrogen bonds and non-bonded interactions holds the host molecules together. Several cephalosporin solvates belong to this type and they can be desolvated and resolvated without destruction of the original crystal lattice and without greatly changing the powder diffraction pattern of the crystal (Byrn, 1982). Sodium cromolyn can take up to 25% water. The water is taken up reversibly and with minimum perturbation of the crystal lattice (Zografi and Hancock, 1994). A study on raffinose pentahydrate (Saleki-Gerhardt et al, 1995) showed that drying of the sample at 30 °C in a vacuum oven for only 24 hours resulted in removal of two water molecules and the transfer to the trihydrate. X-ray powder diffraction of those trihydrate samples showed the same integrated peak intensities as the original pentahydrate sample suggesting that the first two molecules of water removed did not disrupt the crystal structure and hence are most likely two loosely held water molecules. On the other hand, if the pentahydrate is held at 100 °C for 24 hours, it is converted to a completely amorphous structure. Drying of the pentahydrate at 60 °C in a vacuum oven yielded a mixture of the trihydrate and the amorphous solid with no anhydrous crystalline form. The tendency of collapse to an amorphous structure upon dehydration at only 60 °C, reveals the critical structure contributions made by the last three water molecules removed.

1.3.2 WATER AND AMORPHOUS SOLIDS (ABSORPTION):

It was observed that in the case of amorphous solids, the amount of water taken up by the solid is much more than that expected from a 2-3 layer adsorption of water seen in the case of crystalline solids. This significant water uptake into such amorphous solids far in excess of what would be predicted from an adsorption to the surface as that seen in crystalline solids is termed absorption or sorption, to differentiate it from adsorption (Zografi, 1988). Water uptake in this case was correlated to sample mass rather than to surface area (particle size) as is the case in water adsorption for crystalline solids. It has been noted that water vapour can be adsorbed and desorbed reversibly from the surface of crystalline solids with no hysteresis between the sorption and desorption steps. An example mentioned by Ahlneck and Zografi (1990) whereby water vapour was repeatedly

adsorbed and desorbed on freshly crystallized sodium chloride up to its critical relative humidity of 76% (deliquescence point) and neither changes in the amounts of adsorbed water nor physical changes in the solid were seen. On the other hand in the case of water sorption into amorphous solids, there is usually significant hysteresis between the sorption and desorption isotherms (Zografi, 1988). The more polar the amorphous solid is, the higher the solubility of water in the solid, and hence the greater the extent of water absorption into the amorphous solid under any particular conditions of relative humidity and temperature.

1.3.2.1 WATER AS A PLASTICIZER:

When an additive lowers the Tg of a substance we speak of its plasticizing effect (Hancock and Zografi, 1994). Water, due to its very low Tg (-134 °C), its ability of hydrogen bonding and its small molecular weight can have a profound plasticizing effect. So a plasticizer is basically a substance that has the ability to reduce the glass transition temperature of another amorphous substance when added to it. Zografi (1988) stated that, as soon as water penetrates into the amorphous solid structure, it acts as a plasticizer and reduces the glass transition temperature of the amorphous solid. From this it can be concluded that, each point on the sorption isotherm reflects the physical state of both the amorphous solid and water and how each have influenced one another under a certain set of conditions (temperature, RH). Thus in spite of the fact that the temperature of the experiment might be constant (T), the difference between this temperature and the glass transition temperature of the amorphous solid (T-Tg) will differ in conjunction with the difference in amount of water being sorbed. For an amorphous solid with a Tg value higher than experiment temperature, the more water is sorbed by the solid, the more the Tg will be suppressed until eventually Tg reaches a value close to or below T. Once this temperature is reached it will critically jeopardise the physical and chemical stability of this amorphous solid as the increased molecular mobility will be sufficient to allow amorphous solids to undergo solid-state chemical reactions and to support the crystallization of the amorphous regions. As water is dissolved in an amorphous solid, the plasticizer effect of water leads to an increase in free volume of the solid by reducing hydrogen bonding between adjoining molecules of the solid, with a corresponding reduction in its glass transition temperature (Ahlneck and Zografi, 1990). As free volume of the solid is significantly increased, the mobility of the molecules or segments of the

molecules in the solid is greatly increased. This increase in mobility is reflected in a decrease in the viscosity of the solid which is particularly significant if the solid is plasticized enough to pass from the glassy immobile state with lower free volume and higher viscosity to the rubbery liquid like state with more free volume and lower viscosity. Amorphous solids below their glass transition temperature (Tg) exist in the glassy state with less than 3% free volume and viscosities greater than about 10^{13} poise (Zografi, 1988). Based on William-Landel-Ferry (WLF) equation, going just 20 °C above Tg will cause the viscosity to change from 10^{13} poise at Tg to10^{8} poise with a very significant increase in the molecular mobility of the solid and water (Ahlneck and Zografi, 1990). When passing from the glassy to the rubbery state, diffusion of water molecules increases exponentially. Hysteresis in the sorption/desorption isotherm of amorphous solids upon exposure to water vapour, is an indication that absorbed water can result in conformational changes of polymer chains in the solid state and was explained as being due to the ability of water to act as a plasticizer when added to polymers or other amorphous solids (Zografi, 1988). Figure (1.10) shows the effect of water absorbed into an amorphous solid on the glass transition temperature of a typical amorphous solid having very high water solubility and a high Tg in the dry state. It can be seen that water with its very low Tg (-134 °C), increasingly and continuously lowers the Tg of the amorphous solid as its concentration in the solid increases. Combinations of the temperature effect with a change in RH effect show the possible changes in the amorphous solid from the glassy state to the rubbery state (Ahlneck and Zografi, 1990). Both an increase in temperature and an elevation in humidity result in increased molecular mobility of the amorphous solid, which can lead to a transition from the glassy to the rubbery state. The first case results in raising T to a level equal to or above Tg , whereas in the second case water causes lowering of Tg to a level equal to or lower than T. Poly(vinylpyrrolidone) is an amorphous solid whose interaction with water gives a typical behaviour as the one seen in Figure 1.10. It has been shown by Hancock and Zografi (1993) that there is a significant change in Tg of PVP at low water contents, with a levelling-off in the water plasticizing effect as the water content increases. This has been explained as being due to the strong interaction between water and the amorphous solid, leading to a marked plasticizing effect of water at low water contents. As the water content in the amorphous solid increases, the strength of the interaction between water and the amorphous solid is reduced, resulting in a lowering of the plasticizing efficiency

of water. Eventually the affinity of water to the amorphous solid is reduced to such an extent that water becomes preferentially associated with its own molecules

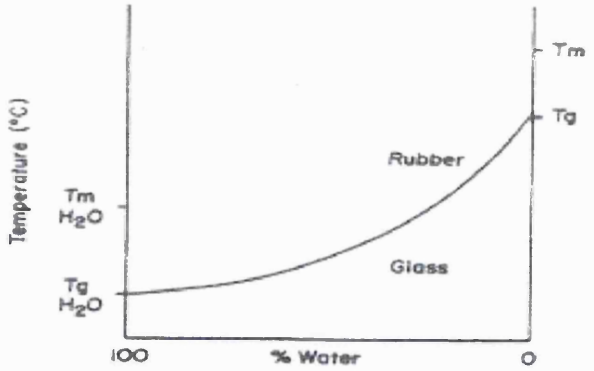

Figure 1.10 *Schematic solute-water state diagram illustrating the effect of water plasticization and its effect on Tg. Adapted from Ahlneck and Zografi, 1990.*

Hancock and Zografi (1994) explained that if two amorphous solids are compared in terms of the extent of water effect on suppressing the glass transition temperature assuming that both solids had the same Tg value, the one with the lower density will be plasticized the least by any certain amount of water. On the other hand, if two amorphous solids having the same density are compared, the one with the lower Tg will be plasticized the least

1.3.2.2 ESTIMATING WATER EFFECT ON GLASS TRANSITION TEMPERATURE (Tg):

The most widely and easily applied equation to estimate the effect of adding a given weight fraction of one amorphous solid to another amorphous solid on the glass transition temperature is the Gordon-Taylor equation (Gordon and Taylor, 1952). It is assumed that there is perfect volume additivity at Tg and no specific interaction between the two components is taking place and so simple mixing rules have been applied.

$T_{g\ mix} = [(w_1.T_{g1}) + (K.w_2.T_{g2})]/ [w_1 + (K.w_2)]$ .....Equation. 1.5

Where:

$T_{g\ mix}$: Glass transition temperature of the mixture of the two components.

w_1 and w_2 : Weight fractions of component 1 and component 2 respectively.

T_{g1} and T_{g2} : Glass transition temperatures of component 1 and component 2 respectively.
K: constant considered to be a measure of the relative free volume contributed to the mixture by each of the two components at any temperature, and is calculated from the densities ρ, and the thermal expansivities, ∝, of the two components as shown below

$K = (\rho_1.\Delta\propto_2)/(\rho_2.\Delta\propto_1)$ .....Equation. 1.6

Where $\Delta\propto = (\propto_{rubbery} - \propto_{glassy})$

Since $(\Delta\propto . T_g) \approx$ constant, Gordon-Taylor equation can be simplified and the constant K can be calculated from the densities and glass transition temperatures of the two components.

$K = (\rho_1. T_{g1})/(\rho_2. T_{g2}$ .....Equation. 1.7

A perfectly miscible system will display a single sharp glass transition event. Immiscibility, incompatibility or, nonideality is often indicated by a poor fit to the equation (Hancock and Zografi, 1997). Hancock and Zografi (1994) investigated a variety of amorphous or partially amorphous compounds. They attempted to fit the data to the Gordon-Taylor equation, and it was noted that the equation could predict fairly accurately the plasticizing effect of water upon both hydrophilic (e.g PVP) and hydrophobic (e.g poly(methylmethacrylate))synthetic linear polymers of pharmaceutical interest. Very few data did not fit the equation well, an example of which was cellulose. In this case the measured depression in the Tg was far greater than predicted by the equation. This behaviour was explained as possibly being due to the presence of crystalline regions in the cellulose, which might have affected the true density of the compound, or that the water content of the sample should be calculated based on the volume fraction of only the amorphous material present. When the density of both components is almost the same, Gordon-Taylor equation can be simplified to the Fox equation. In this case the ratios of the densities will be approximately unity (Hancock and Zografi, 1994).

Fox equation:

$1/T_{g\ mix} = (w_1/T_{g1}) + (w_2/T_{g2})$ .....Equation 1.8

1.3.2.3 PREFERENTIAL WATER ABSORPTION TO AMORPHOUS REGIONS (WATER AMPLIFICATION THEORY):

Partially amorphous solids can be frequently encountered in pharmaceutical processing. A crystalline solid can be rendered partially amorphous by a variety of pharmaceutical

operations such as milling, and compaction. These partially amorphous regions usually exist on the surface of the solid and sometimes they are present in such low percentages that their presence can be missed unless the appropriately sensitive techniques are used to identify and quantify amorphous character. Contact with water was seen to cause preferential water uptake into the amorphous regions rather than onto crystalline portions. Ahlneck and Zografi (1990) explained how water absorption into such low concentrations of amorphous regions lead to a high plasticization of the amorphous part and lowering of Tg below T might take place to such a high extent that molecular mobility is largely increased. This high mobility gained by the molecules in the presence of water can facilitate reordering of the molecules into a crystalline structure and so crystallization will take place. Chemical degradation can take place as well, supported by the molecular mobility, which can lead to exposure of more chemical groups, increase chemical reactivity and facilitate chemical degradation. Slade and Levine (1988) did a study on partially amorphous sucrose having a variety of percentages of the amorphous form ranging from 0.5 to 5 % of the total weight of the solid (Table 1.1). The samples were exposed to two relative humidity values resulting in a water uptake of 0.1 and 0.5 % calculated on the basis of the total mass of the solid. The critical thing was that due to the fact that water got concentrated in the amorphous regions, the less the amorphous content was, the higher was the percentage of water concentrating in that region. Thus a very tiny amount of amorphous content of 0.5 % and at only 0.1 % water uptake (calculated relative to the total mass), this percentage being concentrated in amorphous structure constitutes 20 % of the weight of the amorphous portion. This is a significant concentration of water sufficient to cause plasticization and impart molecular mobility large enough to lower Tg to 9 °C, a temperature that is significantly lower than room temperature (25 °C). This can lead to crystallization of the amorphous part affecting a variety of the physical properties of sucrose such as flow and compaction or promoting chemical degradation. A higher percentage of water of only 0.5 % of the total weight of the solid, which is not unusually encountered in pharmaceutical processing, lowers Tg to a value of −73 °C with significantly high molecular mobility at room temperature. From this work, it can be concluded that it is best to calculate the percentage of water uptake on the basis of the amount of amorphous content in partially amorphous solids, as water tends to be preferentially absorbed into these disordered regions of higher energy levels and higher molecular mobility. This leads to amplification of the percentage of water and

so smaller amounts of amorphous content are more critical in terms of threatening stability of the solid for the same level of total water uptake.

Table 1.1 Moisture content in the amorphous portion of sucrose and the corresponding glass transition temperature if a total of 0.1 or 0.5 % moisture is taken up. Adapted from Ahlneck and Zografi (1990). The value of 52 °C was used as the Tg of totally amorphous sucrose.

Amount of moisture (%)	**Amount of amorphous Material (%)**	**Moisture content In amorphous material (mg H_2O/100 mg solid)**	**Glass transition Temperature (° C)**
0.1	0.5	20	9
	1	10	27
	5	2	49
0.5	0.5	100	-73
	1	50	-36
	5	10	27

1.3.2.4 WATER SORPTION PROFILES IN AMORPHOUS SOLIDS:

Water adsorption on the surface of crystalline solids at a certain temperature and vapour pressure is most commonly fitted to either the BET or its extension the GAB adsorption isotherm (as mentioned previously). In case of amorphous solids however, water is known to be absorbed into amorphous regions rather than being adsorbed. To fit data of water absorption into amorphous materials or amorphous regions, the BET equation or the GAB equation have been used. It is considered to be useful in estimating W_m. Hancock and Zografi (1993) argue however that in the case of amorphous solids, these mathematical models are basically used as they fit data quite well rather than being able to advance our understanding of the molecular processes occurring as water is taken up into amorphous solids. It clearly does not take into account the significant plasticizing effect of water or any structural changes in the solid taking place as water is absorbed. This is a disadvantage in relying on the BET equation to demonstrate water absorption

profile in amorphous solids. In the case of amorphous solids W_m does not indicate monolayer coverage but rather reflects the polarity of the solid, the higher the polarity the higher the value of W_m (Buckton, 1995a). For amorphous solids, W_f is substituted with the term W_g indicating the amount of water needed to convert the amorphous solid from the glassy rigid state to the rubbery state. The significance of W_g being a critical point is quite clear from knowing the greater molecular mobility accompanying the rubbery state relative to the glassy state, which will lead to a significant increase in water uptake above W_g. In the case of W_m, the significance in amorphous materials is not as clear but it was shown that for water-PVP system, the ratio of W_g to W_m over 100° range is quite constant indicating that W_m is related to the plasticizing effect of water (Zografi and Hancock, 1994). Basic solution theories have been used to model data and to achieve a better understanding of water vapour absorption into amorphous solids. This is based on the idea that the water absorption process by amorphous solids is completely analogous to the solution process. Two theories are considered here:

1.3.2.4.1 THE FLORY- HUGGINS THEORY:

This theory is based on the assumption that the solution process is driven by a minimum free energy requirement. A form of the equation that gives the partial pressure of the solvent as a function of the solvent content is a frequently used form of the equation (Hancock and Zografi, 1993).

$$P/Po = \phi_1 \exp \{(1 - 1/x)\, \phi_2 + \chi\, \phi_2^{\,2}\} \qquad \text{.....Equation. 1.9}$$

Where P/Po is the partial pressure of the solvent, ϕ_1 and ϕ_2 are the volume fractions of the solvent and the polymer respectively; x is the ratio of the molar volumes of the solvent and the polymer and χ is the Flory-Huggins polymer-solvent interaction parameter (a constant). This constant ranges from 0 (good solvent) to 0.5 (poorer solvent). The validity of the Flory-Huggins model for predicting water vapour absorption into amorphous pharmaceutical solids was tested by comparing the predicted isotherm with experimental data from the literature (Hancock and Zografi, 1993). Poly(vinylpyrrolidone) (PVP K30)-water system at 30 °C was used as the model to test for agreement with Flory-Huggins model. It was noted that there is an overall agreement between experimental data and predicted isotherm especially when the amount of water vapour sorbed is sufficient to plasticize the sample and convert it from the glassy to the rubbery state where

significantly greater amounts of water will be taken up by the amorphous solid sample. This is not surprising since this theory was derived for non-polar polymer-solvent systems at high solvent concentrations, which are not met by PVP absorbing small amounts of water in the glassy state. It can thus be concluded that this is a suitable model to predict behaviour of the amorphous solid material in the rubbery state upon exposure to water though is less suitable to predict behaviours in the glassy state which is maintained at low partial vapour pressures provided that the temperature of experiment is kept below Tg of the sample mix (Figure 1.11). It has to be mentioned though that the glassy region is the region of interest for most pharmaceutical applications since samples will almost always be dried and then stored at lower vapour pressures.

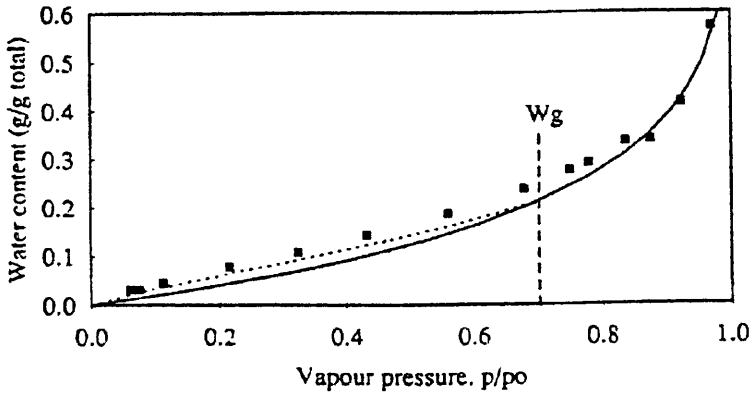

***Figure 1.11** Comparison of data fitting of PVP K30 to both Vrentas model and Flory-Huggins model at 30 °C (▪) Data; (.....) Vrentas equation; (——) Flory-Huggins equation. Adapted from Hancock and Zografi (1990).*

1.3.2.4.2 THE VRENTAS THEORY:

Vrentas proposed that the sorption of a penetrant by a polymer results in a nonideal hole free volume increase. Nonideal, in the sense that, the net hole free volume of the polymer/water system in the glassy state is less than what would be predicted by simple addition of the hole free volumes of the two independent components. This net excess loss in hole free volume is due to local rearrangement of the glassy polymer as the penetrant enters the system and interacts with the polymer (Hancock and Zografi, 1993). Vrentas equation is very similar to Flory-Huggins equation but with the addition of the term $\exp f$ as shown below:

$$P/Po = \phi_1 \exp\{(1 - 1/x)\,\phi_2 + \chi\,\phi_2^{\,2}\}\exp f \qquad \text{.....Equation. 1.10}$$

Where $f = \{M_1 w_2^2 (C_{pg} - C_p) (dT_{gm}/dw_1) ((T/T_{gm}) - 1)\}/RT$

Where M_1 is the molecular weight of the solvent, w_1 and w_2 are the penetrant mass fraction and the polymer mass fraction respectively, C_{pg} and C_p are the heat capacities of the mix in the glassy state and the rubbery state respectively, dT_{gm}/dw_1 is the change in T_g of the mixture with varying penetrant mass fraction, R is the universal gas constant and T is the experimental temperature. It can be noted that the term *f* includes all those factors that reflect the change in structure of the polymer-penetrant mixture below the glass transition temperature. It can further be commented that all components of this term are constant at any given experimental temperature except for dT_{gm}/dw_1, hence it is this term that is most critical in determining the shape of the isotherm below T_g. A significant change in the value of dT_{gm}/dw_1 would produce a large shoulder of the isotherm in the region of W_m. This shoulder is not predicted by the Flory-Huggins model, which basically deals with the rubbery state. Thus, the value of the Vrentas model is that it enables the prediction of sorption isotherms for polymers in both the glassy and the rubbery states as water is absorbed as can be seen in Figure 1.11. It should be noted that at $T = T_g$ the Vrentas equation reduces to the Flory-Huggins equation.

1.3.3 EFFECT OF ADDITIVES OTHER THAN WATER ON Tg OF AMORPHOUS SOLIDS:

Other additives can reduce the time for recrystallization. Colloidal silicon dioxide (Stubberud and Forbes, 1998) has been shown to reduce the onset of crystallization of lactose at 25 °C at both 55 and 75 % RH values in a humidity controlled chamber when it is prepared as a binary physical mixture using a cube mixer for the preparation. It has been proposed that colloidal silicon dioxide reduces time for recrystallization by an isolation or deaggregation mechanism whereby small particles of silicon dioxide are able to penetrate the amorphous lactose bed and increase the dispersion of primary particles of amorphous lactose making it more accessible to water. An antiplasticizer is a material that does the reverse of a plasticizer and that is resulting in an increase in the Tg value of the material to which it is added. The antiplasticizer will have a Tg value that is higher than the original material to which it is added and hence the net glass transition temperature will be somewhere between that of the two individual components. Many studies involved the use of PVP and showed how crystallization can be delayed or even inhibited

by the use of physical mixtures or coprecipitates of PVP with other drugs or excipients (Matsumoto and Zografi, 1999, Shamblin and Zografi, 1999, Lu and Zografi, 1998, Stubberud and Forbes, 1998, Yoshioka and Zografi, 1995). Matsumoto and Zografi (1999) showed that coprecipitates of indomethacin with poly(vinyl)pyrrolidone (PVP) or poly(vinyl)pyrrolidone-co-vinyl acetate (PVP/VA) prepared by colyophilization were capable of inhibiting crystallization of indomethacin at 30 °C for at least 20 weeks at polymer levels as low as 5 % w/w regardless of molecular weight of PVP used ranging from 10^3 to 10^6 g/mole. The extensive inhibition of crystallization noted seems to involve a mechanism more complex than a simple antiplasticizing effect that ideally follows simple mixing theories of free volume as suggested by Gordon-Taylor. The actual suggested mechanism was that of hydrogen bonding taking place between indomethacin and PVP preventing dimerization of amorphous indomethacin at the carboxylic acid group. Such dimerization is essential for γ crystal formation. This sort of interaction in colyophilized mixtures involving inhibition of dimerization of amorphous indomethacin was mentioned in this study and proven in a previous study (Taylor and Zografi, 1997).

Saleki-Gerhardt and Zografi, (1994a) carried out a study involving sucrose and its crystallization from the amorphous state in the presence of a variety of sugars colyophilized with sucrose and all having comparable Tg values but greater than that of sucrose (trehalose, lactose and raffinose). It was shown that these additives at levels as low as 10 % w/w increased the crystallization temperature of sucrose significantly. The glass transition temperatures of these mixes increased with the increase in weight fraction of the sugar used in a manner that is in good agreement with the Fox equation (mentioned earlier and used here since the densities of the individual components are almost the same). This agreement with Fox equation suggests volume additivity taking place with these systems with no strong interaction between the two components. Methylcellulose and several alginic acids were reported to retard conversion from the amorphous to the crystalline state (Byrn, 1982).

Other methods have resulted in delay of crystallization such as that reported by Buckton and Darcy (1995a) whereby a delay in crystallization of lactose (as manifested by a long lag time before crystallization takes place) is reported, when either microcrystalline cellulose or magnesium stearate are added as a middle layer between two layers of lactose in the ampoule of the isothermal microcalorimeter. This restricted the rate of water uptake by the lactose sample and led to a delay in the crystallization of lactose with

microcrystalline cellulose having greater effect resulting in further delay in crystallization of lactose when compared with magnesium stearate.

1.3.4 COLLAPSE PHENOMENON IN AMORPHOUS MATERIALS:

Collapse is a synonym to loss of structure in freeze-dried substances while during storage of amorphous solids collapse is related to viscous flow of the dried powder matrix and is termed stickiness (Tsourouflis et al., 1976). Collapse is a structural transition, which can be seen in amorphous solids when exposed to high temperatures and/or high levels of moisture. In which case either the temperature is raised above the collapse temperature of the solid (Tc) as in heating or Tc of the solid is lowered below experiment or ambient temperature (T) as triggered by moisture uptake. Increase of moisture was found to lower Tc of freeze-dried solids with just a 1 % difference in moisture content of freeze-dried solids resulting in Tc being reduced by 5 °C in most samples studied by To and Flink (1978a). Both increasing the temperature or the moisture content will result in increased mobility and an increase in free volume. This increase in temperature or water content may exceed a critical value specific to the material to such an extent that viscosity is significantly lowered. This reduction in the viscosity to a point where the solid matrix can no longer support its own weight can lead to flow of the matrix and collapse taking place (To and Flink, 1978b). In freeze-dried solids, the collapsed sample visually resembles a highly viscous glassy material compared to the pre-collapsed appearance of a porous solid (Tsourouflis et al., 1976). Collapse phenomenon is usually considered in relation to freeze-drying in food science. This is due to the fact that freeze-drying procedure is unique in the fact that water is removed by sublimation of ice from the frozen solid instead of evaporation from the liquid state as commonly done in drying of solids. This method of drying can give an extensive gross structure with low bulk density (To and Flink, 1978b). The space occupied by ice in the frozen material will eventually be replaced by voids as ice is sublimated in the drying step. Presumably a system with smaller fraction of total void volume is more resistant to collapse as explained by Tsourouflis et al. (1976). Yet, collapse can occur in any amorphous material prepared by methods other than freeze-drying such as spray drying. Particles sticking to the walls of dryers and difficulties in collecting the powder in the collecting zones are a consequence of this stickiness. The sticky-point temperature marks a transition from a dry stable powder to a viscous sticky state and is hence related to collapse (Tsourouflis et al., 1976).

The problem of agglomeration and caking of powders is also related to collapse (Tsourouflis et al., 1976). It is obvious that collapse and glass transition are similar events. However, while glass transitions are generally reversible (unless crystallization took place), collapse behaviour is irreversible (To and Flink, 1978b). Crystallization usually follows collapse as the need to reach the most stable thermodynamic state is met by obtaining a crystalline structure. Crystallization can take place triggered by moisture or heat. However in the absence of moisture collapse of a monohydrate as triggered by heat alone can happen without subsequent crystallization as explained by Flink (1983). Effect of heating rate on Tc was investigated by To and Flink (1978a). They found that while slight differences in degree of collapse were noted for samples heated at 2 °C/min. and 10-40 °C/min., Tc was found to be independent of heating rate. This partial collapse was suggested by To and Flink (1978a) where they found that different extents of collapse are seen on a series of freeze dried sucrose and maltose mixtures at the different temperatures. They showed that collapse is not an all or none phenomenon and that it can be stopped partway or allowed to proceed to a higher level depending on the temperature. They measured collapse under a hot stage microscope whereby the extent of collapse was defined in terms of change in flake area (Figure 1.12). The area of the flake is measured from the beginning of shrinkage of the flake (start of collapse) until the flake becomes a round structureless blob with no further change in area being observed which marks the end of collapse. In most cases the range of temperature over which collapse can be observed is 20-40 °C (To and Flink, 1978a).

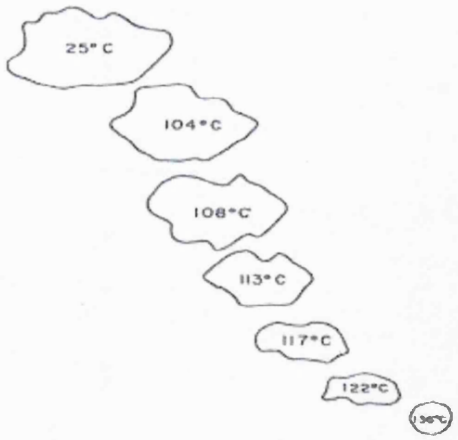

Figure 1.12 *Diagram showing partial collapse indicated by a change in the area of the flake as seen under a hot stage microscope (magnification x 150). Adapted from To and Flink (1978a).*

Buckton and Darcy (1996) studied partial collapse brought about by exposure to a certain RH for a variety of times. Collapse of amorphous lactose was followed in dynamic vapour sorption (DVS) and was seen to start after 60 minutes of exposure to 50 % RH since 60 minutes of exposure to 50 % RH results in a maximum water uptake whereby Tg almost equals T and the sample does not collapse losing all its water during the desorption step back to zero point. At 120 minutes of exposure to 50 % RH the sample is completely collapsed and desorption is controlled by slow diffusion of water through the collapsed structure with minimal amount of water being desorbed. Intermediate levels of collapse where seen at intermediate exposure times at 50 % RH. Buckton and Darcy (1997) followed the collapse of lactose and proved that crystallization of collapsed amorphous lactose occurs in differential scanning calorimeter at lower temperatures (ca. 70 °C) than the non-collapsed samples (ca. 180 °C). This makes the collapsed sample more prone to change during standard pharmaceutical processing. Collapse of freeze-dried structures was related to loss of volatile ingredients, which were frozen in with the matrix during the process of freezing (To and Flink, 1978c). Oxidation of emulsified fat in a freeze-dried matrix was also shown to be related to collapse by To and Flink (1978c). However both complete loss of volatile ingredients and release of trapped oil, which will thus be oxidized, did not occur after collapse but rather after recrystallization where the crystalline structure with its limited free volume can no longer accommodate the presence of other molecules. This is why recrystallization is considered one of the best methods for purification of a substance. Tsourouflis et al. (1976) stated that a collapsed product loses its shape by becoming a highly viscous liquid and often shows poor aroma retention, poor rehydration characteristics and uneven dryness. Obliteration of capillaries and increased vapour flow resistance can result from collapse during freeze-drying.

1.3.5 METHODS OF OBTAINING AN AMORPHOUS FORM OF THE SOLID:

Amorphous structures in solid materials can either be normally present as in the case of some polymeric materials where basically the solid is either in the amorphous form or is partially amorphous or partially crystalline. This is the case in some polymers as for these large molecules it might be difficult to find molecules completely well packed in short and long range order with the absence of any disorder in the molecule. These polymeric solids include many pharmaceutical excipients, as well as packaging materials (Hancock and Zografi, 1997). Amorphous character can also be seen in large peptides and proteins

used as therapeutic agents. Every protein molecule whether crystalline or amorphous can be considered to be a disordered array of structures some of which are more locally ordered than others (Shamblin et al, 1998). The other possibility is obtaining amorphous structures from different sorts of pharmaceutical processing operations carried out on small molecules, which are ordinarily crystalline. These treatments of the sample include:

1. Lyophilization (freeze drying): Preparation of amorphous solids through lyophilization of the crystalline counterpart is widely reported in the literature. Pikal et al (1977, 1997) prepared amorphous forms of different antibacterials and insulin respectively through freeze- drying of their crystalline forms. Different amorphous sugars were prepared by lyophilization in a study carried out by Taylor and Zografi (1998). Larsen et al (1997) used lyophilized amorphous acadesine in a study involving the evaluation of water-catalyzed crystallization of the amorphous form. Saleki-Gerhardt et al (1994b) prepared amorphous sucrose by freeze-drying in order to assess the amount of amorphous sucrose mixed in known ratios with crystalline sucrose by different analytical techniques (the mix is used as a standard curve).
2. Spray drying: widely used in the literature to prepare amorphous solids from the crystalline version of the material. Hill et al (1998), Chidavaenzi et al (1997), Buckton and Darcy (1996, 1997), Buckton et al. (1995a), Brigginer et al. (1994), Sebhatu et al (1994), used spray drying to prepare amorphous samples of lactose. Schmitt et al (1996) used spray drying in the preparation of one of the amorphous samples of lamotrigine mesylate. Bukton et al. (1995b) used spray drying to prepare amorphous samples of salbutamol. Spray drying was used by Pikal et al (1978) as one of the methods to prepare amorphous versions of some cephalosporin antibiotics.
3. Quenching and slow cooling from the melt: Yonemochi et al. (1999) used quenching in liquid nitrogen to prepare amorphous samples of ursodeoxycholic acid. Hancock and Parks (2000) and Andronis et al. (1997) prepared amorphous samples of indomethacin by melting and quenching the crystalline sample in liquid nitrogen. Moustafa et al. (1971) used melting and slow cooling of the melt in preparing amorphous samples of sulphamethoxydiazine. Yoshioka et al (1994) used both quenching and slow cooling from the melt in obtaining two amorphous samples of indomethacin.

All of the above methods are intentionally used to trigger the formation of amorphous forms of the solid. They render the material amorphous as they either involve rapid precipitation from the melt through rapid removal of the solvent as in the case of lyophilization or spray drying (Shamblin et al., 1998, Hancock and Zografi, 1997) or supercooling of a melt as in quenching and slow cooling (Hancock and Zografi, 1997). Condensation from the vapour state is another method through which amorphous structures can be obtained (Hancock and Zografi, 1997).

4. Milling (Comminution): Many workers showed that milling could result in the development of such disordered or amorphous regions (Ward and Schultz, 1995, Briggener et al., 1994, Saleki-Gerhardt et al., 1994, Elamin et al., 1994a, Otsuka and Kaneniwa, 1990, York, 1983). Milling is one of the basic unit operations frequently encountered in the processing of pharmaceutical solids. It is useful in terms of reducing the particle size, which can result in a more homogenous mix of the milled drug and the excipient. A smaller particle size can be achieved that can further improve the rate of solution through an increase in surface area, which in turn can lead to enhanced bioavailability of the drug. This increase in rate of solution can be critical especially when dealing with sparingly soluble drugs. Milling however can improve the apparent solubility through the creation of disordered or amorphous regions or the so-called reactive hot spots, which are chemically and physically unstable and able to take in larger amounts of water in the crystalline solid (Ahlneck and Zografi, 1990). A study on the solubility of comminuted and uncomminuted samples of digoxin was carried out (Florence and Salole, 1975). The milled samples exhibited amorphous character and the apparent equilibrium solubilities at 25 °C of the milled samples showed increases of between 7 and 118 % over those of the unmilled starting materials. Another study on digoxin and digitoxin (Chiou and Kyle, 1979) showed that trituration resulted in a disorder in the crystalline structure, which was associated with an increase in the solubility of the disordered amorphous form in comparison to the crystalline one. The difference in solubility was detected in the dynamic solubility study but failed to show in the equilibrium solubility study. This was thought to be due to the fact that the amorphous form crystallizes within the first hour to the more stable crystalline form.

Milling involves mechanical activation of the solid. The active mechanical energy that is partially transferred to the solid is stored in the form of lattice defects. This causes the solid system to transform from a deactivated (crystalline) state to an activated state with the accompanying disordering and a resulting increase in entropy, enthalpy and volume (Huttenrauch et al., 1985). Formation of disordered regions with higher energy state than that of the crystal means that these regions are thermodynamically unstable (Buckton and Darcy, 1999, Saleki-Gerhardt et al., 1994b). This development of a thermodynamically unstable activated state in the crystal lattice is reversible and deactivation, recrystallization; entropy loss and energy output of the system can follow as seen in Figure 1.13 (Huttenrauch et al., 1985).

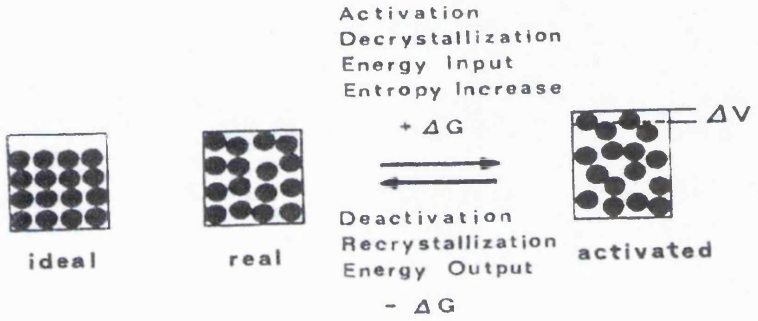

Figure 1.13 *Diagramatic representation of activation and deactivation of solids. Adapted from Huttenrauch (1985).*

The activation can be manifested throughout the entire crystal in which case an amorphous structure is produced, or affect only the surfaces of the crystals and maybe even then be restricted to localized points on that surface (Elamin et al, 1994a). Buckton et al. (1988) showed that surface energetics of a powder can be altered by milling. Samples of aspirin were milled in different types of mills and the surface energy of the powder was noted to increase in proportion to the perceived energetics and efficiency of the mill used. When two consecutive milling processes were used, the powder tended to have energetic properties similar to powders milled by the first rather than the second mill alone.

Elamin et al. (1994a) investigated the aqueous solubility of unmilled (crystalline), quenched (completely amorphous) and milled griseofulvin samples. They found that the milled samples contained about 5.8 % amorphous solid which is concentrated on the surface of the solid particles. They showed that the quenched samples had the highest initial (peak) solubility, followed by the milled sample with the unmilled

sample having the lowest initial solubility. The increased solubility was concluded to be due to presence of amorphous regions as proven by heat of solution measurements since no differences in particle size or surface area were seen between the milled and unmilled samples. However, the solubility tends to fall from that of the peak level for the milled sample with longer exposure to the dissolution medium, and this is argued as being due to conversion of the unstable amorphous form to the thermodynamically stable crystalline one. Ward and Schultz (1995) studied the physical stability of both micronized and unmiconized crystalline albuterol sulfate. They found that micronization resulted in the presence of small amounts of amorphous characters. They concluded that the micronized sample stored at 40 °C and 75 % RH for 24 hours crystallized with the loss of water upon crystallization. These micronized, crystallized particles resulted in the formation of interparticulate bridges and fusion of particles resulting in agglomeration. This is due to the fact that particles were close to each other during crystallization of amorphous regions. Agglomeration of the particles can cancel out the micronizing efforts and is indeed very critical in this case and can dramatically reduce the effectiveness of powder inhalation products. Otsuka and Kaneniwa (1990) studied the relationship between crystallinity and chemical stability in the solid state of cephalothin sodium. The crystalline sample was subjected to grinding in a ball mill for different grinding times. They concluded that milling for 2 hours reduced crystallinity to 30 % with a corresponding reduction of the decomposition point from 215 °C for the original crystalline sample to 187 °C after 2 hours of milling. Milling for 3-10 hours resulted in intermediate crystallinity of 50 % with an intermediate decomposition point of 192 °C. It was explained that the temperature in the ball mill rose by 5 °C after one hour of grinding and that this rise in temperature might have caused crystallization of some of the amorphous regions formed during milling for times more than one hour. A clear correlation between a fall in decomposition point and degree of crystallinity was noted and thus indicated a lower chemical stability of the amorphous form.

Unlike the previous methods (lyophilization, spray drying and quenching or slow cooling of the melt) the presence of such amorphous regions in a milled sample is unintentional and is just a consequence of a basic unit operation carried out in pharmaceutical processing of materials.

5. Presence of impurities: Pikal and Grant (1987) explained that the presence of a small percentage of an additive or impurity creates defects in the crystal lattice of the major component. This disruption of the crystal lattice can take place when a substance comes in contact with the solid accidentally as in being present in water vapour or in solution during crystal growth (in both cases considered as an impurity) as well as if added intentionally as in solvents, cosolvents, surfactants and antioxidants. Hendriksen (1990) studied the effect of incorporating ethyl acetate and sodium chloride during aqueous precipitation of calcium fenoprofen. It was concluded that some level of disruption of calcium fenoprofen crystals was caused by sodium chloride while considerable disruption in crystallinity was caused by ethyl acetate. Uptake of surfactants into the crystal during crystal growth might produce a defect in the crystal structure resulting in the crystal being thermodynamically unstable and hence dissolve faster (York, 1983)

1.3.6 ADVANTAGES AND DISADVANTAGES OF AMORPHOUS CHARACTER IN PHARMACEUTICAL SOLIDS:

Amorphous solids whether completely amorphous or present in tiny amounts in crystalline solids have been widely studied and many of their advantages and disadvantages have been recognized. Amorphous characters are disordered structures associated with a higher energetic level, greater molecular mobility and greater free volume resulting in a thermodynamically activated, less stable state in comparison to the crystalline state (Hancock and Zografi, 1997, Ediger et al., 1996, Saleki-Gerhardt et al., 1994, Ahlneck and Zografi, 1990). Thus, presence of amorphous structures gives rise to some problems as well as some benefits. Amorphous forms are thus expected to provide the biggest advantage in terms of apparent solubility and bioavailability, however the stability might be jeopardized. Many studies have been carried out to verify the solubility advantage of the amorphous form over its crystalline counterpart. Hancock and Parks (2000) studied the solubility of a group of drugs with indomethacin being the most extensively studied in both their amorphous and crystalline forms. They concluded that the amorphous forms are markedly more soluble than the crystalline ones, though they stated that the experimentally measured solubility of the amorphous form was lower than the predicted solubility calculated based on simple thermodynamic considerations. Failure of the amorphous form to achieve the maximum predicted theoretical solubility in

practical experimental conditions was explained as being due to crystallization of the amorphous form in presence of the dissolution media. They stated that even quite low levels of amorphous character (< 10 %) in a drug substance could cause theoretical solubility increases of much more than two fold. At least a two-fold increase in solubility is needed to be clinically meaningful assuming that ± 50 % intersubject variability is typical (Hancock and Parks, 2000). Moustafa et al (1971) showed that sulphamethoxydiazine had 3 polymorphs, 2 solvates and an amorphous form. The apparent equilibrium solubility of one of the polymorphic forms (polymorph II) and the amorphous form was about 1.8 times that of the water stable polymorph, however longer period of contact of the solid with the dissolution medium was found to result in a decrease in solubility to that of the value corresponding to the solubility of the water-stable form. Buckton and Beezer (1992) explained that with metastable polymorphs higher solubility values can be achieved practically but should never be considered as the true thermodynamic equilibrium solubility. It is basically the one achievable in the time scale of the experiment and is thus called apparent solubility. Given enough time, true equilibrium solubility can be achieved.

Both physical and chemical instabilities of the amorphous structures are widely reported in the literature. The problem can be of dramatic effects especially when the presence of such amorphous characters is in tiny amounts which can pass several techniques such as X ray powder diffraction, differential scanning calorimetry and density measurements by helium pycnometry unnoticed since these techniques are not sensitive enough to detect amorphous characters accurately below 10% amorphous content (Saleki-Gerhardt et al (1994b). This is frequently the case in amorphous characters generated by micronization of crystalline powders or by powder compaction (Hancock and Zografi, 1996), which unlike polymeric, lyophilised or spray-dried materials, the amorphous character is present in small amounts and is usually on the surface of the solid. The low amorphous content exists on the surface of the particles in this case, and it is the surface, which will be involved in interactions and indeed reactions (Briggner et al., 1994). Effects of milling on solubility and stability of the solid material are explained in Section (1.3.5 part 4).

Other more sensitive techniques to detect low levels of amorphous content can be used such a water vapour sorption which is claimed to detect as low as 1 % (Saleki-Gerhardt et al., 1994b) or 0.05 % (Buckton and Darcy, 1995b). Isothermal microcalorimetry is another sensitive technique that can be used to detect as low as 0.625 % (Buckton et al., 1995a) 1 % (Briggner et al, 1994) or 2 % (Sebhatu et al., 1994a) amorphous content.

Larsen et al (1997) reported that lyophilized, amorphous acadesine, intended to be administered as an intravenous solution is readily soluble in large amounts of water but when exposed to water vapour the amorphous material converts to a water-repellent, insoluble, anhydrous crystalline form with the formation of an intermediate metastable hydrate which spontaneously converts to the anhydrous crystalline form. In another study carried out by Andronis et al (1997), amorphous indomethacin crystallized to the stable γ crystal when exposed to relative humidity of less than 43 % at 30 °C, whereas exposure of the amorphous form to higher RH values at the same temperature led only to the formation of the metastable α form. In both of the above examples the formation of a metastable form is in agreement with Ostwald's step rule which indicates that the phase that crystallizes is not necessarily the one which is thermodynamically most stable, but the one which crystallizes the fastest that is the one kinetically more achievable (Mullin, 1997).

Schmitt et al (1996) reported moisture dependent crystallization of amorphous spray dried and freeze-dried lamotrigine mesylate samples. Chemical instabilities related to percentage crystallinity are also reported in the literature. Crystalline drugs are normally much more stable toward chemical degradation than the corresponding amorphous solid. This observation is most likely the result of a more rigid and inert molecular environment in the case of crystalline solids in comparison with amorphous ones thus this restricted motion exhibited by crystalline solids does not allow the reaction to readily occur.

Pikal et al (1977) in a study carried out on a group of β-lactam antibiotics noted that even when dry, the amorphous forms obtained by freeze drying were at least one order of magnitude less stable than the corresponding unsolvated crystalline form. They also showed that when water is absorbed by the sample the number of decomposition products as well as decomposition rate increased. The same greater stability of the crystalline form of some β-lactam antibiotics in comparison with the amorphous one was noted by Pikal et al (1978), Oberholtzer and Brenner (1979). However, an exception to the rule was reported in a study by Pikal and Rigsbee (1997). The authors concluded that the amorphous form of insulin prepared by freeze-drying was far more chemically stable than the crystalline counterpart. They noted that increasing water contents resulted in an increase in the degradation rate of crystalline insulin while degradation rate constants of the amorphous form seemed to be independent of moisture up to the maximum water content studied (≈15 %). They explained that differences in stability might be due to structural differences between the two solids although no structural changes were seen in

the amorphous form when tested by both DSC and FTIR. The workers suggested that the rule stating that the crystalline phase provides greater stability toward degradation must be questioned for proteins in general. Shalaev et al (2000) reported acid catalysed inversion of amorphous sucrose even at very low levels of residual water (< 0.1%) to other reducing sugars (capable of reacting with other ingredients in the formula) when sucrose is colyophilized with an acid such as citric acid.

Many workers investigated the effect of presence of amorphous parts in the solid on tablet strength. Sebhatu et al. (1994b) showed that the presence of 15% amorphous content in spray dried lactose resulted in better tablet strength when spray dried lactose was exposed to 57% RH for up to 4 hours prior to compaction in comparison with the dry spray dried sample. However, they noted that there is an optimum exposure time for best strength in tablets and that exposure to 57% RH for more than 6 hours prior to compaction resulted in a decrease in tablet strength. They explained this as being due to water acting as a plasticizer and that when Tg came closer to T, there was an increase in the mobility and plastic flow of the solid mass resulting in an increase in plastic deformation which lead to the formation of stronger tablets. They also showed that tablets made from crystallized spray dried lactose prior to compaction exhibited lower tablet strength and explained this as being due to the fact that an already crystallised system is a deactivated one which exhibits limited molecular mobility, rearrangeability and hence plasticity. They stated that the tablet strength of the crystallized material had almost the same tablet strength as crystalline α-lactose monohydrate at the same compaction pressure. A similar study was carried out by Stubberud et al. (1996) who evaluated the strength of tablets made from microcrystalline cellulose either alone or in combination with poly(vinyl)pyrrolidone (PVP). They proved that there is an optimum level of moisture uptake, which reduces Tg to a level sufficient to impart enough molecular mobility to enhance the formation of strong compacts. However, if this value is exceeded and crystallization or collapse of the amorphous structure occurred prior to compaction a fall in tablet strength is noted. Elamin et al. (1994b) remarked that in post compaction storage of compacts at various RH values, there exists a lower critical relative humidity value probably related to both temperature and moisture content, below which molecular mobility in amorphous regions is too low to trigger crystallization and cause any change in compact strength. They also stated that spontaneous aggregation of particles can occur parallel to surface crystallization such as in milled sucrose samples (in the experimental conditions they used) and that such

changes might drastically affect some of the powder processing properties such as powder mixing, flow and die filling.

1.4 AIMS OF THE THESIS:

- To prepare an amorphous form of a hydrophobic model drug (terfenadine) by two methods (slow cooling and quench cooling from the melt), and to compare the two products.
- To study the effect of water uptake on the potential for crystallization of amorphous terfenadine.
- To prepare salts of terfenadine using homologous dicarboxylic acids and to identify the products.
- To compare the properties of terfenadine with those of its salts in both the crystalline and the amorphous forms.
- To assess the solubility and the potential for crystallization of terfenadine and its salts.
- The general aim of this thesis was to study a homologous series of a parent drug (terfenadine was used as the model in this case) and to compare them in the amorphous state in terms of the relationship between carbon chain length and the glass transition temperature (Tg). This was done in an attempt to prepare amorphous forms that are more stable and at the same time are of higher solubility than the parent drug. If this was achieved, it would be a breakthrough in the field of amorphous materials.

CHAPTER TWO

MATERIALS AND METHODS

2.1 ANALYTICAL METHODS:

2.1.1 GRAVIMETRIC METHODS (DYNAMIC VAPOUR SORPTION (DVS)):

This method of solid sample analysis involves the use of a humidity and temperature-controlled system. The system used in this study was a DVS from Surface Measurement Systems, U.K. (*Figure 2.1*). The ultrasensitive (Cahn) microbalance is capable of measuring changes in sample mass lower than 1 part in 10 million. The microbalance mechanism is sensitive to sorption and desorption which necessitates purging of the balance head with a constant dry flow of nitrogen gas. This will give the best performance of baseline stability. Accurate and desired relative humidities are obtained by mixing both dry and saturated vapour gas flows in the correct proportions through the mass flow controllers. Sample and reference sides are contained in the assembly whereby the sample is placed in a quartz pan held in the sample side and an empty quartz pan is kept in the reference side.

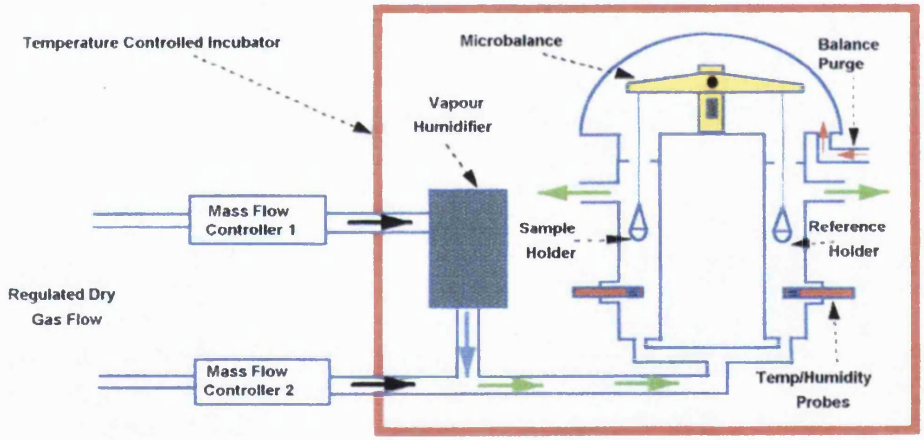

Figure 2.1 *Schematic diagram showing the Dynamic Vapour Sorption System (reproduced from the DVS User Guide manual).*

Humidity and temperature probes are situated just below the sample and the reference holders to give independent verification of the system performance. Different cycles of sorption and desorption can be chosen and performed. Equally, RH values can be varied for different time intervals in the same experiment giving diversity in methods of manipulating and studying the solid sample under investigation. The quartz pans must be extremely clean. Washing is done with distilled water as a first step followed by

rinsing with ethanol or industrial methylated spirit (IMS). The pan is then left to dry at 0% RH. If any static is generated resulting in high level of noise in the balance reading, the RH is raised up to 90-95% for around 5 minutes followed by drying at 0% RH until constant weight is achieved. The experiment is then started.

Both weight and humidity calibration must be performed periodically. Weight calibration is done whenever the operating temperature is changed. It is performed using a 100 mg weight in the sample pan and the value is adjusted if deviation is more than $\pm$ 50 micrograms

2.1.2 ISOTHERMAL MICROCALORIMETRY:

This is a thermal method of analysis whereby both endothermic (heat-absorbing) and exothermic (heat-producing) processes are observed and quantified. It can be used for a variety of purposes where heat change is involved including chemical, physical and biological changes. Information can be obtained concerning the rate and extent of chemical reactions, changes in phase, changes in structure as well as metabolism of living systems.

The equipment used in the current study was the LKB 2277 Thermal Activity Monitor, Sweden. It is an extremely sensitive thermal technique, which gives it a large advantage making it able to detect temperature differences of less than 10^{-6} °C. This high level of sensitivity may, however, be problematic as minute changes may be misinterpreted. The sensitivity and high level of precision is largely due to the stability of the heat sink, which surrounds the measuring cylinders. The heat sink is made up of a closed 25 litre thermostated water bath maintained to $\pm 2 \times 10^{-4}$ °C within the measurement range of 5-80 °C (*Figure 2.2*).

Water is circulated by being pumped upwards into the cylindrical, stainless steel tank where it overflows into a larger outer tank. The water is then re-circulated from the outer tank to the inner one. The thermal activity monitor utilises the heat flow principle where heat produced in a thermally defined vessel flows away in an effort to establish thermal equilibrium with its surroundings (*Figure 2.3*). Measurement takes place in the measuring vessel (cup), which is kept between a pair of sensitive heat sensors (Peltier elements). The system is designed in such a way that any flow of heat to or from the measuring vessel has to take place through those sensors.

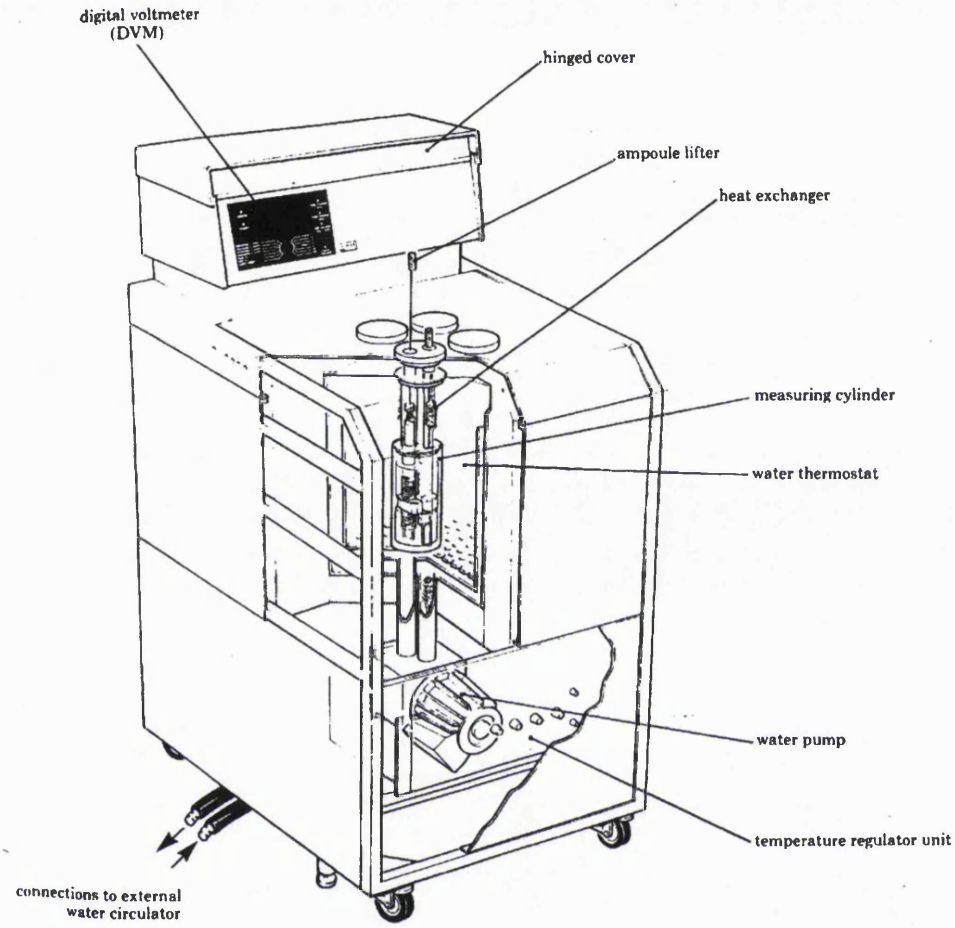

Figure 2.2 *Schematic representation of the isothermal Microcalorimeter System (reproduced from the LKB 2277 Thermal Activity Monitor Instruction manual).*

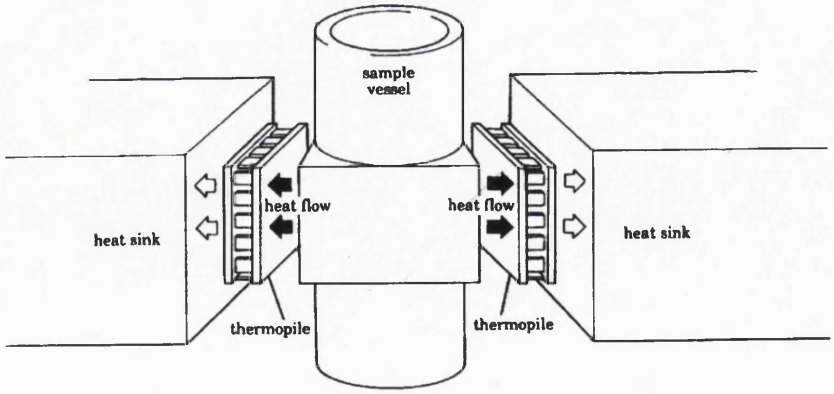

Figure 2.3 *Diagram showing the heat flow principle in the Thermal Activity Monitor (reproduced from the LKB 2277 Thermal Activity Monitor Instruction manual).*

Up to four channels (measuring units) can be housed and operated at the same time in the same Thermal Activity Monitor (TAM) unit. Each measuring unit is made up of two sides, a sample side and a reference side (*Figure 2.4*). The net signal reading represents the difference between both sides. The reading is in power units (usually microwatt) versus time and typical curves are known as power/time curves. Measurements between 3-3000 microwatt (μwatt) can be recorded. All experiments carried out in this work were performed using 3 ml. glass ampoules (*Figure 2.5*) and 3000 μwatt at 25 °C. The TAM is kept in a temperature controlled room maintained at 20 ± 1 °C. The sample is pre-equilibrated to temperature by being lowered on the ampoule lifters into the neck of the measuring cylinder (the half-way mark) before being lowered into the measuring site. This way, both the reference and the sample side are brought to thermal equilibrium with the surrounding water bath before measurement is made.

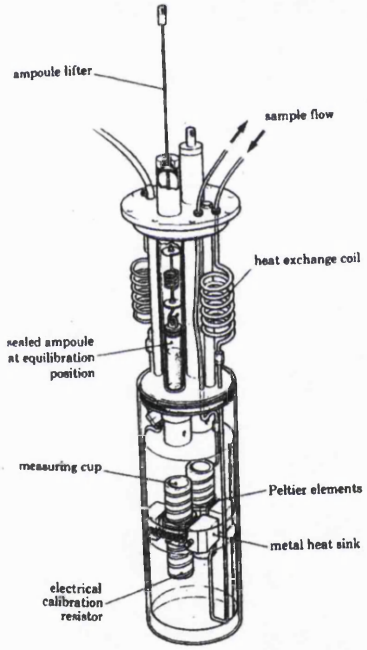

Figure 2.4 *Diagram showing the Microcalorimetric unit with both the sample and the reference sides (reproduced from the LKB 2277 Thermal Activity Monitor Instruction manual).*

Calibration of the measurement unit in the TAM must be performed when the instrument is used for the first time, after a change in any experimental conditions such as a change in operating temperature or level of power output as well as after any power-cut conditions.

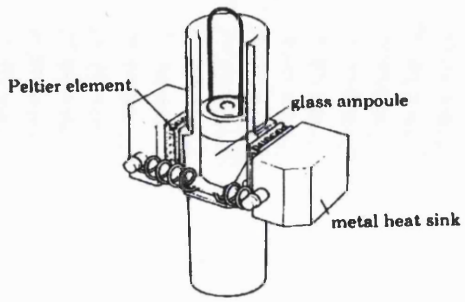

Figure 2.5 *Diagram showing the glass ampoule connected to the ampoule-lifting loop and inserted in the measuring site (reproduced from the LKB 2277 Thermal Activity Monitor Instruction manual).*

2.1.3 DIFFERENTIAL SCANNING CALORIMETRY (DSC):

The DSC is perhaps the most commonly used method of thermal analysis. Thermal methods of analysis generally have the following advantages over some other analytical methods (Hatakeyama and Quinn, 1999):

1. Samples can be studied over a wide temperature range using different temperature programs.
2. A small sample is required for analysis (few milligrams)
3. Time needed to carry out an experiment ranges from several minutes to several hours.
4. Using the proper type of vessel or attachment, almost any physical form of the sample can be analysed (solid, liquid or gel).

However, since the results are indirect and may be misinterpreted a combination of thermal methods with other spectroscopic methods of analysis such as nuclear magnetic resonance (NMR), infra red (I.R.) and X-ray diffractometry may be needed whereby better understanding of molecular structure or physicochemical changes occurring in the sample can be obtained.

DSC is one method of thermal analysis which involves measurement of differences in heat flow into a substance and a reference as a function of sample temperature while both the sample and reference are subjected to a controlled temperature program (Skoog et al., 1998). Both endothermic processes such as melting and vaporisation and exothermic processes such as crystallization can be measured using this technique. Glass transitions of amorphous solids typically appear as baseline shifts on the DSC thermograms (*Figure 2.6*).

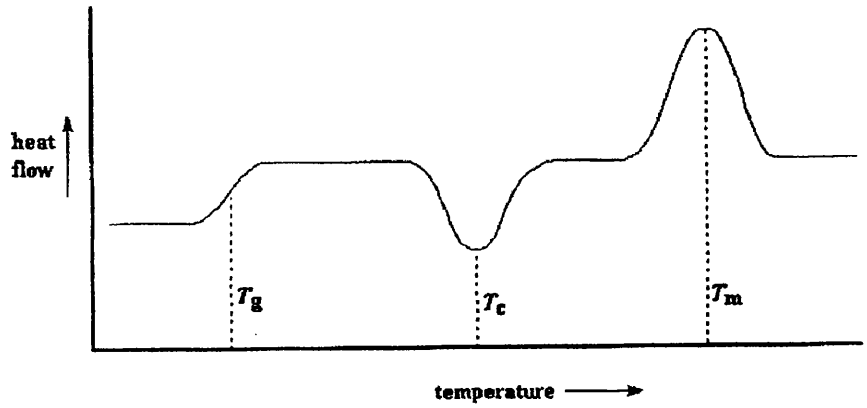

***Figure 2.6** Typical DSC thermogram showing glass transition and crystallization of the amorphous solid and melting of the crystalline one.*

DSC 7 (Perkin- Elmer) was used in this study, which is of the power compensation DSC type. In power compensation DSC, the instrument has two independent furnaces; one for heating the sample and the other for heating the reference side (*Figure 2.7*). The furnaces are usually small giving the advantage of rapid rates of heating, cooling and equilibration. The furnaces are imbedded in a larger temperature controlled heat sink, which is kept at a constant cooler temperature than the targeted temperature range used in running the experiment. This is to allow for possible dissipation of heat from the furnace into the sink rapidly. Above the furnaces are the sample and reference holders that contain the platinum resistance thermometers in the base. The platinum resistance thermometers are employed to monitor both temperature and energy measurements. The temperature of both the sample and reference is kept the same and if a temperature difference is detected, due to a phase change in the sample, energy is then supplied and measured in order to maintain this equal temperature state.

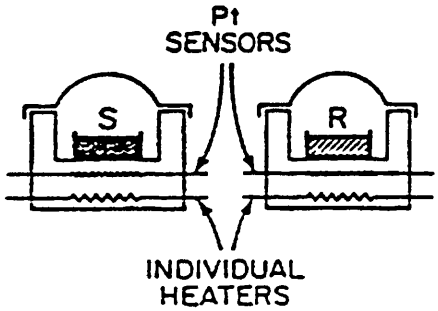

***Figure 2.7** Diagram showing the design of a power compensated DSC (reproduced from Perkin-Elmer, DSC 7 Users Manual).*

Many factors may affect the results of the DSC including heating/cooling rate, sample's dimensions (particle size) and weight, as well as type of aluminium pans used (open, closed, hermetically or non hermetically sealed). In general, larger heating rate shifts the peaks to a higher temperature and better peak sharpness is achieved with smaller samples that are thinly spread in the bottom of the pan. Smaller particle size as well as smaller sample size results in lower onset temperature of the thermal event. Hermetically sealed pans prevent the escape of any available vapours. Furthermore, the atmosphere within the sample in the case of closed pans can have an impact on the obtained results.

Indium was used to calibrate the instrument each time before use. Occasionally, both Indium and Zinc (high purity standards) were used in the calibration process. Theoretically, calibration is only needed if a change in heating/cooling rate is done, if a change in the temperature range of the experiment run is to be made or if a power cut was encountered.

2.1.4 DYNAMIC DIFFERENTIAL SCANNING CALORIMETRY (DDSC):

This is a new thermal analysis technique offered by Perkin- Elmer as an accessory for the Perkin- Elmer power compensation DSC. DDSC is a type of a modulated temperature DSC that allows running a temperature program consisting of a repetition of short isothermal or constant scanning rate steps. The repetition program leads to a dynamic heat flow signal (a modulated signal instead of the linear signal obtained in DSC) that is analysed to get many specific heat curves. The advantage here is that in this case reversible thermal processes such as glass transitions can be separated from other irreversible (sometimes overlapping) thermal events such as moisture loss, enthalpic relaxations and crystallization. This makes DDSC a useful and straightforward technique for measuring glass transition temperatures. Three curves can be obtained from a modulated signal in the DDSC. These are: the storage, loss and complex Cp curves.

The storage Cp curve is the one related to energy stored in the sample as the sample is heated. It is exactly equal to equilibrium Cp as measured by a standard DSC in the absence of structural changes or reactions. The loss Cp curve involves that part of the energy, lost or dissipated, which is involved in a structural change rather than a temperature raise of the sample. This curve is zero in temperature regions where no

structural change is expected such as above the melt or below Tg. Complex Cp is the vector sum of storage and loss Cp curves. It is almost identical to the storage Cp except in the melting region where the loss term dominates.

In this study, DDSC was used in order to compare the resulting Tg values with those obtained from DSC. The instrument used was a Perkin-Elmer Pyris 1 DSC. Non-hermetically sealed flat-bottomed aluminium pans were used. The samples were run with an initial temperature of 20 °C, second temperature of 22 °C and an end temperature of 180 °C. The sample is kept isothermally to equilibrate at the beginning for 30 seconds. A total of 80 repetitions were used for this experiment. Conditioning of the instrument is done by heating up to 500 °C for a couple of minutes in the absence of the pans. A baseline check was established by running two empty pans (one in the sample side and another in the reference side) in the same conditions of the experiment.

2.1.5 THERMOGRAVIMETRIC ANALYSIS (TGA):

In thermogravimetric analysis the mass of a sample in a controlled atmosphere is recorded continuously as a function of temperature or time while the temperature of the sample is increased (usually linearly with time) (Skoog et al., 1998). Modern available thermogravimetric instruments consist of: 1) Sensitive analytical balance, 2) Furnace, 3) Purge gas system to provide either inert or reactive atmosphere (as required), and 4) A computer which is used for instrument control and for data acquisition and display. Thermogravimetric analysis (TGA) is one of the thermal methods of analysis. In TGA, the mass change of a sample can be measured in two modes, a scanning mode in which the mass change is measured as a function of temperature at a certain heating rate and an isothermal mode in which the mass change of the sample is measured as a function of time at a constant temperature. Thermogravimetric analysis only shows thermal events that are accompanied by a mass change such as decomposition, oxidation, dehydration and desolvation. It is hence of great value in studying solvates, as the weight loss can be calculated and stoichiometric correlations can be made to the weight of solvent lost from the sample. However, those thermal events that are not associated with mass loss such as melting, crystallization and glass transition cannot be studied by TGA (Hatakeyama and Quinn, 1999).

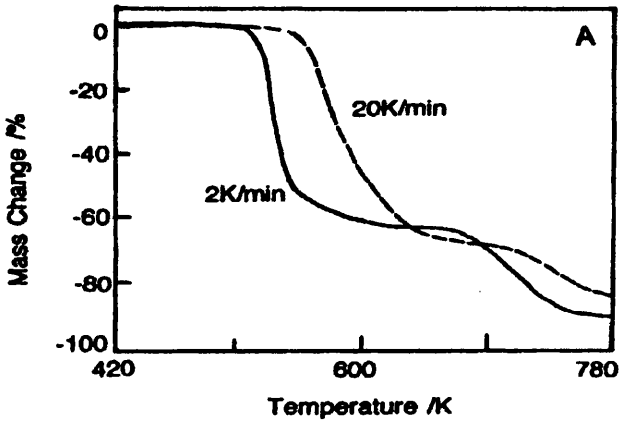

***Figure 2.8** A typical TGA trace for a single-state mass loss at two heating rates (adapted from Hatakeyama and Quinn, 1999).*

Many experimental conditions influence TGA results such as heating/cooling rate, sample mass and particle size in a similar manner as that described for DSC (Section 2.1.3). It has been noted that at a lower heating rate the sample undergoes change more gradually than at a higher heating rate. This leads to a change in mass within a narrower temperature range and an onset of mass change at a lower temperature (*Figure 2.8*). The TGA used in this study is a TGA 2950 thermogravimetric analyser, TA instruments (*Figure 2.9*). The balance in the TGA is the key component of the system and it provides precise measurement of sample weight. This is kept at a null position. The beam of the balance is kept in a horizontal position by an optically controlled meter movement. A small flag situated at the top of the balance beam blocks an equal amount of light (emitted from a LED) from reaching the two photodiodes. Any change in sample mass causes a deflection of the beam and accordingly the flag. This results in unequal amount of light reaching the two photodiodes. The resulting imbalance in the photodiode current is amplified and fed into a coil situated between the poles of a permanent magnet. The magnetic field that is generated in the coil by the current restores the beam to its original null position.

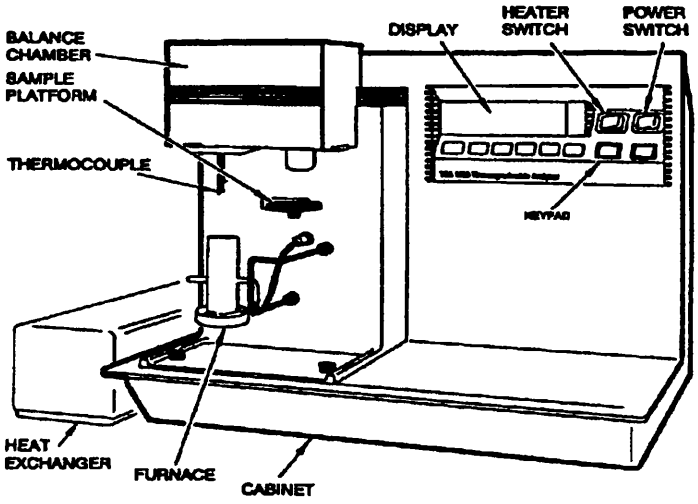

Figure 2.9 Diagram of the TGA 2950, TA instruments (reproduced from TGA 2950 Thermogravimetric Analyzer Operator's Manual).

The amplified current is monitored and transformed into mass or mass loss information by the data acquisition system. The balance provides an accuracy of $\leq \pm$ 0.1 % and a resolution of 0.1 μg. The furnace can be heated up to 1000 C° and is cooled between runs by means of a compressed air supply. A thermocouple is used to measure the temperature of the environment and is positioned just above the sample pan. Both the balance and the furnace are purged with gas in order to prevent contamination of the furnace and balance assemblies. The gas line is split before entering the module and two flow meters are used to set the flow rates to 60cc/min through the purge inlet and 40cc/min through the balance inlet. The purge gas used in this study was dry nitrogen gas. The region of the balance should be constantly kept under an inert flowing atmosphere such as dry nitrogen or dry helium gas. Atmospheres in the sample chamber can be classified into two categories, interactive and non-interactive. Non-interactive such as helium or nitrogen gas is used to standardize the conditions of the experiment without affecting the sample. An interactive atmosphere on the other hand can be chosen to play a direct desired role in the reaction processes taking place in the sample. Oxygen is a type of a gas used for this purpose (Hatakeyama and Quinn, 1999). Two types of calibration procedures are carried out on the TGA namely weight and temperature calibrations. Weight calibration is usually performed monthly using 100 mg and 1 g standards in order to calibrate the weight signal. Temperature calibration is done

using indium as a standard whenever purge gas flow-rate or heating rate is altered or if for any reason the position of the thermocouple is changed.

2.1.6 HOT STAGE MICROSCOPY:

This method involves the visual observation of a sample under an optical microscope equipped with a heated sample stage. Hot Stage Microscopy is a method of sample analysis, which is sometimes referred to as Thermomicroscopy (Hatakeyama and Quinn, 1999). The heating rate can be controlled and kept at a certain desired value and the sample is observed under the microscope while it is being heated. A number of changes in a material can be detected by use of Hot Stage Microscopy; these include solid-state transformations such as melting and crystallization. In addition; decomposition, swelling, shrinking, evaluation of volatiles (seen as bubbling) and changes in colour and texture can be followed using Hot Stage Microscopy.
The instrument used in this study was a Mettler FP5 heating control unit with a connected heating stage. The microscope was an Olympus BX50 model. Heating was done at 2C°/min from ambient conditions until 180 C° and magnification of the objective lens was set at 40x.

2.1.7 POWDER X-RAY DIFFRACTION:

X-ray diffraction was discovered by Von Laue in 1912 and it can be said that much that is known about spacing and arrangement of atoms in crystalline solids has been owed to diffraction studies (Skoog et al., 1998). X-ray powder diffraction method relies on exposing a powdered sample to X-ray beams. The beam will hit the crystal surface at an angle (θ). Part of the beam will be scattered due to interaction with the layer of atoms at the surface. The unscattered part of the beam will penetrate to the second layer of atoms where again a fraction of the penetrating beam will be scattered while the rest passes on to the third layer. The cumulative effect of this scattering from the regularly spaced centres of the crystal is the diffraction of the X-ray beam. This method is thus based on the fact that each crystalline solid has a unique and distinctive X-ray diffraction pattern. Thus, a complete match of the diffractogram between an unknown and an established reference sample indicates that both samples have the same chemical identity, whereas a complete lack of match indicates difference in identity. It is also known that through

measuring the intensity of diffraction lines and comparing them with standards, quantitative analysis of crystalline mixtures is possible. X-ray beams diffract in much the same way as visible light diffraction. Figure 2.10 represents a diagram of a typical Powder X-ray diffractometer.

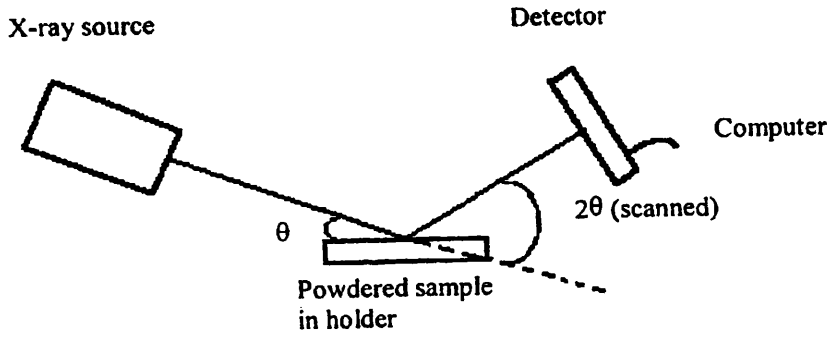

***Figure 2.10** Diagram representing a typical X-ray diffractometer.*

Bragg showed in his equation (Equation 2.1), that X-rays appear to be scattered from a crystal only when the angle of incidence of the X-ray beam (θ) satisfies the condition:

$$\sin\theta = \frac{n\lambda}{2d} \qquad \text{.....Equation 2.1}$$

Where n is a multiple of the wavelength (λ) and d is the interplanar distance in the crystal. The diffraction angle (2θ) is determined from the spacing between a certain set of planes and with the aid of the Bragg equation the distance (d) can be calculated from the known wavelength of the X-ray source and measured angle. Identification of any crystalline solid is established from the position of the lines (in terms of 2θ) and their relative intensities. It is an efficient technique for both qualitative and quantitative determination of crystalline compounds provided that grinding of the crystalline sample into a homogenous fine powder is carried out prior to testing. This way, a huge number of small crystallites are oriented in every possible direction; thus, when the X-ray beam passes through the sample, a significant number of particles can be expected to be oriented in a way that fulfils the Bragg condition for reflection from every possible interplanar spacing (Skoog et al., 1998). The X-ray powder diffraction technique is not considered as efficient for characterization of amorphous solids as it is for crystalline ones since amorphous solids lack a three-dimensional long-range order. Saleki-Gerhardt et al., (1994b) showed that lower values of standard deviation of the measured amorphous content are noticed for samples with higher percentage of amorphous

material. On the other hand, they stated that differences in measured amorphous content in a sample that is 90% crystalline and that which is 100% crystalline could not be distinguished using X-ray powder diffraction. This relatively low detection limit of amorphous content is due to the fact that this technique measures bulk properties and thus the entire sample is analysed as a whole. This makes the amorphous content, comprising a small part of the total signal, difficult to detect with sufficient confidence (Buckton and Darcy, 1999).

The instrument used in this thesis was a Philips PW 1840 using copper alpha X-ray tube with a compact diffractometer. Scan range of 2- 60° at 2θ step size. Goniometer speed is 0.02 2°θ/sec. Chart speed is 10 mm/ 2°θ. Receiving slit width is 0.2 mm. The experiments were carried out at ambient conditions (temperature and relative humidity).

2.1.8 SCANNING ELECTRON MICROSCOPY (SEM):

This is a microscopic method, which can be used for imaging, defining morphology and shape of solid surfaces. Detailed knowledge of the physical nature of the surfaces of solids is of great importance in many fields including materials science as the surface of a solid usually differs substantially from its interior in many aspects including its physical properties. The classical method for surface monitoring of solids was by optical microscopy, but its use has been superseded by Scanning Electron Microscopy (SEM) as the latter provides considerably higher resolution and depth of focus than the optical microscope (Skoog et al., 1998). In a scanning electron microscope, the surface of a solid sample is swept in a raster pattern with a beam of energetic electrons. A raster is a scanning pattern in which an electron beam is swept across a surface in a straight line in the direction of x-axis and is then returned to its starting point followed by a downward shift of the beam in the direction of y-axis (Skoog et al., 1998). It can thus be said that using the raster pattern, a sample is scanned in a series of parallel tracks. This process is repeated until a desired area of the surface has been scanned. While the scanning process is carried out, a signal is received above the surface and stored in a computer where it can be converted to the produced image. Several types of signals are produced from the surface as a result of interaction with the electrons. These signals most commonly include, backscattered electrons, secondary electrons and X-ray emission (Skoog et al., 1998). All of these signals can be captured and digitally displayed. In this study, samples were adhered to an SEM stub using double sided

carbon impregnated tape. Samples were gold coated prior to viewing in an Emitech K550 Sputter Coater for 3 minutes at 40 mA. Images were captured using a Philips XL20 Scanning Electron Microscope.

2.1.9 ELEMENTAL ANALYSIS (EA):

This analytical method is used for the determination of CHN and is based on the quantitative "dynamic flash combustion" method, which converts all organic and inorganic substances into combustion products. The procedure is carried out by holding a sample in a tin container and dropping it into a vertical quartz tube maintained at 1020 °C (combustion reactor), the sample is purged with a continuous flow of helium gas, but when it is dropped inside the furnace, the helium flow is temporarily mixed with pure oxygen gas to trigger combustion of the sample. The sample and tin container will then flash combust. The mixture of evolved gases is then passed over a catalyst to promote quantitative combustion. The mixture of gases is then passed over copper, which will get rid of excess oxygen and will reduce nitrogen oxides into elemental nitrogen (N_2). The resulting mixture is then passed to a chromatographic column where individual components such as nitrogen (N_2), carbon dioxide (CO_2), water (H_2O) and sulphur dioxide (SO_2) are separated and eluted from the gas. These eluted components are detected by thermal conductivity detector (TCD), which feeds a potentiometric recorder giving an output signal proportional to the concentration of each component in the gaseous mixture. Figure 2.11 shows a schematic diagram of an Elemental Analyser.

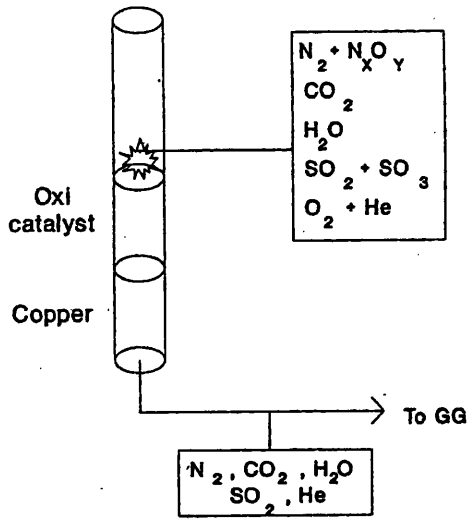

***Figure 2.11** Schematic diagram showing the principle of operation of an Elemental Analyser (reproduced from Carlo-Erba EA 1108 Users Manual).*

Since determination of the Carbon, Hydrogen and Nitrogen percentage (CHN) depends on the original weight of the sample, it is essential that the sample be dry and free from any foreign substance (such as dust, hair, parafilm or fibres of filter paper).

The instrument used in our studies was a Carlo-Erba Elemental Analyser EA 1108 with PC based data system (Eager 200 for windows). A Sartorious ultra microbalance 4504 MP8 was used for weighing the sample. A Gas Chromatographic column (Porapak QS 50-80 mesh) was employed for GC separation. The combustion reactor was made of translucent silica and was filled with silvered cobalt oxide, which was deposited on top of 40mm of silica wool. Another layer of silica wool separates the chromium oxide from the silvered cobalt oxide. The reduction reactor was made of alternating layers of silica wool and copper oxide wires.

2.1.10 NUCLEAR MAGNETIC RESONANCE (NMR):

This is a powerful method used widely by chemists and biochemists to elucidate the structure of chemical species. NMR spectroscopy is based on the measurement of electromagnetic radiation absorbed by a sample in the radio frequency range of roughly 4-900 MHz. In this case, nuclei of atoms instead of outer electrons (as is the case in infrared, visible and ultraviolet spectroscopy) are involved in the absorption process. It is essential however in order for the absorption of electromagnetic radiation to occur, to place the analyte in an intensive magnetic field which supplies the nuclei with sufficient energy state that is required for absorption of radiation. The importance of NMR in elucidating chemical structures was made clear when chemists became more aware that molecular environment affects the absorption of radio frequency (RF) radiation by a nucleus in a magnetic field and that this type of effect can be linked to the molecular structure of the chemical species in question. Two types of NMR spectrometers are available, continuous and pulsed or (Fourier transform) spectrometers (FTNMR). Nearly all-modern NMR instruments are of the FT type, which gives a much better resolution (high resolution spectra). The four nuclei that have been of greatest use to organic chemists and biochemists are ^{1}H, ^{13}C, ^{19}F and ^{31}P. Proton (^{1}H) NMR analysis is the most frequently used and in this case, exact positions of different protons in a molecule can be determined and shown in the spectra and the molecular structure can thus be elucidated. Second to proton NMR in popularity is the carbon (^{13}C) NMR

though this method is about 6000 times less sensitive than proton NMR due to a weaker NMR signal from the ^{13}C nucleus. Proton NMR will be discussed here, as it was the one used in this study.

In proton NMR, the frequency of RF radiation, which is absorbed by a certain nucleus, is strongly affected by its chemical environment that is the presence of electrons or nuclei in the nearby environment. Different types of effects can be encountered:

1- Chemical shift: Taking pure ethanol as an example (*Figure 2.12*), three regions of peaks are seen (3 peaks to the far left, 5 peaks in the middle and 3 peaks to the far right). The 3 peaks to the far left are attributed to the proton of the hydroxyl group (OH). If the hydrogen atom of the hydroxyl group is replaced by deuterium, the three peaks to the far left will disappear and 4 peaks will replace the 5 peaks in the middle. The displacement of the hydroxyl proton by deuterium will lead to some changes in the absorption frequency of the proton; such changes depend on the group to which the hydrogen atom is bonded. This type of effect is called a chemical shift.

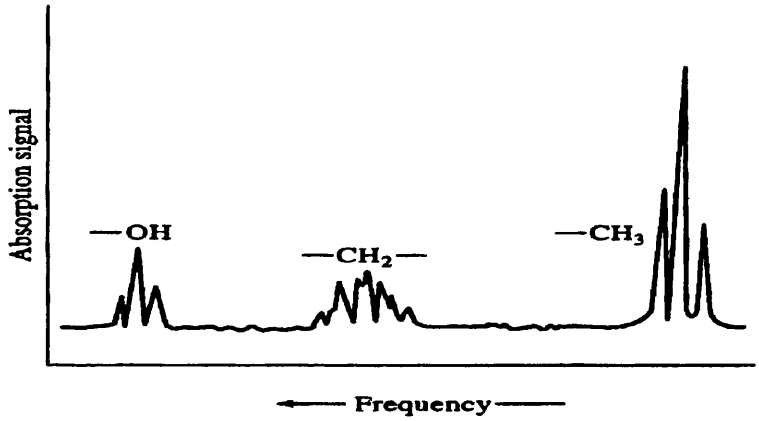

***Figure 2.12** A typical proton NMR spectrum of highly purified ethanol showing splitting of OH and CH_2 peaks (adapted from Skoog et al., 1998).*

2- Spin-spin splitting: The magnetic field produced by a spinning nucleus causes changes in electron distribution in its bonds to other nuclei. This will cause changes in the magnetic field of adjacent nuclei and leads to splitting of energy levels that will therefore lead to multiple transitions. In the example on pure ethanol (Figure 2.12), it is noted that the methylene (CH_2) group appears in the NMR spectra as 5 peaks in the middle, whereas the methyl (CH_3) group appears as 3 peaks in the far right side of the spectra. A general rule is suggested for the calculation of the number of peaks in a spectrum and that is, the number of

peaks in a split band, which is termed as multiplicity (M), is equal to the number (n) of magnetically equivalent protons plus 1.

$$M = n + 1$$

The splitting of the hydroxyl peak into 3 smaller peaks is due to the adjacent methylene (CH_2) protons. The adjacent methyl (CH_3) and hydroxyl (OH) protons on the other hand cause the splitting of the methylene peak into 5 smaller peaks. The methyl group is split into 3 peaks due to the effect of the adjacent methylene group. Splitting of peaks can take place when protons are spaced no more than 2 bonds apart.

The best solvents for proton NMR spectroscopy contain no protons; hence, carbon tetrachloride (CCl_4) is an ideal solvent, though its low ability to dissolve many compounds limits its use as a solvent for NMR experiments. Many deuterated solvents are used instead such as deuterated chloroform, benzene, ethanol and methanol. The instrument used in our study was a Bruker AM500 NMR instrument with an ASPECT 3000 computer processed on the PC using WINNMR software. Deuterated methanol and residual solvent peak was used to reference spectra (CD_3OD = 3.31 ppm).

2.1.11 KARL FISCHER TITRATION:

This is a Coulometric titration method of analysis. Coulometry is based on reducing the analyte by electrons that are supplied by a source of electrical power. According to Faraday's law, if one molecule of the analyte reacts with one electron, then 1 mole of analyte will react with 96485 Coulombs of electricity (Watson D.G., 1999). Karl Fischer is a widely used method for the determination of water content in pharmaceutical materials. The Karl Fischer reagent used for the determination of water content contains anhydrous methanol, anhydrous pyridine, iodine and sulphur dioxide. The reagent is added to the sample during titration and reaction of water with the reagent takes place as follows:

$$H_2O + I_2 + SO_2 + 3C_5H_5N + CH_3OH \longrightarrow 2C_5H_5N.HI + C_5H_5NH.SO_4CH_3 \quad \text{.....Equation 2.2}$$

The presence of water basically causes the conversion of iodine into iodide through reduction in presence of sulphur dioxide. A potential is supplied through the

reacting solution but no flow of current will occur until all water has been titrated, then the first excess of the Karl Fischer reagent causes the current to flow in the solution and reduction of iodine into iodide takes place (Equation 2.3) indicating the end point.

$I_2 + 2e \longrightarrow 2I$ .....Equation 2.3

The instrument used was a 701 KF Titrino (Metrohm) connected to a 703 Ti stand (Metrohm). The experiments were carried out using methanol- free Karl Fischer solution from BDH laboratory supplies. Dried methanol was supplied by BDH chemicals (Analar). Standardisation of the instrument was done against di-sodium tartrate, which contains a known amount of water representing 15.66% of its weight, supplied by BDH chemicals (Analar). Standardization results had a relative standard deviation (RSD) of 0.23 % (should be less than 1 %). Experiments were carried out in a fume hood to contain the toxic vapours of the Karl Fischer reagent.

2.1.12 THIN LAYER CHROMATOGRAPHY (TLC):

This is one of the earliest chromatographic techniques. A mobile phase (usually a mixture of organic solvents) triggers the migration of the analyte up a layer of a stationary phase (most frequently used is silica gel). A few microlitres of the analyte solution are spotted onto the silica gel plate at the origin. The bottom 0.5 cm of the plate is immersed in the mobile phase which in turn is placed in a tank and then the liquid mobile phase is left to travel up the silica gel plate by capillary action. More polar compounds adsorb more to the silica gel leading to a faster elution of the compound onto the stationary phase, which results in a shorter distance being travelled up the plate in a given time. Different detection techniques are available and can be used to locate the eluted spot of the compound on the stationary phase (depending on the type of the compound), including different chemicals such as iodine vapour, potassium permanganate and ninhydrin solution. Another technique involves detection by ultraviolet light where light with a wavelength of 254 nm is used to illuminate the plate (after elution) and the compound that absorbs UV light appears as a black spot on the plate of the stationary phase. In this case, silica gel that is impregnated with a fluorescent material must be used. The Rf value, which equals the distance travelled by the compound from the point of origin divided by the distance travelled by the solvent from the origin (solvent front) is hence

calculated and is indicative of the compound in the system being used. The Rf is usually reported as Rf x100. The mobile phase is typically a mixture of different solvents. Water, however is rarely used alone since most organic compounds are of low water solubility. Thus, water is usually used in mobile phases containing a water miscible organic solvent such as methanol. In the current study, TLC experiments were carried out in the conditions devised by Badwan et al. (1990) as follows:

5 microlitres (μl) of 5 mg /ml solution strength of the analyte in methanol were dropped on the silica gel plate at the point of origin (marked at 3 cm from the bottom of the plate). The stationary phase used was plates made of silica gel coating aluminium sheets 20 cm x 20 cm (silica gel 60 F_{254} supplied by Merck). The mobile phase consisted of methanol, butanol, water, toluene and acetic acid mixed in proportions of 2: 3: 1: 2 :0.1 respectively and the mobile phase was left to travel up the stationary phase to around 11 cm solvent front. The developed plates were read using UV light at 254 nm.

2.1.13 HIGH PRESSURE LIQUID CHROMATOGRAPHY (HPLC):

HPLC is the technique most commonly used for quantitative analysis of drugs whether in formulations or in body fluids. In this technique, the liquid mobile phase is pumped under pressure through the stationary phase, which is contained in a stainless steel column at a certain chosen flow rate. A solution of the sample to be analysed is delivered to the column by injecting a sample into a loop that carries the sample to the head of the column. Separation of the analysed sample into its components and the elution of the components on the stationary phase take place. Detection of the separated, eluted components is done by a detector that is attached to the column. HPLC columns are of different types and most commonly used are; silica gel and octadecylsilane coated (ODS-coated) silica gel with average particle size of 3.5 or 10 μm. Since silica gel is polar, more polar compounds are retained more and faster on silica gel than non-polar compounds. The mobile phase is made up basically of a mixture of organic solvents in which the drug to be tested is soluble. The mobile phase carries the drug through the stationary phase where the drug will partition. Different types of detectors are available and the type of detector to be used is chosen based on the drug to be analysed. Yet, the most commonly used

type of detector is a UV/ visible detector. pH of the mobile phase has an effect on elution rate of compounds in which the degree of ionisation is dependent on the pH such as basic and acidic compounds. Through ionisation, retention time for the elution of the compound on a polar stationary phase can be reduced.

The HPLC parameters used in the current solubility study are adapted from the study of Arafat and Kaddoumi (1995) and they were:

Column: BDS phenyl column (25 cm, Hypersil).

Mobile phase: 40% acetate buffer (pH = 6, prepared in HPLC grade water from Merck), 60% acetonitrile (Merck, HPLC grade) with the final pH adjusted to 6.45.

Injection volume: 100 µl.

Flow rate: 1.2 ml/ min.

Detector: UV detector at 240 nm (Lachrom Merck- Hitachi, L-7400)

Pump: Lachrom Merck- Hitachi, L-7100.

Integrator: Merck- Hitachi integrator, D-7500 was used for data capturing and analysis.

2.2 MATERIALS:

The main chemical substance on which this study was carried out is Terfenadine. Terfenadine used here was produced by Ricordati chemicals (Italy) and was supplied by the Jordan Phamaceutical Manufacturing Company (JPM).

2.2.1 TERFENADINE:

Terfenadine is an antihistamine of the H1 antagonist type. The drug does not cross the blood brain barrier and thus CNS depression is minimal. Terfenadine was withdrawn from the market due to many drug-drug interactions, some of which were life threatening such as cardiac arrhythmias due to concomitant use of terfenadine with certain imidazole and macrolide antibiotics. The interest here in terfenadine is not as a drug of potential use but simply as a good physical model of a hydrophobic drug that is a glass former at the same time.

2.2.1.1 DESCRIPTION OF TERFENADINE:

Terfenadine is a white crystalline powder, odourless, but with very bitter taste (Badwan et al., 1990).

Empirical formula $C_{32}H_{41}NO_2$, Molecular weight: 471.69 g/mole.

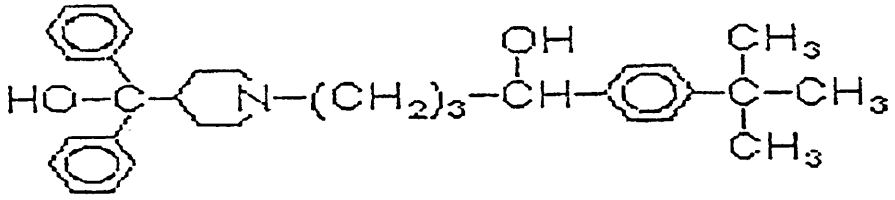

Figure 2.13 Structural formula of terfenadine

2.2.1.2 POLYMORPHISM, PSEUDOPOLYMORPHISM AND GLASS FORMATION:

Three polymorphs of terfenadine and two solvates were found by recrystallizing terfenadine from different solvents (Badwan et al., 1990).

The study of Badwan et al. (1990) showed that polymorph I (the most stable one) was obtained by recrystallization from an ethanol/water solvent mixture. Polymorph II was obtained by recrystallization from methanol. Polymorph III was obtained by recrystallization from propylene glycol and a glass can be formed by rapid cooling from the melt.

2.2.1.3 PHYSICO-CHEMICAL PROPERTIES OF TERFENADINE:

Table 2.1 shows the melting range of the three polymorphs of Terfenadine and Tg values for the glass obtained from the melt.

Table 2.1 Melting ranges of terfenadine polymorphs and glass transition temperature of amorphous form (°C). Adapted from Badwan et al (1990)

Polymorph I	149-152
Polymorph II	146-148
Polymorph III	142-144
Glass from cooled melt	Tg: 55.93, 57.91, 59.88 *

* The Tg values are quoted as reported by Badwan et al. (1990). My speculation is that the different Tg values were most probably due to variable water content in the prepared amorphous samples.

2.2.1.4 DIFFERETIAL SCANNING CALORIMETRY OF TERFENADINE:

Badwan et al. (1990) reported that the thermograms of the terfenadine samples were obtained by heating a sample with a weight range of 3-10 mg at a heating rate of 10 °C min^{-1} and that no signs of decomposition were noticed upon melting of the sample.

Table 2.2 Enthalpies of fusion and peak temperature for the three-terfenadine polymorphs using DSC as reported by Badwan et al (1990).

POLYMORPH	ΔH J/g	PEAK TEMPERATURE (°C)
I	102.0	151.1
II	100.5	147.8
III	82.4	143.5

2.2.1.5 SOLUBILITY OF TERFENADINE IN DIFFERENT SOLVENTS:

The solubility of the most stable polymorph of terfenadine was obtained by placing an excess amount of the drug together with the solvent (different solvents used), shaking at 30 °C until equilibrium is reached (Badwan et al, 1990).

Table 2.3 Equilibrium solubility of terfenadine at 30 °C. Adapted from Badwan et al.(1990).

SOLVENT	SOLUBILITY g/100 ml at 30 °C
Water	0.001
Ethanol	3.780
Methanol	3.750
Hexane	0.034
0.1 M Hydrochloric acid	0.012
0.1 M Citric acid	0.110
0.1 M Tartaric acid	0.045

2.2.1.6 SPECTROPHOTOMETRIC PROFILE OF TERFENADINE:

Molar absorptivities of terfenadine were determined using an ultra violet spectrophotometer.

Table 2.4 Molar absorptivity values and wavelength of maximum absorbance (λ_{max}) for terfenadine. Adapted from Badwan et al (1990).

SOLVENT	WAVELEGTH OF MAXIMUM ABSORBANCE (λ_{max})	MOLAR ABSORPTIVITY
Methanol	260	660.4
Ethanol	260	671.7

2.2.1.7 X-RAY POWDER DIFFRACTION PROFILE OF TERFENADINE:

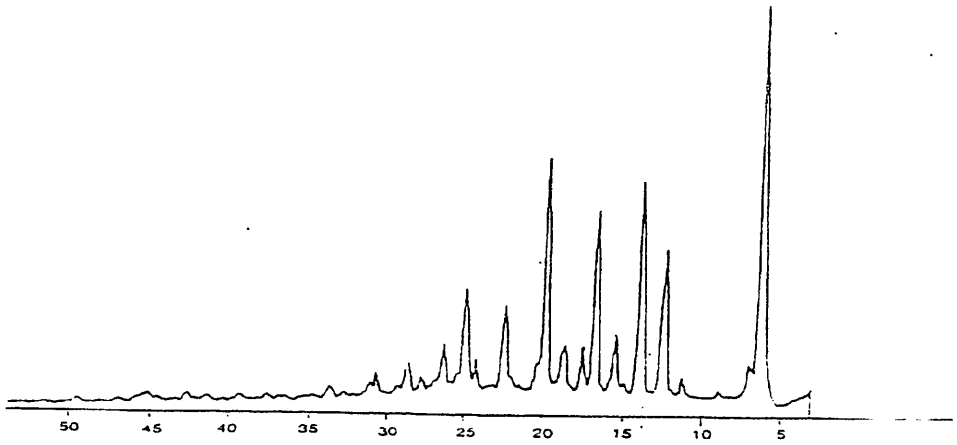

***Figure 2.14** X-ray powder diffraction pattern of polymorph I of terfenadine. Adapted from Badwan et al (1990).*

2.2.2 SATURATED SALT SOLUTIONS:

In an enclosed space and at a certain given temperature, a constant relative humidity can be obtained via the presence of a saturated aqueous salt solution provided that the amount of salt is in excess of that which can dissolve. The salt solutions were prepared by dissolving the salt in distilled water with the aid of heat, leaving the solution to cool down to room temperature and making sure that an obvious excess amount of the salt was present in the bottom of the container. Three salt solutions, selected to three different relative humidities at a controlled room temperature of 20 $\pm$ 1, (Nyqvist, 1983) were prepared. The prepared salts with their corresponding relative humidities are listed in Table 2.5 below.

Table 2.5 Saturated salt solutions and their corresponding relative humidities at a controlled room temperature of 20 ± 1 °C (values taken from Nyqvist, 1983).

Salt	Relative humidity value (RH) at a Temperature of 20 ± 1 °C
Potassium chloride, KCl	85-86
Sodium chloride, NaCl	75-76
Potassium carbonate, K_2CO_3	43-44

2.2.3 MISCELLANEOUS CHEMICALS:

Other chemicals used in this study are listed with their suppliers in the table below.

Table 2.6 List of miscellaneous chemicals used in this study

Chemical	Supplier
Absolute ethanol	Analytical grade (Merck chemicals)
Acetic acid	Analytical grade (GCC chemicals)
Acetonitrile	HPLC grade (Lab-scan analytical sciences)
Adipic acid	Merck chemicals
Butanol	Analytical grade (GCC chemicals)
di-sodium tartrate	BDH chemicals (AnalaR)
Dried methanol	BDH chemicals (AnalaR)
Glacial acetic acid	Analytical grade (GCC chemicals)
Glutaric acid	ACROS chemicals
Hydrochloric acid	Analytical grade, about 32%V/V (Frutarom)
Karl Fischer reagent	Methanol free (BDH chemicals)
Methanol	BDH chemicals
n-propanol	Analytical grade (GCC chemicals)
Oxalic acid	T.S.E.S chemicals
Potassium carbonate	Sigma chemicals ACS grade (> 99% pure)
Potassium chloride	Sigma chemicals ACS grade (> 99% pure)
Potassium hydroxide	As pellets (Chemilab co.)
Sodium acetate	Merck chemicals
Sodium Chloride	Sigma chemicals ACS grade (> 99% pure)
Succinic acid	Merck chemicals
Toluene	Analytical grade (GCC chemicals)
Water (HPLC)	HPLC grade supplied by Merck chemicals
Water (purified)	Obtained from a reverse osmosis system

CHAPTER THREE

CHARACTERIZATION OF CRYSTALLINE AND AMORPHOUS FORMS OF TERFENADINE

3 INTRODUCTION:

General characterization of the as-received terfenadine was essential before doing any further work with the material in order to verify purity and polymorphic form(s) of the received sample. These methods are used to prepare amorphous form of the solid as explained in Section 1.3.5 part 3. The aim of this study was to investigate the original terfenadine material, prepare an amorphous form of terfenadine and analyse the prepared samples in order to investigate percentage crystallinity in the prepared amorphous form in comparison with the as-received (crystalline) terfenadine. The prepared amorphous form would later be used for further investigations.

3.1 CRYSTALLINE TERFENADINE:

3.1.1 CHARACTERIZATION OF CRYSTALLINE TERFENADINE:

Two methods were used in the characterization of crystalline (as received) terfenadine, Differential Scanning Calorimetry (DSC) and X-ray powder diffraction.

DSC is one of the most widely used thermal methods of analysis. It has been used by many workers to show crystallization as well as melting peaks, enthalpies of crystallization and fusion of crystalline solids as well as determination of the glass transition temperatures of amorphous solids. Examples of workers who used DSC in their studies include Yoshioka et al. (1994, 1995), Chidavaenzi et al. (1997), Chiou and Kyle (1979), Schmitt et al. (1996), Guo et al. (2000), Pikal and Rigsbee (1997), Oberholtzer and Brenner (1979), Oksanen and Zografi (1993), Stubberud et al. (1996), Matsumoto and Zografi (1999), Andronis and Zografi (1998), Her et al. (1995), Hofer et al. (1991), Taylor and Zografi (1998), Hancock et al. (1995), Elamin et al. (1994a), Kajiwara et al. (1999), Hogan and Buckton (2001a), Shamblin and Zografi (1999). Homan and Desantis (1992) used DSC in order to identify the different polymorphic forms of terfenadine available in suspension preparations after separating terfenadine from the other suspension components.

The general principles of the DSC are discussed in Section 2.1.3. In this study, DSC was used to get information regarding the melting point and the enthalpy of fusion of terfenadine and to compare it with the values reported in the literature.

X-ray powder diffraction (XRPD) is widely used in the literature to quantify the crystallinity of a solid, to detect the presence of different polymorphs and that of solvates due to the differences in their diffractograms. Examples from the literature on workers who have used XRPD in their studies include Saleki-Gerhardt et al (1994b), Lin (1972), Kordikowski et al. (2001), Ahmed et al. (1996), Hendriksen (1990), Yonemochi et al. (1999), Lu and Zografi (1998), Matsumoto and Zografi (1999), Shamblin and Zografi (1998, 1999), Otsuka and Kaneniwa (1990), Ward and Schultz (1995), Briggner et al. (1994), Oberholtzer and Brenner (1979), Villiers et al. (1998). The general principles of powder x-ray diffraction were described in Section 2.1.7. Amorphous solids are identified by the absence of sharp peaks and instead a halo is seen in the diffractogram due to the lack of the long-range order present in the crystalline lattice. Crystalline solids lead to the diffraction of the x-rays from the lattice resulting in the appearance of peaks in the diffractogram. The less the crystallinity of the sample, the less the intensity of the peaks in the diffractogram.

The aim of this study was to check the crystallinity of the as received terfenadine.

3.1.1.1 METHODS:

The DSC experiments were carried out using hermetically sealed aluminium pans and measurements were made over a temperature range of 30 – 180 °C in a Perkin-Elmer DSC 7 model. A heating rate of 10 °C/ min was used and all experiments were carried out under an atmosphere of nitrogen gas.

The method used in carrying out the XRPD experiments was described in Section 2.1.7.

3.1.1.2 RESULTS:

The results obtained from the DSC are shown in Table 3.1 and the melting point is taken as peak melting point.

Table 3.1 DSC results of crystalline (as received) terfenadine.

Sample No.	Melting point Tm °C	Enthalpy of fusion ΔH_f J/ g
1	152.3	101.0
2	153.0	102.5
3	151.9	101.0
Average	152.4	101.5
S.D	0.6	0.8

Figure 3.1 shows a typical DSC thermogram of the as received terfenadine

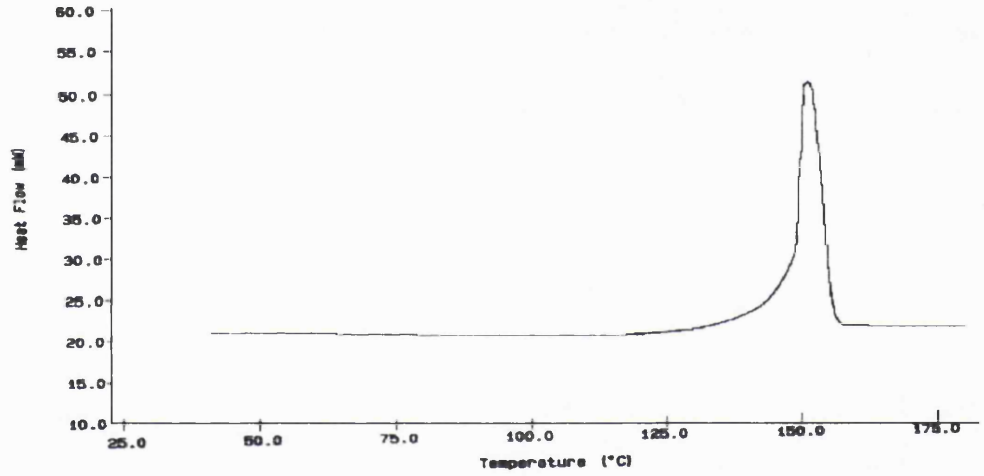

Figure 3.1 *Typical DSC thermogram of the as- received terfenadine showing the melting peak of the crystalline solid.*

The results obtained above are in keeping with those reported by Badwan et al. (1990) and confirm that the as received sample is the most thermodynamically stable polymorph of terfenadine having a melting point within the range of polymorph I (149- 152 °C).
The X-ray diffractogram of the as- received terfenadine is shown in Figure 3.2.

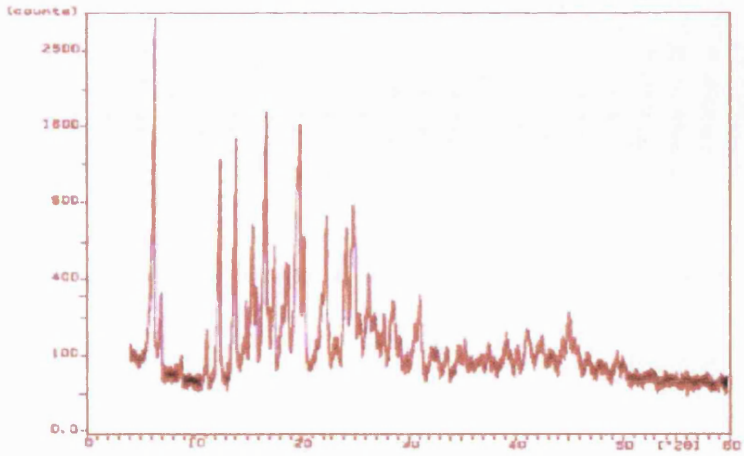

Figure 3.2 *Typical x-ray diffractogram of the as received terfenadine.*

The presence of sharp peaks in the diffractogram confirms that the sample is crystalline which is in keeping with the DSC results.

3.2 AMORPHOUS TERFENADINE:

A definition and general discussion of the amorphous form of the solid, its advantages and disadvantages as well as the different states of an amorphous solid were presented in Section 1.2. An amorphous form of a solid material can be obtained by different methods of sample preparation and manipulation, as outlined in Section 1.3.5.

3.2.1 PREPARATION OF AN AMORPHOUS FORM OF TERFENADINE:

3.2.1.1 PREPARATION OF THE AMORPHOUS FORM BY MELTING AND SLOW COOLING OF THE MELT:

In this case, amorphous terfenadine was prepared by melting crystalline terfenadine in a beaker over a hot plate. The temperature did not exceed ~ 160 °C. The molten mass was dropped through a Pasteur pipette over tin foil and the resulting beads were left to slow cool to ambient temperature. The procedure was then repeated but while leaving the molten mass for 5 minutes on the hot plate before dropping the melt through the Pasteur pipette and leaving it to slow cool. This is done in order to ensure the absence of any crystalline seeds in the melt (this is the procedure that was used in the preparation of all

amorphous solids that were prepared and analysed in the rest of the chapters in this thesis).

3.2.1.2 PREPARATION OF THE AMORPHOUS FORM BY MELTING AND QUENCH COOLING OF THE MELT:

Amorphous terfenadine was prepared by melting crystalline terfenadine over a hot plate as described in Section 3.2.1.1 above but in this case instead of leaving the melt to slow cool to ambient temperature, liquid nitrogen was poured over the molten mass present in the beaker. The liquid nitrogen then evaporated leaving behind a quenched sample of terfenadine.

3.2.2 CHARACTERIZATION OF AMORPHOUS TERFENADINE (QUENCH COOLED AND SLOW COOLED):

Diferential Scanning Calorimetry (DSC), Thermogravimetric Analysis (TGA), Karl-Fischer analysis, Thin Layer Chromatography (TLC) and hot stage microscopy were used in the characterization of amorphous terfenadine samples.

Saleki-Gerhardt et al. (1994b) showed that DSC could be used to estimate the degree of disorder with an overall sensitivity of $\pm$5%. They pointed out however that for highly crystalline samples, this method is not able to differentiate low levels of amorphous content when the level of disorder decreases below 10%. The DSC measures the heat capacity (Cp) as well as the glass transition temperature (Tg) of amorphous solids.

In the case of amorphous solids there is an increase in the heat capacity of the solid at the glass transition temperature, which shows as a shift in the DSC thermogram baseline. At the same time, it should be mentioned that the heat capacity of an amorphous material is always higher than that of its crystalline counterpart (Hancock and Zografi, 1997).

The basic principles of hot stage microscopy were described in Section 2.1.6. A heating stage is incorporated on the optical microscope, which allows viewing of structural transitions on a microscale. Many transitions such as collapse, crystallization, melting and decomposition can be viewed via hot stage microscopy. A built in temperature programmer is used to control the temperature of the sample as well as the heating rate.

The general principles of TGA were explained in Section 2.1.5, Karl Fischer titration was discussed in Section 2.1.11, TLC was described in Section 2.1.12.

3.2.2.1. METHODS:

The DSC was performed by placing one bead of slow cooled terfenadine (12 mg $\pm$ 2mg) in the aluminium pan for testing to be performed. Since the quenched sample shatters while quenching, the only thing that could be done was to take almost the same sample weight as that of the slow cooled terfenadine in the same pan type. Hermetically sealed and open aluminium pans (Perkin-Elmer) were used in the experiments and heating was carried out over a temperature range of 5 – 180 °C while holding isothermally for two minutes at the start temperature. The heating rates used were as shown in Table 3.2 and Table 3.3. The Tg was calculated as the mid point value with half Cp extrapolated. The results reported in Table 3.2 and Table 3.3 are those obtained at a first run on the DSC.

TGA experiments were carried out in a ramp mode from ambient temperature to a maximum temperature of 170 °C at a heating rate of 20 °C/min. Open aluminium pans supplied by Perkin-Elmer were employed. For comparison purposes, the TGA experiments were carried out under purged nitrogen gas within the same temperature range and at a heating rate used in the DSC. The Karl-Fischer method and the instrument used in the analysis were discussed in Section 2.1.11.

The method used in Thin Layer Chromatography (TLC) consisted of a mobile phase, a stationary phase and a detection method. Those were described in Section 2.1.12. Terfenadine was dissolved in HPLC grade methanol. The solution was prepared in a concentration of 5 mg/ ml. Samples were prepared by spotting a 5 µl sample by a micropipette on the silica gel plate, 2 cm away from the bottom of the plate (this is considered as point of origin). Closed, glass TLC jars containing the mobile phase were left for a couple of hours to saturate the glass chamber with organic vapours before placing the spotted silica gel plates inside. When the mobile phase travelled up the stationary phase a distance of around 11 cm, the developed plates were taken out, left to dry and later read using UV light at 254 nm.

In carrying out the experiments using hot stage microscopy, a sample was taken and placed on an Ultima plain glass slide having the dimensions of 76 x 26 mm and a thickness of 1 – 1.2 mm. In the case of the slow cooled sample, the bead was lightly crushed with a spatula before being placed on the slide. The sample was then covered by a slide's cover made from borosilicate glass with the dimensions of 22 x 26 mm (BDH). The slide was then placed on the heating stage and was heated from ambient temperature up to complete melting of the sample at a heating rate of 2 °C/min. The magnification

used was 10x (objective lens) in the case of the slow cooled terfenadine sample and 40x (objective lens) in the case of the quenched sample, multiplied by the magnification of the eyepiece (ocular lens), which was 10x. The net magnification was hence equal to 100x and 400x respectively.

3.2.2.2 RESULTS:

Crystallization of the amorphous quenched and slow cooled samples of terfenadine was noticed to take place during the DSC experiments when the DSC experiments were carried out at the lowest heating rate of 10 °C/ min. However, no crystallization of either the quenched or the slow cooled terfenadine samples was noted at the higher heating rate of 20°C/ min during the DSC experiments. A typical DSC trace of amorphous terfenadine showing crystallization to occur just prior to melting when the experiments were carried out at a heating rate of 10 °C/ min is shown in Figure 3.3 for slow cooled sample and Figure 3.4 for quench cooled sample. Figures 3.5 and 3.6 show the lack of crystallization of the amorphous samples when the DSC experiments were performed at a higher heating rate of 20°C/ min. It is well known that the heating/cooling rate has an effect on the crystallization of the sample from the amorphous state (Ediger et al., 1996; Hancock et al., 1998; Moynihan et al., 1974). At a higher heating rate, sample crystallization can be avoided through rapid increase in temperature, which does not give sufficient time for crystallization of the amorphous sample to occur since crystallization takes place at a temperature between Tg and Tm. Table 3.2 shows the DSC results of quench cooled terfenadine samples in hermetic and open pans where samples are run from 5 – 180 °C at two heating rates (10, 20 °C min). The samples are basically amorphous with an average enthalpy of fusion of the crystalline portion of 3.1 J/g (Table 3.2). This corresponds to ca. 3.0 % crystallinity of the quenched sample (knowing that the enthalpy of fusion of the completely crystalline sample is 101.5 J/g as seen in Table 3.1). This average, crystallinity value was obtained when the DSC experiments were carried out at a heating rate of 10 °C/min where some crystallization took place during the DSC experiments and hence it reflects the total crystallinity in the sample (the crystalline content present prior to the DSC and that achieved during the DSC experiments). The results in Table 3.2 show that lower average Tg values were achieved when hermetically sealed pans were used as opposed to open pans at the same heating rate. This is probably due to entrapment of water leading to an inability of water to escape when sealed pans were used (the

presence of water is confirmed by Karl-Fischer results below). Water can be gathered by the sample during quenching in liquid nitrogen and, being basically amorphous, water may get absorbed by the sample, and cause suppression of Tg due to its plasticizing effect. The Tg value is affected by heating rate and it can be noted from Table 3.2 that at the lower heating rate of 10 °C/ min, a slightly lower average Tg was obtained for the quenched samples (ca. 57 °C at 10 °C/ min versus ca. 59 °C at 20 °C/ min in open pans and ca. 54 °C at 10 °C/ min versus ca. 57 °C at 20 °C/ min in hermetically sealed pans). Table 3.3 shows the DSC results of slow cooled terfenadine samples. The experiments were carried out at two heating rates (10, 20 °C/min) in hermetically sealed aluminium pans. As in the case of the quenched samples, it can be seen that the heating rate affected the obtained Tg value with a slightly lower Tg noted at the lower heating rate (slow cooled terfenadine exhibited a Tg value of ca. 59 °C at 10 °C/min and ca. 61 °C at 20 °C/ min). Ediger et al. (1996) and Moynihan et al. (1974) explained the effect of heating rate on the Tg value of amorphous solids. They clarified that a higher Tg value can be obtained at a faster heating rate than that achieved at a lower heating rate. Hancock et al. (1998) stated that for all the materials they used in their study, the Tg changed by about 7 K for a ten-fold change in scanning rate. The effect of heating/cooling rate on the Tg value was discussed in Section 1.2. Basically a smaller heating/cooling rate means a lower change in temperature with time. This can allow for more molecular rearrangements resulting in a more dense glass and the sample will convert from the rubbery to the glassy state at a lower temperature.

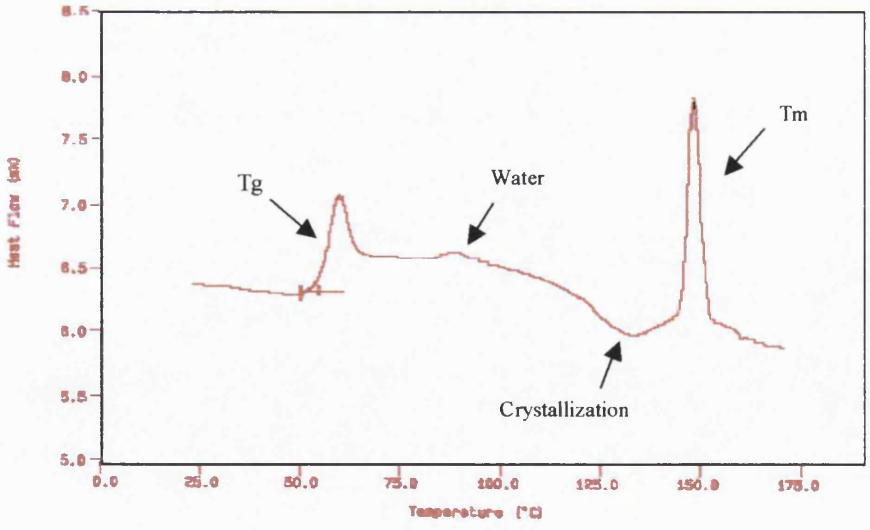

Figure 3.3 *Typical DSC thermogram of the amorphous slow cooled terfenadine at a heating rate of 10 °C/min showing some crystallization prior to melting.*

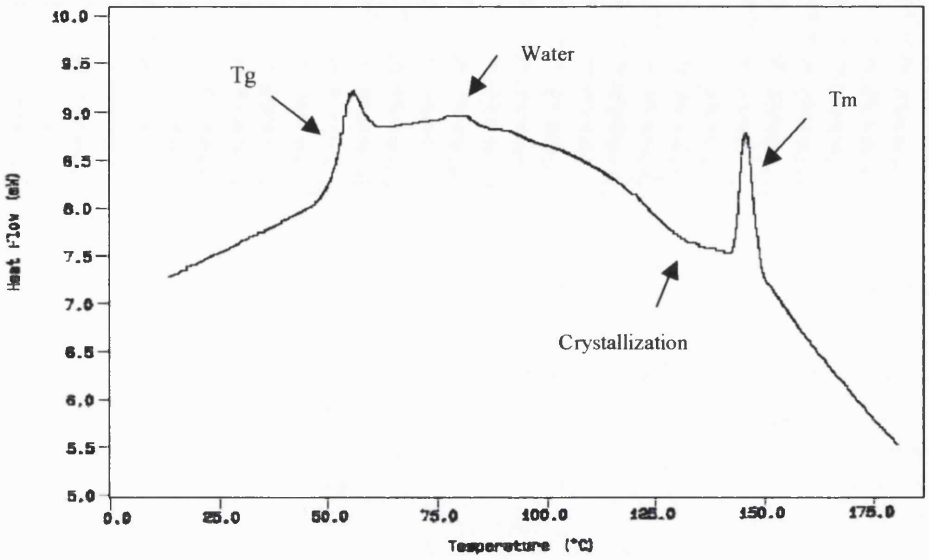

Figure 3.4 Typical DSC thermogram of the amorphous quench cooled terfenadine at a heating rate of 10 °C/min showing some crystallization prior to melting.

Table 3.2 DSC data of the quenched terfenadine sample. Batches were prepared as described in Section 3.2.1.2.

Heating rate (°C/min)	Pan type	Sample no.	Tg (°C)	Tm (°C)	ΔH_f J/g
10	**Hermetic pans**	**1**	55.3	147.2	2.4
		2	54.4	146.8	3.7
		3	53.3	147.2	3.1
		Average	54.3	147.1	3.1
		S.D.	1.0	0.3	0.7
20		**1**	55.8	146.9	0.4
		2	57.0	146.4	1.2
		3	58.2	148.7	0.8
		Average	57.0	147.3	0.8
		S.D.	1.2	1.2	0.4
10	**Open pans**	**1**	57.3	148.8	1.5
		2	56.6	148.5	2.1
		Average	57.0	148.7	1.8
		S.D.	0.5	0.2	0.4
20		**1**	58.1	148.3	0.3
		2	59.3	147.6	0.4
		Average	58.7	147.9	0.3
		S.D.	0.9	0.5	0.1

Table 3.3 DSC data for slow cooled terfenadine using hermetically sealed aluminum pans.

Heating rate (°C/min)	Sample no.	Tg (°C)	Tm (°C)	ΔH_f J/g
10	**1.**	59.5	149.5	7.2
	2.	56.9	148.1	7.6
	3.	58.9	150.1	7.4
	Average	58.5	149.2	7.4
	S.D.	1.3	1.0	0.2
20	**1.**	59.4	149.9	1.6
	2.	61.9	149.0	1.6
	3.	60.2	147.9	0.6
	Average	60.5	148.9	1.3
	S.D.	1.3	1.0	0.6

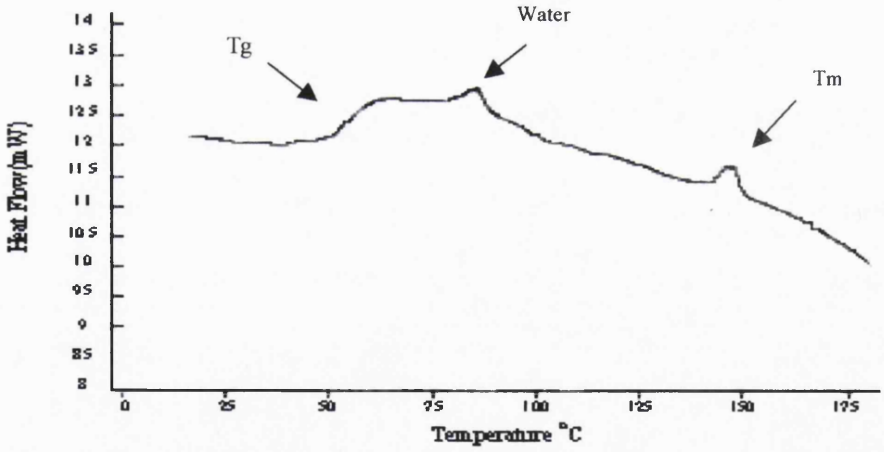

Figure 3.5 *Typical DSC thermogram of quenched terfenadine at a heating rate of 20 °C/min showing the lack of crystallization during the DSC experiment.*

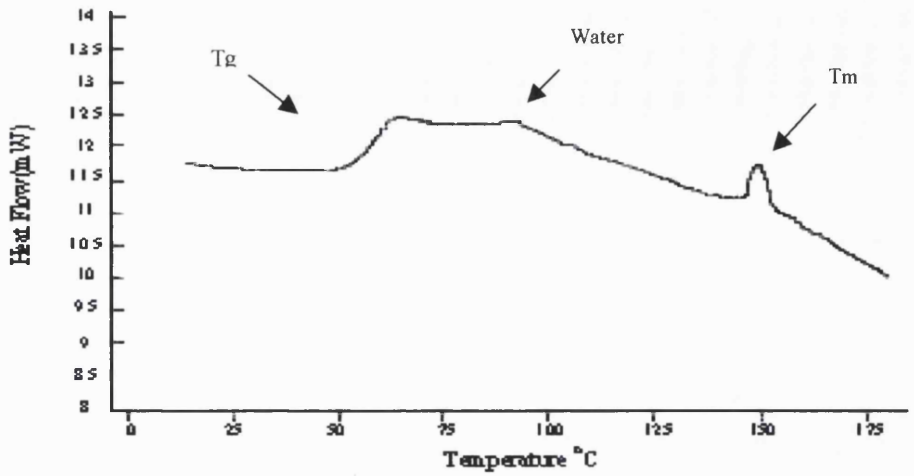

Figure 3.6 *Typical DSC thermogram of slow cooled terfenadine at a heating rate of 20 °C/min showing the lack of crystallization during the DSC experiment.*

Table 3.4 Comparison of average DSC values and average crystallinity for quenched and slow cooled samples of terfenadine using hermetically sealed aluminium pans.

Heating rate (°C/min)	Sample treatment	Average Tg, (S.D.) °C	Average Tm, (S.D.) °C	Average ΔH_f, (S.D.) J/g	% Crystallinity
10	Quenched	54.3 (1.0)	147.1 (0.3)	3.1 (0.7)	3.1
	Slow cooled	58.5 (1.3)	149.2 (1.0)	7.4 (0.2)	7.3
20	Quenched	57.0 (1.2)	147.3 (1.2)	0.8 (0.4)	0.8
	Slow cooled	60.5 (1.3)	148.9 (1.0)	1.3 (0.6)	1.3

Comparison of the DSC results for quenched versus slow cooled terfenadine samples is demonstrated in Table 3.4. It can be noticed that quenching produced the less thermodynamically stable polymorph (polymorph II which shows a melting range of 146 – 148 °C as reported by Badwan et al., 1990), whereas slow cooling produced the most thermodynamically stable polymorph with a melting range of 149 – 152 °C. This was

noticed from the DSC results of experiments carried out at a heating rate of 20 °C/min (where no crystallization of the amorphous sample was seen during the DSC experiments). Comparing the DSC results of quenched and slow cooled samples at a heating rate of 10 °C/ min (where crystallization was seen during the DSC experiments) showed that the slow cooled samples crystallized to the most stable polymorph (polymorph I), whereas the quenched samples crystallized into a metastable polymorph (polymorph II) during the DSC experiments. Yoshioka et al. (1994) reported that rapidly cooled indomethacin crystallized under nonisothermal conditions predominantly to the less thermodynamically stable α form, whereas the slowly cooled sample predominantly gave the more thermodynamically stable γ crystal.

Comparison of the percentage crystallinity between quench cooled and slow cooled terfenadine samples and of the same sample type (quenched or slow cooled) at the two heating rates of 10 and 20 °C/ min is shown in Table 3.4. It can be observed from Table 3.4 that the quenched terfenadine samples exhibited lower crystallinity than the slow cooled samples (3.1% crystallinity in quench cooled sample versus 7.3% crystallinity in the slow cooled sample at a heating rate of 10 °C/ min in the DSC and 0.8% crystallinity in the quench cooled sample versus 1.3% crystallinity in the slow cooled sample at a heating rate of 20 °C/ min in the DSC). Seymour and Carraher (1996) pointed out that quench cooling might result in lower percentage of crystallinity in an essentially amorphous sample whereas slow cooling favours a comparatively higher level of crystallinity. The quenched and slow cooled samples have crystallinity of 0.8 and 1.3 % respectively, which reflects the inherent crystallinity in the samples prior to the DSC run. This is obtained from the enthalpy of fusion seen in the DSC experiments when a heating rate of 20 °C/ min was applied (Table 3.4), since at this heating rate no crystallization of the samples during the DSC experiments was noted (Figures 3.5 and 3.6 for quench cooled and slow cooled terfenadine samples respectively). Since both quench cooled and slow cooled samples showed some crystallization taking place during the DSC experiments when a heating rate of 10 °C/ min was applied, while the same samples failed to crystallize at the higher heating rate of 20 °C/ min during the DSC experiments, the difference in crystallinity for the same sample type (quenched or slow cooled) at the two heating rates corresponds to that amount of amorphous solid that crystallized during the DSC experiments. This amounts to around 2.3% crystallinity of the quenched sample and 6% crystallinity of the slow cooled sample obtained during the DSC experiments.

A stricter control was applied over sample preparation through leaving the sample for a longer time over the hot plate once melting was achieved before slow cooling (fixed at ca. 5 minutes once complete melting was accomplished) and to check the effect that this had on percentage crystallinity of the resulting samples. The temperature of the samples did not exceed 165 °C and no change in colour or odour was observed. The data showed substantial reduction in crystalline content of the resulting slow cooled samples with two out of the three samples tested showing the absence of crystalline material with no melting peaks seen in the DSC thermograms and one of the tested samples showing a negligible enthalpy of fusion of a crystalline solid of 0.5 J/g which corresponds to ca. 0.5% crystallinity. The DSC experiments were carried out at a heating rate of 10 °C/min in a temperature range of 5-180 °C in hermetically sealed aluminium pans in a nitrogen atmosphere. This lower level of crystallinity may be due to reducing the possibility of leaving any crystalline seeds in the melted sample, which was achieved through leaving the sample for a longer time over the hot plate once melting was achieved. The lack of crystalline seeds might be the reason behind the failure of crystallization of this slow cooled terfenadine sample during the DSC experiments at a heating rate of 10 °C/ min.
One may thus deduce that the percentage crystallinity is sensitive to the history of sample preparation as indicated by different crystallinity values for quenched versus slow cooled samples and for samples left for a longer time over the hot plate after melting was achieved verses the ones quenched or slow cooled immediately once complete melting was reached. Table 3.5 shows the Tg values of the amorphous slow cooled terfenadine left for 5 minutes over the hot plate (after melting was accomplished) prior to slow cooling.

Table 3.5 DSC data for slow cooled terfenadine left for 5 minutes over the hot plate after melting. DSC carried out at a heating rate of 10 °C/ min from 5 – 180 °C.

Sample no.	Tg (°C)
1.	53.9
2.	55.7
3.	56.4
Average	55.3
S.D	1.3

Thermogravimetric analysis was carried out in order to explain the appearance of a peak at a temperature of ca. 89 °C in the DSC thermogram of quench cooled terfenadine (Figures 3.4 and 3.5) and at ca. 92 °C for slow cooled terfenadine (Figures 3.3 and 3.6). The TGA results are shown in Table 3.6 and Figure 3.7 for quench cooled terfenadine and in Table 3.7 and Figure 3.8 for slow cooled terfenadine.

Table 3.6 TGA results for quench cooled terfenadine at a heating rate of 20 °C. Run was carried out from start until 170 °C under purged nitrogen in open pans.

Sample no.	Approximate temperature range of weight loss (°C)	% Weight loss
1.	Start – 95 °C	0.14
2.	Start – 95 °C	0.16
Average	Start – 95 °C	0.15

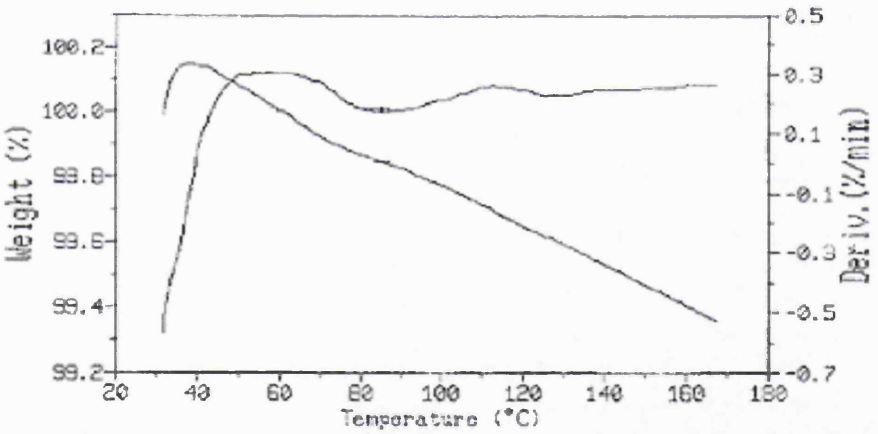

Figure 3.7 *Typical TGA thermogram of quench cooled terfenadine at a heating rate of 20 °C/min.*

Table 3.7 TGA results for slow cooled terfenadine at a heating rate of 20 °C. Run was carried out from start until 170 °C under purged nitrogen in open pans.

Sample no.	Approximate temperature range of weight loss (°C)	% Weight loss
1	Start – 90 °C	0.07
2	Start – 90 °C	0.05
Average	Start – 90 °C	0.06

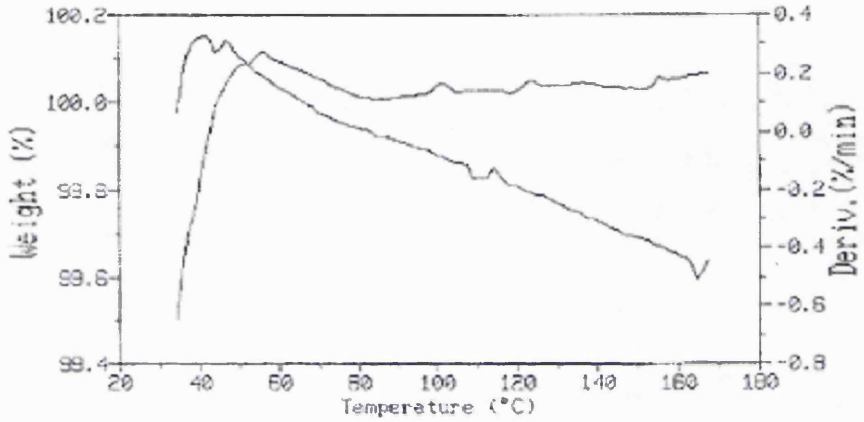

Figure 3.8 Typical TGA thermogram of slow cooled terfenadine at a heating rate of 20 °C/min.

It can thus be concluded from the TGA results above that a loss in weight within the temperature range of the peak seen in the DSC was noticed in the TGA (Table 3.6 and Table 3.7 for quench cooled and slow cooled terfenadine respectively). A Karl-Fischer test was then carried out in order to check if this loss in weight corresponds to the presence of water in the samples. The results from the Karl-Fischer test (Table 3.8) gave a percentage of water, which is very close to that of the percentage weight loss in the TGA (Tables 3.6 and 3.7 for quench cooled and slow cooled terfenadine respectively). Karl-Fischer results thus confirmed that the peaks seen in the DSC thermograms at ca. 92 °C and ca. 89 °C for slow cooled and quench cooled terfenadine samples respectively and the loss in weight in the TGA within the same temperature range corresponded to water loss from the samples.

Table 3.8 Karl Fischer titration results for both quenched and slow cooled terfenadine.

Type of sample	Water % (1^{st} trial)	Water % (2^{nd} trial)	Average water content (%)
Quenched	0.21	0.22	0.22
Slow cooled	0.06	0.06	0.06

An initial weight gain can be seen in the TGA thermograms (Figures 3.7 and 3.8 for quench cooled and slow cooled samples respectively). This can be due to an initial water uptake by the amorphous sample at the beginning of the TGA experiments where nitrogen gas was still incompletely filling the TGA compartment and thus was still unable to get rid of all the air in the atmosphere surrounding the furnace in the TGA, which might contain some humidity. The weight loss was measured until 95 °C in the case of quenched samples and 90 °C for slow cooled samples. This is due to the fact that it can be seen from the derivative curves (Figures 3.7 and 3.8) that the bulk weight loss was concentrated in this region with almost a plateau in the derivative curves beyond these temperatures. This is confirmed to be true with correlation between the weight loss seen in the TGA and water content obtained from Karl –Fischer analysis.

Table 3.4 demonstrates a comparison of the Tg values of both quenched and slow cooled terfenadine samples. The results in Table 3.4 show similar Tg values for both the quenched and the slow cooled samples with the quenched samples having a slightly lower average Tg value than the slow cooled samples. This can be due to the fact that quenched samples contain a higher percentage of entrapped water than the slow cooled samples (as seen from Karl-Fischer data). This resulted in a higher plasticizing effect of water in the case of the quenched samples than in the slow cooled samples, which lead to a lower average Tg value in the case of the quench cooled terfenadine samples.

Slade and Levine (1991) reported higher Tg values of fructose and galactose in hyperquenched glasses than the Tg values of their slow cooled counterparts. On the other hand, Yoshioka et al. (1994) reported similar Tg values of indomethacin for both the slowly cooled and rapidly cooled samples.

To check the effect of heat on the sample of terfenadine and investigate whether heating of terfenadine caused any decomposition in the sample while preparing the amorphous form, TLC was carried out on the slow cooled sample and original crystalline terfenadine for comparison purposes. The TLC Results of slow cooled and crystalline terfenadine are shown in Table 3.9.

Table 3.9 Rf values of slow cooled and crystalline terfenadine done in triplicate.

Sample No.	Rf (Crystalline Terfenadine)	Rf (Amorphous Terfenadine)
1	75.2	74.5
2	75.0	75.2
3	75.3	75.6
Average	75.2	75.1
S.D	0.2	0.6

The Rf values were calculated as follows:

$$\frac{\text{Distance travelled by the sample from the origin}}{\text{Distance travelled by the mobile phase}} \times 100$$

The results in Table 3.9 show that the slow cooled sample showed just one spot on the silica gel developed plates and that there is one Rf value for the spot achieved when the experiment was carried out in triplicate and that the results can be considered the same as those for the crystalline terfenadine (original raw material). This indicates that the sample was still pure terfenadine after heating with no decomposition products produced. This was a necessary procedure to assure purity of the sample and freedom of decomposition products that might be triggered by heating in spite of the fact that while heating terfenadine no change in colour or odour was noticed.

Hot stage microscopy was done for both quench cooled and slow cooled terfenadine samples. Figures 3.9a and 3.9b show the polarized light photomicrographs of slow cooled and quench cooled terfenadine samples respectively. Figures 3.9a and 3.9b indicate the presence of both amorphous (dark) and crystalline (glittering) regions in the prepared slow cooled and quench cooled samples prior to heating of the samples (inherent crystalline regions present in the samples after quench or slow cooling).

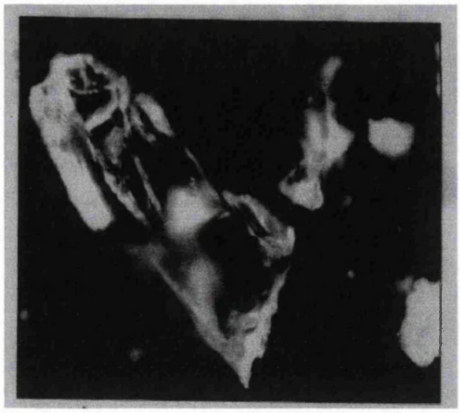

Figure 3.9a *Amorphous regions (dark) and crystalline regions (glittering) of a slow cooled terfenadine sample under a polarized light microscope.*

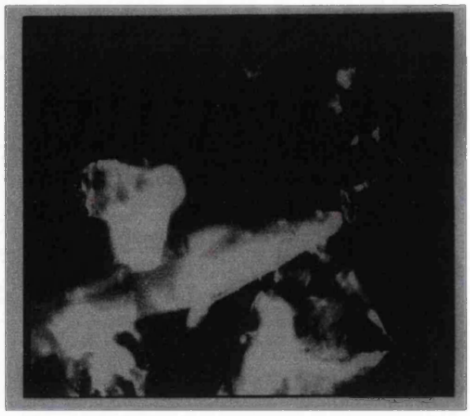

Figure 3.9b *Amorphous regions (dark) and crystalline regions (glittering) of a quench cooled terfenadine sample under a polarized light microscope.*

Figures 3.10a- 3.10j show the photomicrographs under the light microscope in hot stage microscopy for the slow cooled sample at a heating rate of 2 °C/min from ambient conditions until complete melting of the sample. In the case of the quench cooled sample only the stages of crystallization and melting are shown (Figure 3.11a- 3.11d) since crystallization started earlier in the quench cooled sample while there was no difference in the beginning (before crystallization started) between the two samples.

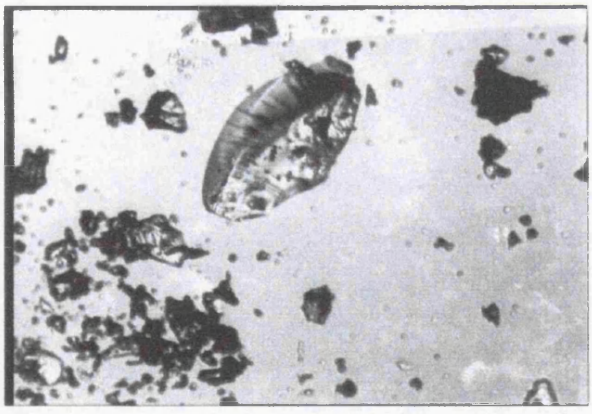

Figure 3.10a *A view under the microscope before the start of heating the sample of slow cooled terfenadine (magnification 100x).*

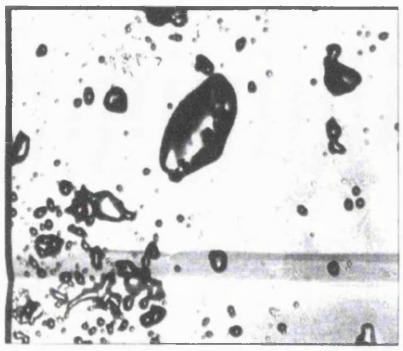

Figure 3.10b

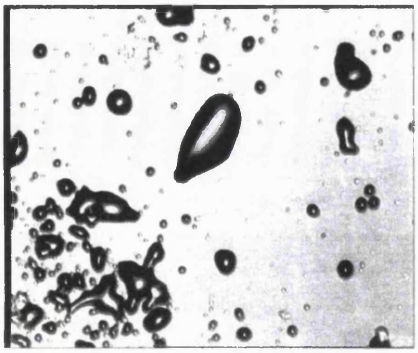

Figure3.10c

Figures 3.10b, 3.10c *A beginning (Figure 3.10b) and continuity (Figure 3.10c) of collapse of the sample can be noted in the form of shrinkage of the slow cooled terfenadine flake (magnification 100x).*

It can be noticed from the slow cooled sample photomicrographs above that in Figure 3.10b the sample started to flow and collapse becoming unable to support its own weight under gravity at a temperature of ca. 74 °C. The sample showed further shrinking in Figure 3.10c where the temperature reached ca. 77 °C. To and Flink (1978a) showed that the extent of collapse under an optical hot stage microscope can be defined in terms of a change in flake area until a round structureless blob with no further change in area was observed indicating maximum possible collapse under the conditions used during the course of the experiment. The principles of collapse were discussed in Section 1.3.4. The sample started to flow and globules gather and merge together (Figure 3.10d)

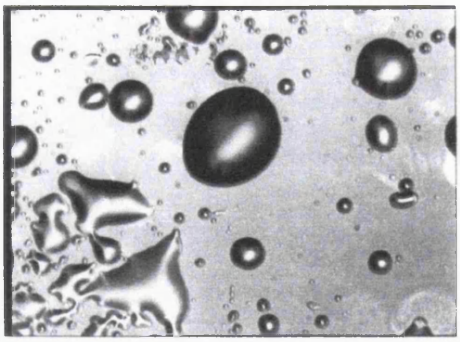

Figure 3.10d *The slow cooled sample is in the rubbery state and is flowing while globules merge together (magnification 100x).*

This is followed by crystallization, which started at ca. 106 °C (Figure 3.10e) and ended at ca. 147 °C (Figure 3.10g).

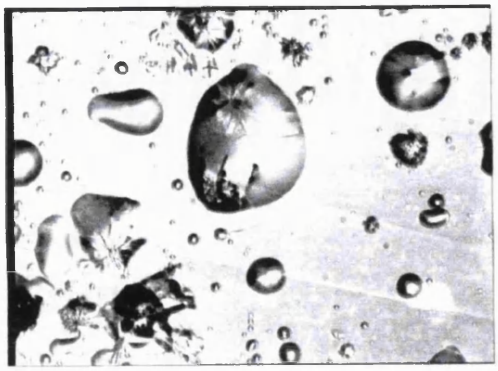

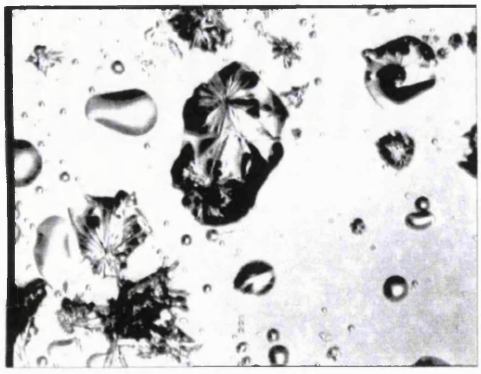

Figure 3.10e ***Figure 3.10f***

Figure 3.10e, Figure 3.10f *Start of crystallization is noted in Figure 3.10e and continues in Figure 3.10f (magnification 100x).*

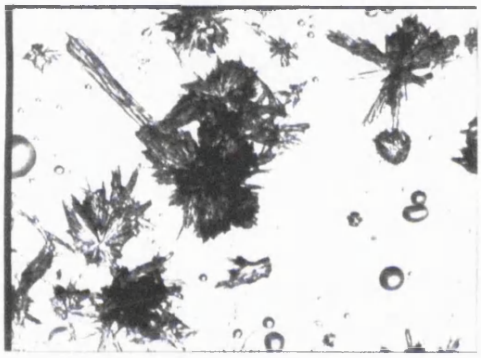

Figure 3.10g *Complete of crystallization of the slow cooled sample at ca 147 ^{0}C (magnification 100x).*

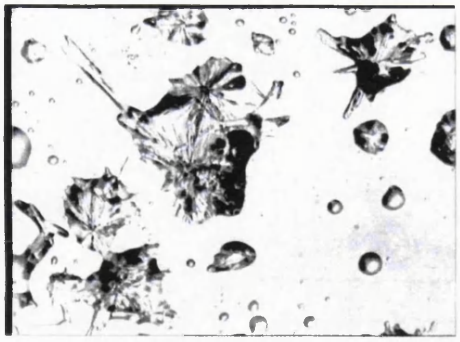

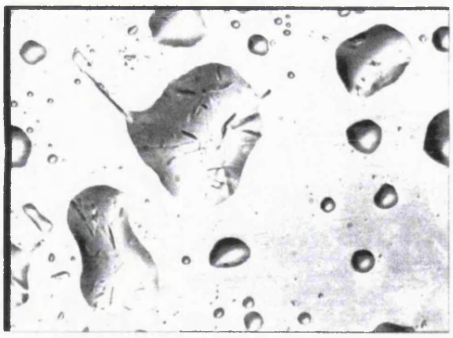

Figure 3.10h ***Figure 3.10i***

Figure 3.10h, Figure 3.10i *Start (Figure 3.10h) and continuity (Figure 3.10i) of melting of the crystalline terfenadine in the slow cooled sample (magnification 100x).*

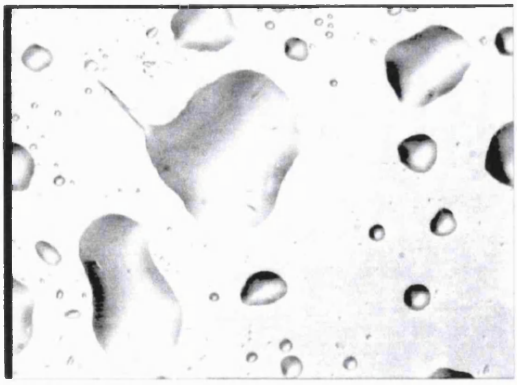

Figure 3.10j *End of melting of the slow cooled terfenadine sample at ca 151 °C (magnification 100x).*

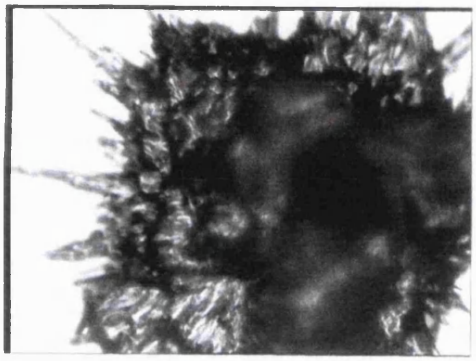

Figure 3.11a

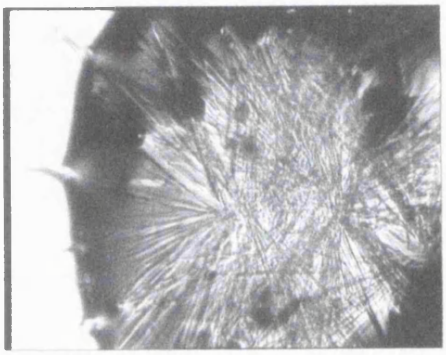

Figure 3.11b

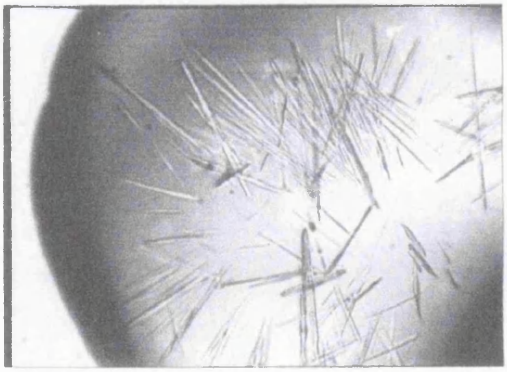

Figure 3.11c

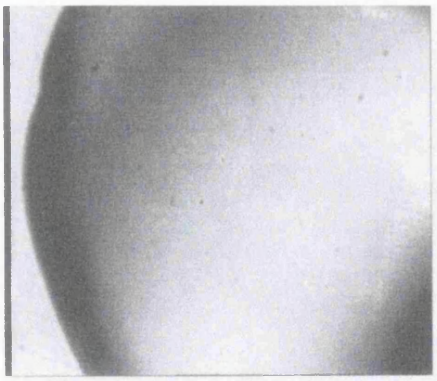

Figure 3.11d

Figures 3.11a- 3.11d *End of crystallization of quench cooled terfenadine followed by start of melting, then further melting until the end of the melting step of the quenched sample respectively (magnification 400x).*

Melting of the slow cooled terfenadine sample started in Figure 3.10h at a temperature of ca 148 °C and ended at ca. 151 °C (Figure 3.10j) indicating that the sample crystallized into the most stable polymorph (polymorph I in Table 2.1).

Though no differences in the melting or collapse behaviour of the quench cooled or slow cooled samples were seen as collapse started in the quench cooled sample at ca 72 °C and that of the slow cooled sample at ca 74 °C and melting started for both samples at ca. 148 °C, yet for the quench cooled sample crystallization started at ca. 95 °C while that of the slow cooled sample started at ca. 106 °C. This difference in crystallization temperature (Tc`) was not noticed in the DSC at a heating rate of 10 °C/ min (Figures 3.3 and 3.4). The lower heating rate used in hot stage microscopy (2 °C/ min) might have allowed the differences in temperature of crystallization between the slow cooled and the quenched terfenadine samples to be noticed. This lower Tc` for the quenched sample might be due to a relatively higher mobility (as the sample contains a higher amount of water and is hence more plasticized than the slow cooled sample), which triggers crystallization at a slightly lower temperature in the case of the quench cooled sample than that of the slow cooled sample. A change in the Tg value that is accompanied with a change in the crystallization temperature (Tc`) is reported in the literature. For example, Schmitt et al. (1996) reported lower Tg values accompanied with lower Tc` values as the moisture content in the sample is increased. Yoshioca et al. (1995) reported an increase in Tg with a corresponding increase in Tc` as the concentration of poly(vinylpyrrolidone) (increases Tg by its antiplasticizer effect) is increased. Melting started at ca. 148 °C in both quenched and slow cooled samples indicating that both of those samples crystallized to the most stable polymorph of terfenadine (polymorph I) when a heating rate of 2 °C/ min was applied. This is not in agreement with the DSC results where the quenched sample crystallized to a metastable polymorph (polymorph II) while the slow cooled sample crystallized to the most stable polymorph at a heating rate of 10 °C/ min during the DSC experiments (as discussed earlier and seen in Table 3.4). This discrepancy in results can be attributed to differences in heating rate applied during the DSC from that used during hot stage microscopy where the lower heating rate of 2 °C, that is applied in hot stage microscopy, gave the material the chance to crystallize into the most stable polymorph. In both DSC and hot stage microscopy experiments carried out at a heating rate of 10 °C/ min and 2 °C/ min respectively (where some crystallization of both quenched and slow cooled samples of terfenadine took place), melting involved that of the original crystalline material that was present in the prepared amorphous samples (quenched and slow cooled)

as well as that crystalline portion which was formed due to crystallization during the DSC or the hot stage microscopy experiments.

3.3 DISCUSSION:

The original (as received) terfenadine is crystalline and proves to be of the most stable polymorph type of terfenadine when tested on the DSC. Amorphous terfenadine was prepared using two methods, slow cooling and quench cooling from the melt. The quenched sample exhibited lower crystallinity in the DSC than the slow cooled samples (3.1 % for quench cooled versus 7.3% for slow cooled samples) while crystallizing into a metastable polymorph (polymorph II) during the DSC experiments carried out at a heating rate of 10 °C/ min. The slow cooled samples crystallized during DSC experiments carried out at a heating rate of 10 °C/ min into the most stable polymorph (polymorph I). Heating of both the slow cooled and quench cooled samples in the DSC at a heating rate of 20 °C/min did not lead to crystallization of the amorphous samples during the DSC experiments. The fact remained though that the quench cooled samples contained lower crystallinity than the slow cooled samples (0.8% for the quench cooled versus 1.3% for the slow cooled samples). The above lead to the conclusion that around 2.3% of the crystallinity in the quenched sample and 6% of the crystallinity in the slow cooled sample was obtained due to crystallization during the DSC experiments. Quench cooling and hermetically sealed pans resulted in lower Tg values than those obtained in slow cooled samples or when open pans were used. This was explained as being due to the presence of larger amount of water in the quenched sample collected from exposure to liquid nitrogen as proven by higher water content in the Karl-Fischer data of the quenched samples versus that of the slow cooled sample. Hermetically sealed pans prevented the escape of water resulting in lower Tg values than those noted when open pans were used. A lower heating rate of 10 °C/ min gave a slightly lower Tg value in the DSC than when a higher heating rate of 20 °C/ min was used in both quenched and slow cooled samples. An endothermic peak in the DSC traces of both quenched and slow cooled samples was seen at ca.89 °C and ca. 92 °C respectively. These peaks were thought to be due to water evaporation as the loss in weight seen in the TGA overlapped with the temperature range of these endothermic peaks in the DSC. Karl-Fischer analysis proved that the percentage of water corresponded with the percentage weight loss seen in the TGA in both the slow cooled and the quench cooled samples with a higher percentage of water in the quenched

sample than that in the case of the slow cooled sample. Hot stage microscopy revealed the presence of both amorphous and crystalline regions in the quenched and slow cooled samples of terfenadine, which were not exposed to a stricter control in sample preparation (through leaving the molten mass for around 5 minutes over the hot plate before being quenched or slow cooled). This was in agreement with the DSC data of samples that were quenched or slow cooled directly once melting was achieved over the hot plate. Hot stage microscopy was carried out at a low heating rate of 2 °C/ min and crystallization was seen in both quench cooled and slow cooled samples. Due to the difference in heating rate used in the DSC (10 °C/ min) from that used in the hot stage microscopy (2 °C/ min), the difference in crystallization temperature between slow cooled and quench cooled samples could be detected using hot stage microscopy. The quench cooled sample had a slightly lower crystallization temperature (Tc`) than that of the slow cooled sample. This was attributed to a greater mobility in the quench cooled sample due to a larger water content resulting in higher plasticization, lower Tg and lower Tc` values than those noted for the slow cooled sample. Due to the lower heating rate used in hot stage microscopy than that used in the DSC experiments, both the quench cooled and the slow cooled samples crystallized into the most stable polymorph in hot stage microscopy.

CHAPTER FOUR

INVESTIGATION OF CRYSTALLIZATION BEHAVIOUR OF AMORPHOUS TERFENADINE USING ISOTHERMAL MICROCALORIMETRY AND DYNAMIC VAPOUR SORPTION

4 INTRODUCTION:

Isothermal microcalorimetry is used extensively as an analytical tool due to its high sensitivity and ability to follow changes in materials in real time. The method gives information regarding thermodynamics, kinetics (mechanism) and concentration (analysis) of the sample under investigation as shown by Buckton and Beezer (1991). The general principles of isothermal microcalorimetry are discussed in Section 2.1.2. The principles and fields of application of isothermal microcalorimetry, which include investigations of microbiological metabolic processes, chemical and physical stability of a material are discussed by Buckton (1995b) and Wadsö (1997). Discussion of the advantages and disadvantages of isothermal microcalorimetry and the wide fields of its application as well as mentioning of the different experimental techniques that can be used including the flow cell, solution calorimetry (breaking ampoule) and glass or stainless steel ampoule method was presented by Buckton and Beezer (1991). In the current study, the glass ampoule method was used, which involves placing the sample under investigation in a glass ampoule with a most commonly used capacity of 3 ml. A small Durham tube containing an aqueous saturated salt solution or a mixture of organic liquids is added to the ampoule in such a way that the liquid in the tube will be separated from the sample yet the vapours of the liquid will be able to interact with the sample. The ampoule is then crimp-sealed before lowering into the isothermal microcalorimeter (Figure 4.1). Any thermal changes occurring in the ampoule can be detected and recorded to the sensitivity level mentioned in Section 2.1.2. The glass ampoule method has been used by many workers with the tube containing a saturated salt solution, with different salts giving rise to different relative humidity values, examples of which are (Ahmed et al., 1998; Briggner et al., 1994; Buckton et al., 1995a; Buckton et al., 1995b; Chidavaenzi et al., 1997;). Ahmed et al (1996) used organic vapours (ethanol or mixtures of ethanol and water) in the tube inserted in the ampoule of the isothermal microcalorimeter in order to trigger crystallization of the amorphous form of a drug used in panic disorders.

Figure 4.1 *Glass ampoule of isothermal microcalorimeter containing the sample under investigation and the Durham tube with either a saturated salt solution or an organic vapour.*

Dynamic vapour sorption (DVS) is a gravimetric method for sample analysis. Water sorption by solid samples and the corresponding weight change in the sample can be monitored by DVS. Crystalline samples can adsorb water on their surfaces and water uptake depends on surface area of the solid material; whereas in the case of amorphous solids water is absorbed into amorphous regions and the extent of moisture uptake is more determined by sample mass (Ahlneck and Zografi, 1990). A sample with both amorphous and crystalline domains shows a preferential water uptake into the amorphous regions, which makes the amount of water taken up by the amorphous content very high in comparison with water uptake relative to the total sample mass. This behaviour is explained by the water amplification theory (Ahlneck and Zografi, 1990). It is well known that water acts as a powerful plasticizer often causing the glass transition temperature (Tg) of an amorphous solid material to drop below the temperature of the experiment (T). Once sufficient mobility is imparted to the molecules by the plasticizing effect of water, crystallization of the amorphous solid usually follows (Hancock and Zografi., 1994; Ahlneck and Zografi, 1990). Crystallization is reported to take place even at temperatures below the glass transition temperature, however the rate of crystallization is markedly increased at higher temperatures due to an increased molecular mobility (Yoshioka et al., 1994). Crystallization of an amorphous solid can be identified by the DVS apparatus as the sample loses weight when crystallization takes place due to the expulsion of absorbed water as the ordered crystalline structure is formed. Hence crystallization is indicated when loss in weight is seen during the water uptake step in the DVS apparatus. However, Hogan and Buckton (2001a) showed that

weight loss alone cannot be relied upon to confirm crystallization of samples where multiple hydrates form as in the case of raffinose where the amorphous sample does not seem to be losing weight on the DVS but proven to be crystallizing by NIR. Hence if weight loss alone were used to judge crystallization of the sample then it would be possible to miss the crystallization event. Lane and Buckton (2000) reported that a combination of DVS and near infra- red (NIR) techniques showed that loss in weight due to water desorption precedes crystallization and continues after crystallization was complete. This is contrary to the common belief that crystallization precedes water expulsion from the crystallized sample.

The water sorption technique can also be used for quantitative determination of amorphous content even when detecting low amorphous contents in predominantly crystalline solids. Water vapour sorption has been widely used as a technique to produce a controlled targeted relative humidity in order to trigger crystallization and quantify amorphous content using a highly sensitive Cahn microbalance for weight determination. Schmitt et al. (1996) stated that weight loss associated with crystallization in a moisture sorption microbalance could be used to detect as little as 2% disorder in physical mixtures of crystalline and amorphous forms of the drug under investigation (lomotrigine mesylate). Buckton and Darcy (1995b) showed that a water sorption technique can readily be used to reveal the existence of amorphous lactose down to a low level of 0.05 % w / w with calculations being based on residual water content which correlated well with the formation of α-lactose monohydrate. However the authors later clarified (Buckton and Darcy, 1999) that when larger amounts of the amorphous solid are present not all of the sample will crystallize into a hydrate and in fact not all of the sample will crystallize to the α-lactose form. Thus quantification of the amorphous content in the sample based on the calculation of the amount of hydrate that forms will only be possible if all of the sample forms a hydrate which was not the case with lactose as explained by Buckton and Darcy (1999). Saleki-Gerhardt et al. (1994b) were able to detect a level of disorder in the solid as low as 1% with a high degree of accuracy of $\pm$ 0.5% by using water sorption measurements. Hogan and Buckton (2001b) quantified low amorphous contents in predominantly crystalline lactose samples down to the 1 mg level. Andronis et al. (1997) triggered crystallization of the hydrophobic drug indomethacin through moisture. Indomethacin has very limited water solubility in the crystalline form but demonstrates significant water sorption in the amorphous state. Water sorption of the amorphous sample thus caused plasticization

and reduction of Tg below T ending in crystallization of the hydrophobic amorphous indomethacin. Andronis et al. (1997) reported that isothermal crystallization of indomethacin at 30 °C and RH values in the range of 0 - 43% resulted in the γ crystal form while the α crystal form was obtained at higher RH values ranging from 56-97% RH. Crystallization took place after ca. 100 days when the sample was stored at 0% RH while increasing the RH resulted in an increase in the crystallization rate. Buckton and Darcy (1996), Darcy and Buckton (1997), used DVS to detect and determine whether partial or complete collapse was taking place in an amorphous lactose sample. Collapse started when the sample was exposed to 50% RH in the DVS for more than 60 minutes. All of the above show the diversity and significance of the moisture sorption technique in studying and characterizing solid samples.

The aims of this study were:

- To check if crystallization of the amorphous form of a hydrophobic drug (terfenadine) could be triggered by humidity effect through exposure to water vapour in the isothermal microcalorimeter.
- To see if organic vapours were able to crystallize the amorphous sample in the isothermal microcalorimeter in an overnight experiment at 25 °C
- To study the slow diffusion of water and the extent of water uptake into freshly prepared amorphous terfenadine as a model of a hydrophobic amorphous material in order to develop an understanding of its physical stability and potential for crystallization under the influence of humidity using DVS.
- To compare the rate of water uptake by a freshly prepared amorphous terfenadine sample with that of an aged one.
- To derive an expression from a regression analysis of the data, relating the percentage mass change (due to sorption) to time.
- To evaluate the potential for crystallization of terfenadine under the combined effect of humidity (75% RH) and an elevated temperature of 50 °C in the DVS.
- To investigate the use of non-aqueous vapours (ethanol) in the Dynamic Vapour Sorption apparatus (DVS) in an attempt to recrystallize amorphous terfenadine.
- To check the time it takes the amorphous terfenadine sample to start crystallizing and the time it needs in order to crystallize completely upon exposure to water vapour at different relative humidities and ambient temperature of 21 + 1 °C.

4.1 METHODS:

4.1.1 PREPARATION OF AMORPHOUS SAMPLES:

Preparation of amorphous samples of terfenadine was carried out by melting and slow cooling the melt as explained in Section 3.2.1.1. The resulting beads had a diameter of approximately 3mm and an average weight of 11.7 mg (n = 100, S.D. = 0.72).

4.1.2 ANALYTICAL METHODS:

4.1.2.1 METHOD USED IN THE ISOTHERMAL MICROCALORIMETRY:

Experiments were carried out by placing 10 beads in the 3 ml glass ampoule. A Durham tube containing either saturated salt solution, ethanol/water or ethanol/n-propanol mixtures (depending on the experiment being carried out); was placed on top of the beads inside the glass ampoule. The ampoule was then crimp-sealed with rubber and aluminium over seal. A reference side glass ampoule was prepared in the same way as the sample ampoule without the addition of the amorphous beads. Both the sample and the reference ampoules were pre-equilibrated in the isothermal microcalorimeter (TAM) for 20 minutes at the experimental temperature set at 25 °C before lowering into the measuring position. The monitoring of the heat flow signal was started once the ampoules were lowered to the measuring site. Results were recorded as rate of change of heat (power) verses time.

The amorphous sample has a maximum ΔH_f of the crystalline portion of 0.5 J/g (in comparison with an average value of 101.5 J/g as seen in Table 3.1 and 102 J/g as reported by Badwan et al., 1990 for the completely crystalline sample) with some data showing the lack of any crystallinity as concluded from their DSC results in Table 3.5.

4.1.2.2 METHODS USED IN THE DVS FOR THE CHARACTERIZATION OF THE AMORPHOUS FORM OF TERFENADINE:

Six beads of the amorphous form of terfenadine were placed in the sample side quartz pan of the DVS apparatus. The reference side quartz pan was kept empty. The system

was conditioned and dried at 0% RH until an almost flat baseline with minimal noise was obtained prior to the start of any experiment.

1. Using water in the DVS, an experiment was set in steps where amorphous terfenadine was exposed to one cycle of sorption and desorption. The experiment was carried out at a temperature of 25 °C going from 0% RH up to 90% RH and back to 0% RH again. Each step was kept for a period of 10 minutes.
2. Amorphous terfenadine was exposed to a ramp method in the DVS going from 0% RH at which the samples were equilibrated for 1 hour, up to 44% RH, 75% RH, or 90% RH where samples were kept for 20 hours at the target RH. This was followed by a final drying step at 0% RH for 1 hour. The experiments were carried out at a controlled temperature of 25 °C.
3. A third approach was used in an attempt to trigger crystallization of the amorphous forms by a combined effect of humidity and temperature. The experiments were applied to amorphous form of terfenadine. The temperature in the DVS was set to 50 °C and using a ramp method, the DVS was equilibrated at 0% RH for 1 hour followed by 75% RH for 20 hours and ended with a drying step at 0% RH for 1 hour.
4. Replacing water with ethanol in the DVS, a series of experiments were carried out:
    a. The system was first equilibrated at 0% RH for 10 minutes. The flow of ethanol was then adjusted to a variety of percentages ranging from 50-95% in the total gas flow (ethanol vapour mixed with dry nitrogen), the flow of ethanol was kept at the specified percentage for 3 hours. The experiments were carried out at 25 °C.
    b. Experiments were set with an initial equilibration step at 0% RH for 1 hour followed by exposure to 95% ethanol in the total gas flow (mixed with nitrogen gas) for 20 hours and ended with a one hour step at 0% RH. Experiments were carried out at 25 °C.

4.2 RESULTS:

4.2.1 MICROCALORIMETRY RESULTS:

4.2.1.1 RESPONSE OBSERVED IN ISOTHERMAL MICROCALORIMETER AS A RESULT OF EXPOSURE TO WATER VAPOUR AND VAPOURS OF WATER/ETHANOL MIXTURES:

An attempt to quantify amorphous content and study the characteristic crystallization profile of amorphous terfenadine by exposure to humidity was carried out using the glass ampoule method as mentioned above and by placing saturated potassium chloride (KCl) solution in the Durham tube containing an excess amount of the salt which produces a relative humidity of 85% at 25 °C as reported by Nyqvist (1983). The samples failed to crystallize in the isothermal microcalorimeter at this combination of temperature (25 °C) and RH (85%) over a period of 20 hours as indicated by the flat power/time curve obtained in the isothermal microcalorimeter (Figure 4.2).

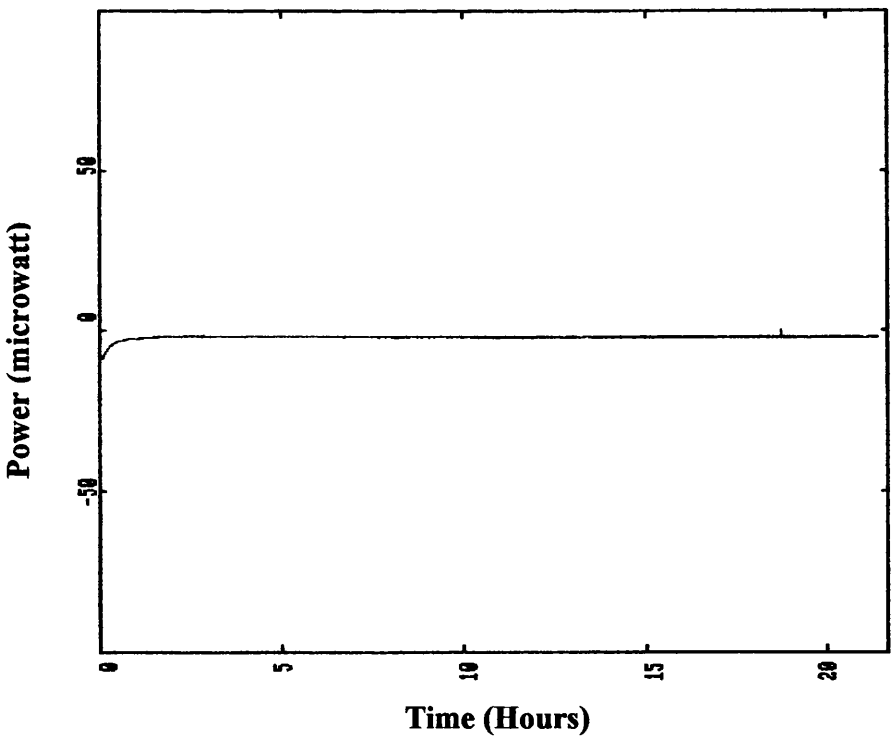

Figure 4.2 Typical microcalorimetry response for the amorphous terfenadine sample after exposure to 85% RH at 25 °C.

Crystallization of the amorphous hydrophobic samples of terfenadine was thus attempted by the use of a mixture of ethanol/water in the Durham tube producing a percentage of organic vapour instead of the KCl saturated salt solution which gave water vapour in the inner environment of the ampoule. It can be seen from Figure 4.3 that crystallization starts to take place at a percentage of ethanol somewhere between 25 – 40 % as there is lack of any crystallization taking place in the isothermal microcalorimeter at 25% ethanol and some crystallization is noticed at 40 % ethanol in the ethanol/water mixtures. Ahmed et al. (1996) carried out a similar study whereby crystallization failed to take place in the presence of water vapour, so organic vapours had to be used in order to crystallize the amorphous sample in the isothermal microcalorimeter. Although terfenadine is a hydrophobic drug with aqueous solubility of 0.001 and solubility in ethanol of 3.78 g/100 ml at 30 °C (as seen in Table 2.3), hydrophobicity per se cannot justify the lack of crystallization of the amorphous sample. This is due to the presence of previous studies that reported crystallization of hydrophobic materials taking place under the influence of a humid environment. Examples of which include griseofulvin with low aqueous solubility which was converted from the amorphous to the crystalline form by exposure to 65 –85 % RH as reported by Ahmed et al., (1998). Indomethacin is another example of a hydrophobic drug, which was crystallized upon exposure to humid air as shown by Andronis et al., (1997). Ahmed et al., (1996) though reported the need for organic vapours to crystallize a drug used for anxiety and panic disorders, yet the drug has a Tg value in the amorphous state of around 398 K (125 °C) which makes this sample less likely to be plasticized by water at ambient temperatue than the amorphous terfenadine sample which has a Tg value of around 60 °C. Hence, the lack of crystallization of amorphous terfenadine by the effect of humidity may in part be due to the large size of the beads and as moisture is taken up by the amorphous sample, water might be localized in certain amorphous regions on or close to the surface. This amount of water relative to the whole size of the sample might be too small to be able to trigger sufficient plasticization and lowering of Tg below the experimental temperature (T). This is combined with the fact that the hydrophobic nature of the sample will contribute in repelling moisture and minimizing the extent of water absorbed by the amorphous sample together with the possibility that the structural orientations of the hydrophobic molecule might be in such a way that favours the presence of the hydrophobic chemical

groups on the surface of the particles thus further enhancing water repellence and resistance to wetting.

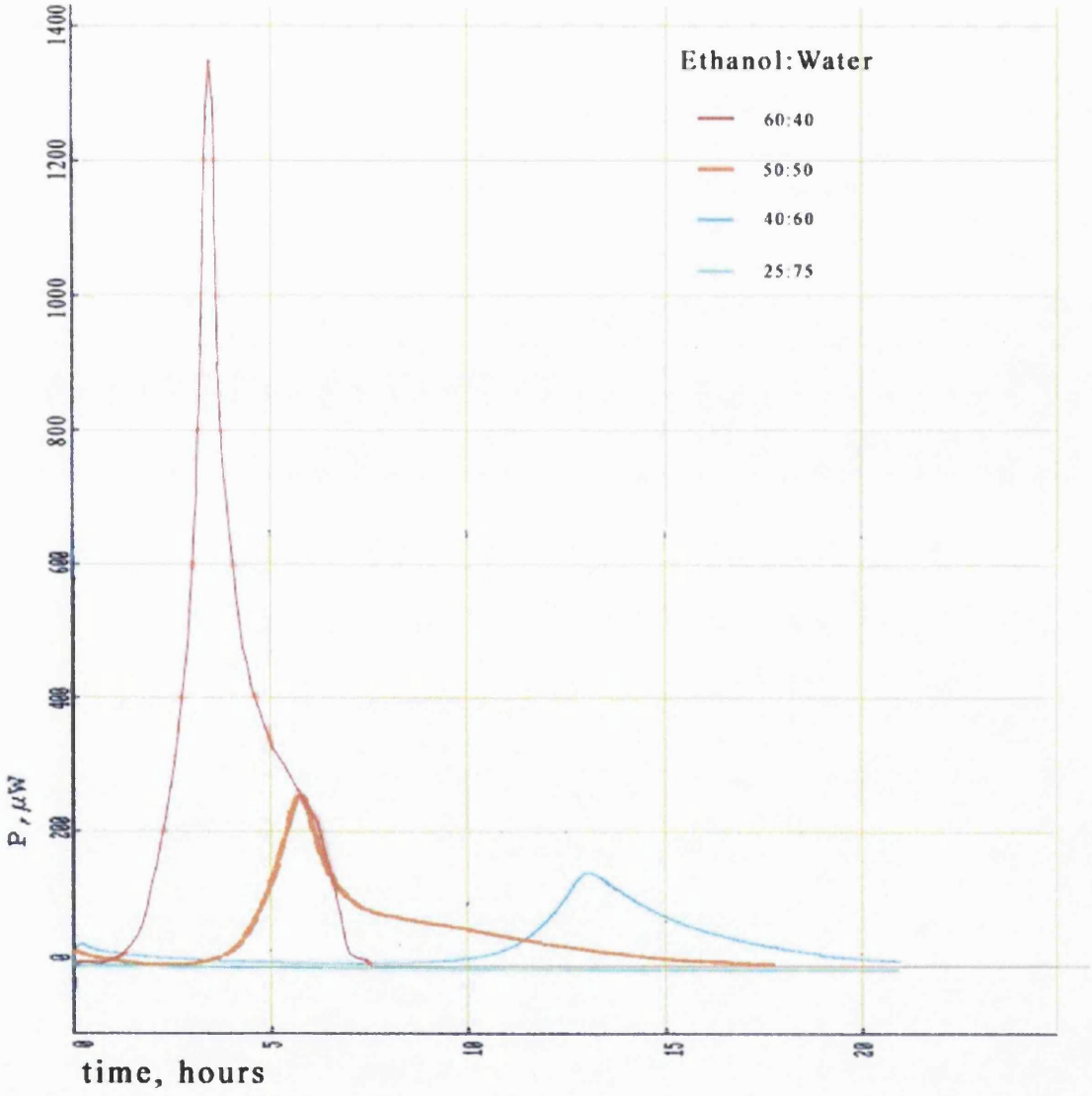

Figure 4.3 *Typical microcalorimetry profiles for amorphous terfenadine samples exposed to different percentages of ethanol/water vapour.*

In previous experiments carried out by Briggner et al. (1994) on the hydrophilic material lactose, it was found that the onset of crystallization could be delayed by reducing the relative humidity of the atmosphere inside the ampoule of the isothermal microcalorimeter. The highest relative humidity (85% RH) resulted in the fastest crystallization while the lowest relative humidity used (53% RH) lead to the most

delayed onset of crystallization with intermediate onsets of crystallization at in-between RH values. Sebhatu et al. (1994a) reported delayed onsets of crystallization of spray dried amorphous lactose at lower relative humidity values in the sealed glass ampoule method experiments in the microcalorimeter. Ahmed et al. (1996) reported a similar finding in a study carried out on a hydrophobic drug used for panic disorders whereby 96% ethanol and different ratios of 96% ethanol/water were used for the crystallization of the amorphous form in the isothermal microcalorimeter. Comparison of areas under the curve and normalizing those values per unit weight of the sample gave more or less the same values indicating the existence of the same amorphous content in the samples and that complete crystallization was taking place.

To investigate whether an equivalent situation was obtained in this study, an isothermal microcalorimetric study was carried out at 25 °C using different ratios of ethanol in the ethanol/water mixture placed in the Durham tube. The initial small exothermic peak seen in the microcalorimetric trace of some graphs in Figure 4.3 is due to the standard disruption caused by lowering of the ampoule into the measuring site. The main upward shifted exothermic peak that follows the initial tiny exothermic peak (Figure 4.3) is indicative of crystallization of amorphous regions. It can be seen that the fastest onset of crystallization was for the sample being crystallized with the highest percentage of ethanol (60%), with progressively increasing onsets of crystallization going from 60 to 50 to 40 % ethanol in ethanol/water mixtures and eventually no crystallization was taking place in the sample over 20 hours when the percentage of ethanol dropped to 25% (Figure 4.3). Samples tested on the isothermal microcalorimeter with percentages of ethanol of 40, 50 and 60 % ethanol/water mixtures were tested on the DSC after being taken out from the isothermal microcalorimeter. DSC experiments were carried out at a heating rate of 10 °C/ min in a temperature range of 20 - 180 °C under nitrogen atmosphere using hermetically sealed aluminium pans. It was noted that though crystallization was detected in the isothermal microcalorimeter, crystallization was still taking place in the same samples when tested on the DSC. This indicates that incomplete crystallization of the amorphous samples took place at the percentages of ethanol used in the isothermal microcalorimeter. A typical DSC thermogram showing crystallization of the sample still taking place after exposure to 40% ethanol in the isothermal microcalorimeter is seen in Figure 4.4. A comparison of the areas under the curve in the isothermal microcalorimeter thermograms showed that at the higher percentages of ethanol, more crystallization was taking place (as indicated by larger

area under the curve in the isothermal microcalorimetry trace) with values of 14.57 mJ/mg, 26.6 mJ/mg and 47.1 mJ/mg for samples crystallized using 40 %, 50 % and 60 % ethanol in ethanol/water mixture in the isothermal microcalorimeter respectively. This indicates that at higher percentages of ethanol more crystallization of the amorphous content was taking place. Yet, since incomplete crystallization was achieved in the isothermal microcalorimeter, quantification of the amorphous content of the slow cooled amorphous samples was not possible with these ethanol/water mixtures.

Terfenadine has three polymorphic forms and it can be noted that the crystalline form obtained subsequent to exposure to microcalrimetry and DSC was the most thermodynamically stable form (Polymorph I).

The formation of the thermodynamically stable form has also been reported by Giron et al. (1997) for a purine derivative crystallized by exposure to different relative humidities and evaluated using the DSC. Buckton et al. (1995b) reported obtaining the thermodynamically stable form of salbutamol sulphate subsequent to exposure to different RH values in the microcalorimeter.

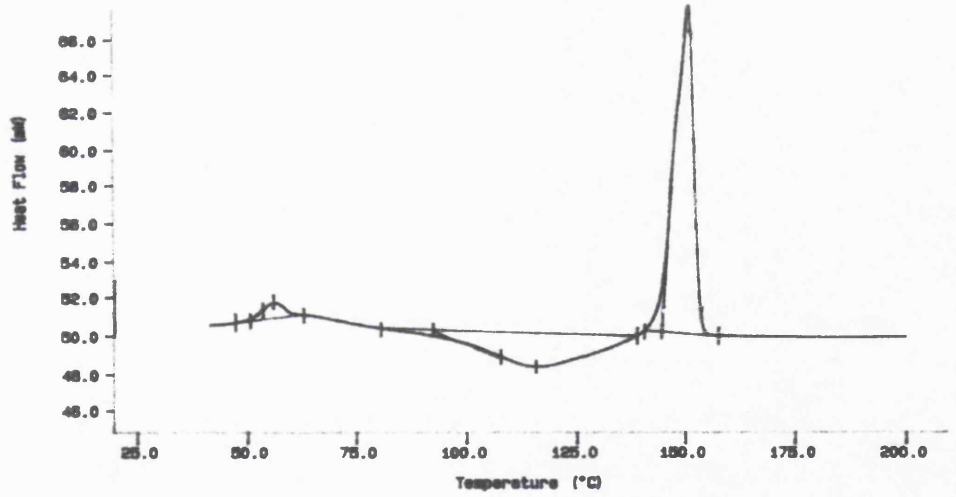

Figure 4.4 *Typical DSC thermogram showing crystallization still taking place in amorphous terfenadine sample tested after exposure to a mixture containing 40: 60 ethanol: water respectively in the isothermal microcalorimeter.*

In this study, at the lower percentages of ethanol in the total vapour, a longer onset for the crystallization of the sample was noted. This can be due to the fact that at lower percentages of ethanol it will take longer to saturate a sample with ethanol vapour and those lower percentages might be insufficient to plasticize the whole sample and bring

its Tg below experimental temperature (T) and trigger complete crystallization of the sample. At the same time, the percentages of ethanol picked up might be localized on the surface or close to the surface of the amorphous beads causing plasticization and crystallization to take place in just those local surface regions with the rest of the sample staying in the amorphous state. In all previous studies, (eg. Buckton et al., 1995b; Ahmed et al., 1996; Briggner et al., 1994; Giron et al., 1997; Angberg, 1995) saturation of the whole amorphous bed of the sample was assumed prior to initiation of crystallization and crystallization took place in the form of a very sharp exothermic peak in the microcalorimeter indicating simultaneous (though not necessarily spontaneous) crystallization of the whole amorphous sample.

4.2.1.2 RESPONSE OBSERVED IN ISOTHERMAL MICROCALORIMETER AS A RESULT OF EXPOSURE TO ETHANOL/ n-PROPANOL MIXTURES:

Since incomplete crystallization was obtained by ethanol/ water mixtures, another approach was tried and entailed the use of a mixture of organic liquids, hence a 50 : 50 mixture of ethanol : n-propanol was used in the Durham tube (using the same glass ampoule method described in section 4.1) in an attempt to crystallize the amorphous samples of terfenadine at 25 °C in the isothermal microcalorimeter.

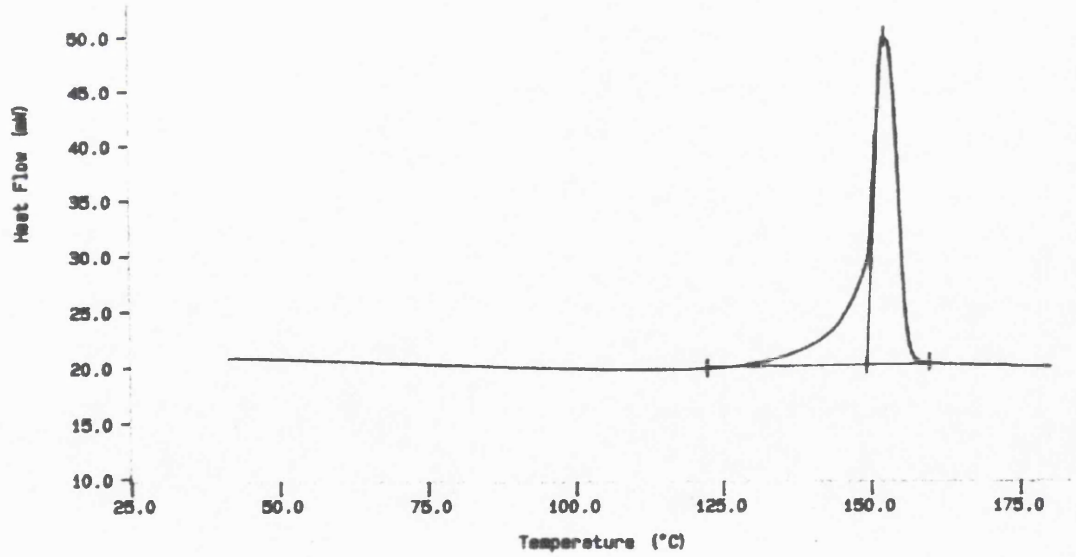

Figure 4.5 *Typical DSC thermogram of slow cooled samples exposed to isothermal microcalorimetry at 25 °C using 50 : 50, ethanol: n-propanol mixture showing complete crystallization has already taken place in the microcalorimeter prior to DSC.*

Table 4.1 DSC results of slow cooled terfenadine beads already exposed to isothermal microcalorimetry at 25 °C and using 50 : 50, ethanol: n-propanol mixture.

Sample Number	Enthalpy of Fusion ΔH_f(J/g)	Melting Point Tm (°C)
1	102.8	150.8
2	101.4	150.6
3	102.9	150.5
4	104.4	150.8
5	99.9	154.8
6	102.4	151.3
7	106.1	151.3
8	104.9	150.1
9	101.9	151.6
10	101.0	152.3
11	100.8	152.4
12	100.4	153.5
13	102.8	153.7
14	100.7	153.2
15	104.9	152.8
16	102.7	153.4
Average	102.5	152.1
S.D.	1.8	1.4

The heating rate in all of the above DSC experiments was 10 °C/min in a temperature range of 20- 180 °C using open aluminium pans under an atmosphere of nitrogen gas. It can be concluded that slow cooled samples of terfenadine were rendered completely crystalline by exposure to a 50 : 50 mixture of ethanol : n-propanol in the isothermal microcalorimeter as indicated by the absence of any glass transition temperature and more accurately by the lack of crystallization exotherms in the DSC trace (Figure 4.5) and by the values of the enthalpies of fusion (Table 4.1) in comparison with that of the completely crystalline sample (Table 3.1 and Table 2.2). The sample again crystallized

into the most thermodynamically stable polymorphic form as seen previously with the samples exposed to ethanol/ water mixtures in the isothermal microcalorimeter (Figure 4.3) before being tested on the DSC (Figure 4.4). In all of those cases however, it cannot be ascertained whether crystallization in the isothermal microcalorimeter resulted in the formation of one of the less stable polymorphs but subsequent heat exposure while testing in the DSC resulted in conversion and crystallization of the sample into the most stable polymorph, or that the most stable polymorph was achieved from the beginning when exposed to ethanol/water mixtures in the isothermal microcalorimeter. From Table 4.1, it can be concluded that the average enthalpy of fusion for the crystallized terfenadine samples (102.5 J/g) is in agreement with the average value obtained of the completely crystalline sample (101.5 J/g as seen in Table 3.1) and with that of 102 J/g as reported by Badwan et al. (1990). A typical microcalorimetry response is shown in Figure 4.6 for a sample of slow cooled terfenadine comprised of 10 beads and crystallized using 50 : 50, ethanol : n-propanol.

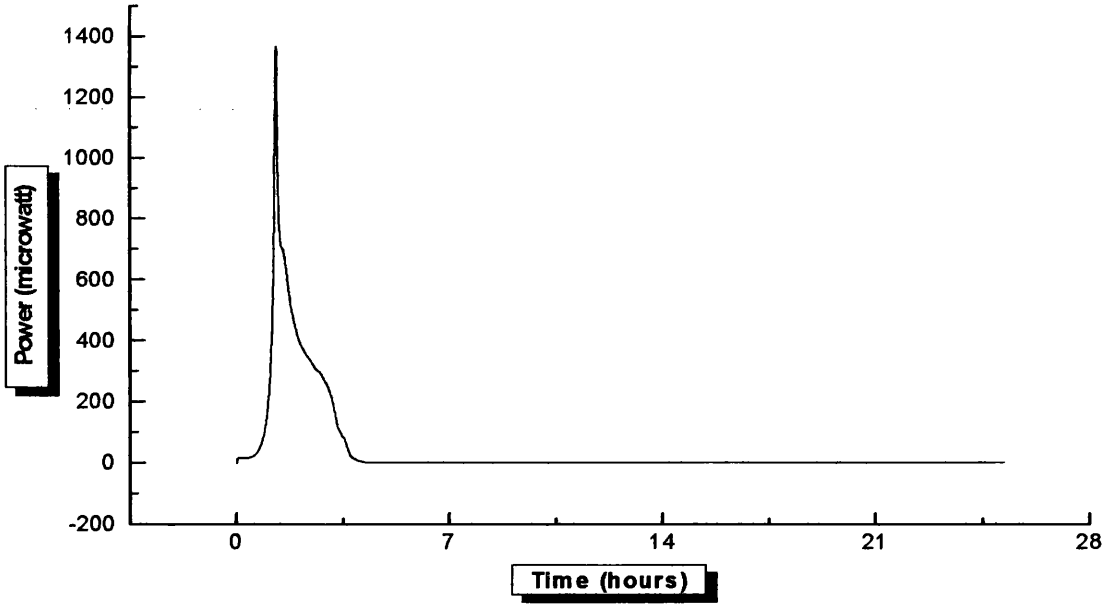

Figure 4.6 *Typical microcalorimetry response for the crystallization of freshly prepared amorphous terfenadine on exposure to 50 : 50, ethanol : n-propanol.*

4.2.1.2.1 INTERPRETATION OF PEAKS SEEN IN ISOTHERMAL MICROCALORIMETRY:

Evaporation of liquids (endothermic) followed by wetting of the sample (exothermic) are almost equal yet opposite processes and hence cancel each other out. This is the case since the vapours are generated and the sample is wetted in the same vessel when using the glass ampoule method termed as a Miniature Humidity Chamber (MHC) (Angberg et al., 1992a,b; Angberg, 1995). Sometimes a tiny wetting response can be noticed as a comparatively small exothermic peak at the beginning of the microcalorimetric trace as reported by Briggner et al., (1994), though this same peak was later attributed by Buckton and Darcy, (1996) to a collapse of the amorphous structure. If water vapours are to be generated outside of the sample vessel, a huge wetting response is expected to be seen as reported by Sheridan et al. (1993) since in such a situation the endothermic vaporization response will be absent. In this case, the wetting peak interferes with the crystallization peak thus making it an obstacle in calculating the crystallization peak separately. The current study involved the use of a MHC but with a mixture of 50: 50 ethanol: n-propanol instead of water and as can be seen in Figure 4.6 and Figure 4.7 there was no obvious exothermic response (might be caused by vapour uptake into the sample) at the beginning of the microcalorimetric trace prior to crystallization when organic vapours were used. This is indicated as no clear deviation from the baseline was noticed as suggested by a close to zero heat flow signal. The main peak (seen in Figure 4.6) is a very sharp exothermic peak, which is indicative of a cooperative process in which the amorphous material crystallizes at the same time or within a very short time (cooperative process of crystallization was explained in section 4.2.1.1). However, since in the current study the exothermic sharp peak (Figure 4.6) was followed by multiple shallow peaks or shoulders (Figure 4.7), it can be argued that a more gradual type of crystallization followed the initial stage of spontaneous crystallization. This second more gradual crystallization can be explained as being due to crystallization of the amorphous regions in the inner parts of the amorphous beads as organic vapours diffuse into the inner parts of the amorphous sample.

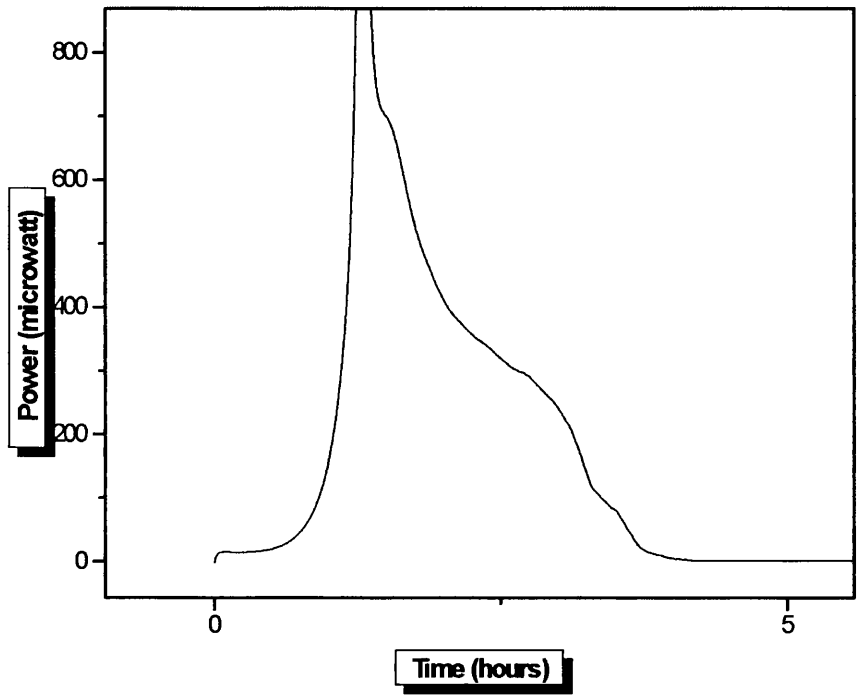

***Figure 4.7** Enlargement of microcalorimetry response for the crystallization of amorphous terfenadine seen in Figure 4.6 showing multiple shallow peaks or shoulders following and connected to the initial crystallization peak.*

In the beginning the core of the beads was less accessible to the vapours but with crystallization starting at the surface, cracks and pores enlarge on the surface of the beads allowing more vapours to pass through and giving a chance for complete crystallization of the amorphous beads to occur. Figure 4.9 shows Scanning Electron Micrographs (SEM) of a sliced incompletely crystallized bead of amorphous terfenadine exposed to ethanol vapours and removed from the apparatus prior to complete crystallization. It is obvious that crystallization of the surface took place while the inner part was still amorphous as indicated by its smooth appearance thus confirming the speculation that crystallization starts on the surface and progresses inwards. The appearance of larger pores subsequent to surface crystallization can be noticed by comparing the surface of a fresh amorphous bead with that of a crystallized bead (Figure 4.8 and Figure 4.10 respectively).

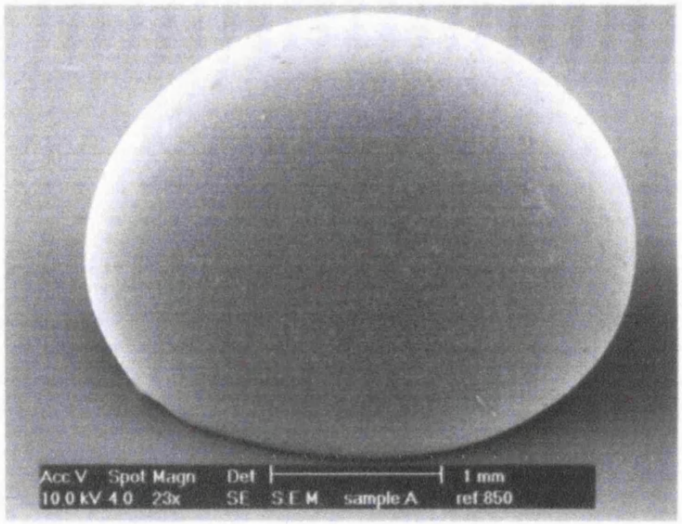

Figure 4.8 *Scanning Electron Micrograph showing the surface of a freshly prepared amorphous terfenadine bead.*

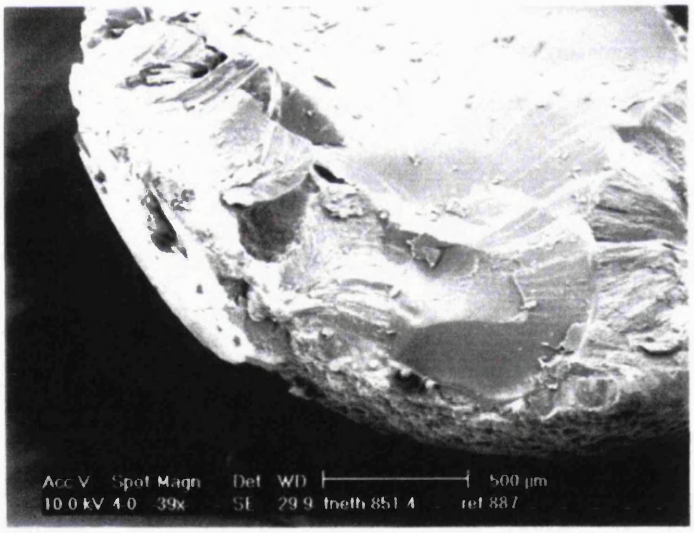

Figure 4.9 *Scanning Electron Micrograph showing the crystallized surface and the amorphous core of a sliced incompletely crystallized terfenadine bead.*

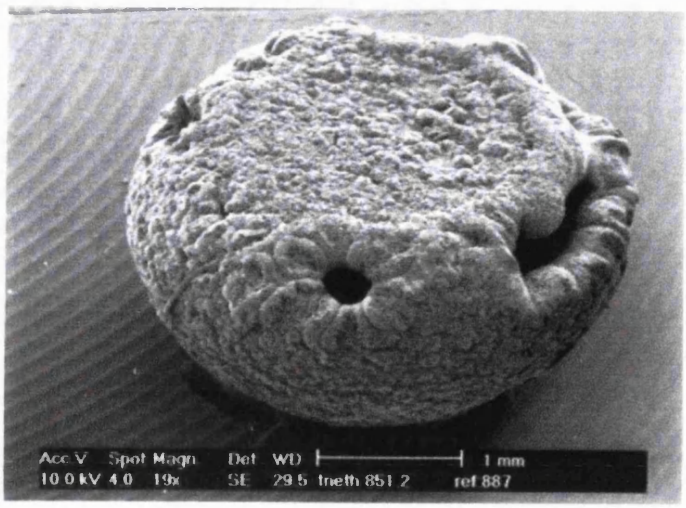

Figure 4.10 *Scanning Electron Micrograph showing the large pores on the surface of a crystallized terfenadine bead.*

Crystallization seems to start at cracks and pores (Figure 4.14) and develops leading to the appearance of larger openings or cracks (Figure 4.10). The formation of those larger pores or cracks allows the vapours to reach the inner parts of the amorphous bead and result in complete crystallization of the amorphous sample deep to the core. It can be postulated that saturation of the surface of the amorphous beads with organic vapours occurs prior to the beginning of crystallization with crystallization starting on the surface of the beads as indicated by the sharp exothermic peak in the microcalorimetric trace (Figure 4.6) and by surface confined crystallization of all the beads if the experiment were to be stopped and samples were inspected by SEM (Figure 4.9).

Figure 4.3 shows the presence of a lag period before the initiation of crystallization and shows that the lag period was increased as the percentage of ethanol in an ethanol/ water mixture was decreased which further suggests that saturation of the surface takes place prior to crystallization. This is the same as the finding of Ahmed et al. (1996) where the lag time prior to crystallization of a hydrophobic material increased as the ethanol content in the Durham tube decreased. From Figure 4.3, it is also noted that the shoulder was not seen in the samples where incomplete crystallization of the amorphous beads took place at ethanol percentages lower than 60% ethanol in an ethanol/water mixture. A shoulder was however detected at 60% ethanol in ethanol/ water mixture, where crystallization was closer to being complete. This further confirms that the presence of these shoulders or multiple shallow peaks is a result of further and slower crystallization taking place which most probably is the result of crystallization of the

inner parts of the amorphous beads. Buckton et al. (1995b) suggested that the presence of multiple peaks or shoulders can be the result of sequenced events of crystallization (exothermic) followed by expulsion of moisture (endothermic) and condensation of expelled moisture back into the salt solution and that although desorption of water and condensation will be approximately equal and opposite thermodynamically, yet they might not necessarily be kinetically synchronized. In this case (Buckton et al., 1995b) multiplicity reflects these kinetic imbalances superimposed on the crystallization event. Lehto and Laine (1997) reported the presence of a shoulder in the microcalorimetric trace showing crystallization of sterotex at different temperatures. Lehto and Laine (1997) argued that the appearance of the shoulder suggested that the crystallization process consisted of at least two overlapping processes. Ahmed et al., (1996) argued that multiple peaks could be interpreted as being due to a more gradual (less cooperative) crystallization taking place superimposed with expulsion of ethanol vapour (endothermic) and condensation of ethanol back into solution (exothermic). It can thus be argued that the presence of shoulders or shallow multiple peaks (Figure 4.7) subsequent to the initial crystallization event of the amorphous beads is a result of a more gradual crystallization superimposed with expulsion of ethanol/ n-propanol vapour and condensation of this vapour back into solution.

4.2.1.3 QUANTIFICATION OF CRYSTALLINITY OF AMORPHOUS TERFENADINE STORED AT DIFFERENT RELATIVE HUMIDITY VALUES:

Since the amorphous terfenadine samples did not crystallize under the influence of humidity over 24 hours at 25 °C, a different approach was used in order to check the time it takes water to plasticize the amorphous sample and bring Tg below the ambient temperature (T) and trigger crystallization.

4.2.1.3.1 METHOD:

Ten beads of slow cooled amorphous terfenadine (prepared as explained in Section 3.2.1.1) ranging in total weight from almost 110 to 125 mg were placed in 3ml open glass ampoules of the isothermal microcalorimeter. The ampoules were left open and stored in desiccators containing saturated salt solutions to give RH values of 44 % (potassium carbonate), 75 % (sodium chloride) and 86 % (potassium chloride) at a

controlled room temperature of 21 °C ±1. This was done in order to check the time it takes the amorphous sample to be plasticized sufficiently by water to start to crystallize and the time it takes (if it can be measured) in order to achieve complete crystallization of the amorphous sample at the different, previously set relative humidities. Schmitt et al., (1996) showed the importance of time scale effects for determining critical moisture levels for crystallization of solids from the amorphous state. They studied the behaviour of amorphous lomotrigine mesylate and their results showed that the sample did not exhibit any crystallization below 60 % RH in an overnight experiment in the moisture sorption microbalance, whereas crystallization took place at a slightly lower RH value (57 % RH) after 14 days of storage. In our study, it was preferred to leave the beads without any crushing and to take a constant number of beads (10) for testing rather than crushing the beads and taking a constant weight of the sample which might change the original amorphous sample and trigger crystallization. Normalization of the data with respect to weight was done in the current calculations as in the case of amorphous materials weight rather than surface area is used since water is absorbed into amorphous regions rather than being adsorbed onto the surface of the solid as is the case in crystalline solids (Zografi, 1988). Samples were tested periodically up to almost 2 years by taking out an ampoule containing 10 beads of the amorphous terfenadine sample, adding a Durham tube containing 50 : 50, ethanol : n-propanol mixture (established to result in complete crystallization of the sample as seen in Section 4.2.1.2). The ampoule was wiped dry from the outside in order to avoid any heat exchange in the microcalorimeter due to water evaporation from the outer surface of the ampoule. Subsequently, the same procedure was used as described in Section 4.1.2.1. In this case however, the amorphous solid that was in the microcalorimeter was that portion that was left in the amorphous state after some sample crystallization took place in the desiccator under the influence of humidity.

4.2.1.3.2 MICROCALORIMETRIC RESULTS OBTAINED AFTER STORAGE OF AMORPHOUS TERFENADINE AT DIFFERENT RH VALUES:

Areas under the curve equivalent to the total heat output were calculated per mg of the sample for all amorphous samples stored at the three RH values used. Results are reported in Table 4.2, Table 4.3 and Table 4.4 for samples stored at 44 % RH, 75 % RH and 86 % RH respectively. The net area reflecting crystallization of the amorphous

sample was calculated as area of the sharp exothermic peak plus the area under the multiple shallow peaks (connected to the main peak) as seen in Figure 4.7. Since the final crystallization of the inner parts in the amorphous sample might be superimposed with desorption of organic vapours from the sample (subsequent to crystallization) and condensation of the vapours (which are two processes that are thermodynamically equal yet opposite), it is a reasonable assumption to include the whole area in the calculations of amorphous content as done by Buckton et al. (1995b). The net calculated area is reasonably accurate in determining the crystallinity of the sample as indicated by the high reproducibility in the data sets of the samples tested after a certain storage time at a certain RH value. This reproducibility is manifested by the low standard deviations obtained for experiments carried out in triplicates as seen in Tables 4.2 – 4.4.

Table 4.2 Microcalorimetric areas under the curve of amorphous terfenadine stored at 44% RH since time of preparation (n = 3).

Time since storage at 44 % RH (Weeks)	1st run (mJ/mg)	2nd run (mJ/mg)	3rd run (mJ/mg)	Average (mJ/mg)	S.D. (mJ/mg)
0	53.5	54.2	54.1	54.0	0.4
1.7	51.1	50.9	51.2	51.1	0.2
3	49.1	48.1	49.2	48.8	0.6
6	48.5	47.9	49.5	48.6	1.5
31	46.2	47.8	46.2	46.8	0.9
55	47.4	47.1	46.8	47.1	0.3
93	46.6	47.3	46.6	46.8	0.4

Table 4.3 Microcalorimetric areas under the curve of amorphous terfenadine stored at 75% RH since time of preparation (n = 2-3).

Time since storage at 75 % RH (Weeks)	1st run (mJ/mg)	2nd run (mJ/mg)	3rd run (mJ/mg)	Average (mJ/mg)	S.D. (mJ/mg)
0	53.5	54.2	54.1	54.0	0.4
1	50.1	49.8	50.3	50.1	0.3
2	48.7	48.9	-	48.8	0.1
3	48.0	47.1	-	47.5	0.6
4	47.5	44.7	47.4	46.5	1.6
6	46.2	46.4	46.2	46.2	0.1
9	45.0	46.3	45.3	45.5	0.7
11	43.4	44.7	45.8	44.6	1.2
55	43.9	44.7	45.6	44.7	0.9
93	43.0	43.8	44.5	43.8	0.8

Table 4.4 Microcalorimetric areas under the curve of amorphous terfenadine stored at 86% RH since time of preparation (n = 2-3).

Time since storage at 86 % RH (Weeks)	1st run (mJ/mg)	2nd run (mJ/mg)	3rd run (mJ/mg)	Average (mJ/mg)	S.D. (mJ/mg)
0	53.5	54.2	54.1	54.0	0.4
0.7	51.0	51.4	51.3	51.2	0.2
2	48.4	48.9	-	48.6	0.4
3	46.9	47.4	46.3	46.9	0.6
4	47.2	46.9	47.6	47.2	0.4
9	44.6	44.9	44.8	44.7	0.1
55	44.0	44.6	-	44.3	0.4
93	43.8	44.1	44.5	44.2	0.3

From the DSC data in Table 3.1, it can be seen that the average enthalpy of fusion of the completely crystalline original terfenadine sample was equal to 101.5 J/g, and that of the crystalline part of the slow cooled terfenadine sample (slow cooled after being left for 5 minutes over the hot plate once melting was achieved) tested immediately after preparation was equal to a maximum of 0.5 J/g (as explained in Section 3.2.2.2), while some tested samples of the slow cooled terfenadine did not show any melt indicating that the sample was completely amorphous. The minimum amorphous content in the slow cooled terfenadine samples based on the DSC data can thus be calculated from equation 4.1 and is equal to 99.5 % (calculations made based on the data in Table 3.5).

$$\% \text{ Amorphous content} = 100 - \frac{\Delta H_{fs} \times 100}{\Delta H_{fc}} \qquad \text{.....Equation 4.1}$$

Where:

ΔH_{fs} is the enthalpy of fusion of the crystalline part in the amorphous slow cooled sample.

ΔH_{fc} is the enthalpy of fusion of the completely crystalline sample.

The amorphous content in the samples tested on the isothermal microcalorimeter can be calculated based on Equation 4.2.

$$\% \text{ Amorphous content} = \frac{A_{un} \times 99.5\ \%}{54} \qquad \text{.....Equation 4.2}$$

Where:

A_{un} is the area under the crystallization peak (calculated per mg of sample) from the microcalorimetry trace of the tested sample.

Table 4.5 Average percentage amorphous content in slow cooled terfenadine after storage at 44%, 75 % and 86 % RH over a period of approximately 2 years as calculated from areas under the curve in microcalorimeter.

Time since storage at designated RH (Weeks)	Average % Amorphous content in samples stored at 44 % RH	Average % Amorphous content in samples stored at 75 % RH	Average % Amorphous content in samples stored at 86 % RH
0	99.5	99.5	99.5
0.7	-	-	94.4
1	-	92.3	-
1.7	94.1	-	-
2	-	89.9	89.6
3	90.0	87.6	86.3
4	-	85.7	87.0
6	89.6	85.2	-
9	-	83.9	82.4
11	-	82.2	-
31	86.1	-	-
55	86.7	82.4	81.6
93	86.3	80.6	81.4

It can be noted from Table 4.5 and Figure 4.11 that at the higher relative humidity values, more of the sample will crystallize leaving behind a lower amorphous content as quantified from isothermal microcalorimetry data. This is in agreement with the action of water as a plasticizer. The experimental measurements in the isothermal microcalorimeter reflect the amorphous content left in the sample after being exposed and crystallized by humidity effect (Table 4.5 and Figure 4.11).

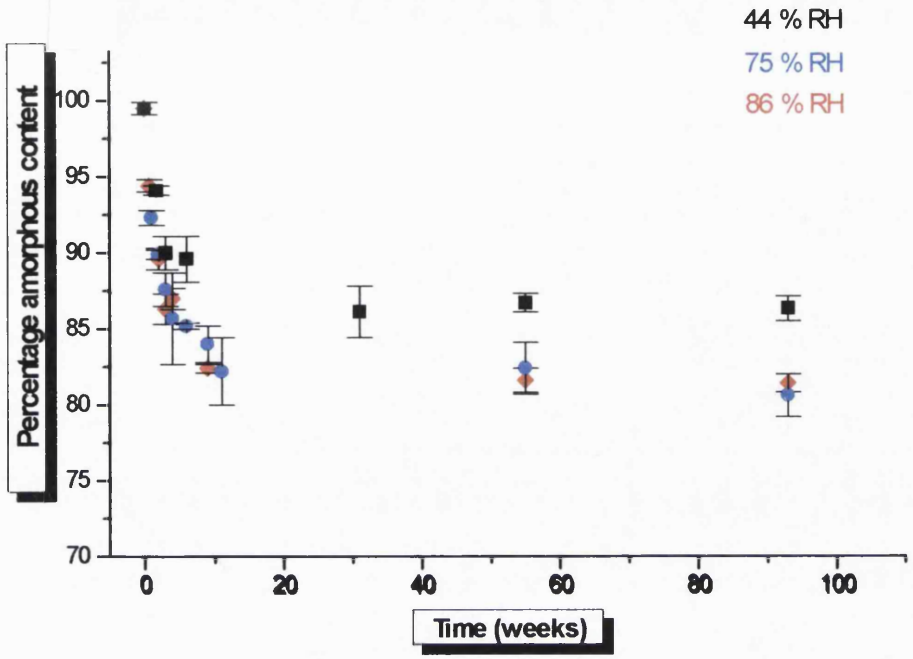

Figure 4.11 *Percentage amorphous content left in the amorphous slow cooled terfenadine samples after being stored in desiccators over different RH values as calculated from microcalorimetry data.*

The effect of moisture content on the amorphous materials was discussed in Section 1.3.2. Amorphous slow cooled terfenadine has a higher amorphous content left in the samples after being stored at 44 % RH (less has crystallized) compared with samples stored at 75 or 86 % RH. At the same time, the amorphous content for samples stored at both 75 and 86 % RH is comparable and there seems to be a levelling off in the water plasticization effect as RH is raised above 75 % (Figure 4.11). This levelling off effect has been discussed by Slade and Levine (1991); Hancock and Zografi, (1993), and can be attributed to a decreased strength of solid-water interactions resulting in a decreased plasticizing efficiency of water and eventually water preferentially associates with itself. Slade and Levine (1991) showed that in the case of hydrophobic materials (termed as water-sensitive solutes), the levelling off effect of the water plasticizing power starts at a lower moisture content than that for hydrophilic (water-compatible) materials. Another levelling off is related to the time effect and which results in an eventual levelling off in the amorphous content in the samples as seen by individual graphs at

each RH value (Figure 4.11). This levelling off indicates a plateau in water plasticization effect, which might be attributed to a time related saturation of possible sites (for water binding on the terfenadine molecule) with water. This saturation at low levels of water uptake might result in an insufficient water content in the sample in order to trigger complete crystallization and hence levelling off in this case is seen at relatively high amorphous content (not less than 80 % after around 2 years of exposure to 86 % RH). Using exponential decay regression analysis, it was found that the sample would stay slightly below 80 % amorphous after 10 years of storage at 44 % RH, and that storage at 86 % RH leaves the sample around 74 % amorphous after 10 years. This indicates a relatively high physical stability of the amorphous sample as reflected in the slow crystallization of the sample into the thermodynamically stable crystalline form. Scanning Electron Micrographs (SEM) of amorphous slow cooled terfenadine beads stored for over a year at 44 % RH are seen in Figures 4.12 and 4.13 and those for samples stored at 86 % RH are seen in Figures 4.14 and 4.15. It can be noted from Figure 4.12 through to Figure 4.15 that the bulk of the sample is still amorphous with some crystallization on the surface of the beads. This is in agreement with the microcalorimetry results, which show the samples to stay basically amorphous with a minimum amorphous content of more than 80 % after being stored in desiccators at different RH values for around two years. The amorphous sample seems to absorb moisture in localized amorphous regions on or close to the surface causing nucleation triggered crystallization to start on the surface. From Figure 4.14, it can be seen that crystallization appears at a crack and around a pore in the amorphous surface suggesting that crystallization started at cracks and pores. From the microcalormetry and SEM results above, it can be assumed that in this case, the levelling off in the water plasticization effect and hence in crystallization of the amorphous terfenadine sample might be due to water accessing the sample only through pores and cracks where crystallization started followed by sealing of some of the pores and cracks with crystalline material (closure of pores can be suggested from Figure 4.15). This can hence lead to prevention of water access to the inner parts of the beads, which results in limited extent of crystallization of the amorphous terfenadine sample. This is in contrast to the enlargement of pores and/or cracks that takes place due to crystallization of the amorphous beads by ethanol/ n-propanol mixture (as seen in Figure 4.10) and which results in further diffusion of organic vapours into the inner parts of the amorphous beads resulting in complete crystallization.

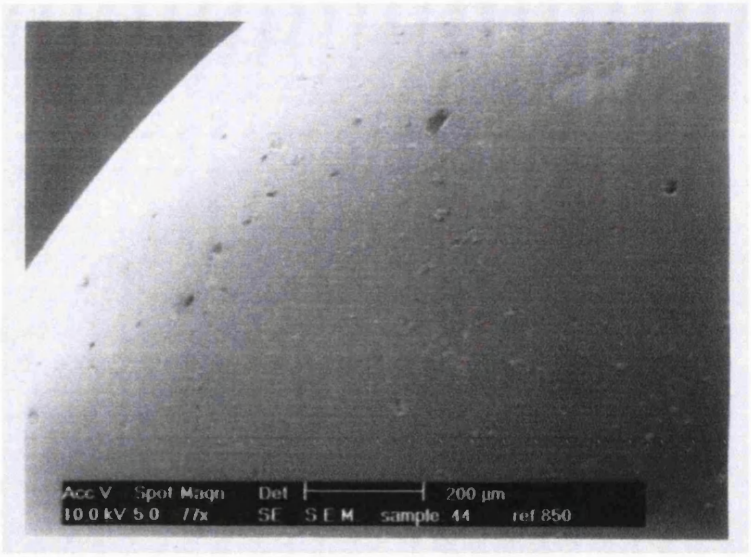

Figure 4.12 *Scanning Electron Micrograph showing the basically amorphous surface of a slow cooled terfenadine bead after being exposed to 44 % RH for over a year.*

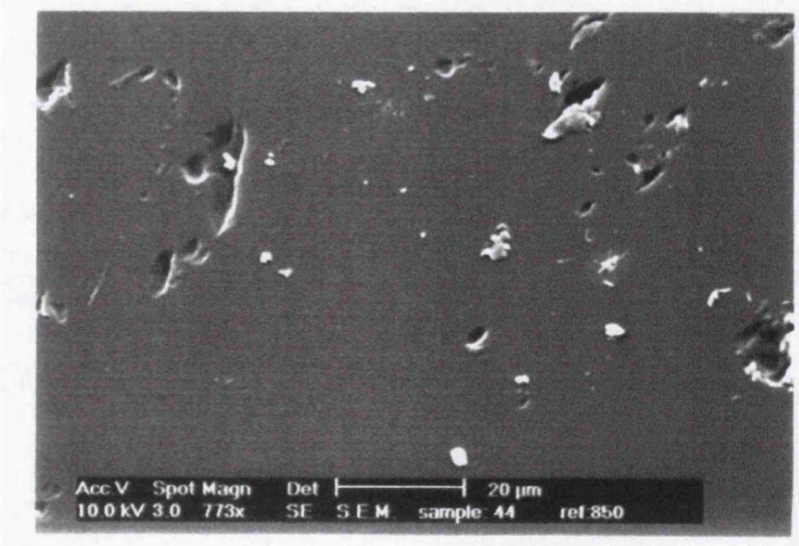

Figure 4.13 *Scanning Electron Micrograph showing the basically amorphous surface of a slow cooled terfenadine bead with pores seen and some crystals formed after being exposed to 44 % RH for over a year.*

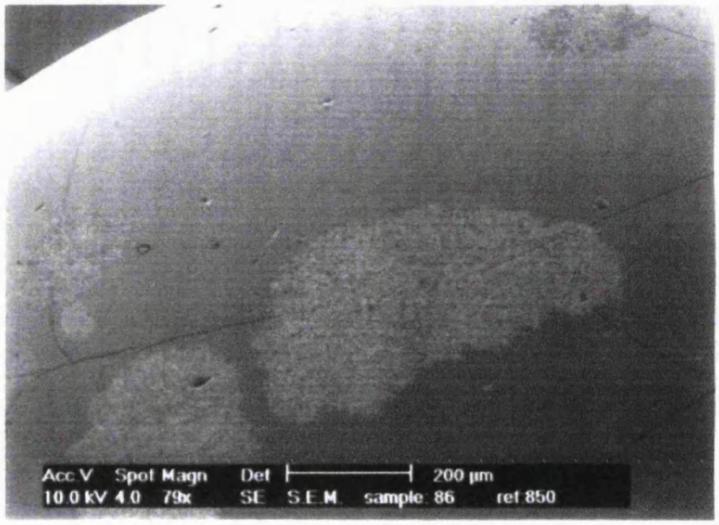

Figure 4.14 *Scanning Electron Micrograph showing the surface of a slow cooled terfenadine bead illustrating crystallization at cracks after exposure to 86 % RH for over a year.*

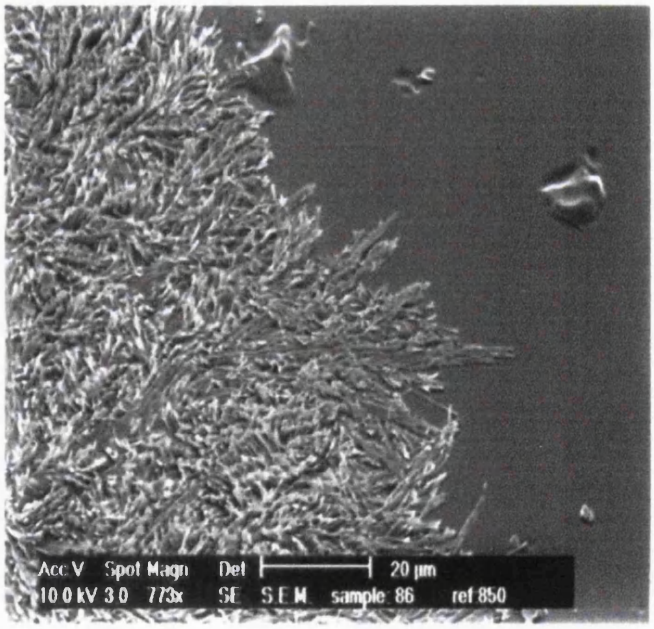

Figure 4.15 *Scanning Electron Micrograph showing the surface of a slow cooled terfenadine bead and manifesting nucleation initiated crystallization on the surface after exposure to 86 % RH for over a year.*

Furthermore, the sites on the terfenadine molecule that are available for hydrogen bonding with water are limited in such a hydrophobic molecule. The assumption that sorbed water is concentrated primarily in polar regions for a hydrophobic material was mentioned by Andronis et al., (1997) for the hydrophobic drug indomethacin where they expected water to be primarily concentrated at the location of the carboxyl groups as well as some of the other polar regions in the indomethacin molecule. In correlation, terfenadine is expected to attract water at the location of the hydroxyl groups in the molecule and if the orientation of the chemical groups subsequent to slow cooling was such that those polar hydroxyl groups were partly imbedded in the inner part of the molecule rather than projecting outwards or that these polar groups were actually situated at the cracks and pores in the terfenadine amorphous beads, then the chemical sites available to hydrogen bond with water are limited and/or are available at sites where water already gets into the sample (pores and cracks). This makes the polar hydroxyl groups unable to reveal or increase the sites available for water to get into the amorphous terfenadine sample.

4.2.2 DYNAMIC VAPOUR SORPTION (DVS) RESULTS:

4.2.2.1 AMORPHOUS TERFENADINE EXPOSED TO WATER VAPOUR:

4.2.2.1.1 AMORPHOUS TERFENADINE EXPOSED TO WATER VAPOUR IN STEPS AND IN RAMP METHODS:

A DVS experiment in steps was carried out on slow cooled terfenadine in order to check the extent to which the sample picks up moisture, the rate at which water uptake takes place and finally to evaluate whether or not the sample equilibrates when held at a certain relative humidity for a certain period of time. The experiment was carried out as described in Section 4.1.2.2 part 1. Figure 4.16 shows the water sorption profile of amorphous terfenadine exposed to a cycle of sorption and desorption in steps in the DVS. The diagram shows that the sample failed to equilibrate at every RH value and rather kept on picking up moisture. This made it impossible to determine the equilibrium moisture content from which we can calculate the expected decrease in the glass transition temperature caused by the retained moisture. Calculations of the extent of depression in Tg caused by the presence of water are based on the Gordon-Taylor

equation (Section 1.3.2.2, equation 1.5). It can also be noted that the sample picked up a low maximum amount of water (ca. 0.1% from Figure 4.17) by the end of the experiment without crystallizing indicating that the tiny amount of moisture that was picked up was insufficient to plasticize the sample and lower its Tg below the ambient temperature of the experiment (T) and thus impart sufficient mobility for crystallization to take place.

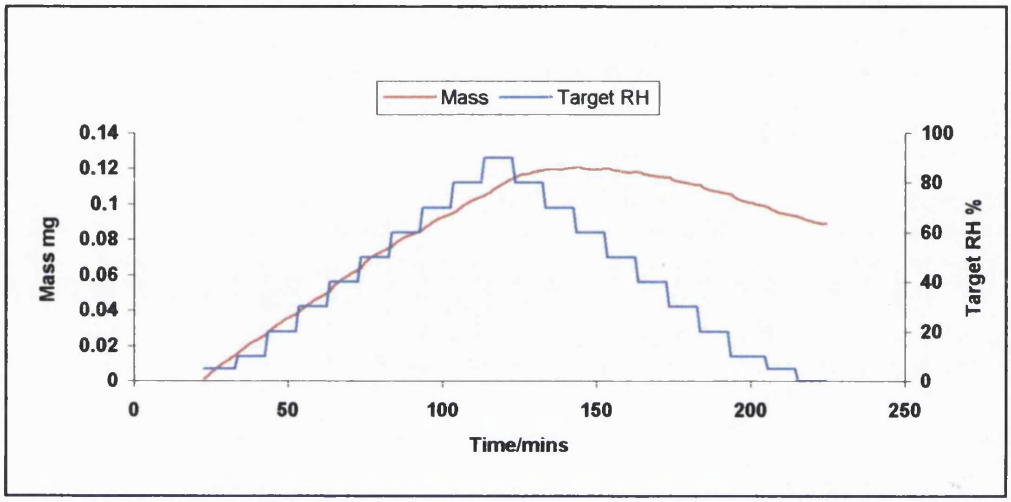

Figure 4.16 *Water sorption profile of amorphous terfenadine exposed to humidity ranging from 0 – 90% RH and back to 0% RH in steps of 10 minutes each at 25 °C.*

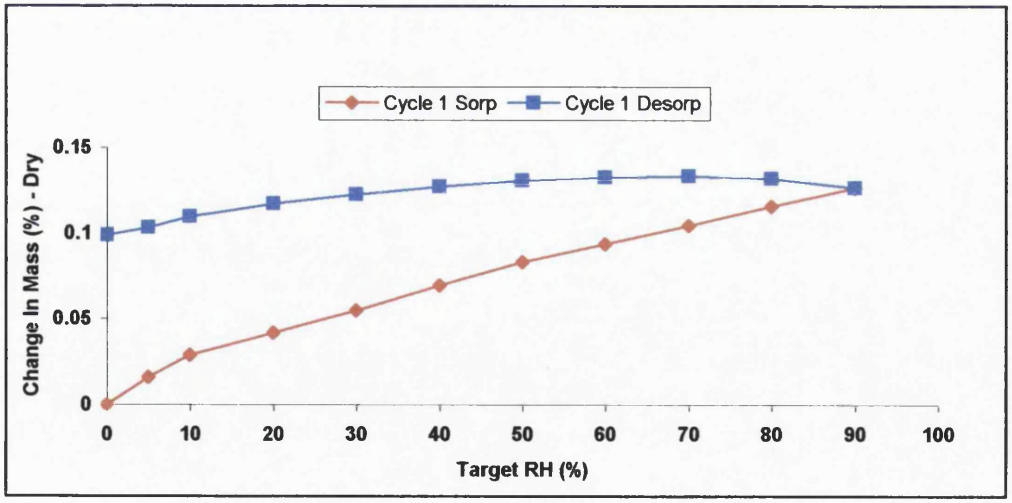

Figure 4.17 *Water sorption isotherm of amorphous terfenadine exposed to humidity ranging from 0 – 90% R and back to 0% RH H in steps of 10 minutes each at 25 °C.*

Figure 4.17 shows the water sorption isotherm of amorphous terfenadine going from 0 – 90% RH and back to 0% RH in steps. The sample did not lose all the moisture it picked up by the end of the desorption step and hysteresis was noted. Zografi (1988) argued that in amorphous solids where water is absorbed rather than adsorbed, hysteresis is usually noticed between the sorption and desorption isotherms and can be best attributed to conformational changes in the structural arrangements of the amorphous molecule as triggered by water plasticizing effects.

In the current study however and since tiny amounts of water are picked up by the amorphous sample (ca. 0.1%), hysteresis is better explained as being due to water entering and leaving the amorphous terfenadine beads only through cracks and pores on the surface of the beads. Hence, water evaporation might be occurring by a slow diffusion process from the pores and cracks on the surface of the beads where limited amount of water was able to escape from the amorphous sample within the time scale of the desorption step of the experiment. This is in agreement with the argument on crystallization of the amorphous terfenadine beads after prolonged exposure to humidity in desiccators where water seems to access the amorphous sample only through pores and cracks showing crystallization starting at those points as argued previously in Section 4.2.1.3.2 and seen in Figure 4.14.

Since carrying out the experiment in steps did not turn out to be of value given that equilibrium could not be achieved, another approach was tried.

Experiments were carried out in a ramp method as described in Section 4.1.2.2 part 2. Three RH values in separate experiments were applied (44%, 75% and 90%). The water sorption profile of amorphous terfenadine using the ramp method was identical in its shape at all three RH values and a typical DVS profile of water sorption at 90% RH is shown in Figure 4.18. The DVS profile shows tiny amounts of moisture being picked up by the sample (ca. 0.6%, n = 4, S.D. = 0.04) while not showing any loss in weight during the sorption step suggesting a lack of sample crystallization. Terfenadine was reported by Badwan et al (1990) to have the ability to form a solvate. Hogan and Buckton (2001a) explained that the absence of loss in weight on the DVS in case of crystalline solids that form multiple hydrates such as raffinose does not necessarily mean a lack of crystallization of the sample. The possibility of crystallizing without losing weight in case of amorphous terfenadine was excluded since a tiny amount of water was picked up by the sample, which was much lower than the percentage needed to form a hydrate. A water percentage of ca. 3.82% corresponds to the formation of a

monohydrate in case of terfenadine. This is clearly much greater than the percentage obtained in the DVS experiments of ca. 0.40 % by the end of the desorption step (knowing that loss in weight was still taking place at the end of the desorption step). Hence the formation of a hydrate was excluded and the lack of loss in weight reflects in fact a lack of crystallization in the sample. The lack of crystallization in the amorphous sample after exposure to 90% RH at 25 °C for 20 hours in the DVS is in agreement with the microcalorimetry results of amorphous terfenadine exposed to ca. 85% RH (using KCl saturated salt solution in the Durham tube in the ampoule method of the isothermal microcalorimeter) at 25 °C for 20 hours where a flat line was seen in the microcalorimetric trace (Figure 4.2 in Section 4.2.1.1).

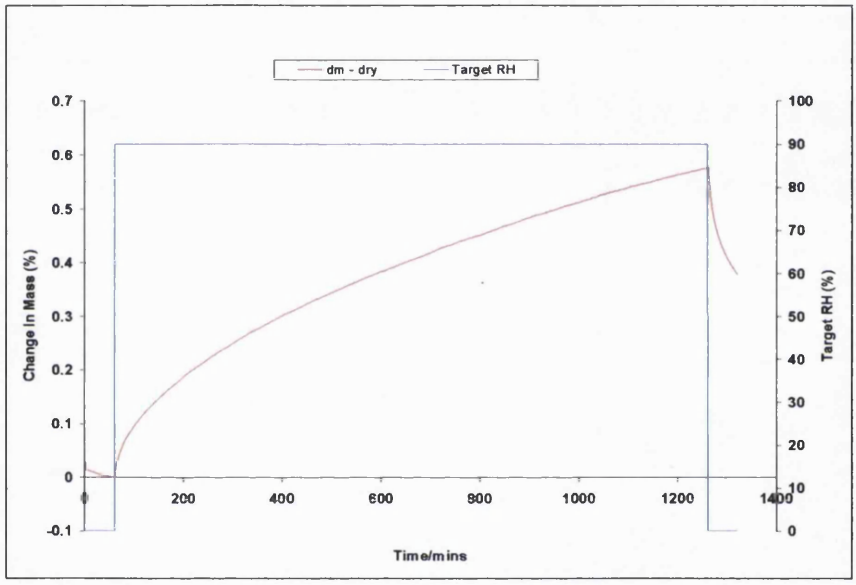

Figure 4.18 *Typical water sorption isotherm for amorphous terfenadine exposed to 90% RH after 1 hour of drying at 0% RH, followed by a 1 hour drying step at 0% RH. (sorption step at 90% RH was for 20 hours) Experiment carried out at 25 °C.*

Visual inspection of the amorphous beads following exposure to humidity in the DVS showed that the samples stayed as transparent glassy beads with no evidence of crystalline appearance subsequent to exposure to the DVS experiments. Being hydrophobic in nature is not sufficient to explain this high resistance to crystallization and the lack of sufficient plasticizing effect of water. Indomethacin, though highly hydrophobic (practically insoluble in water) was strongly plasticized by water and this was indicated by a 10 °C decrease in Tg with a water content of 1% (Andronis et al., 1997). In view of the large size of the beads of the amorphous slow cooled form of terfenadine in combination with its hydrophobic nature, it can be hypothesized that

water under the previously described conditions was only sufficient to absorb into certain areas on the surface or close to the surface of the beads (low percentage mass change of ca. 0.6% by the end of the sorption step) without being able to result in crystallization.

DSC was then used to check if a depression in Tg was noted after exposure to moisture in the DVS. The basic principles of DSC were explained in Section 2.1.3. A DSC study on the amorphous samples of terfenadine was done subsequent to exposure to 90% RH in a ramp method at 25 °C in the DVS (as explained in Section 4.1.2.2 part 2). The DSC experiments were carried out in Perkin-Elmer (DSC 7) using hermetically sealed aluminium pans from 25 – 180 °C at 10 °C/ min under nitrogen atmosphere.

The samples did not show a melting peak of crystalline terfenadine (expected at ca. 152 °C as seen in Table 3.1) and only the amorphous form of terfenadine was present as indicated by the presence of a step in the baseline of the DSC trace (trace not shown) at an average Tg value of 55.7 °C, n = 3, S.D. = 0.6. Tg was calculated as the mid point value with half Cp extrapolated. It can be noted that a slight depression in the Tg was achieved in comparison with the original Tg of slow cooled amorphous samples (ca. 58.5 from Table 3.4). Hence the Tg was still far from the temperature of the experiment (T) after picking up tiny amounts of moisture and thus it was inevitable that crystallization of the amorphous terfenadine sample could not be triggered within the temperature and time scale of the DVS experiment.

4.2.2.1.2 COMPARISON OF THE DVS WATER SORPTION CHARACTERISTICS BETWEEN FRESH AND AGED AMORPHOUS SAMPLES OF TERFENADINE:

Fresh and aged slow cooled amorphous samples of terfenadine were tested for comparison of their water sorption characteristics in the DVS knowing that the previous experiments (Section 4.2.2.1.1) were carried out on freshly prepared amorphous terfenadine samples. Experiments were carried out by placing six beads of amorphous (aged or fresh terfenadine) in the quartz sample pan of the dynamic vapour sorption (DVS, surface measurement systems). Aged samples were those samples left in the desiccator at 0% RH over silica gel for ca. 1 year since the time of preparation while fresh samples were those tested within a month since the time of preparation while being kept at 0% RH over silica gel until the time of experiment. The tested beads were

of relatively different sizes; hence a larger mass would reflect larger beads. The masses of the six beads used in the study ranged from ca 66 to 79 mg. The method used for the DVS characterization was as described in Section 4.1.2.2 part 2. The DVS water sorption profiles at 44 % RH, 75 % RH and 90 % RH are shown in Figures 4.19 – 4.21 respectively. In all of these graphs percentage mass change was computed relative to initial mass (Mo) to enable comparison between different tests. Figures 4.19 – 4.21 illustrate the data and the curve fitting results for the percentage mass change versus time. Curve fitting was applied to data from the start of the sorption step until the end excluding the drying steps and was applied to data of eight runs at each of the three RH values. An expression was derived from a regression analysis of the data, relating the percentage mass change due to sorption with time. The resulting data exhibited a trend, which was first fitted to a square root function but was improved through regression analysis to a function of $T^{0.57}$ (Equation 4.3). This was found to fit data remarkably well.

The expression took the form of:

$$100\,(M-Mo)/Mo = C\,(T-To)^{0.57} \qquad \text{.....Equation 4.3}$$

Where:

M: Mass of sample at time T.

Mo: Initial mass of the sample at time To.

T: Time from the beginning of the experiment.

C: Sorption rate constant calculated relative to initial mass (Mo).

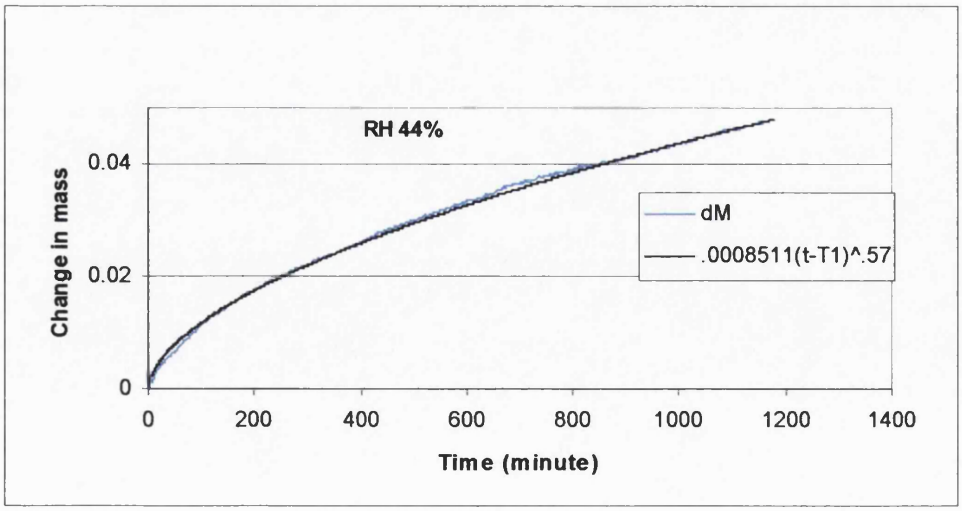

Figure 4.19 *Typical water sorption profile for amorphous terfenadine with curve fitting result for mass change at 44% RH.*

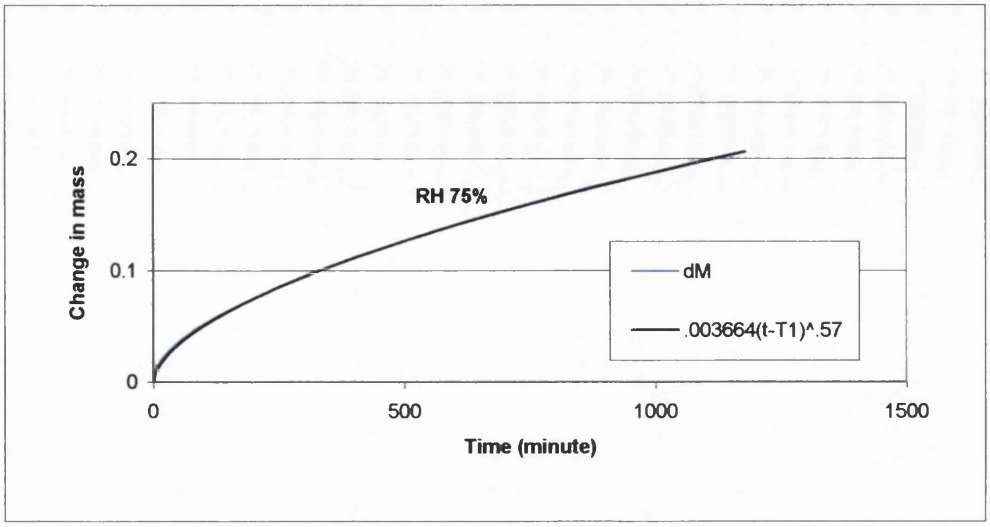

Figure 4.20 *Typical water sorption profile for amorphous terfenadine with curve fitting result for mass change at 75% RH.*

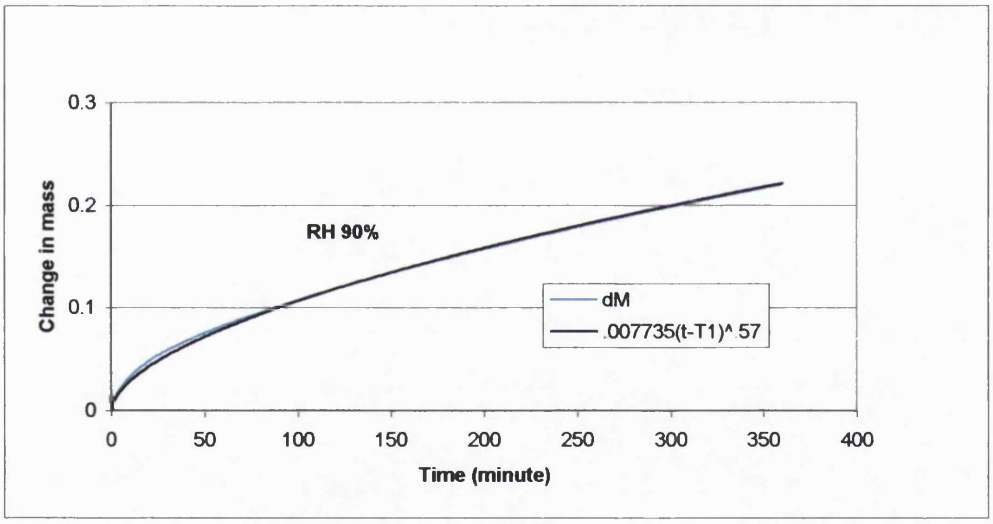

Figure 4.21 *Typical water sorption profile for amorphous terfenadine with curve fitting result for mass change at 90% RH.*

From Figures 4.19 – 4.21, it can be noted that the slow cooled terfenadine picked up moisture at the beginning of the sorption step at a faster rate than later on. This can be explained as being due to the fact that the pores and cracks on the surface of the slow cooled terfenadine bead (seen in Figure 4.14) took up moisture quickly at the beginning since the sample was dried for one hour at 0% RH. Moisture had to diffuse then from the pores and cracks to more inner parts of the bead, which seemed to be a slower process and was slowed even further by the hydrophobic nature of the drug. At the same

time, the chemical groups which might be on the surface of the bead and that were able to take up moisture such as the hydroxyl groups in the terfenadine molecule (Figure 2.13 shows chemical structure of terfenadine) could be already bound to water from the initial amount of water that was sorbed by the amorphous sample. Consequently, the rate of water uptake by the slow cooled terfenadine bead was lowered at prolonged exposure times. Table 4.6 shows the extent of water uptake as percentage from initial mass of amorphous terfenadine in aged and fresh samples. It was found that higher water uptake was seen at higher RH values and in fresh samples when compared to aged samples at the same RH value

Table 4.6 Maximum water uptake as percentage of initial mass (% w/w) in fresh and aged samples of amorphous terfenadine at the three RH values (44%, 75% and 90%), n = 4.

RH	**44%**		**75%**		**90%**	
	Fresh	**Aged**	**Fresh**	**Aged**	**Fresh**	**Aged**
Water	0.18	0.12	0.37	0.26	0.62	0.29
Uptake	0.21	0.08	0.31	0.25	0.60	0.30
(%w/w)	0.17	0.12	0.36	0.24	0.52	0.28
	0.16	0.12	0.30	0.20	0.58	0.30
Average	0.18	0.11	0.34	0.24	0.58	0.29
S.D.	0.02	0.02	0.04	0.03	0.04	0.01

Figure 4.22 shows the sorption rate constant (C) versus % RH for both aged and freshly prepared samples of amorphous terfenadine. The sorption rate constant was obtained by regression analysis (Equation 4.3) of curve fitting data applied on four aged samples and four fresh samples at each RH value. Figure 4.22 shows that aged samples (kept in the desiccator over silica gel at 25 °C for ca. one year) show a smaller sorption rate than that of freshly prepared slow cooled terfenadine samples (prepared fresh and stored over silica gel at 25 °C) with a larger difference in sorption rate between fresh and aged samples at the higher RH values. The difference in sorption rate between fresh and aged samples got smaller as the RH was decreased until reaching 44 % RH where the difference in sorption rate was basically negligible. It is common knowledge that water uptake by crystalline materials is linked to surface area of the particles rather than the sample's mass since water gets adsorbed on the surface of the particles. On the other

hand, for amorphous materials water uptake is more linked to sample's mass as water gets absorbed into the sample (Ahlneck and Zografi (1990). However, in the case of slow cooled terfenadine, the sample being hydrophobic with no significant water uptake and penetration, it is more reasonable to assume that water uptake was associated with surface area rather than the mass and more precisely water accessed amorphous terfenadine through the pores and cracks that are present on the surface of the amorphous beads.

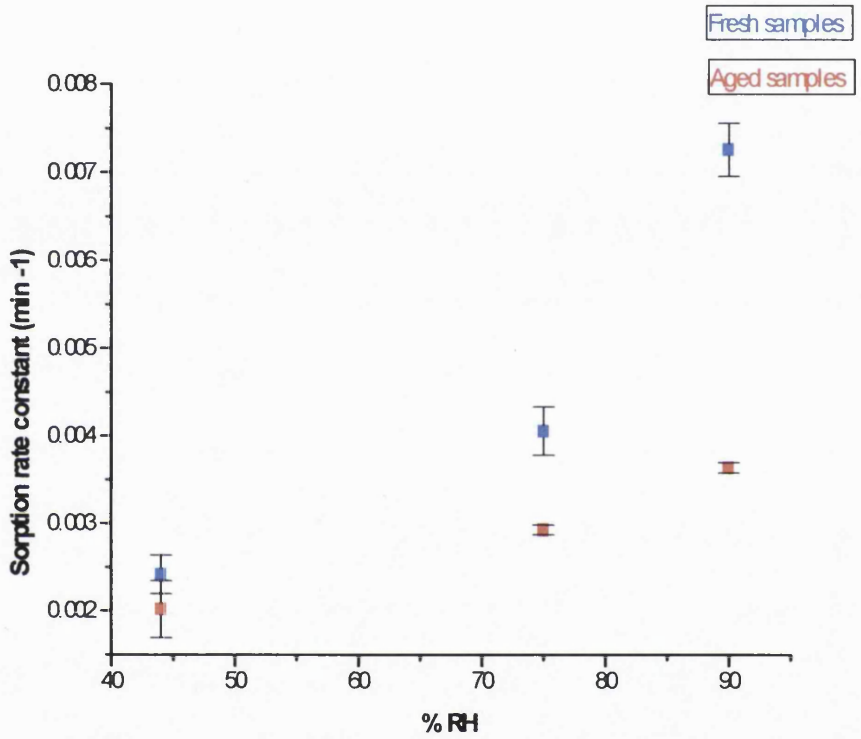

Figure 4.22 *Sorption rate constant versus % RH for both aged and freshly prepared samples of amorphous terfenadine at 44%, 75% and 90% RH.*

Knowing that the extent of water sorption is related to amorphous content in the sample (Hogan and Buckton, 2001b, Buckton and Darcy, 1995b) it might be thought that the difference in the extent of water sorption between aged and fresh samples was related to a higher crystallinity of the aged samples as opposed to the fresh samples (prior to initiation of the DVS experiments). A comparison of crystallinity between fresh and aged slow cooled terfenadine was undertaken using DSC. The results showed a tiny difference in amorphous content with the fresh sample containing ca. 99.5 % and the aged sample containing ca. 99.1% amorphous terfenadine. This difference in

crystallinity does not explain the difference in sorption rate between the two sample types (aged versus fresh).

Thus, the difference in sorption rate between aged and fresh samples suggested that changes were taking place within the amorphous state, which might be changes in surface properties. To further evaluate the difference in surface properties between aged and fresh amorphous terfenadine samples, Scanning Electron Microscopy (SEM) was carried out on both aged and fresh samples of amorphous terfenadine and the micrographs are shown in Figures 4.23a and 4.23b respectively. The basic principles and the procedure followed in carrying out the SEM were described in Section 2.1.8.

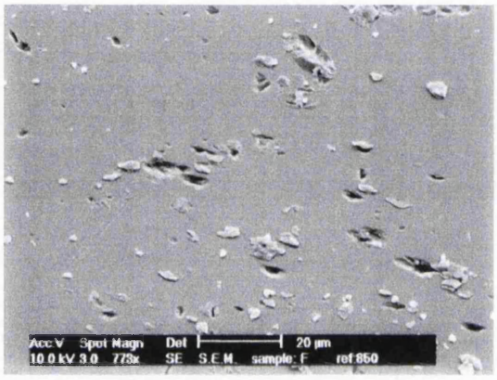

Figure 4.23a *SEM of the surface of fresh slow cooled terfenadine.*

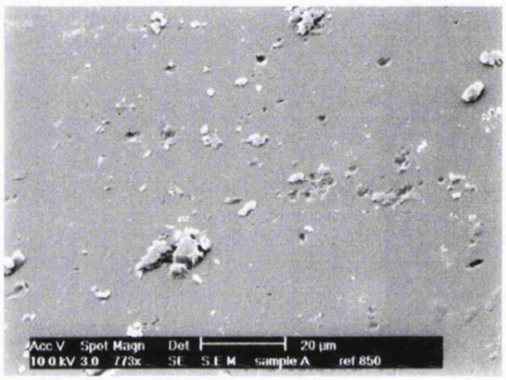

Figure 4.23b *SEM of the surface of aged slow cooled terfenadine.*

From Figures 4.23a and 4.23b, it can be noted that the surface of aged sample (Figure 4.23b) appears to contain relatively smaller pores than the fresh one (Figure 4.23a). This means that a contraction of the amorphous surface leading to closing or narrowing of some available pores might have occurred with aging. This can result in less accessibility to water penetration, which can explain the lower sorption rate and lower extent of water uptake of the aged sample in comparison with that of the fresh one. This also confirms that water accessibility was basically through the pores on the surface of the slow cooled amorphous beads, which is in agreement with the results seen and argued previously with respect to the isothermal microcalorimetry study (Section 4.2.1.3.2).

Hence, this part of the study showed that water sorption for amorphous terfenadine using DVS varied with time according to a function of $T^{0.57}$ (Equation 4.3). This function was shown to be independent of the RH value and sample's age. However, the rate of sorption, which is the constant C in Equation 4.3, was found to be dependent on

both of those parameters (RH and sample's age). This constant (C) was found to increase with RH and decrease with sample's age.

Since upon aging of amorphous terfenadine no significant change in crystallinity was observed, changes in water sorption rate were proposed to be related to changes within the amorphous state notably surface changes.

4.2.2.1.3 EFFECT OF HUMIDITY AND TEMPERATURE COMBINATION IN THE DVS ON THE POTENTIAL FOR CRYSTALLIAZATION OF AMORPHOUS TERFENADINE:

Amorphous slow cooled terfenadine was exposed to a combination of a higher temperature of 50 °C and a humidity of 75% RH (as described in Section 4.1.2.2 part 3). This was carried out in order to investigate if the combination could further enhance molecular mobility and facilitate crystallization of the amorphous terfenadine sample. A typical DVS profile of amorphous terfenadine exposed to 75 % RH for 20 hours at 50 °C after being equilibrated for an hour at 0% RH and ending with a one hour desorption step at 0% RH is shown in Figure 4.24. The experiment was carried out in 4 trials and all exhibited the same profile as the one seen in Figure 4.24.

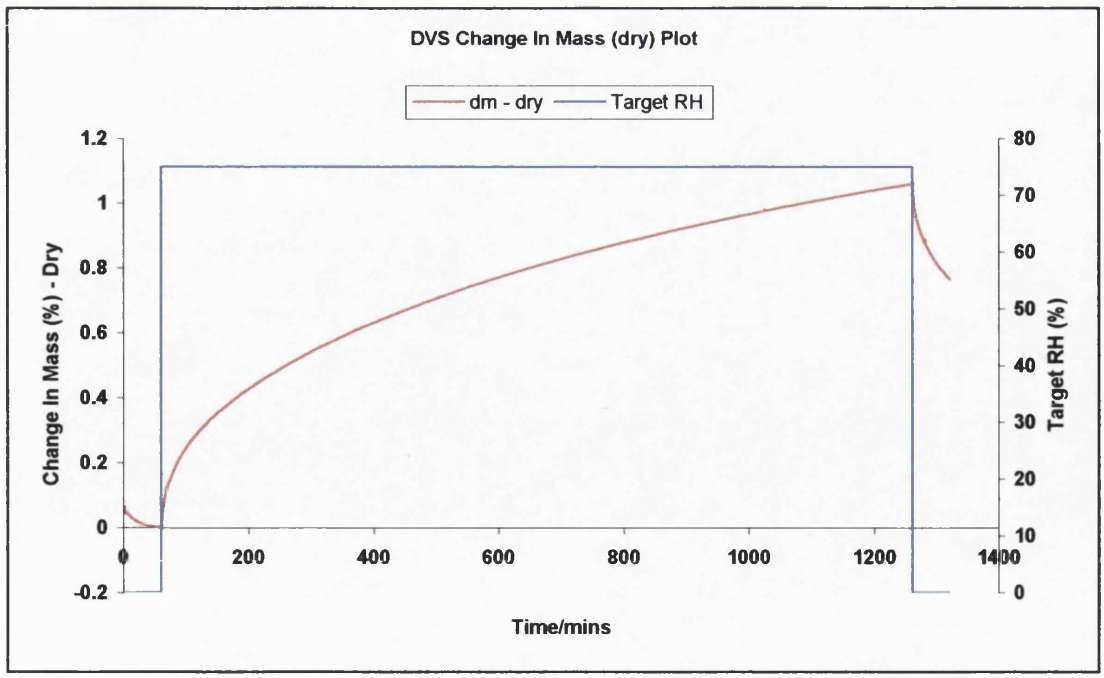

Figure 4.24 *Typical water sorption isotherm for amorphous terfenadine exposed to 75% RH for 20 hours at 50 °C.*

Figure 4.24 shows that amorphous terfenadine picked up moisture while again failing to crystallize at the experimental conditions used. Oksanen and Zografi (1990) investigated the water sorption isotherms of poly(vinylpyrrolidone) at four temperatures.

Amorphous samples were studied on the DSC to determine if any change occurred in the glass transition temperature after exposure to 75% RH at 50 °C in the DVS apparatus. The DSC study on the amorphous samples of terfenadine was carried out following the exposure to 75% RH in a ramp method at 50 °C in the DVS (as explained in Section 4.1.2.2 part 3). The DSC experiments were carried out in a Perkin-Elmer (DSC 7) using hermetically sealed aluminium pans from 25 – 180 °C at 10 °C/ min under nitrogen atmosphere.

The samples did not show a melting peak of crystalline terfenadine (expected at ca. 152 °C) and only the amorphous form of terfenadine was present as indicated by the appearance of a small peak in the baseline of the DSC trace (trace not shown) at an average Tg value of 55.2 °C, n = 4, S.D. = 0.8. The Tg was calculated as the mid point value with half Cp extrapolated. It can be noted that the obtained Tg value was slightly lower than the original Tg of slow cooled amorphous terfenadine samples (ca. 58.5 from Table 3.4) and comparable to that of 55.7 °C (achieved after exposure to 90% RH at 25 °C as seen in Section 4.2.2.1.3). Thus the Tg was still far from the temperature of the experiment (T) after picking up moisture at the experimental conditions used and hence crystallization of the amorphous terfenadine sample could not be detected.

4.2.2.2 AMORPHOUS TERFENADINE EXPOSED TO ETHANOL VAPOUR:

4.2.2.2.1 DVS STUDY RESULTING IN PARTIAL CRYSTALLIZATION OF AMORPHOUS TERFENADINE:

Since crystallization of the amorphous form of terfenadine failed in the presence of humidity even at an elevated temperature of 50 °C, water was replaced by ethanol in the DVS apparatus in an attempt to prompt crystallization of the amorphous sample. Ahmed et al (1996) used 96% ethanol in the isothermal microcalorimeter in order to trigger crystallization of the amorphous form of a drug used for anxiety and panic disorders after the drug failed to crystallize under the influence of humidity. The DVS experiments were carried out as explained in Section 4.1.2.2 part 4a. Figure 4.25 shows

the DVS profiles of fresh amorphous terfenadine beads exposed to ethanol in percentages ranging from 50 – 95 % ethanol in the total gas flow (mixed with nitrogen gas). Each experiment was performed using 6 amorphous beads at either 50%, 70%, 85% or 95% ethanol in the total gas flow (mixed with nitrogen).

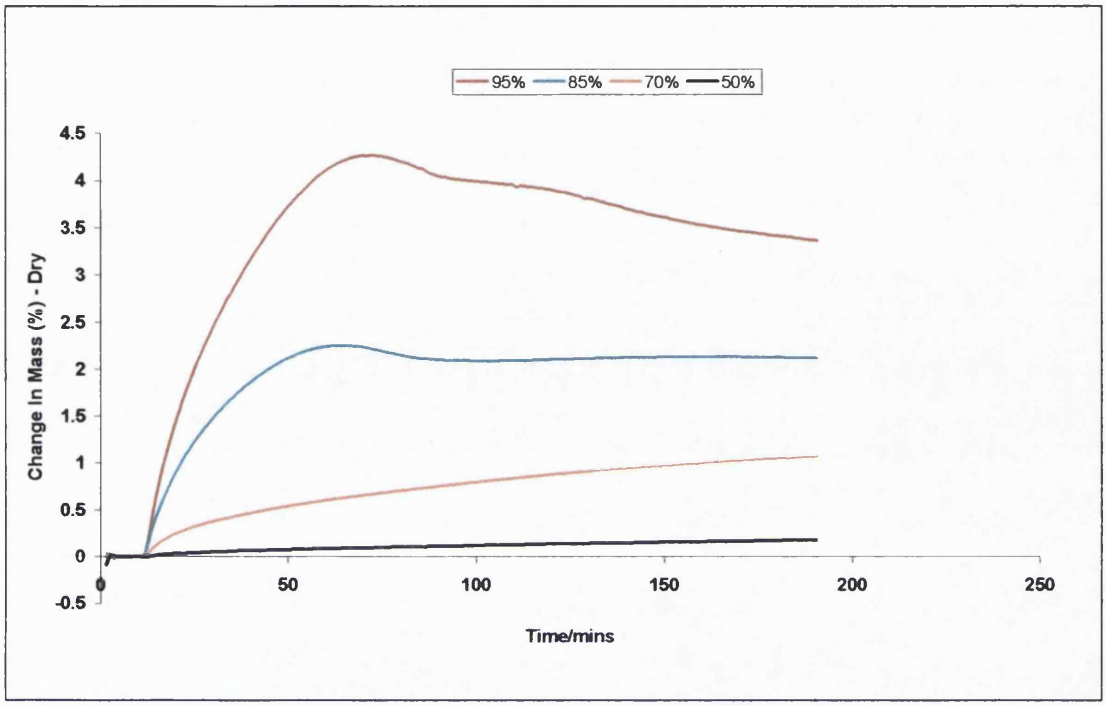

Figure 4.25 *Ethanol sorption isotherm for amorphous terfenadine exposed to varying percentages of ethanol (in the total gas flow) for 3 hours at 25 °C after being equilibrated at 0% RH for 10 minutes.*

As seen in Figure 4.25, the amorphous samples did not show any substantial crystallization (i.e. no detectable mass loss) following 3 hours at 50% or 3 hours at 70% ethanol in the total gas flow (separate experiments were performed and each experiment was carried out at the specified percentage of ethanol for 3 hours). It must be explained though that, minor crystallization could be starting to take place but that the loss in weight caused by crystallization was less than that gained due to sorption of ethanol into the amorphous terfenadine sample. Visual inspection of the amorphous terfenadine samples after exposure to ethanol vapour in a percentage from 50 – 70% showed that the samples were identical in appearance to slow cooled amorphous terfenadine beads (transparent glass beads). Figure 4.25 also shows that the amorphous terfenadine sample

started to crystallize in the DVS at 85% ethanol (indicated by the loss in weight seen in the DVS profile). Samples removed from the DVS following exposure to 85% ethanol were run on the DSC from 25 – 180 °C at 10 °C/ min in hermetically sealed aluminium pans in a nitrogen atmosphere. The samples had both a glass transition temperature at 51.6 °C (n = 4, S.D. = 1.4) and a melting endotherm at 153.9 (n = 4, S.D. = 1.9)) with an average enthalpy of fusion (ΔH_f) of 81.5 J/g. (n = 4, S.D. = 6.9). A typical DSC trace of amorphous terfenadine samples following exposure to 85% ethanol in the DVS for three hours is seen in Figure 4.26.

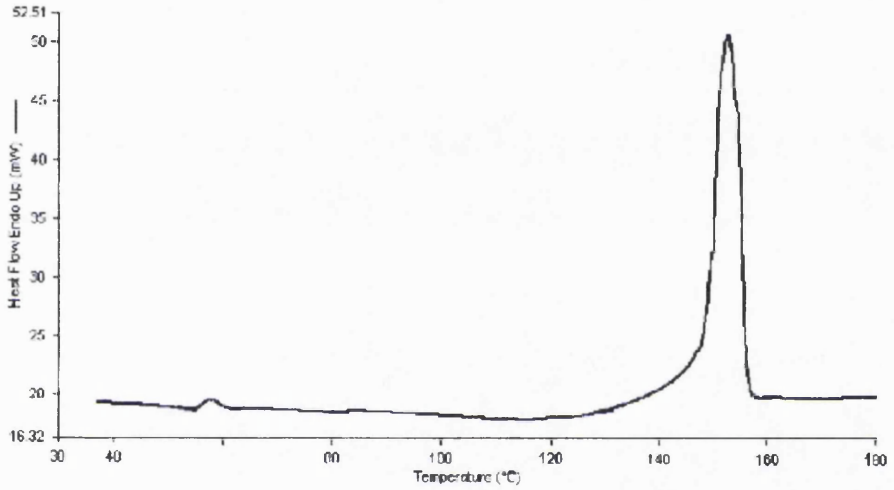

Figure 4.26 *DSC trace of amorphous terfenadine showing a Tg and a melt after being exposed to 85% ethanol for three hours in the DVS at 25 °C.*

The Tg value of the amorphous regions in the terfenadine sample after exposure to 85 % ethanol in the DVS (51.6 °C) was higher than expected from a sample that had gained sufficient molecular mobility whereby Tg was expected to drop below T (25 °C) thus giving the sample a chance to start to crystallize. This might be explained as being due to partial evaporation of ethanol during handling and transfer of the samples from the DVS apparatus to the DSC pans. Thus reducing the amount of ethanol available to impart mobility to the amorphous regions of the terfenadine sample resulting in a higher Tg value on the DSC than would be expected. Another possible explanation is that ethanol was not equally distributed in the amorphous regions of terfenadine and thus some amorphous regions were more plasticized than others in the same amorphous

sample resulting in a net Tg value that was higher than ambient conditions (25 °C) contrary to what was expected from a crystallizing sample.

The enthalpy of fusion of the crystalline part of terfenadine after exposure to 85% ethanol for three hours in the DVS (average value of 81.5 J/g) was lower than that of the completely crystalline sample (ca.102 J/g as seen in Table 3.1). Percentage crystallinity however cannot be calculated from the DSC results based on the enthalpy of fusion since loss of ethanol on the TGA was seen at the region of the melt and this is possibly the cause of the relatively high standard deviation (S.D. = 6.9) in the ΔH_f values. Testing of the samples on the TGA from ambient temperature to 180 °C at 10 °C/ min in open aluminium pans after exposure to 85% ethanol in the DVS showed a weight loss in a temperature range from ca. 90 °C to the end of the run (180 °C). The weight loss had an average value of 0.88% (n = 2, S.D. = 0.02). A typical TGA trace of terfenadine beads subsequent to exposure to 85% ethanol on the DVS is shown in Figure 4.27.

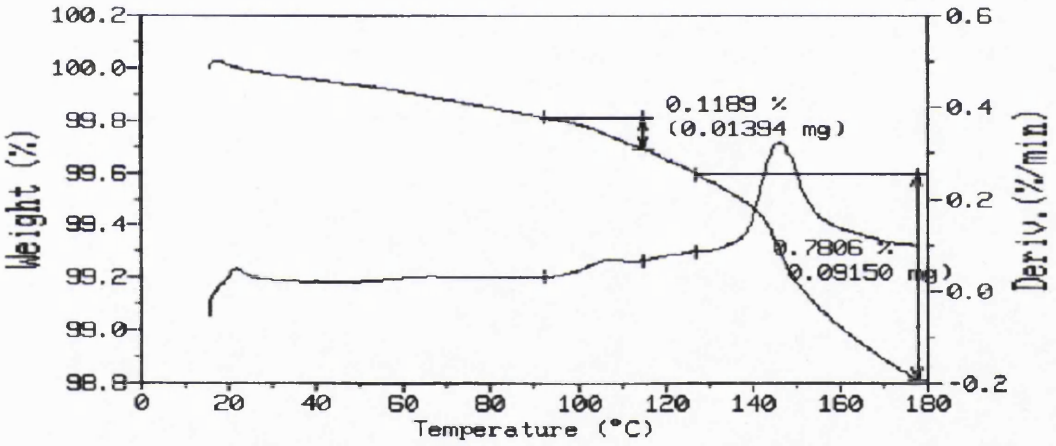

Figure 4.27 *TGA trace of amorphous terfenadine after being exposed to 85% ethanol for three hours in the DVS at 25 °C.*

Scanning electron microscopy (SEM) carried out on sliced and un-sliced crystallized beads showed incomplete crystallization of the beads with crystallization starting on the surface of the beads by nucleation while the inner parts of the beads stayed amorphous (indicated by the smooth appearance) (Figures 4.28 – 4.31). This can be explained as being due to ethanol vapour accessing the amorphous beads through pores and cracks available on the surface of the beads (seen previously in Figure 4.14) triggering crystallization to start at these surface sites. At the same time, the large bead size (ca. 3mm in diameter) and the relatively low uptake of ethanol vapour was only sufficient to

absorb into and plasticize some local surface regions without being sufficient to diffuse into the inner parts of the beads and trigger complete crystallization of the sample within the time scale of the DVS experiment (3 hours). The absorption of ethanol had a plasticising effect giving increasing molecular mobility at the surface relative to the bulk. Increased molecular mobility at the surface relative to the bulk can result in surface initiated crystallization (Andronis et al., 1997).

In Figure 4.28, crystallization around a crack on the surface of the sliced bead can be noticed with the core staying amorphous (smooth appearance). It can also be noted from Figures 4.29 - 4.31 that larger pores form due to surface crystallization of the terfenadine beads (compare with pores of the original, fresh amorphous terfenadine bead seen in Figure 4.23a) but that due to insufficient percentage of ethanol or insufficient exposure time in the DVS at 85% ethanol, further diffusion of ethanol vapours through these larger pores into the inner parts of the beads was limited and thus could not trigger complete crystallization of the amorphous terfenadine beads.

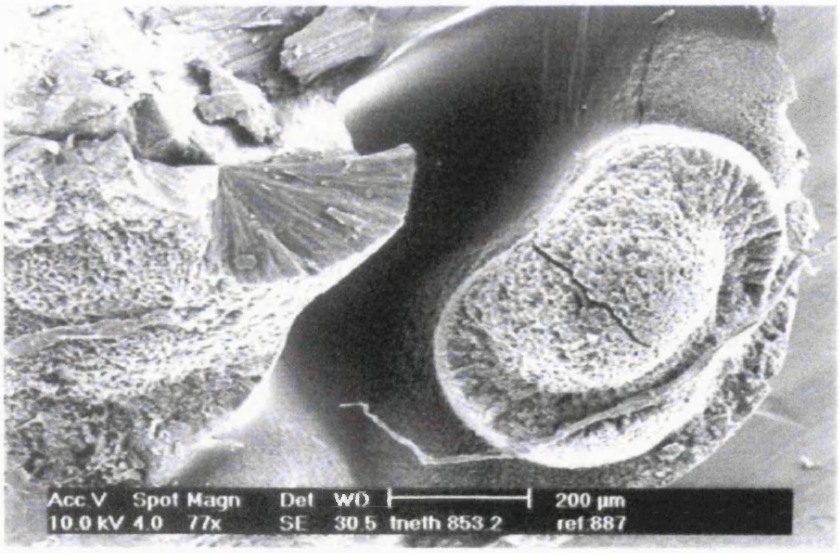

Figure 4.28 *Scanning Electron Micrograph showing the crystallized surface and the amorphous core of a sliced partially crystallized terfenadine bead exposed to 85% ethanol for 3 hours at 25 °C in the DVS.*

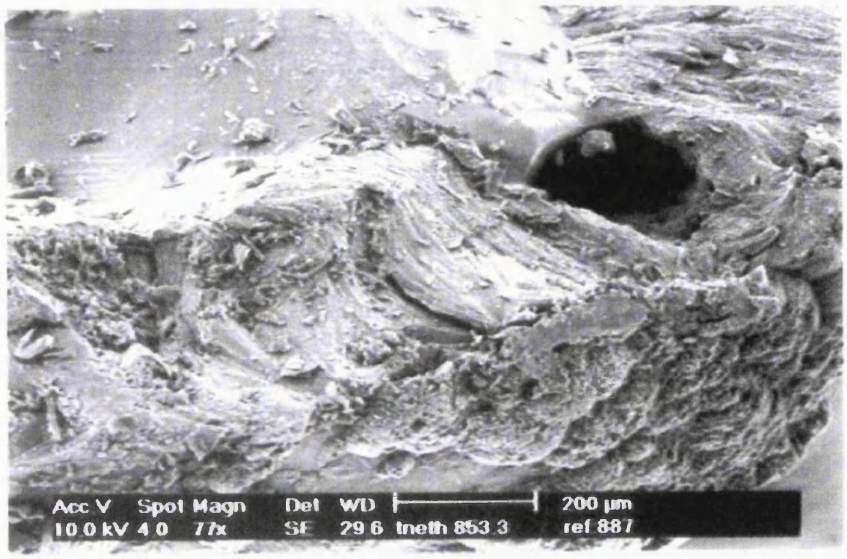

Figure 4.29 *Scanning Electron Micrograph showing the crystallized surface and the amorphous core of a sliced partially crystallized terfenadine bead with a large pore showing on the surface. Sample exposed to 85% ethanol for 3 hours at 25 °C in the DVS.*

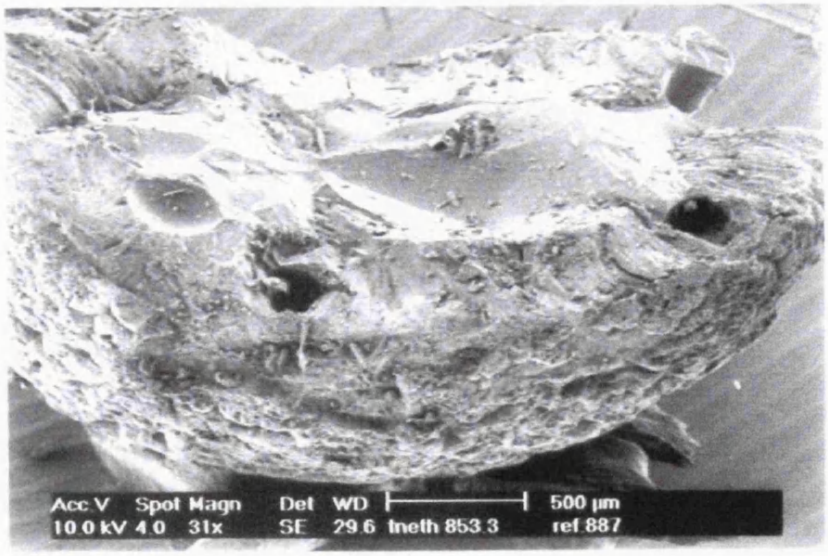

Figure 4.30 *Scanning Electron Micrograph showing the crystallized surface and the amorphous core of a sliced partially crystallized terfenadine bead with the appearance of larger pores forming due to surface crystallization.*

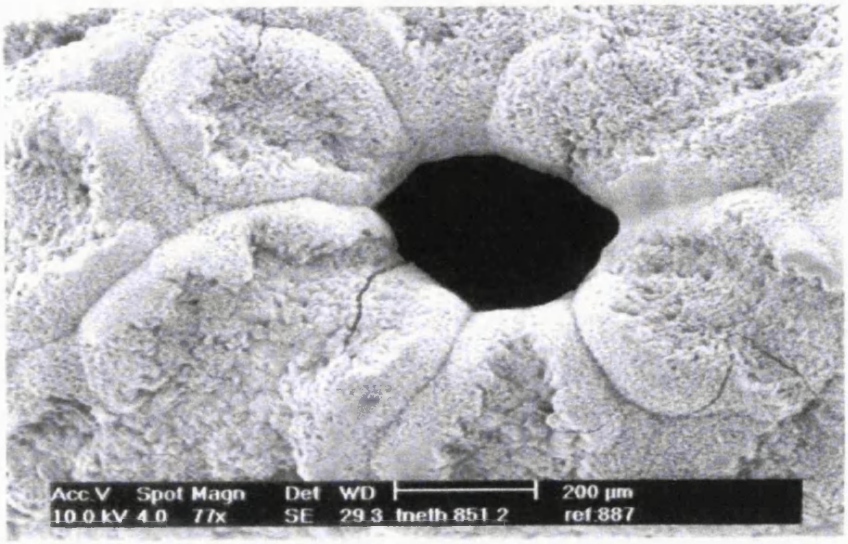

Figure 4.31 *Scanning Electron Micrograph showing a larger pore forming on the crystallized surface of a whole un-sliced terfenadine bead exposed to 85% ethanol for 3 hours at 25 °C in the DVS.*

Amorphous terfenadine samples exposed to 95% ethanol were obviously still crystallizing in the DVS apparatus by the end of the 3 hours, as indicated by the clear continued loss in weight during the sorption step (Figure 4.25). This is in contrast to the weight change at 85% ethanol which appeared to have reached a plateau (presumably due to insufficient ethanol sorption to drive crystallisation beyond the surface of the bead, or due to an exact match between the amount of ethanol that was sorbed by the beads and that which was desorbed from the beads as crystallisation proceeded slowly), and 50% ethanol where mass uptake continued slowly as the bead sorbed ethanol vapour (indicated by the minute increase in mass over the exposure period of 3 hours) while failing to crystallise on the DVS as suggested by the lack of weight loss in its DVS profile (Figure 4.25).

From Figure 4.25, it can be noted that the rate and extent of sorption of ethanol increases as the percentage of ethanol was raised in the total flow of gas. This can be caused by a larger concentration gradient of ethanol between the surface of the bead and that in the operating chamber as the percentage of ethanol increased in the total gas flow.

4.2.2.2.2 DVS STUDY RESULTING IN COMPLETE CRYSTALLIZATION OF AMORPHOUS TERFENADINE:

Ethanol at 95 % in the total gas flow was used in the DVS experiments but for a longer exposure time of 20 hours instead of the previously used 3 hours (resulting in incomplete crystallization of the amorphous terfenadine beads as seen in Figure 4.25). The DVS experiments were carried out as explained in Section 4.1.2.2 part 4b.
Figure 4.32 shows a typical DVS ethanol sorption profile obtained from exposure of fresh terfenadine beads to 95% ethanol (in the total gas flow) for 20 hours.

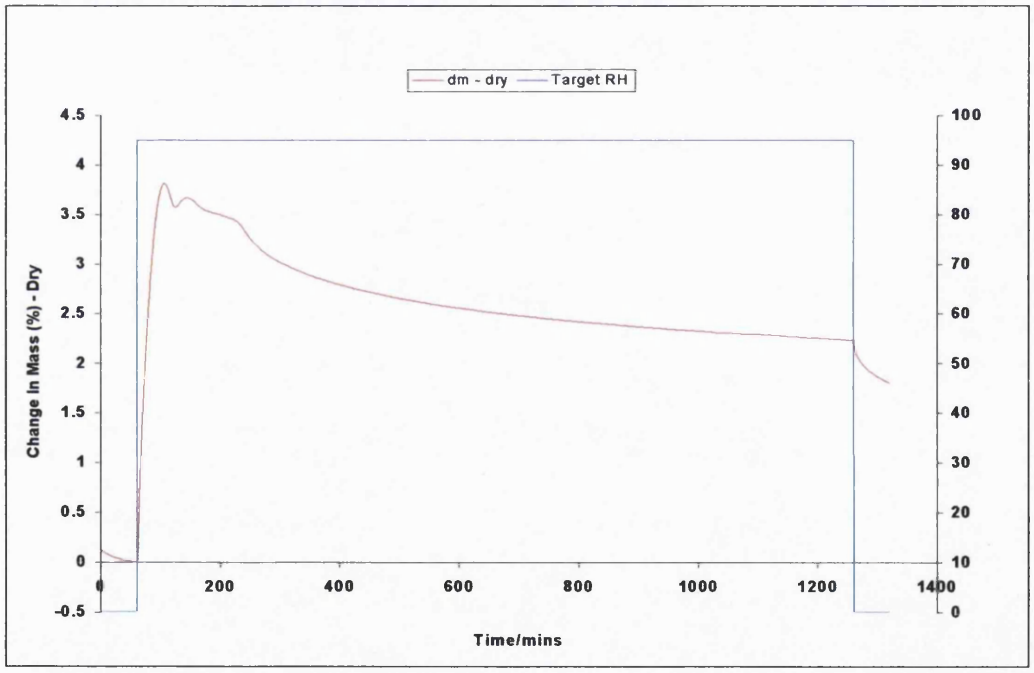

Figure 4.32 *A typical ethanol sorption isotherm for fresh amorphous terfenadine exposed to 95% ethanol (in the total gas flow) for 20 hours after 1 hour of drying at 0% RH and followed by a 1 hour drying step at 0% RH. Experiment carried out at 25 °C.*

DSC was carried out on the crystallized beads from 25 – 180 °C at 10 °C/ min in a nitrogen atmosphere. The DSC thermograms show the absence of a glass transition temperature and only a melting endotherm is observed with an average melting peak of 153.3 °C (n = 4, S.D. = 0.4) and an enthapy of fusion (ΔH_f) ranging from ca. 138-150 J/g (average of 146.0 J/g, n = 4, S.D. = 5.7). The melting point corresponds well with

the melting point of the most stable polymorph of terfenadine (152.4 °C, seen in Table 3.1). The enthalpy of fusion was higher than that of the completely crystalline sample (ca. 102 J/g) with high variation among the samples as judged from the standard deviation. This can be explained as being due to ethanol evaporating from the completely crystallized samples while melting took place which was confirmed by a loss in weight on the TGA (ca. 1.43% of the total sample mass) within the same temperature range (weight loss noted from ca. 110 – 180 °C) of the melting endotherm seen in the DCS and using the same heating rate as that used on the DSC (10 °C/ min). These samples were fresh slow cooled terfenadine samples. When aged slow cooled terfenadine samples were used (stored for ca. one year at 0% RH over silica gel) and exposed to the same experiment in the DVS (explained in Section 4.1.2.2 part 4b), the DSC traces again showed just an endothermic melting peak with the absence of a glass transition temperature when the DSC experiments were carried out from 25 – 180 °C at 10 °C/ min in hermetically sealed aluminium pans. The melting point was almost the same (average of. 152.4 °C, n = 4, S.D. = 2.4), however, the enthalpy of fusion (ΔH_f) reached an average value of ca. 97.5 J/g (n = 4, S.D. = 1.0). The average enthalpy of fusion corresponded to a sample that was ca. 96 % crystalline. However this value was not exact as testing of the aged sample on the TGA after exposure to 95% ethanol in the DVS showed a weight loss of ca. 0.8 % overlapping with the melting endotherm seen on the DSC (weight loss noted from ca. 90 – 180 °C). TGA was carried out from ambient temperature to 180 °C at 10 °C/ min in open aluminium pans. Comparison of the enthalpy of fusion and the weight loss results seen on the TGA between fresh and aged slow cooled terfenadine beads suggest that the smaller pores seen in the aged sample when compared with those of the fresh sample (as seen in Figures 4.23a and 4.23b) resulted in less diffusion of ethanol into the aged terfenadine beads. Hence, the higher weight loss and higher enthalpy of fusion noted for the fresh samples suggest that a loss in weight due to the presence of ethanol was the one responsible for the higher enthalpy of fusion (146.0 J/g) than that of a completely crystalline sample (ca. 102 J/g from Table 3.1).

Consequently, it can be assumed that the amorphous sample of terfenadine following exposure to 95% ethanol for 20 hours was basically crystalline, but an exact value of crystallinity could not be determined. A typical DSC trace of amorphous terfenadine beads after exposure to 95% ethanol for 20 hours in the DVS is seen in Figure 4.33.

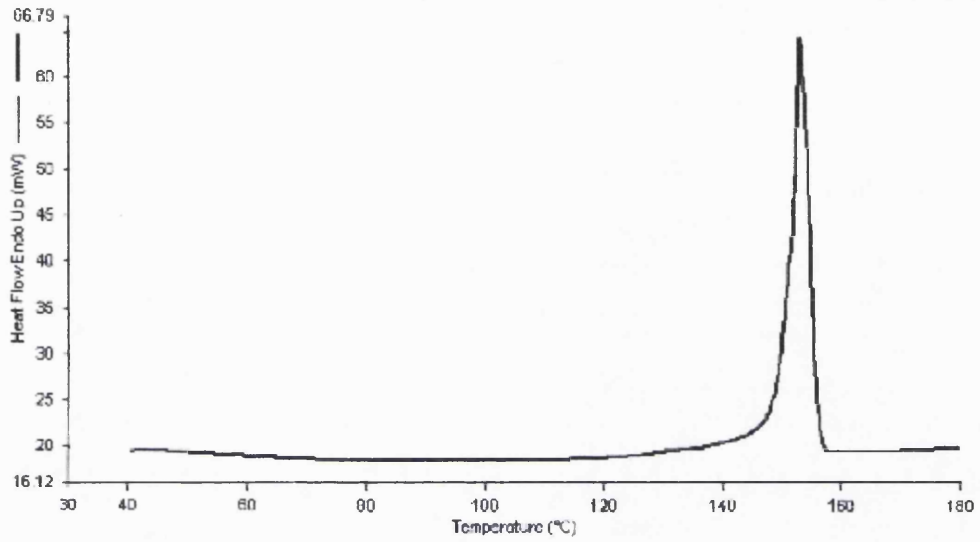

Figure 4.33 A typical *DSC trace of amorphous terfenadine after being exposed to 95% ethanol for 20 hours in the DVS at 25 °C.*

Figure 4.32 shows that following the first sorption of ethanol seen in the DVS profile; an initial decrease in weight was followed by a slight weight gain at ca. 120 minutes, which precedes the continuous slow weight loss in the sorption step. This type of response was reproducible and thus provided information concerning the mechanism of crystallisation. It was clear that there was an initial crystallisation event (the first peak at ca.120 min) followed by an enhanced sorption and then a much more protracted crystallisation. SEM photomicrographs show that the material started to crystallise on the surface (Figures 4.28 and 4.29), thus the first event can be interpreted as being due to initial surface crystallization of the amorphous beads (first decrease in weight). It was also clear from SEM photomicrographs (Figures 4.30 and 4.31) that certain pores become extremely large during crystallisation compared to the very small size of pores that existed in the beginning (Figures 4.23a and 4.23b for fresh and aged samples respectively). Consequently, it can be hypothesised that crystallisation started at the surface, leading to the change in local geometry (the crystal having greater density than the amorphous form), which in turn gave rise to the formation of larger pores in the crystallizing beads. The formed pores allowed further sorption of ethanol into the inner parts of the beads (weight gain) resulting in additional crystallization of the inner parts

of the beads (second continuous weight loss). It can be seen from SEM micrographs of sliced crystallized beads (Figures 4.34 – 4.35) that both the surface and the inner core of the crystallized beads turned crystalline suggesting an almost complete crystallization of the samples as suggested from the DSC data of freshly prepared amorphous terfenadine beads exposed to 95% ethanol for 20 hours at 25 °C in the DVS. Figures 4.36 and 4.37 show crystallization on the surface of the whole terfenadine bead with the appearance of larger pores than those found in the original amorphous sample. Figure 4.38 shows crystallization on the surface of a whole terfenadine bead. Complete crystallization of the amorphous fresh terfenadine beads subsequent to exposure to organic vapours at 25 °C for 20 hours was proven by isothermal microcalorimetry with crystallization (as in the DVS) occurring in stages (indicated by the sharp peak which is followed by tiny peaks or shoulders in the isothermal microcalorimetry trace) (Sections 4.2.1.2 and 4.2.1.2.1).

Figure 4.34 *Scanning Electron Micrograph of a sliced terfenadine bead showing complete crystallization down to the core after exposure to 95% ethanol for 20 hours at 25 °C in the DVS.*

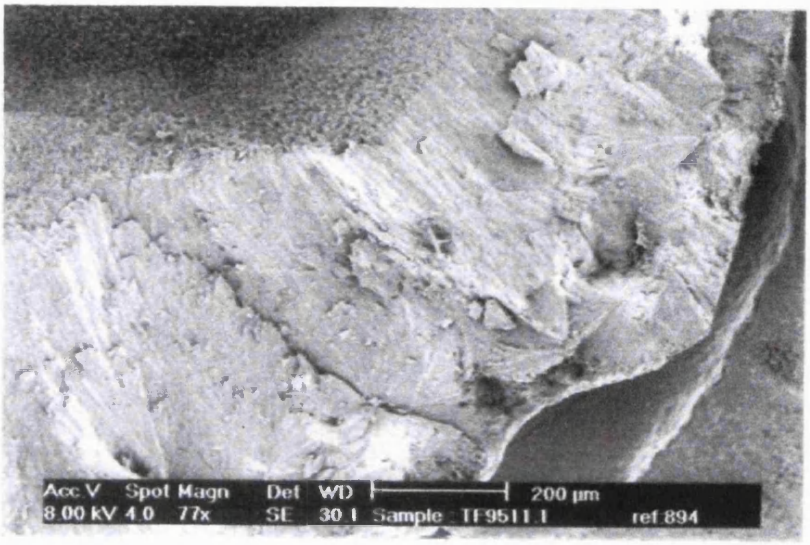

Figure 4.35 *Scanning Electron Micrograph of a sliced terfenadine bead showing complete crystallization down to the core after exposure to 95% ethanol for 20 hours at 25 °C in the DVS.*

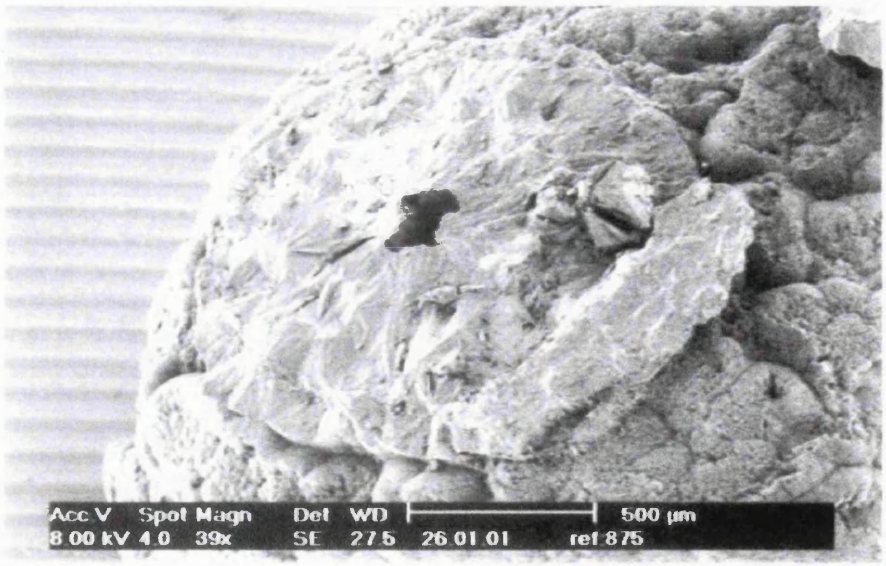

Figure 4.36 *Scanning Electron Micrograph of a whole terfenadine bead showing crystallization with a pore on the surface after exposure to 95% ethanol for 20 hours at 25 °C in the DVS.*

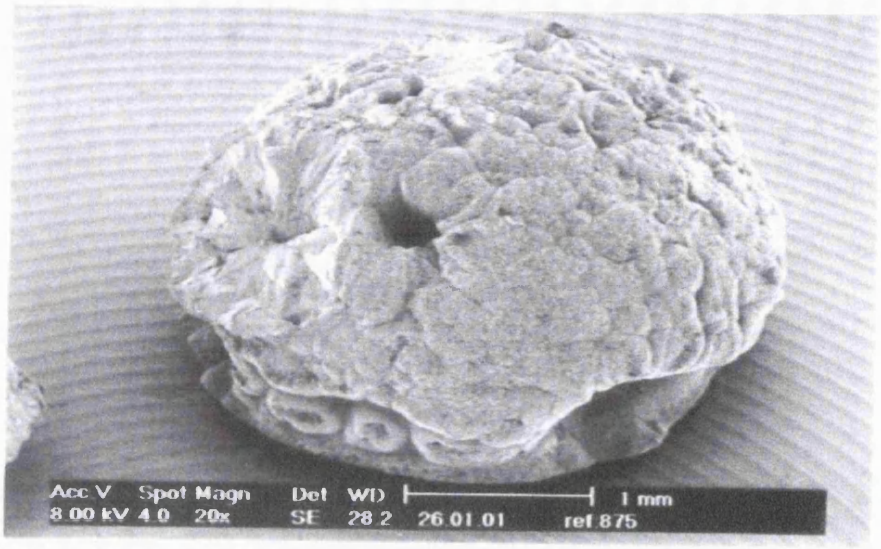

Figure 4.37 *Scanning Electron Micrograph of a whole aged terfenadine bead showing crystallization with appearance of larger pores on the surface after exposure to 95% ethanol for 20 hours at 25 °C in the DVS.*

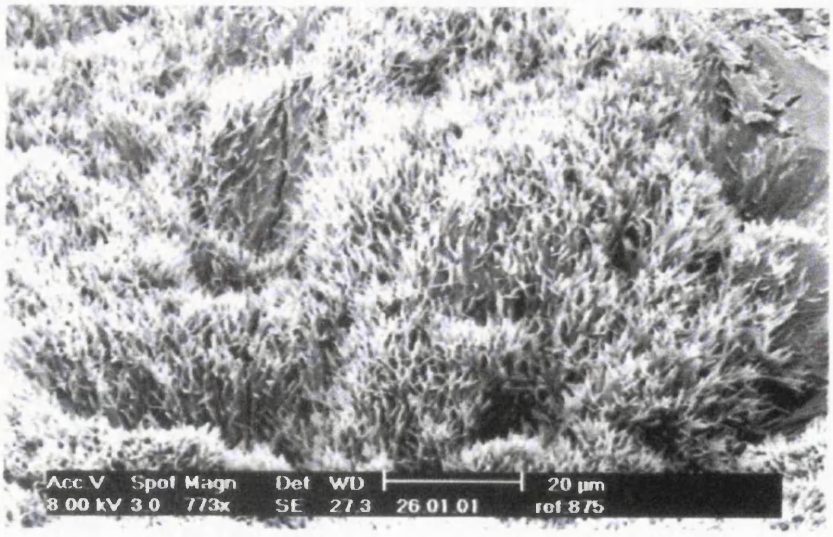

Figure 4.38 *Scanning Electron Micrograph of a whole terfenadine bead showing intensity of crystallization on the surface of the bead after exposure to 95% ethanol for 20 hours at 25 °C in the DVS.*

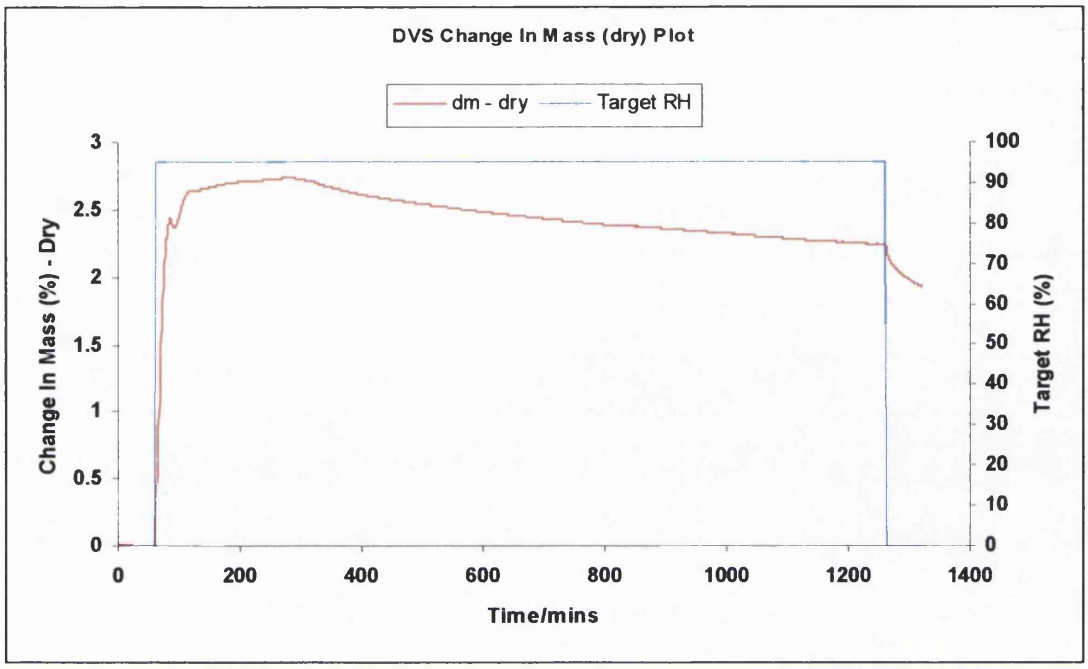

Figure 4.39 *A typical ethanol sorption isotherm for aged amorphous terfenadine exposed to 95% ethanol (in the total gas flow) for 20 hours after 1 hour of drying at 0% RH and followed by a 1 hour drying step at 0% RH. Experiment carried out at 25 °C.*

The DVS profiles obtained in both fresh and aged amorphous terfenadine samples are shown in Figures 4.32 and 4.39 respectively. It can be seen from Figures 4.32 and 4.39 that the amount of ethanol that was sorbed by the amorphous sample was higher in the fresh (average value of ca. 3.9 %, n = 10, S.D. = 0.4) than in the aged sample (average value of ca. 2.7 %, n = 2, S.D. = 0.1). The difference in crystallinity between the fresh and aged samples does not explain the difference in the extent of sorption between the two samples (as explained earlier in Section 4.2.2.1.2). Thus based on the fact that differences in the sizes of the pores (available on the surface of the amorphous beads) exist with the fresh beads possessing larger pores than those available on the surface of the aged beads, it can be hypothesized that easier diffusion of ethanol and better accessibility to the amorphous parts was achieved in the fresh samples resulting in a more complete crystallization than in the case of the aged samples. It can also be noted that after the initial loss in weight due to crystallization a more gradual and protracted increase in weight was noted in the aged sample as caused by the rush of ethanol

through the relatively smaller pores on the surface of the terfenadine beads than in the case of the fresh samples. SEM photomicrographs of crystallized samples at 95% ethanol for 20 hours in the DVS did not show the differences in pore sizes between aged and fresh samples. This might be due to crystallization causing enlargement of the pores as it progresses thus making the differences between fresh and aged samples in the sizes of their enlarged pores unnoticeable by SEM subsequent to crystallization (compare Figure 4.10 with Figure 4.37). However it can be seen from Figure 4.40 That in the case of aged samples, a closure of a pore with crystalline material could be seen (which was not seen in any of the fresh samples) which might suggest that closure of some of the smaller pores of the aged samples resulted in sealing of the pores which reduced the access of ethanol to the interior of the bead and resulted in incomplete crystallization of the aged samples as opposed to the fresh samples.

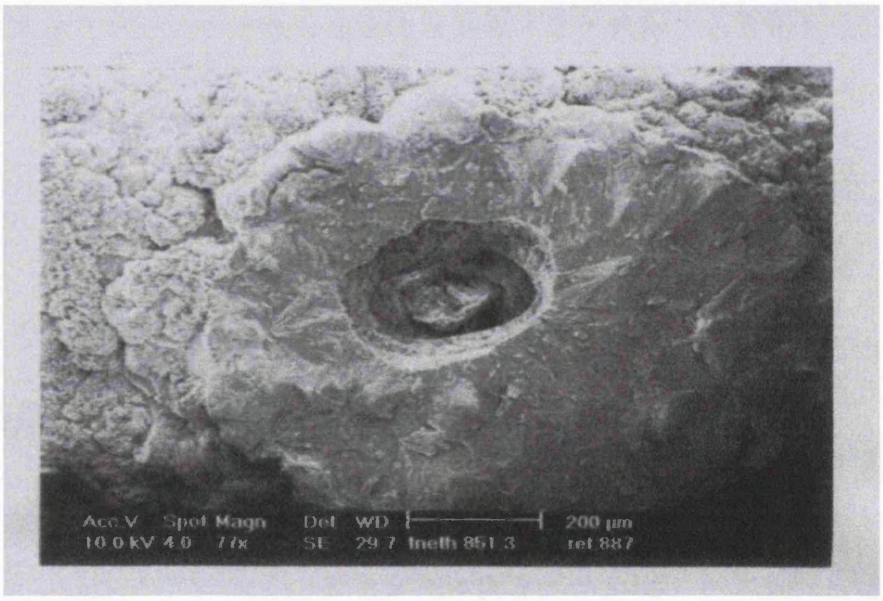

Figure 4.40 *Scanning Electron Micrograph of a whole aged terfenadine bead showing crystallization with closure of a large pore on the surface after exposure to 95% ethanol for 20 hours at 25 °C in the DVS.*

4.3 DISCUSSION:

Amorphous terfenadine was shown to be highly stable and resistant to crystallization triggered in the presence of elevated humidity, with no crystallization seen in the isothermal microcalorimeter at 25 °C over a period of 20 hours. The time scale effect for

the influence of humidity on crystallization was followed by storing the amorphous terfenadine samples at different relative humidities (44, 75 and 86 % RH) in an atmosphere of a controlled temperature of 21 ± 1 °C. The samples were analyzed over a period of close to 2 years using 50 : 50, ethanol : n-propanol in the glass ampoule method of the isothermal microcalorimeter. This method of analysis in the microcalorimeter resulted in complete crystallization of the remaining amorphous content in the samples. It was seen that the samples still stayed basically amorphous with more than 80 % amorphous content for samples stored at 75 % and 86 % RH and a higher amorphous content (86 %) for samples stored at 44 % RH after storage of the samples for around 2 years at the specified RH value. Crystallization of samples stored at different RH values leveled off with time with exponential decay regression analysis showing that it will take very long time for the sample to crystallize completely under the influence of humidity. The percentages of amorphous terfenadine (no more than 20 %) that have crystallized after 2 years seem to be localized on or close to the surface of the amorphous sample as indicated by SEM photomicrographs of slow cooled amorphous samples stored for more than a year at different RH values. The high resistance of the sample to crystallization cannot be attributed to just its hydrophobic nature although its being hydrophobic might restrict hydrogen bonding with water to the polar hydroxyl groups in the molecule of terfenadine. This high resistance to crystallization however, can also be attributed to the large size of the beads of terfenadine localizing the amount of absorbed water to certain regions on the surface of the beads with the possibility that water accesses the sample only through cracks and pores with crystallization resulting in closure of some of those cracks and/or pores with crystalline material. This further limits the water uptake by the sample and leads to a leveling off effect in the water uptake by the amorphous terfenadine samples. Added to that the possibility that the polar groups (2 hydroxyl groups) present in the molecule might be oriented in such a way that makes those groups or one of them projecting inwards or situated at cracks and/or pores, which further restricts water uptake by the amorphous sample.

Crystallization of the amorphous samples was found to be cooperative though incomplete in nature as indicated by the initial sharp peak and the increase in lag time when the percentage of ethanol is decreased in ethanol/ water mixtures used to crystallize the sample in the microcalorimeter.

Using organic vapours (50% ethanol/n-propanol mixture) to crystallize the amorphous terfenadine samples resulted in complete crystallization with larger pores forming on the surface of the beads as seen in Figure 4.10 in comparison with the small pores on the surface of the basically amorphous sample.

The amorphous terfenadine sample failed to crystallize under the influence of humidity at 75% RH for 20 hours at an elevated temperature of 50 °C in the Dynamic Vapour Sorption (DVS). Curve fitting was applied to data of the water sorption profiles of terfenadine kept for 20 hours at 44%, 75% and 90% RH at 25 °C for both fresh and aged amorphous terfenadine samples. An equation was derived from a regression analysis of the data, relating the percentage mass change (due to sorption) to time. The resulting data showed a trend and the water sorption for amorphous terfenadine using DVS was found to vary with time according to a function of $T^{0.57}$. This function was found to be independent of the RH value and the sample's age, yet the rate of sorption (i.e, the constant C in Equation 4.3) was dependent on those parameters. SEM showed that aged samples possessed smaller pores on the surface of the amorphous beads than those present on the surface of the fresh amorphous samples. This lead to higher water uptake at all three RH values (44%, 75% and 90%) and a more complete crystallization under 95% ethanol in the total gas flow in the case of the fresh amorphous samples of terfenadine than in the case of the aged samples.

DVS results obtained from exposure of the amorphous terfenadine samples to ethanol vapour in percentages ranging from 50 – 95% in the total gas flow for three hours showed that crystallization (as indicated by loss in weight in the DVS) did not start until a percentage of 85% ethanol was reached. SEM photomicrographs of the crystallized terfenadine samples at 85% ethanol showed that crystallization started by nucleation on the surface of the amorphous beads and pores enlarged during crystallization.

This observation led to the conclusion that while the amorphous sample starts to crystallize, larger pores form which result in greater diffusion of organic vapours into the inner parts of the terfenadine beads. This penetration of organic vapours results in complete crystallization of the amorphous, hydrophobic terfenadine sample. It was also found that amorphous terfenadine crystallizes into the most stable polymorphic form (polymorph I) when exposed to organic vapours.

CHAPTER FIVE

PREPARATION AND CHARACTERIZATION OF TERFENADINE DERIVATIVES IN CRYSTALLINE AND AMORPHOUS FORMS

5 INTRODUCTION:

The aim of this study was to investigate terfenadine together with a homologous series of acids that are to be reacted with the basic terfenadine and to identify their properties in comparison with the parent compound. A number of dicarboxylic acids that fall in sequence were used to react with terfenadine. Characterization included chemical identification of the prepared terfenadine derivatives and a physical characterization of both the crystalline and the amorphous forms. The aims of this study were:

- To prepare derivatives of the parent compound (terfenadine) in a homologous series in order to be able to compare their characteristics relative to terfenadine as well as to each other.
- To identify the chemical structures of the prepared derivatives using Nuclear Magnetic Resonance (NMR) and Elemental Analysis.
- To identify the physical forms of the prepared terfenadine derivatives and establish whether they are amorphous or crystalline using Differential Scanning Calorimetry (DSC) and X-ray Powder Diffraction (XRPD).
- To determine the purity of the prepared derivatives using Thin Layer Chromatography (TLC).
- To study the physical stability of the prepared derivatives by storage for around 6 months in a vacuum oven at 50 °C and 400 mbar and checking on DSC.

5.1 METHOD OF PREPARATION OF TERFENADINE DERIVATIVES:

Terfenadine derivatives were prepared by dissolving an excess amount of the acid (assuming 2 : 1 stoichiometry for acid : base as it was thought that the acid may react at two sites of the terfenadine molecule) in 20 ml of absolute ethanol. The chemical structure of terfenadine was illustrated in Figure 2.13.

The volume of ethanol was chosen to be just enough to dissolve the acid and keep the terfenadine derivative produced in solution and to result in quick precipitation of the product once purified water is added. The acidic solution was placed over a hot plate set at a temperature of ca. 85 °C with magnetic stirring. The hot acidic solution was then poured over terfenadine and the resultant mixture was placed on the hot plate at ca. 85 °C while maintaining stirring. Once terfenadine dissolved in the hot acidic solution, it was left for ca. 5 minutes on the hot plate with stirring. The heater was then turned off whilst

stirring was kept on and purified water was added up to a total volume of ca. 250 ml in order to precipitate the formed product. The precipitate was then removed from the hot plate and left to cool to ambient temperature. Filtration was done through medium/fast filter paper, followed by three rinses of the precipitate with purified water. Drying was either at ambient temperature or in an oven set at 25 °C after spreading of the precipitate over filter paper.

5.2 CHARACTERIZATION OF TERFENADINE DERIVATIVES:

5.2.1 CHARACTERIZATION OF TERFENADINE DERIVATIVES: DIFFERENTIAL SCANNING CALORIMETRY (DSC)

5.2.1.1 METHOD:

The basic principles of DSC were explained in Section 2.1.3. DSC was carried out initially from 30 – 300 °C and later from 30 – 180 °C (to avoid decomposition) at 10 °C/ min in pin hole aluminium pans.

5.2.1.2 RESULTS:

The main purpose of checking the prepared terfenadine derivatives on DSC was to investigate whether a single product (manifested in one peak on the DSC) was obtained and to compare the obtained peak(s) with those of the original two reacting materials. DSC was also used in order to determine whether the solids produced were amorphous or crystalline. The DSC thermograms of the four terfenadine derivatives prepared are shown in Figures 5.1 - 5.4.Mettler DSC 20 with a TA 4000 processor was used in the current study.

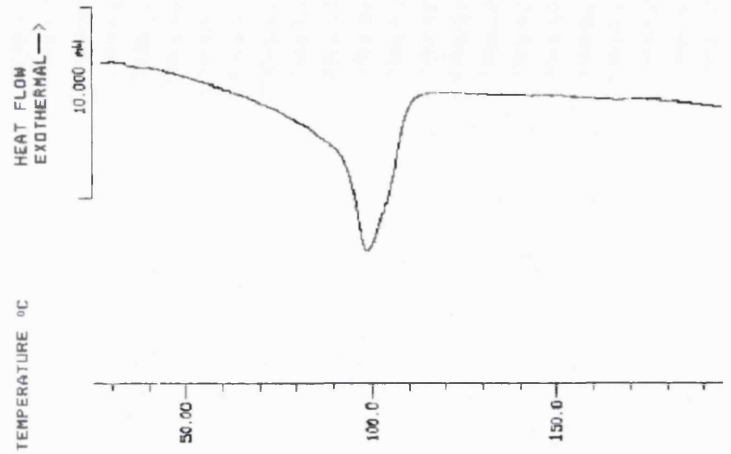

Figure 5.1 *DSC trace of terfenadine oxalate within a heating range of 30 - 180 °C at 10°C/min using pierced aluminium pans in nitrogen atmosphere.*

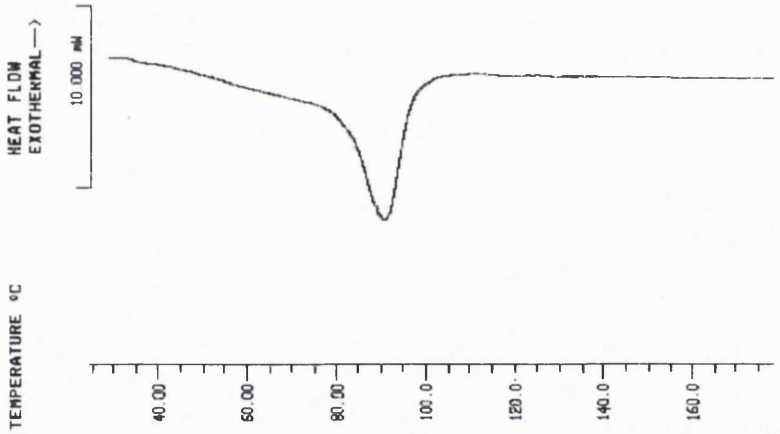

Figure 5.2 *DSC trace of terfenadine succinate within a heating range of 30 - 180 °C at 10°C/min using pierced aluminium pans in nitrogen atmosphere.*

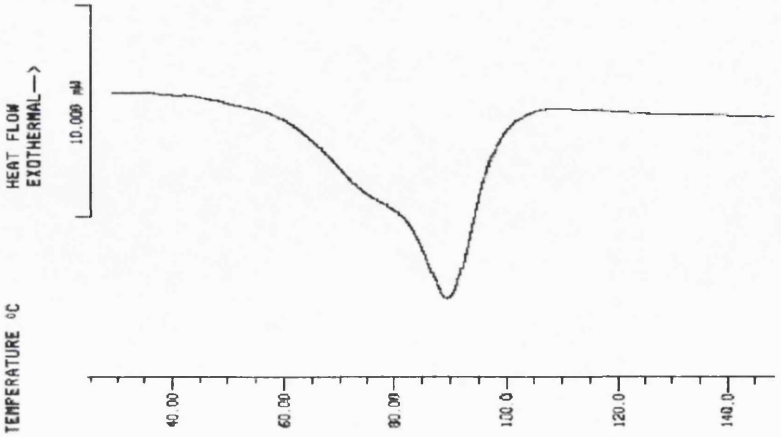

Figure 5.3 *DSC trace of terfenadine glutarate within a heating range of 30 - 180 °C at 10°C/min using pierced aluminium pans in nitrogen atmosphere.*

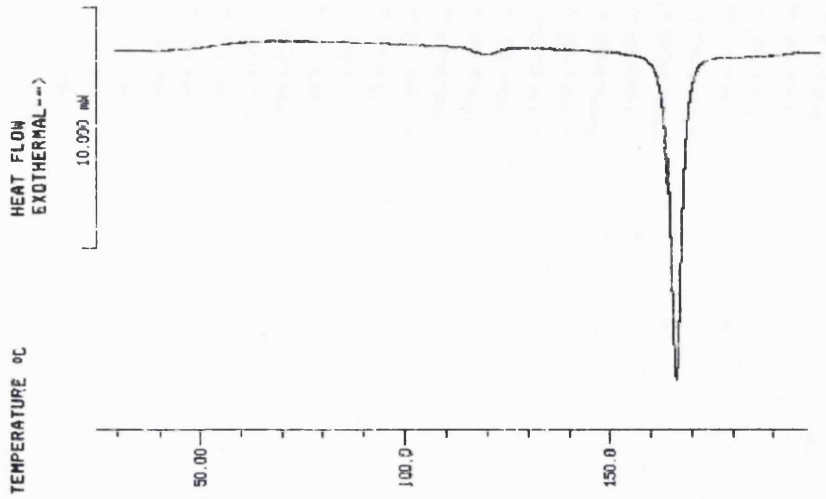

Figure 5.4 *DSC trace of terfenadine adipate within a heating range of 30 - 180 °C at 10°C/min using pierced aluminium pans in nitrogen atmosphere.*

Table 5.1 shows the melting points of the prepared terfenadine derivatives (as described in Section 5.1) and Table 5.2 shows the melting points of the dicarboxylic acids used in the preparation of the terfenadine derivatives.

Table 5.1 DSC results showing peak melting points and enthalpies of fusion of the terfenadine derivatives prepared (n = 4).

Terfenadine Derivative	Peak Melting Point (°C), (S.D.)	Enthalpy of Fusion (ΔH J/g), (S.D.)
Oxalate	97.8 (0.3)	113.2 (2.6)
Succinate	90.9 (0.4)	65.2 (3.8)
Glutarate	88.2 (0.3)	57.3 (2.6)
Adipate	162.2 (0.8)	78.5 (0.2)

Table 5.2 Melting points of dicarboxylic acids used in the preparation of terfenadine derivatives as specified by their sources and confirmed by DSC.

Dicarboxylic acid (Source)	Chemical structure of the acid	Molecular weight of the acid (g/mole)	Melting point of acid (°C) (Source)	Melting point of acid (°C) (DSC)
Oxalic (T.S.E.S chemicals)	HOOC - COOH	90	208-212	210.9
Succinic (Merck chemicals)	HOOC- $(CH_2)_2$ - COOH	118.1	187-190	188.8
Glutaric (ACROS chemicals)	HOOC- $(CH_2)_3$ - COOH	132.1	98.5	98.3
Adipic (Merck chemicals)	HOOC- $(CH_2)_4$ - COOH	146.1	152-154	153.7

It can be seen from Figures 5.1- 5.4 and Table 5.1 that all four terfenadine derivatives exhibited single endothermic peaks prior to decomposition at higher temperatures ($\geq$ 200 °C). The endothermic peaks most probably correspond to melting of a crystalline material that is distinct for each derivative (the endothermic peak of each derivative differs from the endothermic melting peaks of either one of the reactants, terfenadine with a peak melting point of ca. 152 °C and that of dicarboxylic acids seen in Table 5.2). This finding confirms that a new product formed by the method used in the preparation of the terfenadine derivatives (described in Section 5.1). To investigate whether the products were physical mixtures of terfenadine with the acids or new products resulting from a chemical interaction between the two reacting parent compounds (terfenadine and dicarboxylic acids), different molar ratios of terfenadine to adipic acid were used and prepared in the same way as described in Section 5.1. If a simple physical mixture of the two reacting species was obtained, then almost the same DSC trace is expected to be achieved regardless of the molar ratios of terfenadine to the dicarboxylic acid used. On the other hand, if a chemical interaction was taking place, different endothermic peaks may be seen in the DSC thermograms at different ratios of terfenadine to the dicarboxylic

acid. The results showed different endothermic peaks from those of the previously prepared compounds and were seen in Table 5.1. For example, when 2 moles of terfenadine were reacted with 1 mole of adipic acid, one endothermic peak was seen in the DSC trace at 70.7 °C (n = 2, S.D. = 1.3) at a heating rate of 10 °C /min using pierced aluminium pans (Figure 5.5). This is in contrast with an endothermic peak of ca. 162 °C (Table 5.1) when one mole of terfenadine was reacted with two moles of adipic acid as seen in the original procedure followed (Section 5.1). This means that a different product was obtained and that preliminary indications show that the product at hand was not a simple physical mixture.

Another way of checking was by physically mixing the two components (terfenadine and adipic acid) in the same ratio used in the reaction procedure followed (Section 5.1) and leaving the physical mixture in an oven at 85 °C (the same temperature used in preparing the terfenadine derivatives as seen in Section 5.1) for 42, 71 hours and 11 days. DSC run of these physical mixtures gave one endothermic peak at 131.2 °C as seen in Figure 5.6 (n = 3, S.D. = 0.3). The same endothermic peak was achieved in the DSC traces of the physically mixed terfenadine and adipic acid at all exposure times in the oven at 85 °C using the same DSC conditions. This indicated that the physical mixture gave the same product regardless of the time of storage at 85 °C and that this product was again different from that achieved by reacting two moles of adipic acid with one mole of terfenadine showing an endothermic peak at ca. 162 °C (Table 5.1). Another physical mixture was prepared by dry mixing of one mole of terfenadine with one mole of succinic acid followed directly by a DSC run of this physical mixture (Figure 5.7). Three endothermic peaks were seen in the DSC trace at 122.7, 145.3 and 175.3 °C (different from the endothermic peak obtained from succinic acid reacted with terfenadine as obtained from the procedure followed in Section 5.1 and seen in Table 5.1). This again indicated that the product obtained by reacting one mole of terfenadine with two moles of succinic acid as described in Section 5.1 was not a simple physical mixture. The adipate and the succinate derivatives were tested as examples of the group and as a preliminary way of checking whether the products were physical mixtures or products of a chemical interaction before a confirmation is established by NMR analysis for all terfenadine derivatives (seen later in Section 5.2.5.2). All of the above DSC results indicate that the terfenadine derivatives prepared as described in Section 5.1 form at a certain molar ratio of terfenadine to the dicarboxylic acid and most probably are not simple physical mixtures of terfenadine and the dicarboxylic acid.

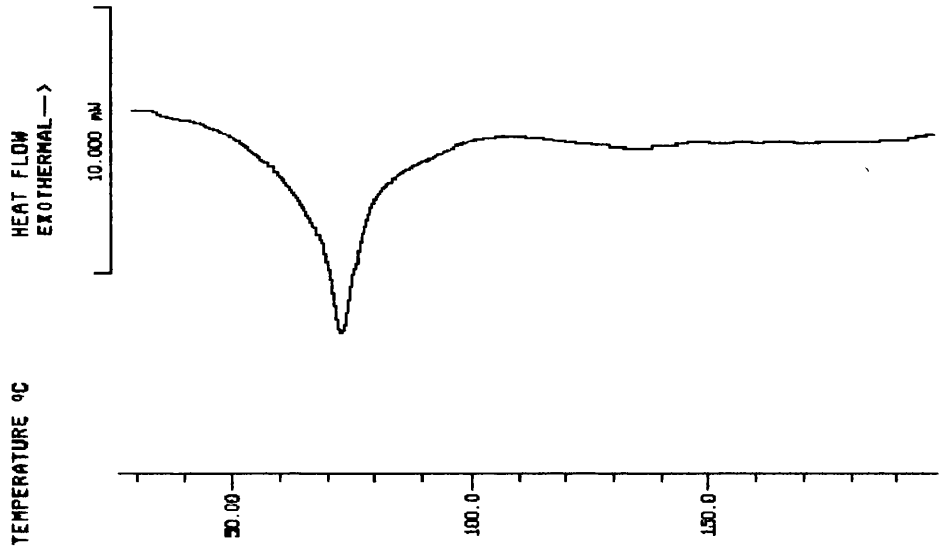

Figure 5.5 *DSC trace of the product from chemically reacting 2 moles of terfenadine with 1 mole of adipic acid, DSC run at 10 °C/min using pierced aluminium pans.*

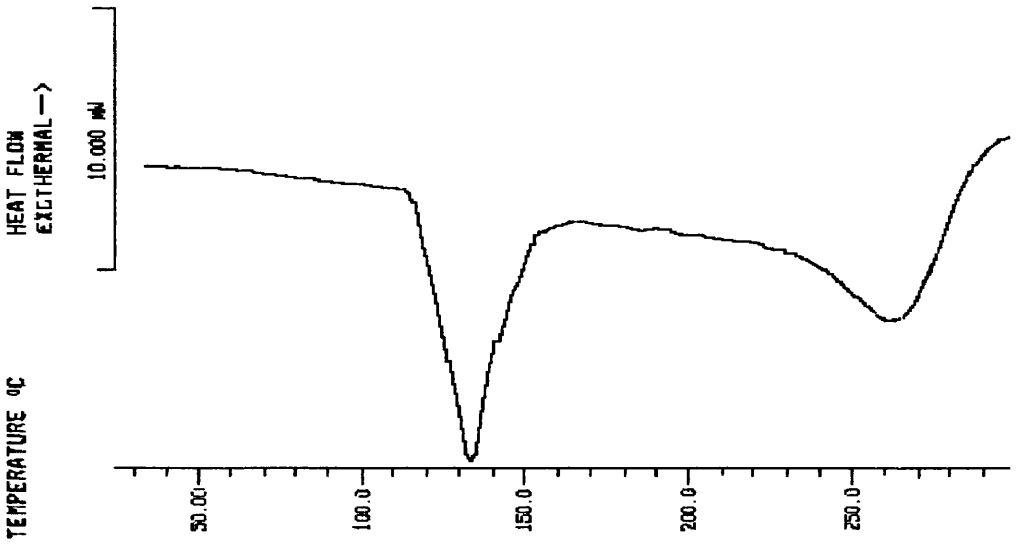

Figure 5.6 *DSC trace of the product from physically mixing terfenadine and adipic acid and storage at 85 °C, DSC run at 10 °C/min using pierced aluminium pans.*

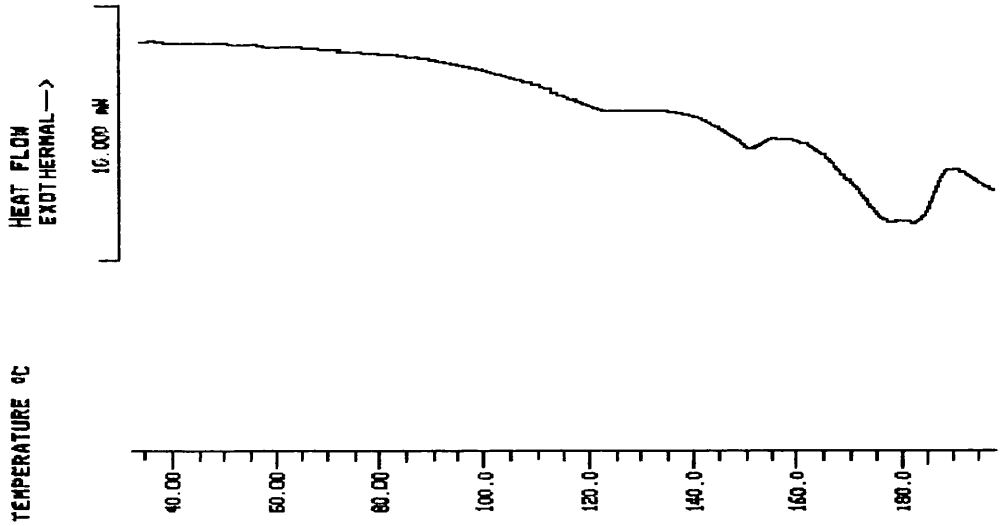

Figure 5.7 DSC trace of the product from physically mixing terfenadine and succinic acid, DSC run at 10 °C/min using pierced aluminium pans.

5.2.2 CHARACTERIZATION OF TERFENADINE DERIVATIVES: THERMOGRAVIMETRIC ANALYSIS (TGA)

5.2.2.1 METHOD:

Thermogravimetric analysis was discussed in Section 2.1.5. Samples weighing 5 ± 2 mg were used and were run in open aluminium pans from ambient conditions up to 180 °C using a ramp method at 10 °C/min under a nitrogen atmosphere.

5.2.2.2 RESULTS:

TGA was carried out in order to check whether the endotherms seen in the DSC thermograms coincided with any weight loss in the samples.
TGA traces of the terfenadine and its derivatives are seen in Figures 5.8 – 5.12 and the TGA results are summarized in Table 5.3.

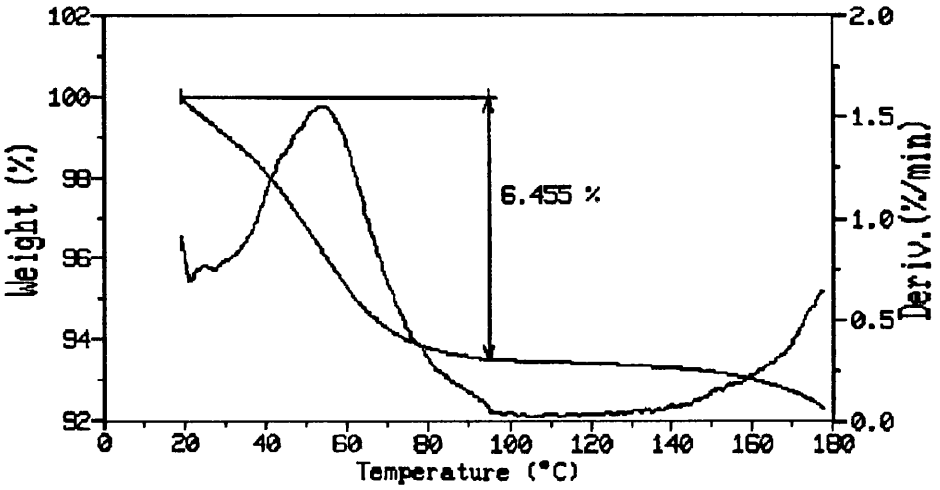

Figure 5.8 TGA trace of terfenadine oxalate from ambient conditions to 180 °C at 10 °C/min.

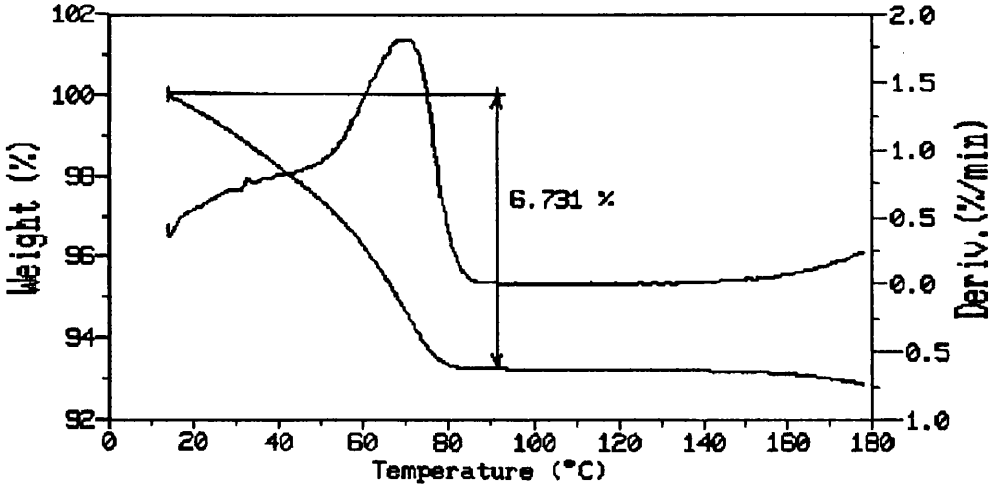

Figure 5.9 TGA trace of terfenadine succinate from ambient conditions to 180 °C at 10 °C/min.

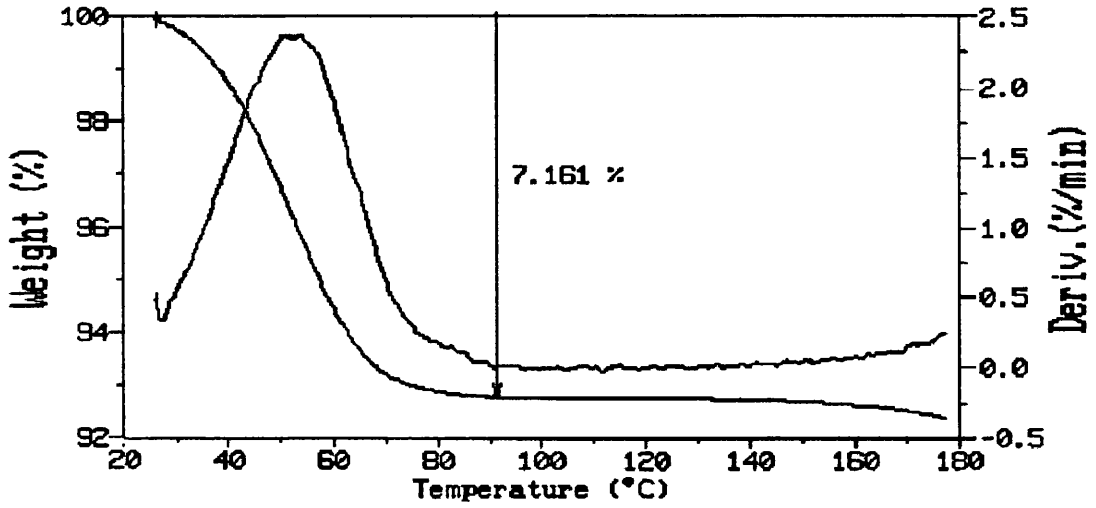

Figure 5.10 *TGA trace of terfenadine glutarate from ambient conditions to 180 °C at 10 °C/min.*

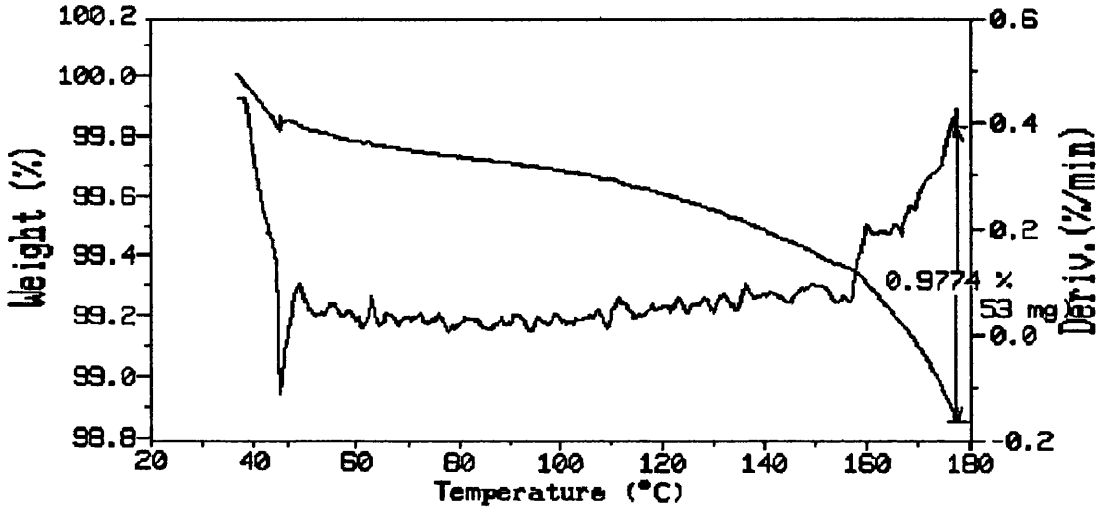

Figure 5.11 *TGA trace of terfenadine adipate from ambient conditions to 180 °C at 10 °C/min.*

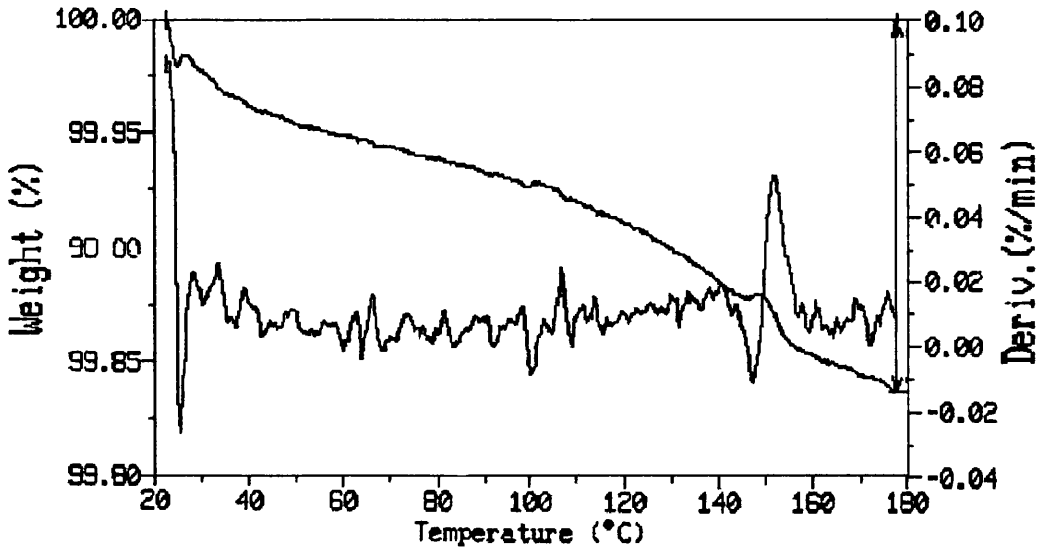

Figure 5.12 TGA trace of terfenadine from ambient conditions to 180 °C at 10 °C/min.

Table 5.3 TGA results of terfenadine derivatives run from ambient conditions to 180 °C, ramp10 °C/min in open aluminium pans under nitrogen gas (n = 3 - 4).

Compound	Percentage weight loss, (S.D.)	Temperature range of weight loss (°C)
Terfenadine	0.2 (0.05)	Beginning to 180 °C
Oxalate	6.4 (0.3)	Beginning to ca. 95 °C
Succinate	6.5 (0.4)	Beginning to ca. 90 °C
Glutarate	7.1 (0.1)	Beginning to ca. 90 °C
Adipate	1.0 (0.03)	Beginning to 180 °C

It is obvious from Table 5.3 that a substantial weight loss takes place in the case of the oxalate, succinate and the glutarate derivatives of terfenadine whereas a negligible percentage of weight loss takes place in the adipate sample (1%) and in terfenadine (0.2%). This substantial weight loss coincides with the melting endotherms seen in the

DSC for the three derivatives (terfenadine oxalate, terfenadine succinate and terfenadine glutarate). It was essential to carry out further tests in order to determine if the weight loss observed in the samples was due to loss of water, loss of ethanol, a combination of both (knowing that those two solvents were the ones used in the preparation of the terfenadine derivatives as explained in Section 5.1) or anything else causing the loss in weight in these compounds such as a sort of decomposition which has to be identified. Karl- Fisher titration was carried out in order to determine whether the weight loss seen in the TGA is due to the presence of water or anything else.

5.2.3 CHARACTERIZATION OF TERFENADINE DERIVATIVES: KARL-FISCHER TITRATION

5.2.3.1 METHOD:

The basic principles of Karl-Fischer titration and the method used to quantify water in the samples were discussed in Section 2.1.11.

5.2.3.2 RESULTS:

Since weight loss was noticed in the terfenadine derivatives when they were tested on the TGA (Section 5.2.2.2), Karl-Fischer titration was used to verify whether the weight loss seen on the TGA was due to the presence of water in the prepared solids or due to another solvent which was used in the preparation procedure of the terfenadine derivatives (ethanol in this case) or any other reason. Water will be confirmed to be the cause for the weight loss in the TGA if the percentage weight loss seen on the TGA matched the quantity of water detected by Karl-Fischer titration.

Table 5.4 shows the percentage of water in the samples of terfenadine and its derivatives as determined by Karl-Fischer titration in comparison with weight loss results seen using thermogravimetric analysis. All Karl-Fischer results were carried out in triplicate.

Table 5.4 Percentage water content as determined by Karl-Fischer (n = 3) and the corresponding weight loss seen on TGA (n = 3 - 4) for the four terfenadine derivatives.

Terfenadine derivative	Water content from Karl-Fischer titration (%), (S.D.)	Weight loss as detected by TGA (%), (S.D.)
Terfenadine	0.1 (0.01)	0.2 (0.05)
Oxalate	7.0 (0.03)	6.4 (0.3)
Succinate	7.6 (0.1)	6.5 (0.4)
Glutarate	8.0 (0.3)	7.1 (0.1)
Adipate	0.8 (0.02)	1.0 (0.03)

From the results in Table 5.4 it can be noted that the percentage weight loss seen on the TGA is in good agreement with the percentage of water in the samples quantified by Karl-Fischer titration with a slightly higher apparent water content seen in the Karl-Fischer data than the corresponding weight loss noted for each of the three derivatives which exhibited the highest weight loss on TGA (terfenadine oxalate, terfenadine succinate and terfenadine glutarate) on the TGA. This difference is expected due to the difference in the methods of analysis used (TGA versus Karl- Fischer titration) and since Karl-Fischer was carried out on freshly prepared samples which are expected to contain a slightly higher amount of water. It can thus be concluded that the weight loss seen on the TGA is due to the presence of water in the terfenadine samples and not due to any decomposition of the terfenadine derivatives. Hence, the terfenadine derivatives were stable in heat up to a temperature of ca. 180 °C and the loss in weight simply indicated loss of water from those samples. The loss of water, which coincided, with melting of terfenadine oxalate, succinate and glutarate could explain the relatively high standard deviations seen in the enthalpies of fusion of these three derivatives (Table 5.1).

5.2.4 CHARACTERIZATION OF TERFENADINE DERIVATIVES: POWDER X-RAY DIFFRACTION

5.2.4.1 METHOD:

The basic principles and the method used in carrying out the powder X-ray diffraction experiments were explained in Section 2.1.7.

5.2.4.2 RESULTS:

Powder X-ray diffraction was carried out on the terfenadine derivatives (prepared as in Section 5.1.1) in order to verify whether the endotherms seen on the DSC thermograms of the terfenadine derivatives actually represent the melt of a crystalline material, especially that the endothermic peaks seen in the DSC thermograms of terfenadine oxalate, succinate and glutarate overlapped with loss in weights within the same temperature range as seen from the TGA traces of those terfenadine derivatives (Section 5.2.2.2). The loss in weight can be due to solvent evaporation from an amorphous material or from a crystalline solid with a melting peak overlapping with solvent loss. Powder X-ray diffraction qualitative traces of terfenadine and its four derivatives are seen in Figures 5.13 – 5.17.

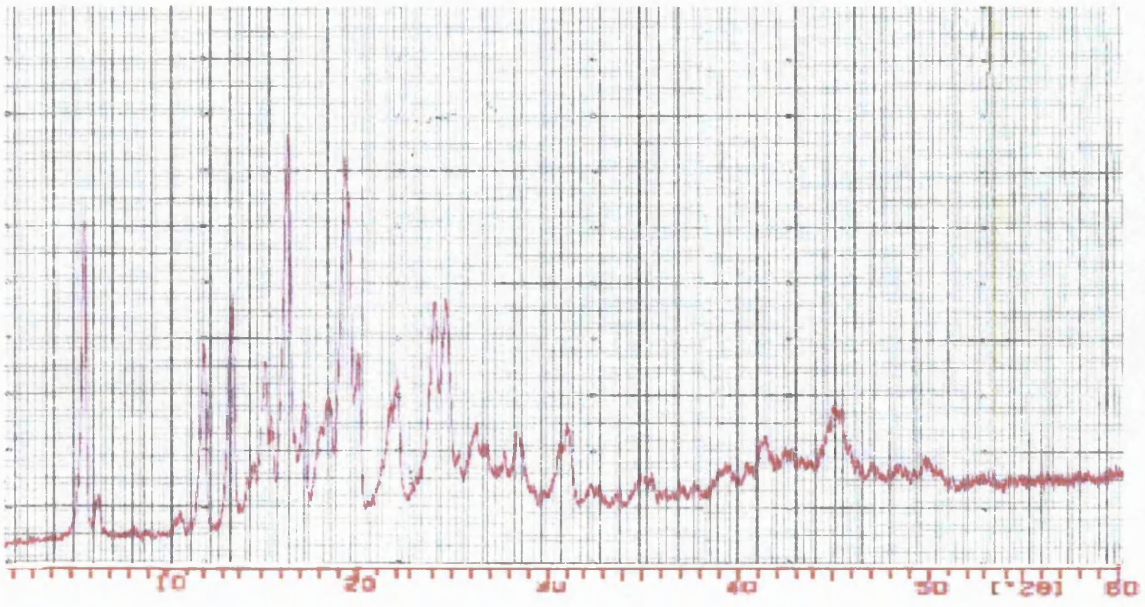

Figure 5.13 *Powder X-ray diffractogram of raw (crystalline) terfenadine.*

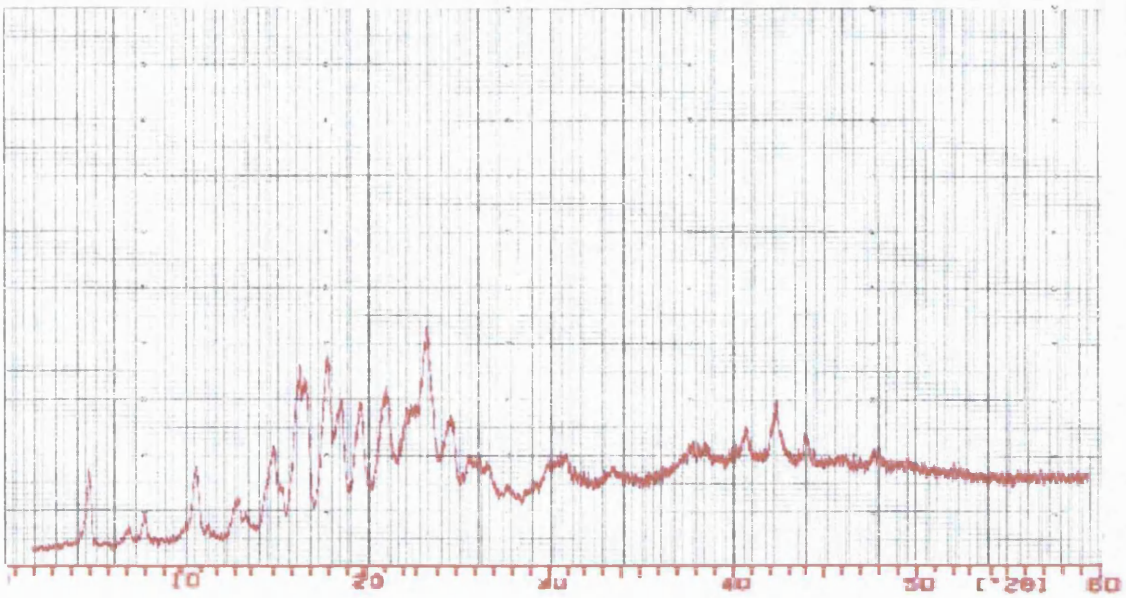

Figure 5.14 *Powder X-ray diffractogram of terfenadine oxalate.*

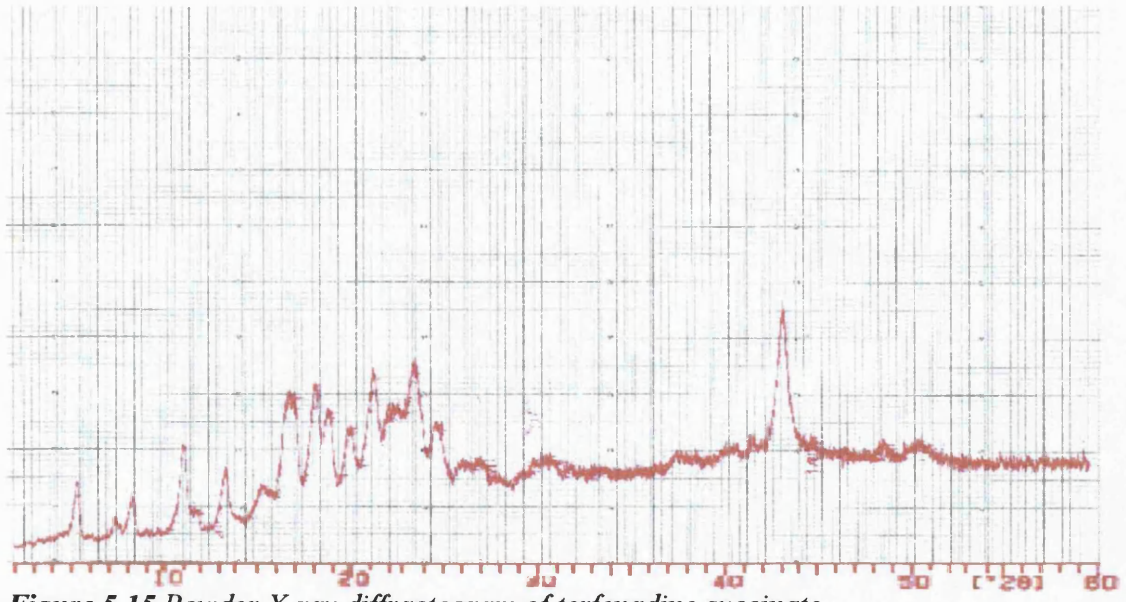

Figure 5.15 *Powder X-ray diffractogram of terfenadine succinate.*

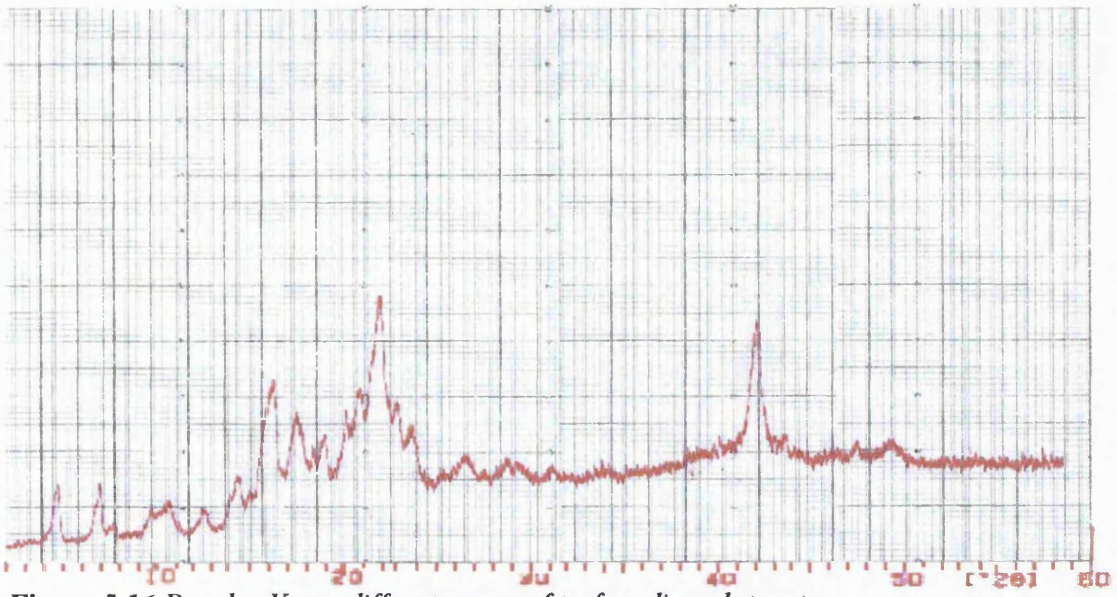

Figure 5.16 *Powder X-ray diffractogram of terfenadine glutarate.*

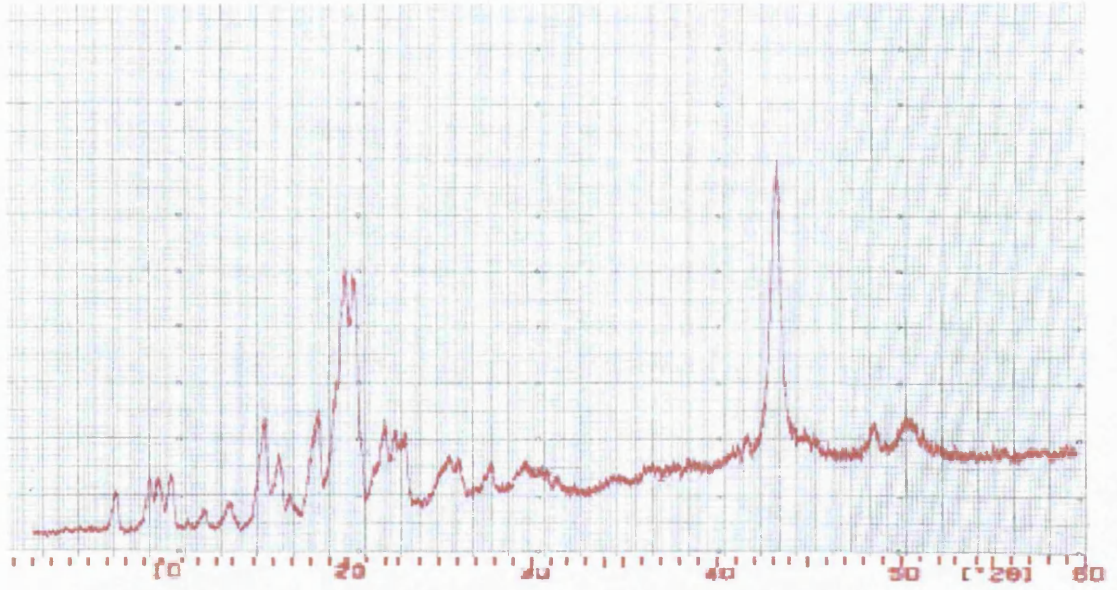

Figure 5.17 *Powder X-ray diffractogram of terfenadine adipate.*

Figures 5.14 – 5.17 show the absence of an amorphous halo in any of the terfenadine derivatives and show the presence of sharp peaks in the diffractograms of terfenadine derivatives. It can thus be concluded that the prepared terfenadine derivatives are crystalline solids which confirms that the endothermic peaks seen in the DSC thermograms of terfenadine derivatives (Figures 5.1 – 5.4) represent melting endotherms of a crystalline solid overlapping with a solvent loss.

Saleki-Gerhardt et al. (1994b) explained that when using the X-ray powder diffraction method, a sample that is 90 % crystalline and that which is 100 % crystalline couldn't be distinguished from one another. This fact has to be kept in mind when looking at X-ray diffraction results, as being crystalline does not necessarily mean that the sample is 100 % crystalline.

5.2.5 CHARACTERIZATION OF TERFENADINE DERIVATIVES: NUCLEAR MAGNETIC RESONANCE

The basic principles of NMR were explained in Section 2.1.10. It was essential to carry out NMR in order to determine whether a physical mixture or a chemical interaction was achieved between terfenadine and the dicarboxylic acids.

5.2.5.1 METHOD:

A sample weighing between 24 – 25 mg of the test compound was placed in a glass vial. Using a Pasteur pipette, 1.5 ml of deuterated methanol (CD_3OD) were added into the vial. Once the powder dissolved, the sample was filtered through glass wool directly into the NMR tube up to a height of 5 – 6 cm. Filtration was done in order to get rid of any solid particles which can distort the homogeneity of the magnetic field. Nitrogen gas was then passed on top of the surface of the solutions in the NMR tubes. This is done in order to prevent any possibility of oxidation of the sample. Samples were prepared in deuterated solvents (solvents that contain deuterium in place of hydrogen) since the NMR signal from the deuterium nuclei is used by the spectrometer for stabilization. Deuterated methanol was chosen since it is a good solvent for terfenadine as well as its derivatives. The above procedure was carried out on terfenadine as well as the other 4 derivatives. Proton ^1H NMR experiments were carried out using a BRUKER AM500 NMR instrument with ASPECT 3000 computer. The offset frequency was 9300 Hz., size of spectrum 16 K, relaxation delay 1.5 seconds. The residual deuterated methanol solvent peak was used to reference the spectra (CD_3OD = 3.31 ppm).

5.2.5.2 RESULTS:

The first step was to check whether all protons of the dicarboxylic acids are incorporated in their corresponding terfenadine derivatives. This would be indicated if the increase in the number of protons relative to terfenadine corresponds to the number of protons in the terfenadine derivative of the specified dicarboxylic acid with splittings of the peaks due to the addition of new protons.

The proton ^{1}H NMR spectra of terfenadine and its derivatives are shown in Figures 5.18 - 5.22. The number of protons incorporated in the terfenadine molecule and its derivatives was calculated from the integral areas in the NMR spectra and the following conclusions were drawn from the NMR spectra:

1. The region at ca. 1.3 ppm. This region represents the C $(CH_3)_3$ group of the chemical structures (the chemical structure of terfenadine is seen in Figure 2.13). This region appears as a singlet peak of 9 protons in the NMR spectra of terfenadine and all the other 4 terfenadine derivatives (Figures 5.18 - 5.22). It is a singlet as there are no adjacent protons to this group with the closest protons being more than 2 bonds away. Protons cause splitting of other adjacent protons if they are spaced no more than 2 bonds apart (Watson, 1999) and since multiplicity (M) = N + 1 (see Section 2.1.10), one peak will be seen in this region in the NMR spectra of terfenadine and its derivatives.

2. The region of ca. 1.4 – 4 ppm. This region represents the aliphatic hydrocarbon chain part in the molecules as well as the tertiary amine group (Figure 2.13). In this region, there is a sequential increase in the number of protons when going from the oxalate to the adipate derivative with terfenadine and the oxalate derivative having the same number of protons but with different peak splittings. It was calculated that terfenadine and the oxalate have 15 protons, the succinate 19 protons, the glutarate 21 protons and the adipate with the highest number of 23 protons with different peaks splitting in this region among the group. The total number of protons in this region for each of the terfenadine derivatives matched the sequential addition of protons from the methylene groups of the dicarboxylic acids in the sequence from the oxalic to the adipic acid (empirical formulas of the dicarboxylic acids are seen in Table 5.2). This indicates a chemical interaction is

taking place between terfenadine and the dicarboxylic acids rather than a simple physical mixture. Different splittings of the peaks in this region (among terfenadine and its derivatives as well as among the derivatives) is another indication of chemically incorporated protons in the parent terfenadine molecule in contrast with a simple physical mixture of the two species (terfenadine and the dicarboxylic acids). Splitting of the peaks in this region could not be specified to each entity of protons, as there is a lot of overlapping. When two protons are close in chemical shift, coupling can cause their signals to overlap (Watson, 1999).

3. The region of ca. 4.6 - 4.8 ppm. This region represents the CH-OH group in terfenadine or CH-COOH (if the reaction took place at this site) of the terfenadine derivatives. This peak shows the presence of 1 proton split into a triplet in the NMR spectra of terfenadine and its derivatives. The proton of the OH group was not seen since it was exchanged with deuterium and hence only 1 proton was detected and a triplet was seen since this group is adjacent to 2 protons.

4. The region between ca 7.1 and 7.3 ppm. This region represents the aromatic part of the molecules (comprised of the of the 3 benzene rings in the molecular structure as seen for terfenadine in Figure 2.13). It shows the presence of 14 protons in the spectra of all 5 compounds. The proton of the OH group present between the two benzene rings in the molecule (Figure 2.13) was not seen as it was exchanged with deuterium.

The above NMR spectral data conclude that terfenadine is not forming a simple physical mixture but rather is chemically interacting with the dicarboxylic acids in a stoichiometric ratio of 1 mole: 1 mole of terfenadine : dicarboxylic acid. This finding confirms the preliminary indications of the DSC regarding the exclusion of a physical mixture of terfenadine and the dicarboxylic acid (Section 5.2.1.2). Although 2 moles of the dicarboxylic acid were reacted with 1 mole of terfenadine, the products showed just 1 mole of the acid incorporated with 1 mole of terfenadine while the rest of the acid remained in the filtrate. This may be due to the short time allowed for the reaction of terfenadine with the dicarboxylic acid (5 minutes after the terfenadine dissolved in the acidic ethanolic solution) which gave the chance for just one mole of the acid to be incorporated with terfenadine or due to a more difficult interaction between terfenadine

and the dicarboxylic acid at the other possible sites of interaction in the terfenadine molecule. This means that the first mole of the acid reacted at the easiest reaction site in the terfenadine molecule.

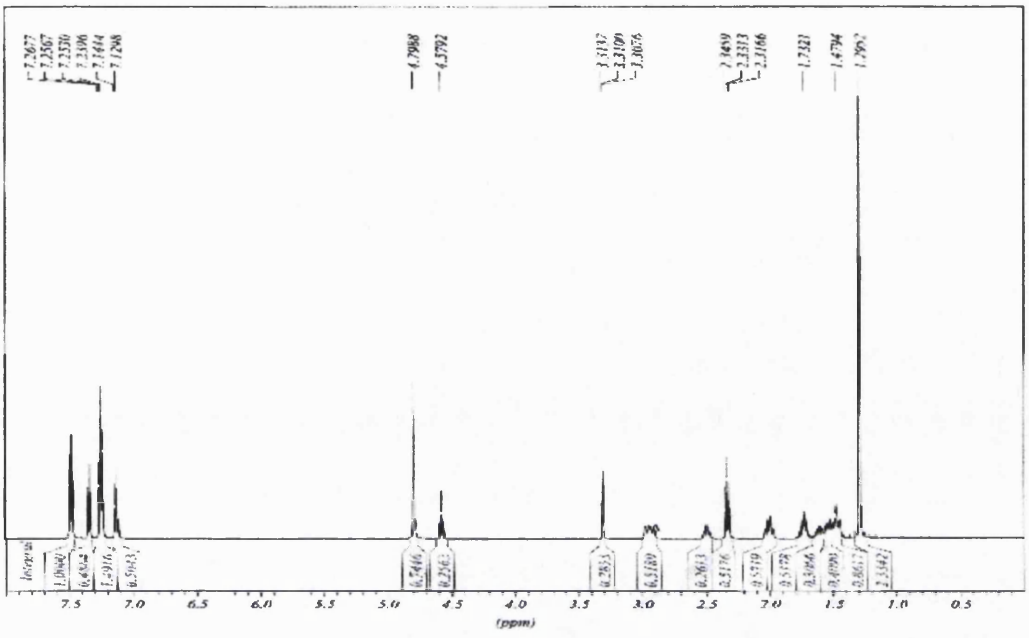

Figure 5.18 *Proton ^{1}H NMR spectrum of terfenadine.*

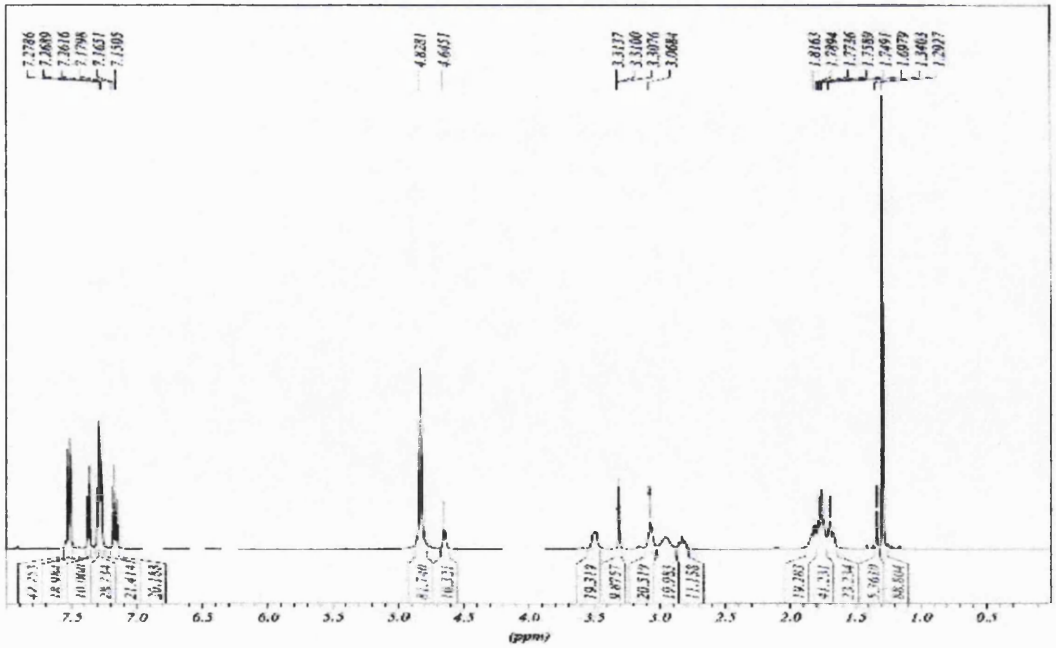

Figure 5.19 *Proton ^{1}H NMR spectrum of terfenadine oxalate.*

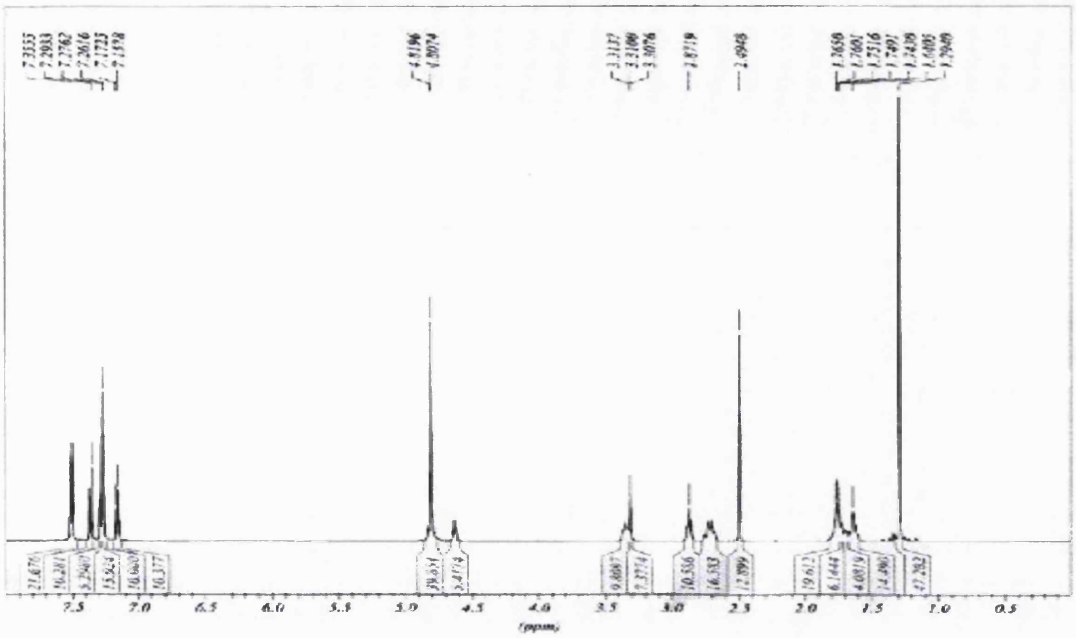

Figure 5.20 *Proton ^{1}H NMR spectrum of terfenadine succinate.*

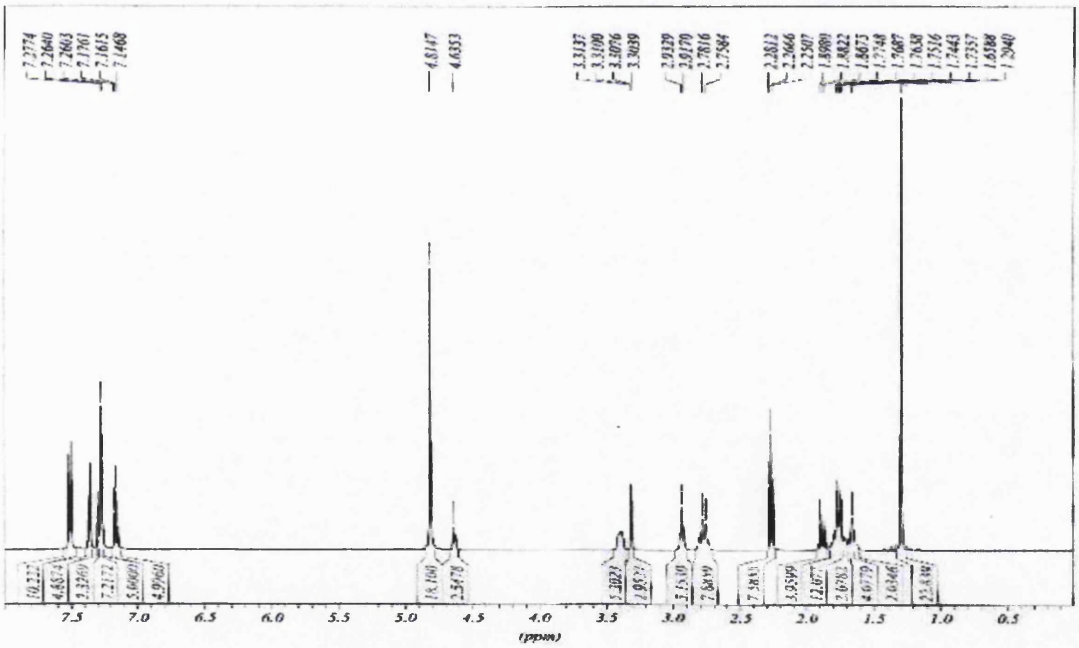

Figure 5.21 *Proton ^{1}H NMR spectrum of terfenadine glutarate.*

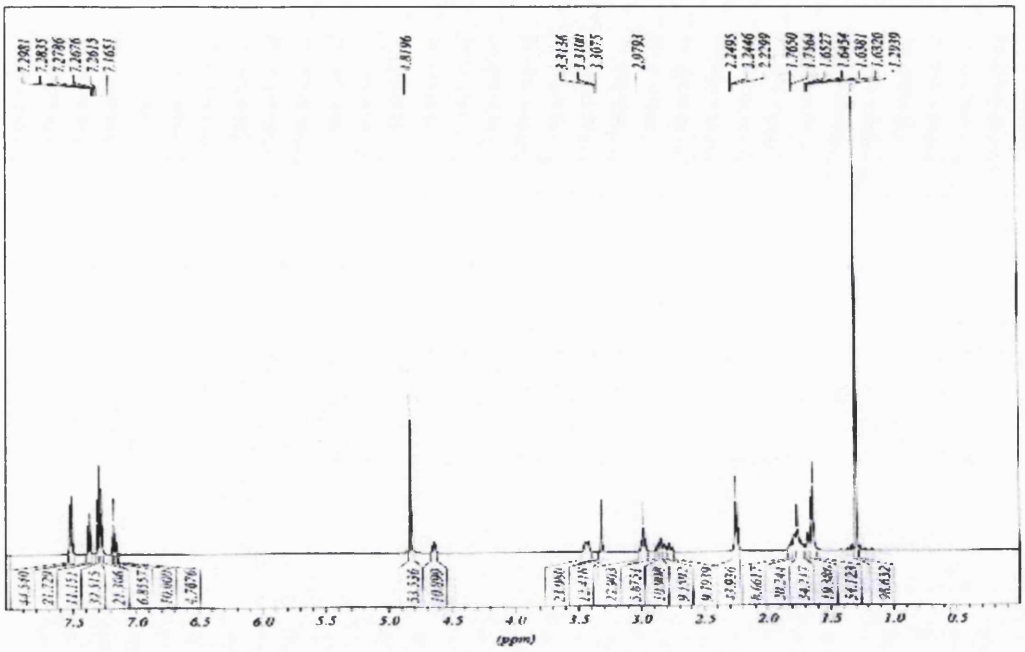

Figure 5.22 *Proton ^{1}H NMR spectrum of terfenadine adipate.*

The next step was the identification of the chemical structure of each of the 4 terfenadine derivatives.

The possible reaction sites between terfenadine and the dicarboxylic acids are summarized in the following points:

1. The basic N: formation of an ammonium salt results from this reaction. This possibility of interaction is the one which most likely took place depending on the procedure carried out (short reaction time of 5 minutes) and one component was the product of the interaction as seen by DSC (Section 5.2.1.2) and proton NMR.

2. The two alcoholic functions (OH): each of them has the potential of forming an ester but this reaction usually leads to an equilibrium and is unlikely to go to completion. Professor Nizar Alrrayyes (Professor of Chemistry at Petra university) explained that an ester could not have formed at the OH group as a longer reaction time is needed for this product to form than that followed in our procedure (5 minutes) besides these reactions are reversible which is contrary to our findings as one product was found in the DSC traces of all terfenadine derivatives (Section 5.1.2.1) and the presence of one compound was concluded from the NMR spectra as based on the number of protons in the terfenadine derivatives relative to those of the reacting species (terfenadine and the dicarboxylic acid) and the occurrence

of splittings in the peaks due to the incorporation of new protons. Hence, the possibility of ester formation was excluded.

3. Another weak possibility of reaction was through water elimination from the OH group present between the two benzene rings resulting in the following change in the molecule (compare with Figure 2.13).

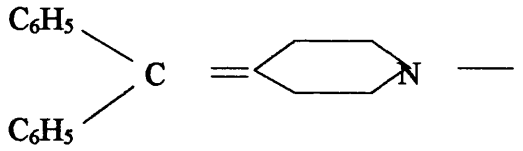

If this reaction took place, there will be a change in the aromatic region but which would not show in the one dimension proton ^{1}H NMR test. Thus a Cozy test (2 dimensional proton NMR) was carried out in order to establish if any change took place in the aromatic region of the chemical structures. Dr Mire Zloh concluded from the results (not shown) that the aromatic region did not show any change in terfenadine derivatives when compared with the same region in terfenadine. This result excluded the possibility of a reaction, taking place at this site.

The NMR results led to the conclusion that the reaction occurred at the tertiary amine resulting in the formation of different terfenadine salts from the different dicarboxylic acids, hence the terfenadine derivatives at hand are actually salts of the parent compound resulting from the reaction of one mole of terfenadine with one mole of the dicarboxylic acid.

5.2.6 CHARACTERIZATION OF TERFENADINE SALTS: ELEMENTAL ANALYSIS

5.2.6.1 METHOD:

The basic principles of elemental analysis and the details of the equipment used in the current study are explained in Section 2.1.9.

Elemental analysis was carried out in order to determine the percentages of carbon, hydrogen and nitrogen (CHN) in terfenadine and its salts.

5.2.6.2 RESULTS:

Theoretical percentages of CHN based on a stoichiometric ratio of 1 mole : 1 mole of terfenadine : dicarboxylic acids as well as practical percentages of CHN for terfenadine and its salts are shown in Table 5.5.

Table 5.5 Theoretical and practical percentages of carbon, hydrogen and nitrogen for terfenadine and its salts as determined by Elemental Analysis (n = 2).

Compound	Theoretical %			Practical % (S.D.)		
	Carbon (C)	Hydrogen (H)	Nitrogen (N)	Carbon (C)	Hydrogen (H)	Nitrogen (N)
Terfenadine	81.4	8.7	3.0	80.0 (0.10)	9.0 (0.03)	2.9 (0.02)
Terfenadine oxalate	72.6	7.7	2.5	68.0 (0.06)	8.1 (0.10)	2.2 (0.05)
Terfenadine succinate	73.3	8.0	2.4	70.2 (0.07)	8.4 (0.05)	2.2 (0.04)
Terfenadine glutarate	73.6	8.1	2.3	69.3 (0.06)	8.4 (0.02)	2.1 (0.08)
Terfenadine adipate	73.8	8.3	2.3	72.7 (0.04)	8.6 (0.02)	2.2 (0.03)

It was proven previously by TGA and Karl-Fischer (Table 5.4) that terfenadine and its salts contain water. The number of moles of water present in terfenadine and the salts was calculated from the TGA and the Karl-Fischer data and is shown in Table 5.6 (calculations were based on results in Table 5.4 and on the fact that one mole of terfenadine reacts with one mole of the dicarboxylic acid).

Table 5.6 Moles of water per 1 mole of compound as calculated from TGA and Karl-Fischer data (n = 3 - 4) and the molecular weights of terfenadine and its salts.

Compound	Moles of water in the sample based on TGA (S.D.)	Moles of water in the sample based on Karl-Fischer (S.D.)	Molecular weight (g/ mole)
Terfenadine	0.05 (0.01)	0.02 (<0.001)	471.7
Terfenadine oxalate	2.1 (0.12)	2.4 (0.01)	560.7
Terfenadine succinate	2.3 (0.14)	2.7 (0.02)	588.7
Terfenadine glutarate	2.5 (0.04)	2.9 (0.13)	602.7
Terfenadine adipate	0.3 (0.01)	0.3 (0.01)	616.7

N.B. Molecular weights were based on the fact that one mole of terfenadine reacts with one mole of the dicarboxylic acid

Taking the presence of water into account in the theoretical calculations of the percentages of carbon, hydrogen and nitrogen (Table 5.7) gives results, which are closer to the practical percentages obtained by elemental analysis, than the original theoretical percentages, which were calculated, based on the assumption that water was absent in the samples (Table 5.5).

Data in Table 5.6 were obtained from the calculations, which were done as follows:

$$\text{No of moles of water} = \frac{mw \times MW}{Wd}$$

Where:

mw: Moles of water present in the sample as calculated from percentage weight loss in TGA or water percentage from Karl-Fischer titration.

MW: Molecular weight of the compound as seen in Table 5.6

Wd: mass of compound in grams as calculated from the percentage of water in the sample (calculated from TGA or Karl-Fischer data in Table 5.4).

Table 5.7 Theoretical percentages of carbon, hydrogen and nitrogen based on the presence of water in terfenadine and its salts.

Compound	Moles of water assumed	Theoretical %		
		Carbon (C)	Hydrogen (H)	Nitrogen (N)
Terfenadine	0.5	79.9	8.7	2.9
Terfenadine oxalate	2	68.3	7.9	2.3
Terfenadine succinate	2-3	67.1-69.0	8.2	2.2
Terfenadine glutarate	2-3	67.5-69.4	8.3-8.4	2.1-2.2
Terfenadine adipate	0.5	72.8	8.3	2.2

The moles of water assumed in the calculations of the theoretical percentages of carbon, hydrogen and nitrogen shown in Table 5.7 were approximations of Karl-Fischer and TGA data seen in Table 5.6 as the samples might have lost some water prior to elemental analysis (samples stored at 0 % RH over silica gel) since TGA was done before elemental analysis while Karl-Fischer was performed on freshly prepared samples which might contain the highest percentage of water. In case of terfenadine and terfenadine adipate half a mole of water was assumed in the calculations of CHN since the moles of water seen by TGA and Karl-Fischer were very low. It can be seen that the theoretical percentages of carbon, hydrogen and nitrogen shown in Table 5.7 and calculated based on the presence of water in the samples are in better agreement with the practical percentages obtained (Table 5.5) than the theoretical data calculated assuming the absence of water in the samples (Table 5.5). The results suggest that all salts from the oxalate to the glutarate (excluding the adipate) may be hydrates with a stoichiometric amount of water suggesting their presence as dihydrates with the possibility of having the succinate and the glutarate derivatives as trihydrates. On the other hand, terfenadine and terfenadine adipate contain water in the physically adsorbed form onto their crystalline structures. Whether these 3 salts (oxalate, succinate and glutarate) are stoichiometric hydrates, non stoichiometric

hydrates or contain water adsorbed onto their crystalline surfaces or a combination of both cannot be known for sure in the absence of a single crystal crystallography which could not be done due to the lack of this piece of equipment. Hydrates are well discussed by Zografi (1988), Zografi and Hancock (1994) and Byrn (1982).

5.3 RELATIONSHIP BETWEEN CARBON CHAIN LENGTH AND MELTING POINTS OF TERFENADINE AND ITS SALTS:

Table 5.8 and Figure 5.23 show the relationship between carbon chain length of the dicarboxylic acid part of the molecule and the melting points in the series of terfenadine and its salts.

Table 5.8 Melting points of terfenadine and its salts in relation to carbon chain length of the dicarboxylic acid side chain.

Compound	No of carbons in dicarboxylic acid side chain	Peak melting points (°C) (S.D.)
Terfenadine	0	152.4 (0.6)
Terfenadine oxalate	1	97.8 (0.3)
Terfenadine succinate	3	90.9 (0.4)
Terfenadine glutarate	4	88.2 (0.3)
Terfenadine adipate	5	162.2 (0.8)

N.B. The melting point of terfenadine is taken from Table 3.1 and the melting points of the other salts from Table 5.1

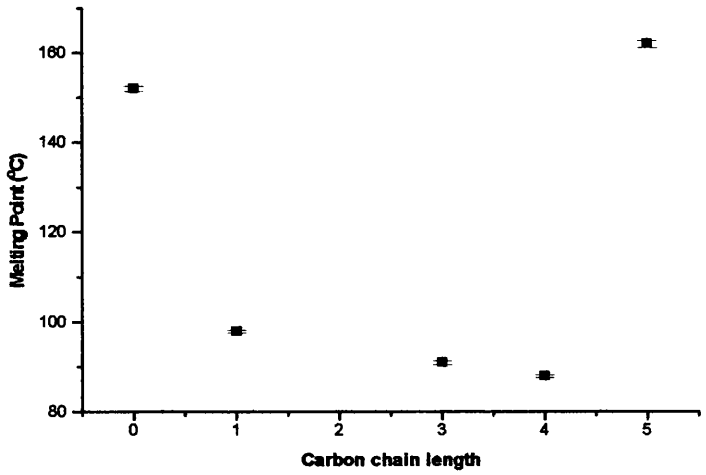

Figure 5.23 Melting points of terfenadine and its salts as a function of the number of carbons in the dicarboxylic acid side chain.

It can be noted from Table 5.8 and Figure 5.23 that there is a large drop in melting points from terfenadine to the shortest chain derivative (terfenadine oxalate). As the chain length of the dicarboxylic acid is increased, the melting point of the resulting terfenadine salt decreases in a linear fashion going from the oxalate to the glutarate and rises sharply from the glutarate to the adipate derivative. These results are in keeping with trends seen for other homologous derivatives of parent molecules (Foster et al., 1991; Yalkowsky et al., 1972; Buckton et al., 1991) whereby changes in trends were observed at a carbon chain length of 5. The reason for changes at 5 C was thought to be because the 5 C chain has sufficient flexibility and length to fold on itself and therefore allow a completely different packing geometry. This relationship shows stronger lattice bonding for terfenadine and terfenadine adipate, with weaker lattices in the crystals of intermediate chain length derivatives. It can be noted form Table 5.8 and Figure 5.23 that the three hydrous salts (terfenadine oxalate, terfenadine succinate and terfenadine glutarate) exhibit a trend in their melting points showing a decrease in its value when going from the oxalate to the glutarate derivative. At the same time, the melting points of these three hydrous salts are closer to each other than to either terfenadine or terfenadine adipate. The anhydrous forms (terfenadine and terfenadine adipate) show close melting points (ca. 152 °C for terfenadine and ca. 162 °C for terfenadine adipate) that are higher than the melting points of the rest of the series (Figure 5.23 and Table 5.8). Thus the trend seen in Figure 5.23 might be related to whether the derivative is a hydrate or an anhydrate.

5.4 AMORPHOUS TERFENADINE SALTS:

5.4.1 PREPARATION OF AMORPHOUS TERFENADINE SALTS:

Amorphous terfenadine salts are prepared by melting and slow cooling from the melt. This is the same method as the one used for the preparation of amorphous terfenadine and described in Section 3.2.1.1. The temperature during preparation did not exceed ~170 °C. Amorphous forms of the salts were also obtained by running the crystalline forms in DSC pans at 10 °C /min up to 180 °C, left to cool to 30 °C and rerunning on the DSC.

5.4.2 CHARACTERIZATION OF AMORPHOUS TERFENADINE SALTS:

5.4.2.1 CHARACTERIZATION OF AMORPHOUS TERFENADINE SALTS: DIFFERENTIAL SCANNING CALORIMETRY (DSC)

5.4.2.1.1 METHOD:

Differential scanning calorimetry was carried out in non-hermetically sealed aluminium pans from 30 to 180 °C at 10 °C/min. The samples weighed 5 $\pm$ 1 mg (when the amorphous form was obtained by a rerun of the crystalline form) or a single bead of the slow cooled form, which weighs 12 $\pm$ 2 mg. The basic principles of DSC were discussed in Section 2.1.3.

5.4.2.1.2 RESULTS:

The DSC traces of amorphous terfenadine salts are shown in Figure 5.24

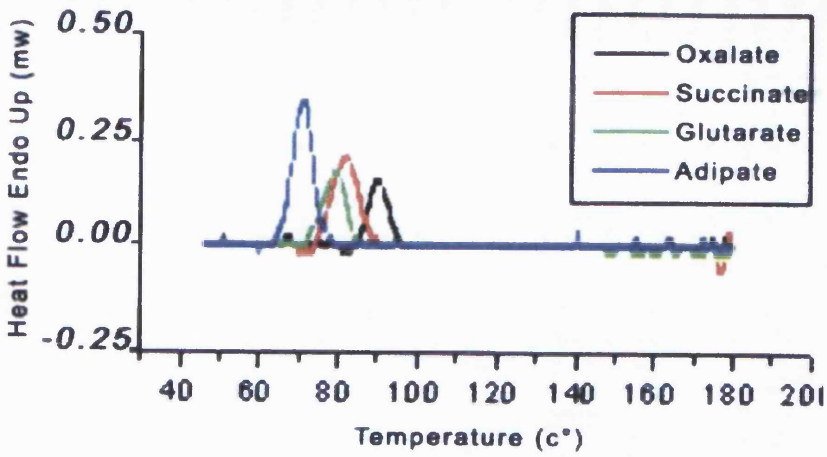

Figure 5.24 *DSC trace showing the glass transition temperatures of terfenadine salts.*

The DSC traces of all amorphous terfenadine salts in Figure 5.24 were taken as first run values in the DSC. They show the absence of a melt and just glass transition temperatures that are indicative of amorphous solids and which appear as tiny peaks are seen. The appearance of these Tg traces in the form of peaks in Figure 5.24 is due to relaxations in the amorphous samples that are overlapping with the Tg event. DSC results of amorphous terfenadine salts are shown in Table 5.9.

Table 5.9 Glass transition temperatures of amorphous salts as determined by DSC (n = 5).

Compound	**Glass transition temperatures (Tg) as measured by DSC (°C), (S.D.)**
Terfenadine Oxalate	89.8 (1.0)
Terfenadine succinate	82.7 (0.8)
Terfenadine glutarate	79.9 (0.7)
Terfenadine adipate	71.7 (1.0)

It can be seen from Figure 5.24 and the data in Table 5.9 that there is a sequential decrease in the glass transition temperature going from terfenadine oxalate to terfenadine adipate. This is explained as being due to a sequential addition of methylene groups going from the oxalate to the adipate which results in an increase in the mobility and flexibility of the molecule as explained by Carraher (1996).

5.4.2.2 CHARACTERIZATION OF AMORPHOUS TERFENADINE SALTS: DYNAMIC DIFFERENTIAL SCANNING CALORIMETRY (DDSC)

5.4.2.2.1 METHOD:

DDSC is a modulated type of a differential scanning calorimeter. The basic principles of DDSC are explained in Section 2.1.4. It is an excellent method for Tg determination of amorphous solids. The purpose of this study was to compare the Tg values obtained by DSC with those obtained by DDSC for terfenadine and its salts. The experiments were carried out using a Perkin Elmer (Pyris 1) in a heat /hold mode and the samples were run from an initial temperature of 20 °C to a second temperature of 22 °C up to 110 - 180 °C, holding the sample isothermally at initial temperature for 30 seconds. Cooling was turned on one hour prior to testing in order to guarantee a stable baseline. Non-hermetically sealed aluminium pans were used in which the bottoms were flattened by applying pressure on the sealed pan using a spatula. The flat bottom of the pan is essential in DDSC experiments in order to achieve a flat baseline.

5.4.2.2.2 RESULTS:

DDSC traces of terfenadine salts are shown in Figures 5.25 – 5.28. The glass transition temperatures were calculated as mid points with half of the heat capacity (Cp) extrapolated.

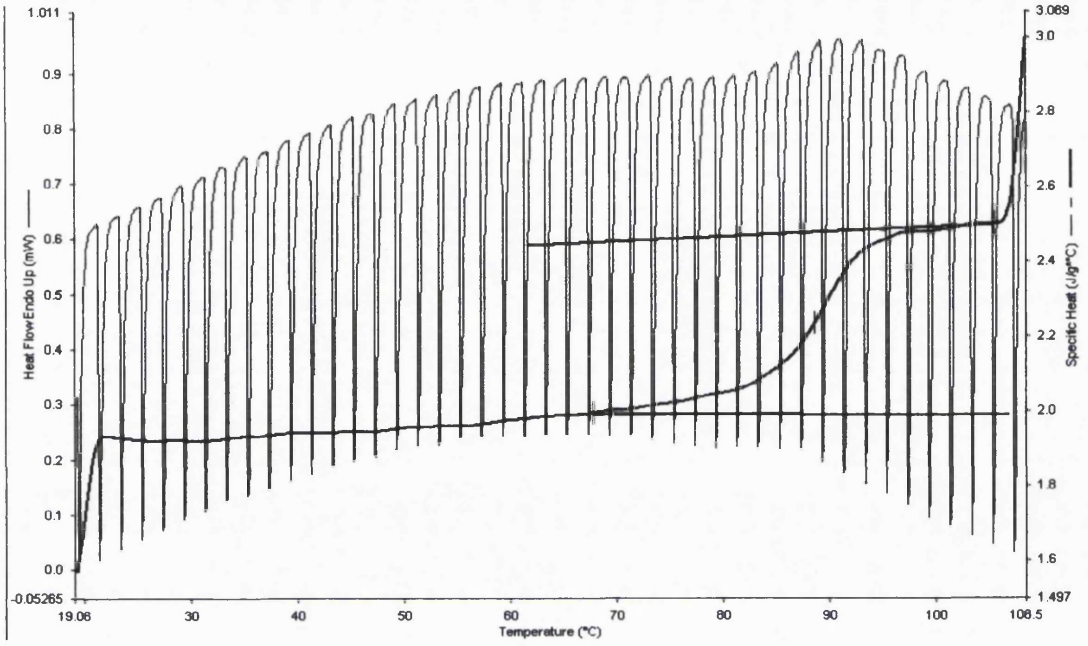

Figure 5.25 *DDSC trace of the heat flow signal and the storage Cp showing the glass transition temperature of terfenadine oxalate.*

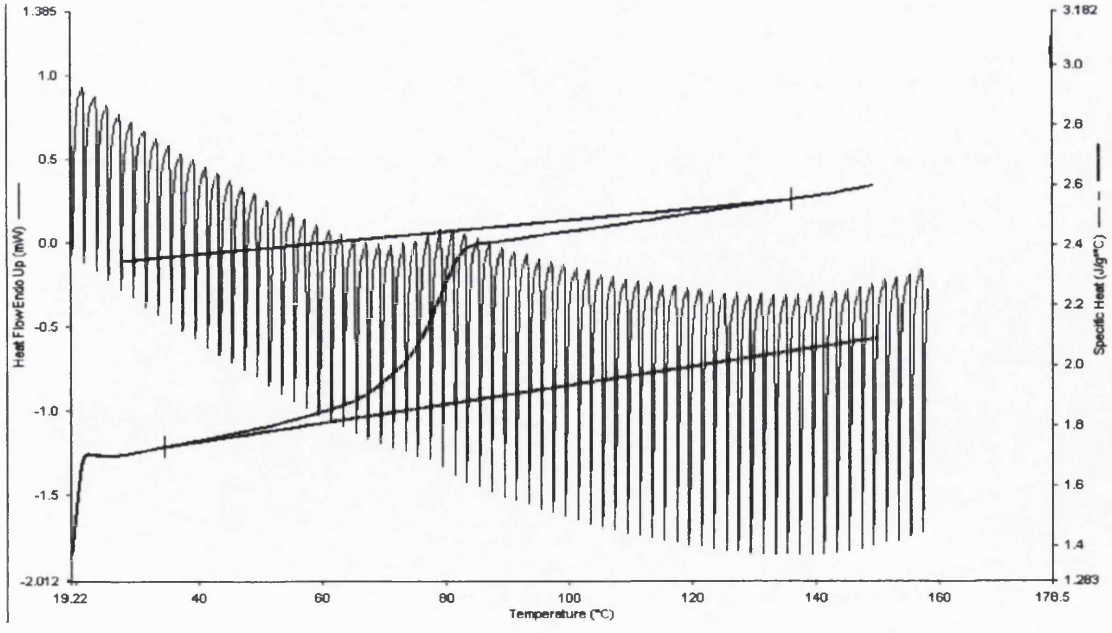

Figure 5.26 *DDSC trace of the heat flow signal and the storage Cp showing the glass transition temperature of terfenadine succinate.*

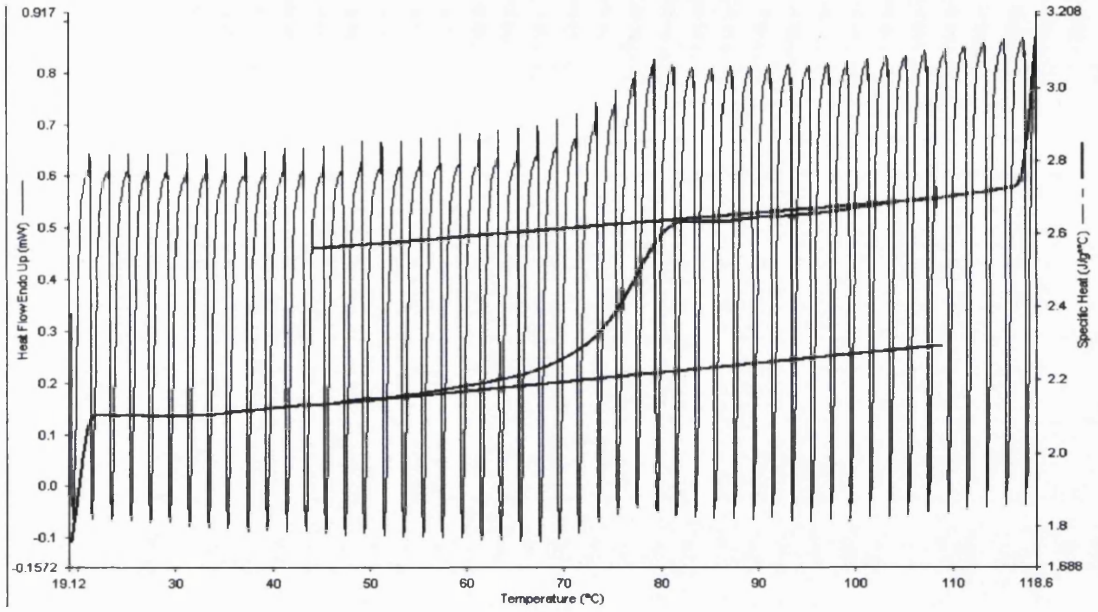

Figure 5.27 *DDSC trace of the heat flow signal and the storage Cp showing the glass transition temperature of terfenadine glutarate.*

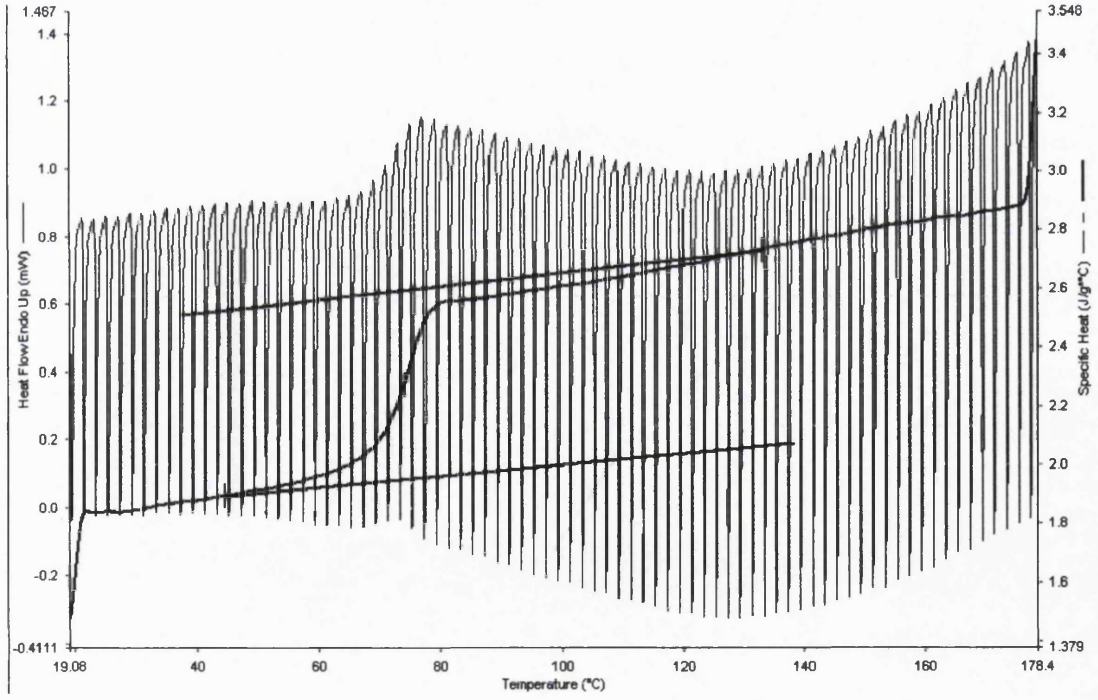

Figure 5.28 *DDSC trace of the heat flow signal and the storage Cp showing the glass transition temperature of terfenadine adipate.*

Glass transition temperatures as determined by DDSC for terfenadine salts are presented in Table 5.10. It can be seen that the Tg values using DDSC are slightly lower than those obtained from DSC (Table 5.9). This is explained as being due to the lower frequency of heating and the longer experiment time in case of DDSC in comparison with DSC experiments. DDSC involves a dynamic heat flow signal in which the thermal effects due to stress relaxation in the region of the glass transition temperature can be separated from and do not show on the dynamic curve and this makes Tg assignment particularly straightforward. This cannot be achieved on a conventional DSC where enthalpic relaxations can make it difficult to get an accurate and clear assessment of Tg by a first run of the sample on the DSC. A rerun of the amorphous sample on the DSC gets rid of the irreversible enthalpic relaxations and maintains the reversible Tg while a second run can be spared in case of DDSC. In DDSC, the in-phase component (storage Cp) of the heat flow signal (related to structural changes such as at Tg) can be separated from out of phase signal, which is related to other thermal events where energy is put in the system but without a consequent increase in temperature.

Table 5.10 Glass transition temperatures of terfenadine salts as determined by DDSC using a heat/ hold mode (n =3).

Compound	Glass transition temperature (Tg) as determined by DDSC (°C), (S.D.)
Terfenadine oxalate	86.2 (1.0)
Terfenadine succinate	77.9 (0.1)
Terfenadine glutarate	76.4 (0.3)
Terfenadine adipate	68.9 (0.1)

A comparison of the DSC traces (Figure 5.24) with the DDSC traces (Figures 5.25 – 5.28) of terfenadine and its derivatives shows that a clearer glass transition temperature, which appears as a step in the baseline, can be seen in the case of the DDSC whereas the glass transition temperature shows as a tiny peak when the DSC was used. This is due to the overlap of relaxations with the glass transition temperatures in the case of the DSC

while relaxations were separated from the glass transition temperature when the DDSC was used which obviously makes the DDSC a better piece of equipment for the measurement of Tg values.

5.5 RELATIONSHIP BETWEEN CARBON CHAIN LENGTH AND GLASS TRANSITION TEMPERATURES OF TERFENADINE AND ITS SALTS:

Figure 5.29 and Table 5.11 show the relationship between carbon chain length in the dicarboxylic acid part of the compound and the glass transition temperatures in the homologous series of terfenadine and its salts.

Table 5.11 Glass transition temperatures of terfenadine and its salts in relation to carbon chain length of the dicarboxylic acid side chain.

Compound	No of carbons in dicarboxylic acid side chain	Tg (°C) (S.D.)
Terfenadine	0	58.5 (1.3)
Terfenadine oxalate	1	89.8 (1.0)
Terfenadine succinate	3	82.7 (0.8)
Terfenadine glutarate	4	79.9 (0.7)
Terfenadine adipate	5	71.7 (1.0)

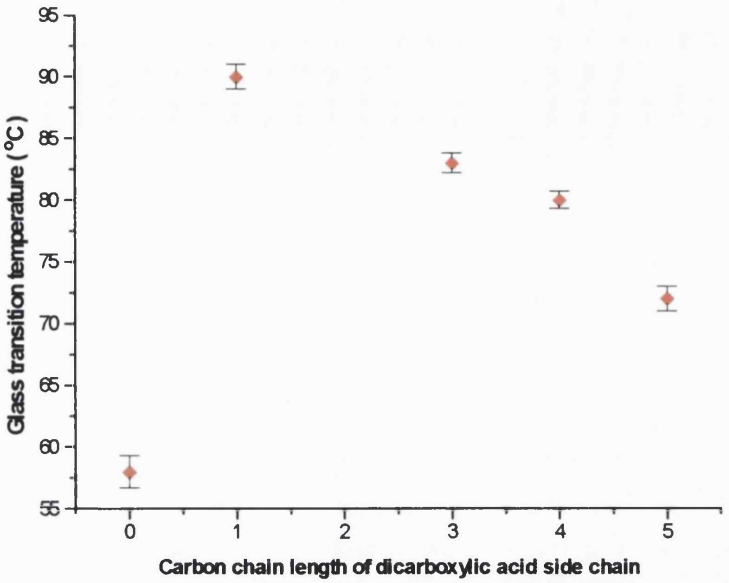

Figure 5.29 *Glass transition temperatures of terfenadine and its salts as a function of the number of carbons in the dicarboxylic acid side chain.*

From Figure 5.29 and the data in Table 5.11, it can be noted that the number of carbon atoms in the dicarboxylic acid chain correlates inversely with the glass transition temperature (Tg) of the resulting compound. The presence of methylene groups contributes to an increase in the flexibility of the molecule Seymour and carraher (1996).This explains the decrease in Tg as the number of methylene groups increases going from terfenadine oxalate to terfenadine adipate. Terfenadine however, does not follow the trend of the salts in terms of its Tg and this parent molecule seems to possess a relatively higher mobility in the amorphous state than any of the salts. Many structural changes have been reported to affect the glass transition temperature of compounds such as the tendency of Tg to increase in the presence of bulky pendent groups, stiffening groups such as carbonyl, sulfone and p-phenylene as well as the addition of polar groups. On the other hand the Tg tends to decrease in the presence of flexible pendant groups and nonpolar groups. Flexibility is increased and Tg is reduced by the presence of many methylene groups between stiffening groups in the molecular chain Seymour and carraher (1996)It follows that terfenadine oxalate is significantly less flexible than terfenadine, as the Tg is greater; this will be due to the stiffening influence of the carboxylic acid group. In this study, following the substantial jump in Tg for the 1 C derivative, there is a subsequent fall, which means that the longer chain derivatives of terfenadine have greater flexibility than the rigid polar oxalate derivative. The author is not aware of a study in which the effect of

homologous derivatives of a parent molecule has been investigated in the amorphous state.

5.6 PURITY DETERMINATION OF AMORPHOUS AND CRYSTALLINE TERFENADINE AND ITS SALTS USING THIN LAYER CHROMATOGRAPHY:

5.6.1 METHOD:

The basic principles of thin layer chromatography (TLC) were discussed in Section 2.1.12. The system used in the TLC study consisted of the following:
TLC aluminium sheets, 20 x 20 cm, silica gel 60 F_{254}, used as the stationary phase. The mobile phase consisted of the following:
methanol, butanol, water, toluene and acetic acid mixed in the proportions of 2.0: 3.0: 1.0: 2.0: 0.1 respectively.
Terfenadine and the salts, each were dissolved independently in HPLC grade methanol. The solutions were prepared in a concentration of 5 mg/ ml. Samples were prepared by spotting a 5 µl sample by a micropipette on the silica gel plate, 2 cm away from the bottom of the plate (this is considered as the point of origin).
Glass, closed TLC jars containing the mobile phase were left for a couple of hours to saturate the glass chamber with organic vapours before placing the spotted silica gel plates inside. When the mobile phase travelled up the stationary phase a distance of around 11 cm, the developed plates were taken out, left to dry and later read using a UV lamp at 254 nm. The TLC method used in this study was adapted from Badwan et al. (1990).

5.6.2 RESULTS:

Thin layer chromatography was performed on both the crystalline and the amorphous forms of terfenadine and its salts in order to check their purity. TLC results are presented in Table 5.12 for both the amorphous and the crystalline forms

Table 5.12 Rf values of amorphous and crystalline forms of terfenadine and terfenadine salts determined by TLC (n = 3).

Compound	Rf in crystalline form (S.D.)	Rf in amorphous form (S.D.)
Terfenadine	75.2 (0.2)	74.3 (0.7)
Terfenadine oxalate	74.7 (0.1)	73.7 (1.1)
Terfenadine succinate	77.0 (0.3)	77.5 (0.3)
Terfenadine glutarate	82.4 (0.5)	78.3 (0.5)
Terfenadine adipate	76.3 (0.5)	75.0 (0.4)

All the samples resulted in the appearance of one spot on the TLC silica gel plates under UV lamp at 254 nm and the results were determined in triplicate.

From the results in Table 5.12, it can be noted that the Rf values are comparable yet slightly different among the five compounds. This indicated that both crystalline and amorphous samples are pure and that the amorphous forms stayed pure after heating and slow cooling during preparation of the amorphous samples.

5.7 STABILITY EVALUATION OF CRYSTALLINE TERFENADINE AND ITS SALTS BY EXPOSURE TO HEAT UNDER VACUUM:

This part of the experimental work was carried out in an attempt to dry the crystalline samples from water and while doing this to try and investigate whether these crystalline salts are hydrates or contain physically adsorbed water. There are two types of solvates in terms of their behaviour upon removal of the solvent involved in their crystalline structures. Those which do not collapse upon removal of the solvent of crystallization from their crystalline solvate structure but rather transform into the anhydrous form. A second type of solvates is one, which collapses into an amorphous form once the solvent of crystallization is removed from the crystalline structure. This was discussed by Byrn (1982), Saleki-Gerhardt et al. (1995), Tong and Zografi (1999), Hogan and Buckton (2001a).

5.7.1 METHOD:

All crystalline salts were stored at 50 °C under vacuum at 400 mbar pressure. In the beginning, samples were followed up for the first two weeks but without any noticed changes in their DSC profiles (in comparison with the original thermograms of the crystalline salts, Figures 5.1 – 5.4). The crystalline salts were then left in the vacuum oven for a total of ca. 5 months before storing over silica gel at 0% RH and testing on the DSC again. The DSC runs were performed from 25 – 180 °C at 10 °C /min using hermetically sealed aluminium pans under nitrogen atmosphere. Hermetically sealed pans were used since the presence of water affects the Tg value obtained if any of the samples collapsed into the amorphous form.

5.7.2 RESULTS:

Table 5.13 shows the DSC results after one year of the preparation of the crystalline salts and after 6 months of storage of the crystalline samples in the vacuum oven at 50 °C and 400 mbar.

Table 5.13 DSC results of terfenadine and its salts after being stored in a vacuum oven for ca. 6 months at 50 °C and 400 mbar (n = 3 – 4).

Compound	Tg (°C) (S.D.)	Tm (°C) (S.D.)
Terfenadine	A	152.7 (0.7)
Terfenadine oxalate	87.4 (1.3)	A
Terfenadine succinate	79.5 (2.2)	A
Terfenadine glutarate	76.7 (0.9)	A
Terfenadine adipate	A	163.4 (0.1)

A: absent from the DSC trace.

DSC results in Table 5.13 show the absence of any melt and just a glass transition temperature corresponding to the Tg of the amorphous form in the case of terfenadine oxalate, terfenadine succinate and terfenadine glutarate. As for terfenadine and terfenadine adipate, the samples did not exhibit any change in their DSC thermograms from their original DSC profiles (Figures 3.1 and 5.4 respectively). Terfenadine and terfenadine adipate stayed crystalline with the absence of any Tg as seen in Table 5.14. Terfenadine adipate gave a melting peak of ca.163 °C in comparison with the original DSC thermogram, which had a melting peak at ca. 162 °C. Terfenadine had a melting peak of ca. 153 °C in comparison with ca. 152 °C for the original crystalline sample.

A rerun of the salts on the DSC from the oxalate to the glutarate, gave reproducible Tg values assuring that these three salts are in the amorphous form. It has been suggested by Saleki-Gerhardt et al., (1995) that the hydrate form of raffinose collapses into an amorphous form when it loses the more intimately bound water molecules that are involved in the crystalline network. Byrn (1982) also suggested that solvates or hydrates could collapse into an amorphous form. Taylor et al. (1998) showed that trehalose dihydrate with a particle size of < 45 μm collapses into an amorphous form upon heating at 80 °C while that with a particle size of > 425 μm gives the crystalline anhydrous form upon heating at 80 °C. Tong and Zografi (1999) reported that sodium indomethacin trihydrate resulted in partial formation of the amorphous form when heated at a slow heating rate of < 10 °C/ min while dehydration at faster heating rates kept the crystalline state intact resulting in a crystal anhydrate form. Hogan and Buckton (2001a) showed that drying of raffinose pentahydrate in a DVS-NIR instrument could detect collapse of raffinose pentahydrate into the amorphous form as indicated by the NIR spectral peaks and that loss of crystallinity occurred when the water level fell to the equivalent of the monohydrate.

We can thus conclude from those results as well as from the TGA and Karl- Fischer results that the first three salts (oxalate, succinate and glutarate) contain water as hydrates and they do collapse into amorphous forms when the water is lost from their structures suggesting that some water is intimately involved in the crystalline structure in the form of a hydrate and not simply a physically adsorbed water. However, whether these hydrates are trihydrates, dihydrates or monohydrates with some physically adsorbed water (refer to TGA and Karl- Fischer results, Table 5.6), cannot be known for sure in the absence of single crystal crystallography.

5.8 CORRELATIONS BETWEEN Tm/Tg RATIO AND SOME PHYSICAL PROPERTIES OF TERFENADINE AND ITS SALTS:

The melting points (Tm) of the crystalline form of terfenadine and of its derivatives can be calculated as a ratio to the glass transition temperatures of their amorphous counterparts (using temperature on the Kelvin scale). These data are reported in Table 5.14. The values range from 1.02-1.28.

Table 5.14 Tm/ Tg ratios and their reciprocal as calculated from DSC data based on Kelvin temperatures.

Compound	Tm/ Tg	Tg/ Tm
Terfenadine	1.28	0.78
Terfenadine oxalate	1.02	0.98
Terfenadine succinate	1.02	0.98
Terfenadine glutarate	1.02	0.98
Terfenadine adipate	1.26	0.79

Similar treatments to the data were carried out by other workers reporting Tm/ Tg values of some carbohydrates (Roos, 1993, Slade and Levine, 1991). Slade and Levine showed that fructose and galactose demonstrated low Tm/ Tg values of 1.06 and 1.16 respectively. It was then debated that these low values reflect higher free volume requirement and lower viscosity in the glassy state with Tg falling near Tm (Tm -Tg much less than 100 °C).

Polymers with high Tm/ Tg ratio (>> 1.5) are considered to be readily crystallisable (Slade and Levine, 1991). Other workers (Kajiwara and Franks, 1997) have reported the ratio for raffinose and its different hydrate forms as Tg/ Tm. The values ranged from 0.74 to 0.94 for different raffinose hydrates. From Table 5.14 it can be observed that an identical Tm/ Tg value (1.02) is obtained for terfenadine oxalate, terfenadine succinate

and terfenadine glutarate. This Tm/ Tg ratio is considered to be low (even lower than the values reported by Slade and Levine, 1991). These low values indicate low local viscosity ($<< 10^{10}$ Pa s) and high free volume in the glassy state with a small difference between Tg and Tm. The Tm/ Tg ratio for terfenadine adipate is very similar to that of terfenadine (1.26 and 1.28 respectively). Consequently, terfenadine and terfenadine adipate have very similar behaviour whereas the shorter chain derivatives have different Tm/Tg ratios. The packing in the crystalline and amorphous states both relate to the derivative structure, however, the consequences of the structural changes are different depending upon whether the material is amorphous or crystalline.

5.9 DISCUSSION:

From the above data it can be concluded that all terfenadine derivatives are ammonium salts. NMR and elemental analysis show that the interaction between terfenadine and the dicarboxylic acids takes place in a 1 : 1 stoichiometric ratio. DSC and powder X-ray diffraction show that all terfenadine salts are crystalline. TGA, Karl-Fischer and elemental analysis are in good agreement in terms of water content and show that terfenadine and its salts contain the percentages of water in the samples as shown in Tables 5.6 and 5.7 and that the loss of this water coincides with their melting points, hence there is the probability that the oxalate, succinate and glutarate salts are hydrates. This was investigated further (Section 5.7) as the crystalline samples of terfenadine and its salts were stored in an oven under vacuum at 50 °C and 400 mbar. Differential scanning calorimetry showed that terfenadine oxalate, terfenadine succinate and terfenadine glutarate have collapsed into their amorphous forms (when checked after 6 months of storage under those conditions). Figure 5.22 and Table 5.8 show the melting points of terfenadine salts as determined by DSC in relation to carbon chain length. From Table 5.8 and Figure 5.22, it can be noted that there is a substantial drop in the melting point from terfenadine to the shortest chain derivative (oxalate). This is followed by a linear decrease in melting point as the chain length of the dicarboxylic acid is increased going from the oxalate to the glutarate derivative (Figure 5.18). The melting point then rises sharply from the glutarate to the adipate derivative. These results are in keeping with trends seen for other homologous derivatives of parent molecules (Foster et al., 1991, Yalkowsky et al., 1972) whereby changes in trends are observed at a carbon chain length of 5. The reason for changes at 5C is thought to be because the 5C chain has sufficient

flexibility and length to hold on itself and therefore allow a completely different packing geometry. This relationship shows a stronger lattice bonding for the terfenadine and the terfenadine adipate, with weaker lattices in the crystals of intermediate chain length derivatives. The trend in melting points in relation to carbon chain length may also be related to the fact the three intermediate compounds (terfenadine oxalate to terfenadine glutarate) are hydrates whereas terfenadine and terfenadine adipate are anhydrates. Table 5.11 and Table 5.28 show the relationship between the carbon chain length of the dicarboxylic acid part of the molecule and the glass transition temperature. The results show a decrease in Tg going from the oxalate salt with 1 C to the adipate with 5 C in its side chain. Terfenadine behaves differently in the amorphous state from the salts as it shows the highest mobility as suggested by its possessing the lowest Tg value among the group. Tm/ Tg ratios prove that the oxalate, succinate and glutarate salts of terfenadine possess the same low Tm/ Tg ratio (1.02). A low Tm/ Tg ratio suggests that these compounds are relatively less readily crystallisable with Tg falling close to Tm, while both terfenadine and terfenadine adipate have similar and higher Tm/ Tg ratios of 1.28 and 1.26 respectively. These ratios indicate that terfenadine and terfenadine adipate are comparatively the most readily crystallisable among the group. Indications of higher Tg values and a lower Tm/ Tg ratios suggest that terfenadine oxalate, terfenadine succinate and terfenadine glutarate are more physically stable than terfenadine adipate or the parent compound (terfenadine).

CHAPTER SIX

SOLUBILITY STUDY OF TERFENADINE AND ITS SALTS IN THE CRYSTALLINE AND AMORPHOUS FORMS USING HIGH PERFORMANCE LIQUID CHROMATOGRAPHY

6 INTRODUCTION:

It is well known that the solubility of basic drugs can be enhanced through salt formation, as in this case the drug becomes more ionised and hence may become more water-soluble. At the same time, the amorphous form of the drug usually possesses a greater solubility than its crystalline counterpart. Moustafa et al. (1971) reported a higher solubility of the amorphous form of sulphamethoxydiazine in 0.1 M HCl than its crystalline polymorphs but with crystallization starting approximately after 15 minutes of contact with the dissolution medium at 70 rpm and 30 °C. Hancock and Parks (2000) reported higher solubility of the amorphous forms of several drugs in comparison with their crystalline forms. They argued that the experimentally obtained solubility of the amorphous forms is less than that predicted from simple thermodynamic considerations (entropy, enthalpy and free energy difference between the amorphous and the crystalline form). They explained that this reduction in the obtained solubility relative to the predicted solubility is due to the difficulty in measuring the true equilibrium solubility of the amorphous form because of the strong driving force for crystallization in the presence of the dissolution medium. Solubility can also be enhanced by presence of amorphous regions in a basically crystalline solid. Chiou and kyle (1979) showed that trituration led to the development of amorphous regions in crystalline digoxin and digitoxin powders leading to higher aqueous solubility, yet with crystallization of the amorphous regions taking place in the dissolution medium. Particle size is another factor that has to be considered when performing a solubility study as particle size can affect the apparent solubility of a solid. Buckton and Beezer (1992) explained that for small particle sizes a larger surface area is obtained which results in an increase in the rate of solution. In this case higher solubility values may be achieved practically but it has to be acknowledged that this solubility value is the one achievable in the time scale of the experiment and is thus called apparent solubility. The apparent equilibrium solubility should never be confused with the true thermodynamic equilibrium solubility, which is achieved when the Gibb's free energy term (ΔG) equals zero. Thus, particle size can alter the rate at which equilibrium is achieved but cannot change the (time independent) equilibrium solubility value. Florence and Salole (1975) explained that the dissolution characteristics of poorly soluble drugs may be complex functions of the surface area and the degree of crystallinity and hence a powder dissolution test is very helpful since it involves the influences of particle size, aggregation and polymorphism

(when present). When both small and large particles are present in the same solution within a system containing suspended particles, the solute diffuses from the layer surrounding small particles to the layer surrounding larger particles and precipitation of the smaller particles occurs on the surface of the larger particles (Lachman et al., 1986). This might apply in a solubility study where an excess amount of the drug of uncontrolled particle size is added while the degree of agitation in the dissolution medium was insufficient to prevent aggregation of the solid.

The aims of this study were:

- To investigate the solubility profiles of both the crystalline and the amorphous forms of terfenadine and its salts in buffer solutions at two pH values of 2 and 6, which are simulating the gastric and intestinal pH respectively.
- To check if the amorphous forms of the salts, of a potentially higher physical and chemical stability (as indicated by higher Tg values and lower Tm/ Tg ratios), exhibit higher solubility than amorphous terfenadine.
- To check the relationship between the carbon chain length in terfenadine and its salts (in both the crystalline and the amorphous forms) and the solubility of these compounds in both chloride and acetate buffers.

6.1 METHODS:

6.1.1 PREPARATION OF BUFFER SOLUTIONS:

Chloride buffer was used as the buffer solution to set the pH to a value of 2. The chloride buffer was prepared as specified in the British Pharmacopoeia (1998). 6.57 g of potassium chloride were dissolved in water (HPLC grade water from Merck was used), 119.0 ml of 0.1 M HCl were added, then the volume was continued up to 1000 ml with the same HPLC grade water. The acetate buffer was the one used to set the pH to a value of 6. It was also prepared according to the British pharmacopoeia (1998). 13.6 g of sodium acetate and 6 ml of glacial acetic acid were dissolved in sufficient water to produce 1000 ml. The pH was later measured using a pH meter (Hanna instruments, HI 8519) after being calibrated using two standard solutions one set to give a pH of 4 and the second to give a pH of 7. The instrument was calibrated and later the pH was checked again in triplicates for each standard solution until the pH readings were 4 ± 0.02 and 7 ± 0.03. The pH of both the acetate and the chloride buffer was adjusted to 6 and 2 respectively by using 8 M phosphoric acid (if lowering of pH is needed) and 5 M potassium hydroxide (if raising of pH is required) solutions.

6.1.2 CALIBRATION AND STANDARDIZATION OF THE HPLC SYSTEM:

Prior to the HPLC solubility study, two types of qualification tests were carried out (according to the specifications provided by Merck for the detector, pump and integrator used) in order to validate the accuracy of the system.

a- Operation qualification test:

Involves the individual testing of pump, UV detector and the integrator.

The pump test entailed a check of the flow rate whereby 5 g of purified water were accurately weighed in a beaker on an analytical balance. The weighed water was then passed through the pump at a flow rate of 1 ml/ min. The pump was turned off after five minutes and the output (amount of water pumped out) was reweighed. The weight was recorded to be 5.0 g (Accepted if the value is 5 ± 0.1 g as specified by the Lachrom Merck-Hitachi L-7100 pump specifications manual).

The UV detector was tested with regards to wavelength accuracy and energy of deuterium lamp. The energy of the deuterium lamp was 413 (should be changed if the energy fell below 250 as specified by Lachrom Merck-Hitachi L-7400 UV detector specifications manual) and the wavelength accuracy was checked at 250 nm and the accuracy of the wavelength was 1 nm (accepted if ± 1 nm).

The integrator was checked for qualification of stored data processing. Twelve peaks that were stored in the software of the system were recalculated and their retention times as well as the areas of the peaks and concentrations of their solutions were reported. The results came out to be identical to those previously set in the software of the system.

b- Performance qualification test: Involves testing of the system as a whole whereby qualification of data processing, noise and drift, system suitability, repeatability and linearity were tested. Qualification of data processing was tested by recalculating a stored peak of anthracene with regards to retention time, peak area and concentration. The results were the same as those values stored in the software of the system for anthracene. Checking of noise and drift was carried out by running pure water in a capillary column (instead of any HPLC separation column). The capillary column had a length of 10 meters and a diameter of 0.25 mm. Water was passed through this column for one hour at a flow rate of 1 ml/ min. Noise and drift in the UV signal were recorded as 5 μV and 13 μV/min respectively (Accepted limits were maximum noise of 30 μV and

a maximum drift of 30 μV/min). System suitability was tested by using 50: 50, methanol: water as the mobile phase, 12.5 cm length Lichrosphere column and injecting a standard 100 mg/ L methyl paraben in methanol (Lichrotest set, Merck) into a 10 μl loop. The appearance of one peak was reported and the retention time and peak area were determined. Repeatability was tested by injecting the same 100 mg/L methyl paraben in methanol solution 6 times and calculating the relative standard deviation (RSD) for both the peak areas and retention times. Peak area gave RSD of 0.13 % (accepted if < 1%) and retention time had a RSD of 0.09 % (accepted if < 1%). Linearity was tested by injecting 4 different concentrations of methyl paraben in methanol (1, 10, 100 and 200 mg/L from Lichrotest set, Merck). Each concentration was injected once and a plot of the area of the peak versus concentration gave a correlation coefficient R = 0.9997 (accepted if R is not less than 0.9990 as specified by Merck system performance qualification test report). A standard mixture consisting of a solution of thiourea, methyl paraben, ethyl paraben and propyl paraben in methanol (Lichrotest set, Merck) was injected through the same loop (10 μl) while using the same mobile phase (50: 50, methanol: water) in order to test efficiency of peak separation in the system. Separation of the individual 4 components was established with retention times and areas under the curve in agreement with the expected results (specified with the test mixture by Merck).

6.1.3 PREPARATION OF STANDARD CURVES:

The standard curves of terfenadine and the four salts (oxalate, succinate, glutarate and adipate) were prepared in both chloride and acetate buffer solutions. Different concentrations of the solid were set up (1, 2.5, 5, 10 and 15 μg/ ml) in the buffer solution by weighing an accurate amount of the solid on a sartorious analytical balance and preparing the different concentrations in volumetric flasks while using volumetric pipettes to add the freshly prepared stock solution of the internal standard (bromhexine in either chloride or acetate buffer). The concentration of the internal standard was kept at a constant value of 1 μg/ ml in all of the solutions prepared for standard curves determination as well as in the whole of this solubility study. All the prepared solutions for standard curves determination were quantitatively analyzed by using High Performance Liquid Chromatography (HPLC) using the same procedure applied for the entire solubility study and described in Section 6.1.5. The areas of the obtained drug

peaks were plotted versus concentration. Arafat and Kaddoumi (1995) used bromhexine as an internal standard in developing an HPLC method for the quantitative determination of terfenadine in raw material as well as in tablets; capsules and suspension dosage forms.

Standard curves of all 5 solids at both pH values are shown in Figures 6.1 – 6.10

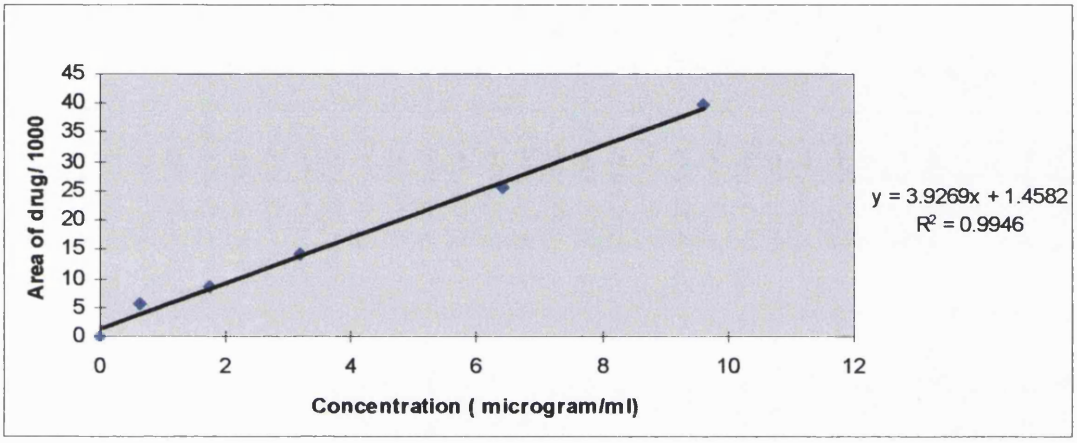

Figure 6.1 *HPLC standard curve of terfenadine in acetate buffer (pH = 6), correlation coefficient* R = 0.997.

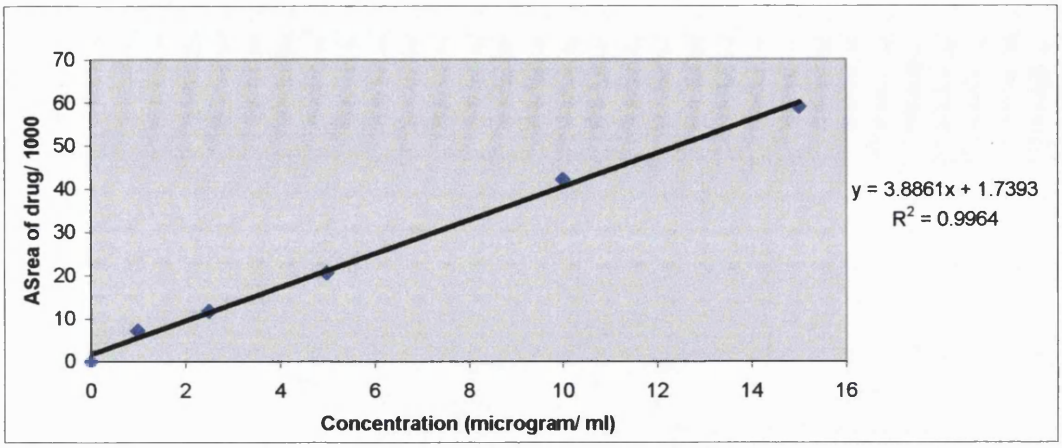

Figure 6.2 *HPLC standard curve of terfenadine oxalate in acetate buffer (pH = 6), correlation coefficient* R = 0.998.

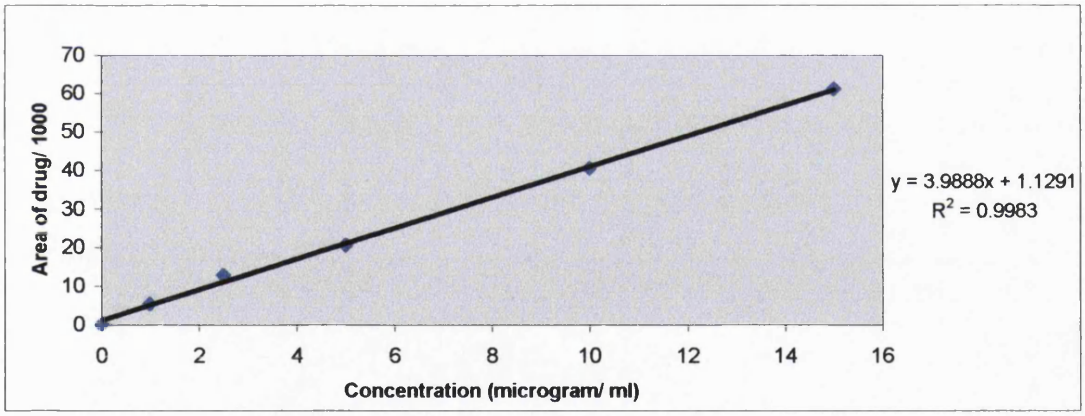

Figure 6.3 *HPLC standard curve of terfenadine succinate in acetate buffer (pH = 6), correlation coefficient* R = 0.9991.

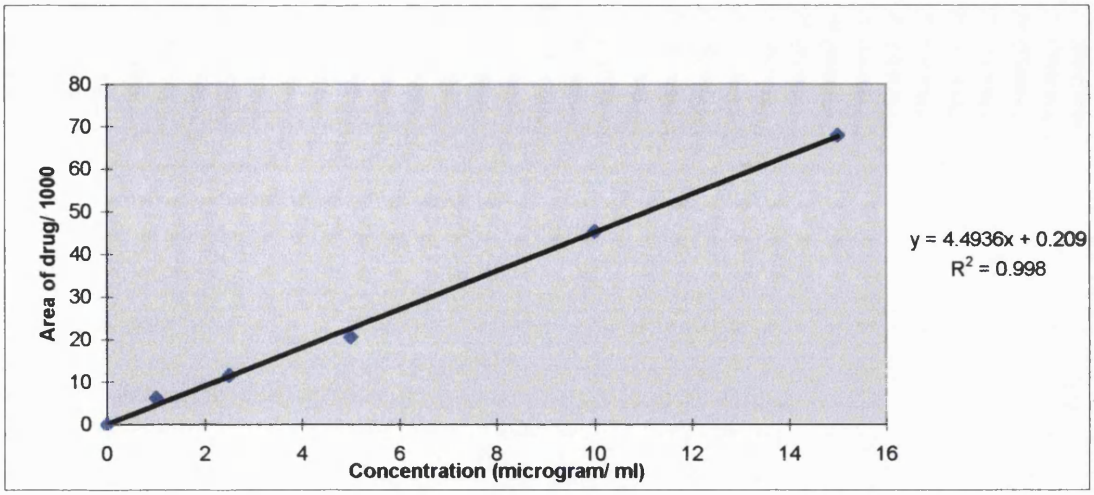

Figure 6.4 *HPLC standard curve of terfenadine glutarate in acetate buffer (pH = 6), correlation coefficient* R = 0.9990.

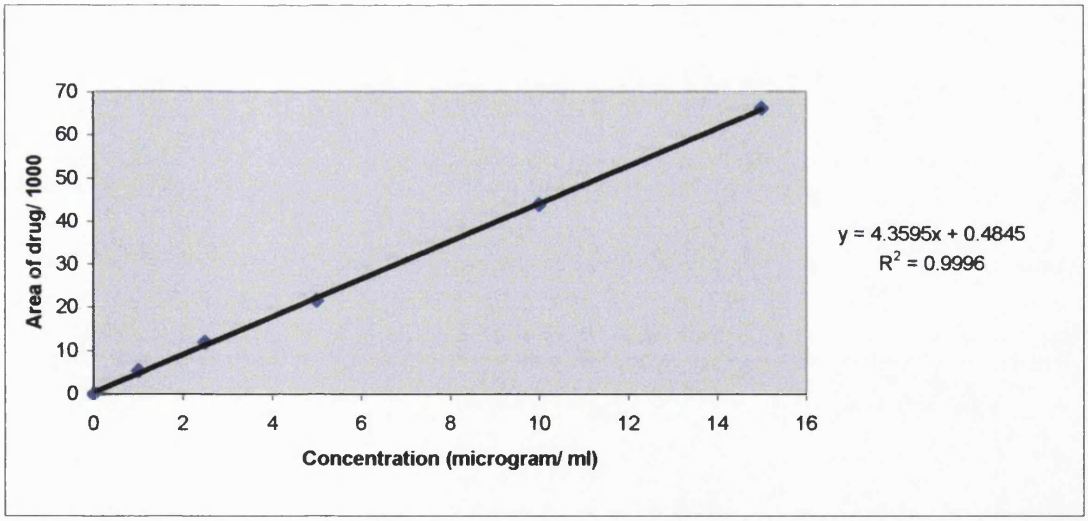

Figure 6.5 *HPLC standard curve of terfenadine adipate in acetate buffer (pH = 6), correlation coefficient* R = 0.9998.

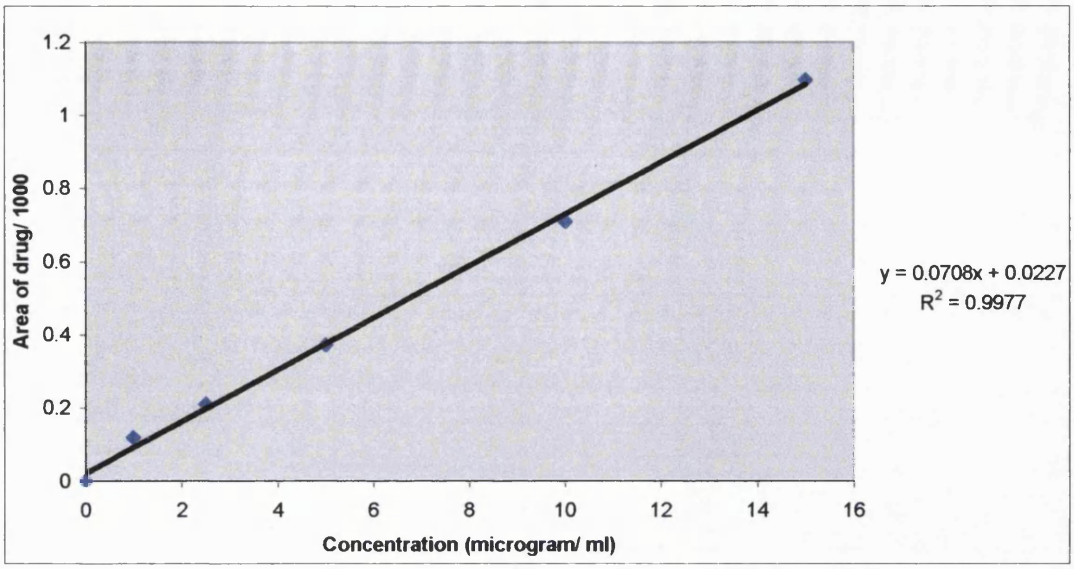

Figure 6.6 *HPLC standard curve of terfenadine in chloride buffer (pH = 2), correlation coefficient* R = 0.9988.

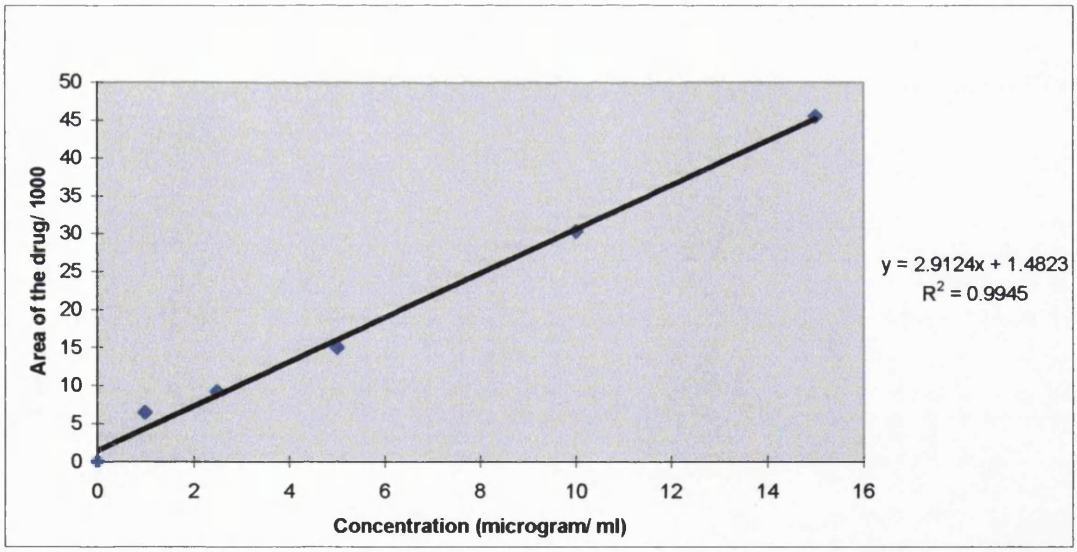

Figure 6.7 *HPLC standard curve of terfenadine oxalate in chloride buffer (pH = 2), correlation coefficient* R = 0.9972.

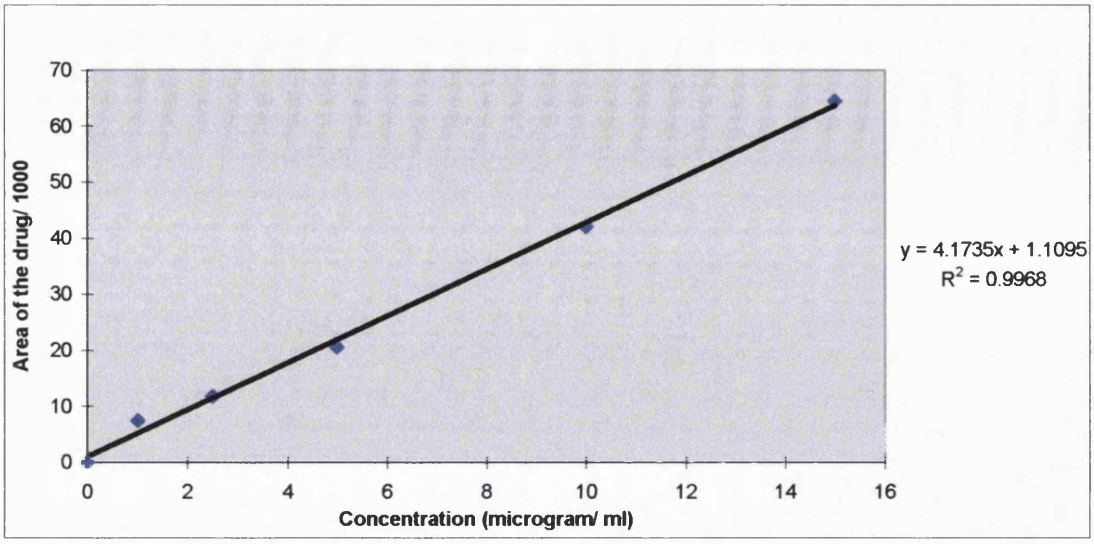

Figure 6.8 *HPLC standard curve of terfenadine glutarate in chloride buffer (pH = 2), correlation coefficient* R = 0.9983.

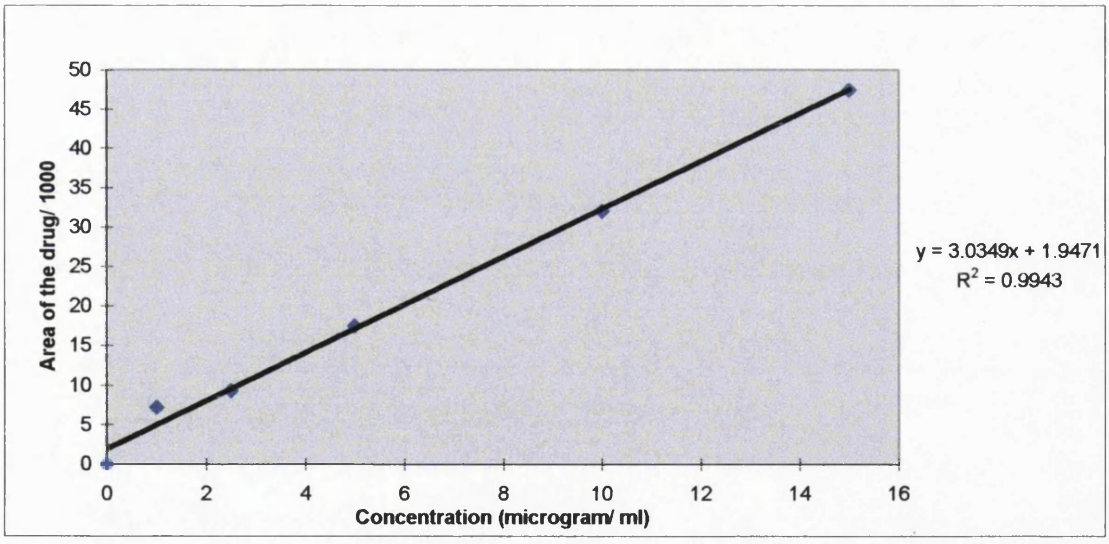

Figure 6.9 *HPLC standard curve of terfenadine adipate in chloride buffer (pH = 2), correlation coefficient* R = 0.9971.

6.1.4 METHOD USED IN THE SOLUBILITY STUDY OF TERFENADINE AND ITS SALTS:

A particle size range of 125 –250 μm was used in this study for crystalline terfenadine oxalate, terfenadine succinate and terfenadine glutarate. The crystalline solids were sieved through a group of sieves (Endecott Ltd., London, UK) using a sieve shaker for 15 minutes (Retsch Type VS 1000 sieve shaker, Germany). Crystalline terfenadine and the adipate salt were very fine and cohesive powders. They passed easily through the smallest sieve of 75 μm upon shaking in the sieve shaker (excluding their aggregates). Milling of the other 3 salts (oxalate, succinate and glutarate) in order to match all particle sizes was avoided in order to keep away from the possibility of triggering some amorphous regions in the crystalline solid which can affect the solubility profile of the crystalline solids. Thus terfenadine and the adipate salt were used as they are with particle size range clearly below 75 μm but with possibility of agglomeration. Amorphous terfenadine and its amorphous salts were prepared by melting and slow cooling from the melt as explained in Section 3.2.1.1 and Section 5.4.1 respectively. The amorphous beads had a large size with a diameter of ca. 3 mm. Crushing of the amorphous beads was avoided since terfenadine adipate crystallized easily even with slight crushing with a spatula and in order to avoid discrepancy, all amorphous forms were used without being crushed. The solubility study was carried out by placing an excess amount of the solid (80 – 100 mg) in a conical flask and adding to it 100 ml of either chloride buffer (pH = 2) or acetate buffer (pH = 6). The flasks were then placed in an ultrasonic water bath at ambient temperature and sonicated for 5 minutes in order to de-aggregate the powders of terfenadine and the adipate salt. In order to avoid discrepancy, all samples were exposed to 5 minutes of sonication regardless of whether or not they form aggregates or whether they are crystalline or amorphous. The flasks were then transferred to a shaking water bath set at a constant temperature of 37 °C and a speed of 40 rpm. The flasks were covered with parafilm in order to prevent water evaporation. Four milliliter samples were withdrawn at 5, 10, 15, 20, 30, 45, 60, 120, 180, 240 and 360 minutes (unless otherwise specified). The samples were filtered into test tubes through medium/ fast filter papers. One milliliter of the filtered, clear sample was then withdrawn by a micropippette and the necessary dilutions were carried out in volumetric flasks with HPLC grade water. Bromhexine was added to all samples to give a final concentration of ca.1-1.5 μg/ ml. This was followed by sonication of the diluted

samples for 5 minutes and leaving them to equilibrate for half an hour before measuring on the HPLC. All results were taken either in duplicate or triplicate.

6.1.5 HPLC METHOD FOR SOLUBILITY STUDY OF TERFENADINE AND ITS SALTS:

The HPLC method used in this study was adapted (with some changes) from the method used by Arafat and Kaddoumi (1995). The mobile phase consisted of 40 % acetate buffer (pH = 6) and 60 % acetonitrile (HPLC grade, Merck). The final pH of the mobile phase was adjusted to 6.45. De-aeration of the mobile phase was carried out by sonication for 20 - 30 minutes prior to use of the mobile phase. The column used was a BDS phenyl column (25 cm, Hypersil) and a 100 µl loop with a 100 µl syringe (giving an injection volume of 100 µl) were employed. The readings were taken at a wavelength of 240 nm using a UV detector. Flow rate was set at 1.2 ml/ min. The basic principles of HPLC were discussed in Section 2.1.13.

6.2 RESULTS:

6.2.1 SOLUBILITY RESULTS OF TERFENADINE AND ITS SALTS AT pH 6:

This study was carried out by studying the solubility of terfenadine and its salts in an acetate buffer adjusted to pH = 6 (prepared as explained in Section 6.1.1). The procedure followed in the solubility study was as described in Section 6.1.4. The HPLC method carried out for the quantitative analysis was the one described in Section 6.1.5. Typical HPLC traces of terfenadine and its salts in acetate buffer are seen in Figures 6.10 –6.14. No degradation was noted in any of the salts nor in terfenadine in the acetate buffer (pH = 6) during the time scale of the experiment as evidenced by the absence of any additional peaks in the HPLC graph apart from the peak belonging to the drug and that belonging to the internal standard (Figures 6.10 – 6.14). Chen et al. (1986) performed an HPLC solution stability study on terfenadine. The authors stated that terfenadine has an excellent stability at pH 5-11 while the maximum stability was achieved in the acetate buffer with 98 % of terfenadine remaining intact after 25 weeks of storage in an acetate buffer (pH =5) under fluorescent light.

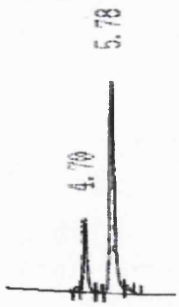

Figure 6.10 *HPLC trace of terfenadine in acetate buffer (pH =6) showing retention times of 4.7 and 5.78 minutes for terfenadine and bromhexine respectively.*

Figure 6.11 *HPLC trace of terfenadine oxalate in acetate buffer (pH =6) showing retention times of 4.88 and 5.76 minutes for terfenadine oxalate and bromhexine respectively.*

Figure 6.12 *HPLC trace of terfenadine succinate in acetate buffer (pH =6) showing retention times of 4.84 and 5.83 minutes for terfenadine succinate and bromhexine respectively.*

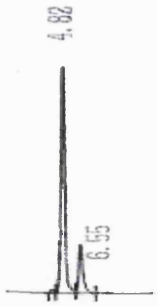

Figure 6.13 *HPLC trace of terfenadine glutarate in acetate buffer (pH =6) showing retention times of 4.82 and 6.55 minutes for terfenadine glutarate and bromhexine respectively.*

Figure 6.14 *HPLC trace of terfenadine adipate in acetate buffer (pH =6) showing retention times of 4.77 and 5.54 minutes for terfenadine adipate and bromhexine respectively.*

Arafat and Kaddoumi (1995) reported retention times of 3.06 and 5.85 minutes for terfenadine and bromhexine respectively in the HPLC chromatographic method that they used.

6.2.1.1 SOLUBILITY OF THE CRYSTALLINE FORMS:

The solubility results of the crystalline forms of terfenadine and those of its salts in the acetate buffer (pH = 6) are shown in Tables 6.1- 6.5

Table 6.1 Solubility results of crystalline terfenadine in acetate buffer at pH = 6 and a temperature of 37 °C (n = 2-3).

Time (minutes)	Concentration in solution (μg/ ml), (S.D.)
5	50.2 (7.9)
10	36.4 (6.9)
15	50.0 (7.4)
30	43.4 (5.8)
45	57.2 (16.9)
60	54.4 *
120	72.3 (0.5)
180	64.5 (6.4)

* A single reading was taken as the other reading was erroneous (reached a high value of ca. 142 μg/ ml).

Table 6.2 Solubility results of crystalline terfenadine oxalate in acetate buffer at pH = 6 and a temperature of 37 °C (n = 2).

Time (minutes)	Concentration in solution (μg/ ml), (S.D)
5	81.5 (0.9)
10	97.2 (0.3)
15	111.1 (0.9)
30	118.7 (4.9)
45	128.3 (0.3)
60	131.9 (9.9)
120	133.6 (1.1)
180	137.2 (0.5)
240	139.0 (1.3)
300	139.1 (1.1)
360	139.2 (0.7)

Table 6.3 Solubility results of crystalline terfenadine succinate in acetate buffer at pH = 6 and a temperature of 37 °C (n = 3).

Time (minutes)	Concentration in solution (µg/ ml), (S.D.)
5	83.4 (2.5)
10	103.8 (3.7)
15	101.9 (2.9)
30	110.5 (3.4)
45	116.4 (1.9)
60	126.5 (6.0)
120	128.5 (2.1)
240	127.4 (4.5)
360	137.3 (0.4)

Table 6.4 Solubility results of crystalline terfenadine glutarate in acetate buffer at pH = 6 and a temperature of 37 °C (n = 3).

Time (minutes)	Concentration in solution (µg/ ml), (S.D.)
5	171.8 (6.6)
10	178.1 (0.1)
15	178.3 (5.5)
30	165.1 (5.8)
45	170.0 (5.0)
60	161.2 (2.3)
120	169.0 (1.9)
240	156.1 (7.1)
360	167.7 (2.1)

Table 6.5 Solubility results of crystalline terfenadine adipate in acetate buffer at pH = 6 and a temperature of 37 °C (n = 2).

Time (minutes)	Concentration in solution (µg/ ml), (S.D.)
5	310.1 (0.3)
10	306.5 (2.3)
15	257.4 (0.4)
30	164.3 (12.3)
45	142.7 (0.8)
60	127.2 (1.1)
120	122.7 (4.4)
240	140.0 (0.5)
360	153.0 (9.2)

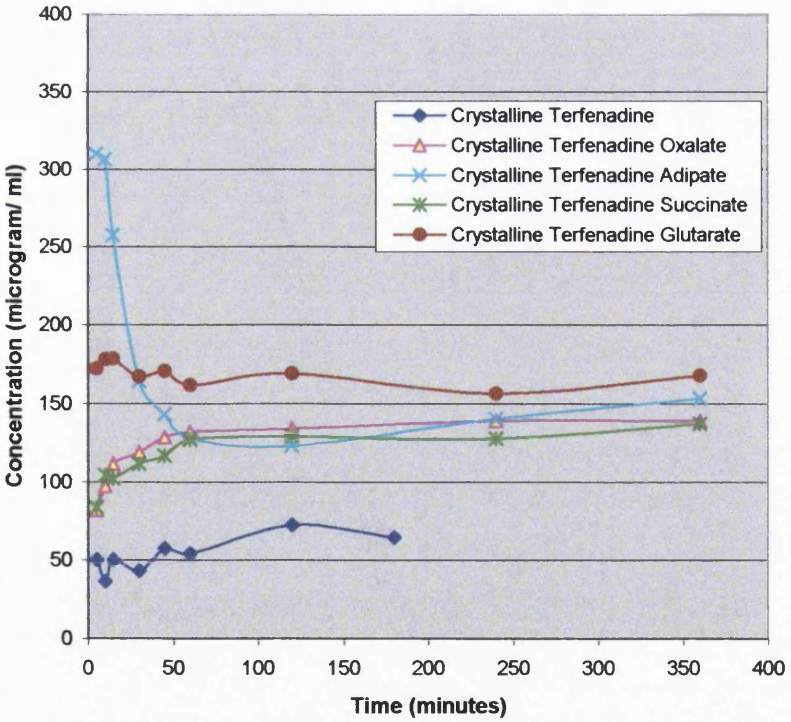

Figure 6.15 *Solubility profiles of the crystalline forms of terfenadine and the four salts at pH =6 in acetate buffer and 37 °C.*

Figure 6.15 and the data in Table 6.6 show the results as obtained from the HPLC analysis study. From these results, it can be noted that all salts have higher apparent equilibrium solubility values (used to indicate the solubility that is achievable within the time scale of the experiment) than terfenadine. The fact that salts enhance the aqueous solubility of acidic or basic drugs is well known and is due to higher ionisation of the salt form relative to the free acid or free base respectively. The apparent equilibrium solubility of the salts increased by at least a factor of 2 for all salts relative to that of terfenadine (with the highest increase in solubility reported for the glutarate salt) (Table 6.6).

Table 6.6 Apparent equilibrium solubility ratios of the crystalline forms of terfenadine salts relative to terfenadine in acetate buffer (pH = 6) at 37 °C, (n = 3-5).

Compound	Average S_{eq} (µg/ ml), (S.D.)	Solubility ratios of compound relative to terfenadine
Terfenadine	65 (7.6)	1.0
Terfenadine oxalate	137 (3.2)	2.0
Terfenadine succinate	130 (5.0)	2.0
Terfenadine glutarate	165 (5.3)	2.5
Terfenadine adipate	137 (12.2)	2.0

S_{eq}: Apparent equilibrium solubility.

In the case of terfenadine adipate, it was noted that the highest solubility reading was at the beginning (5 minutes) and the solubility started to drop from that value onwards until starting to reach a plateau at around 60 minutes. This can be explained as being triggered by the difference in solubility between the sonicated sample (in the dissolution medium) and that solubility which could be achieved for the same sample once transferred to the conditions of the solubility experiment (37 °C with speed of agitation of 40 rpm in the water bath). Crystalline terfenadine adipate had a small particle size (< 75 µm) but with powder aggregates, and in order to break down the aggregates, the

powder sample together with the 100 ml of the dissolution medium (acetate buffer) were sonicated for 5 minutes prior to placing the sample in the water bath for solubility determination. This initial high concentration of the drug in solution subsequent to sonication might have been achieved by de-aggregation of the fine particles of terfenadine adipate. Upon the start of the solubility experiment, agglomeration and separation of the initially dissolved particles might have followed the initial high concentration of the adipate salt in solution. This agglomeration and separation of some particles from solution could have resulted in a continuous decrease in the solubility instead of an increase until reaching a plateau value of the apparent equilibrium solubility of crystalline terfenadine adipate as seen in Figure 6.15. Although in the case of terfenadine (another fine powder which formed aggregates and had a particle size < 75 μm) the reduction in solubility is not as obvious as in the case of terfenadine adipate in the acetate buffer, yet it can be noted from Table 6.1 that the solubility of terfenadine at 5 minutes was ca. 1.4 times that at 10 min indicating an initial decrease in solubility. In the case of the other salts (terfenadine oxalate, terfenadine succinate and terfenadine glutarate), the larger particle sizes (125- 250 μm) with smaller surface areas than either terfenadine or terfenadine adipate lead to the absence of any aggregates in these powders. Thus, sonication did not affect the initial solubility profiles of these three salts, as their powders were already de-aggregated. Chiou and Kyle (1979) used agitation of 200 rpm in an aqueous solubility study of digoxin and digitoxin. The authors mentioned that this high agitation rate was needed in order to overcome the effect of powder aggregation and agglomeration due to the hydrophobic nature of these cardiac glycosides. In contrast, just 40 rpm was used in the current study which might have been insufficient to prevent the aggregation and agglomeration of the two hydrophobic, fine powders namely terfenadine and terfenadine adipate while the force of sonication used succeeded in preventing aggregation prior to the start of the solubility study.

In the case of terfenadine salts that have been screened to a particle size range of 125 – 250 μm (oxalate, succinate and glutarate) and did not show aggregation of their powders (as their particles are relatively large), sonication of the solids in the dissolution medium for 5 minutes did not affect their solubility profiles in the way it affected the profile of terfenadine adipate. This is shown in Figure 6.15 where the solubility profiles of terfenadine oxalate, terfenadine succinate and terfenadine glutarate showed a gradual increase in the concentration of those solids in solution until reaching a plateau value at the apparent equilibrium solubilities of these crystalline salts. This showed the value of

having a uniform particle size of the powders in case a comparison of the solubility profiles of a group of compounds is required. It can be said that though the equilibrium solubility will not be affected (given sufficient time to be achieved), yet the rate at which this equilibrium value is obtained may change with a change in particle size.

6.2.1.1.1 RELATIONSHIP BETWEEN SOLUBILITY IN ACETATE BUFFER AND THE MELTING POINT OR CARBON CHAIN LENGTH OF THE SIDE CHAIN:

Previous studies have investigated the correlation between the aqueous solubility of a homologous series of crystalline drugs with the melting points or the carbon chain lengths of the side chain in the studied series. Yalkowsky et al. (1972) showed that the aqueous solubility (expressed in a logarithmic value) of a homologous series of alkyl p-aminobenzoates falls with an increase in the carbon side chain length in two linear manners having two different slopes. The change in slope occurred at the 5 carbon side chain. Foster et al (1991) studied the aqueous solubility of a homologous series of alkyl p-hydroxybenzoates. Their semi-logarithmic plot showed a linear decrease in aqueous solubility with an increase in the length of the side chain until reaching a length of 4-5 carbon units whereby the solubility is decreased further but with a shallower gradient than that observed for the shorter chains. The decrease in the latter case was in an oscillatory fluctuation manner.

Since our study involves a group of compounds in which there is a sequential addition of methylene groups going from terfenadine (the parent compound with zero additional carbons) until reaching the adipate salt (with 5 additional carbons in its chain), it was worthwhile investigating if there was any correlation between the number of carbons in the side chain and the solubility behaviour in the dissolution medium used (acetate buffer at pH 6). Table 6.7 shows the melting points of the studied series (terfenadine and its salts) (taken from Tables 3.1 and 5.1 respectively) together with the average apparent equilibrium solubilities of the crystalline forms and their logarithmic values as related to the number of carbons in the side chain of the compounds.

Table 6.7 Apparent equilibrium solubilities in acetate buffer as related to carbon chain length in the dicarboxylic acid chain and to melting points of terfenadine and its salts.

Compound	No. of carbons in side chain	Tm (°C)	Average S_{eq} (µg/ ml)	Log S_{eq} (S.D.)
Terfenadine	0	152.4	65	1.81 (0.05)
Terfenadine oxalate	1	97.8	137	2.14 (0.01)
Terfenadine succinate	3	90.9	130	2.11 (0.02)
Terfenadine glutarate	4	88.2	165	2.22 (0.01)
Terfenadine adipate	5	162.2	137	2.14 (0.04)

Figure 6.16 shows the semi-logarithmic relationship between solubility of the crystalline forms in the series of terfenadine and its dicarboxylic acids salts and the carbon chain length of the acidic chain in the compounds.

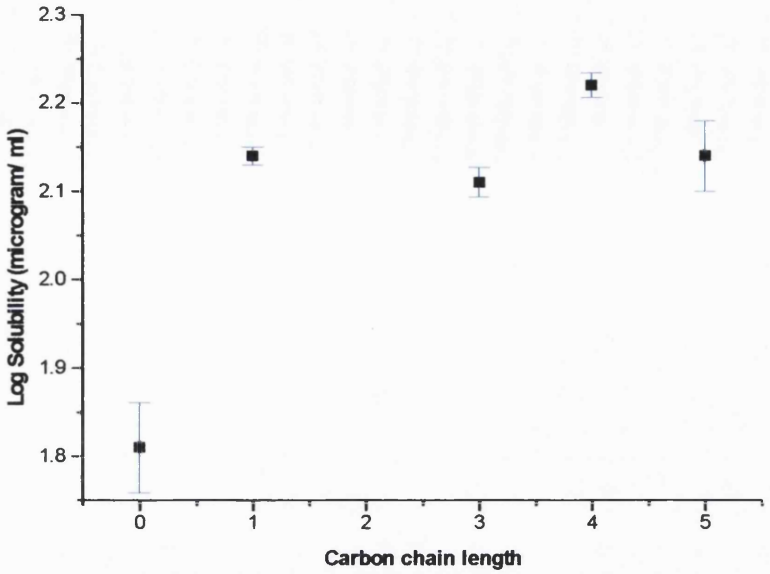

Figure 6.16 *The solubility of crystalline terfenadine and its salts in acetate buffer at pH 6 as a function of the number of carbon atoms in the dicarboxylic acid side chain.*

From Figure 6.16, it can be seen that the semi-logarithmic plot shows a large increase in solubility going from terfenadine with zero carbons in the side chain to terfenadine oxalate with 1 carbon in the side chain. Figure 6.16 shows that all salts have comparable (yet fluctuating) solubilities, which are close to each other yet all much larger than the solubility of terfenadine. This indicates that the behaviour of the crystalline salts in the acetate buffer is similar yet is different from the parent molecule (terfenadine). Hence no trend could be seen in the solubility of either terfenadine or its salts in relation to carbon chain length. These findings (Figure 6.16) are not in agreement with those reported for the aqueous solubility of a series of alkyl p-hydroxybenzoates by Foster et al. (1991) and the findings of Yalkowsky et al. (1972) regarding the aqueous solubility of a series of alkyl p-aminobenzoates. In both of those studies a fall in solubility was reported with an increase in the carbon chain length with a change in slope at the 5 C derivative in the case of the alkyl p-aminobenzoates and an oscillatory fluctuation at the 4 – 5 carbon units in the case of the alkyl p-hydroxybenzoates. The solubility in this case study (Table 6.7 and Figure 6.17) might be somewhat dependent on the breakage of the crystal lattice as terfenadine with a higher melting point exhibited a lower solubility than the rest of the series while terfenadine oxalate and terfenadine succinate showed similar solubility values with similar melting points (Table 6.7 and Figure 6.17). Terfenadine glurtarate possessing the lowest melting point exhibited the highest solubility. The only one which did not follow the trend was terfenadine adipate and

showed a much higher solubility than can be predicted from its melting point (Table 6.6) It is well known that hydrates generally possess lower aqueous solubilities than the anhydrates. Terfenadine oxalate, terfenadine succinate and terfenadine glutarate are hydrates whereas terfenadine adipate is anhydrous. This might have resulted in a higher solubility in the case of terfenadine adipate than what would be expected to be seen in the trend of the salts if they were all hydrates or all non- hydrates. Consequently, this might have lead to a lack of break in solubility value at the 5C derivative (terfenadine adipate) and a much higher apparent solubility than that expected if it were a hydrate.

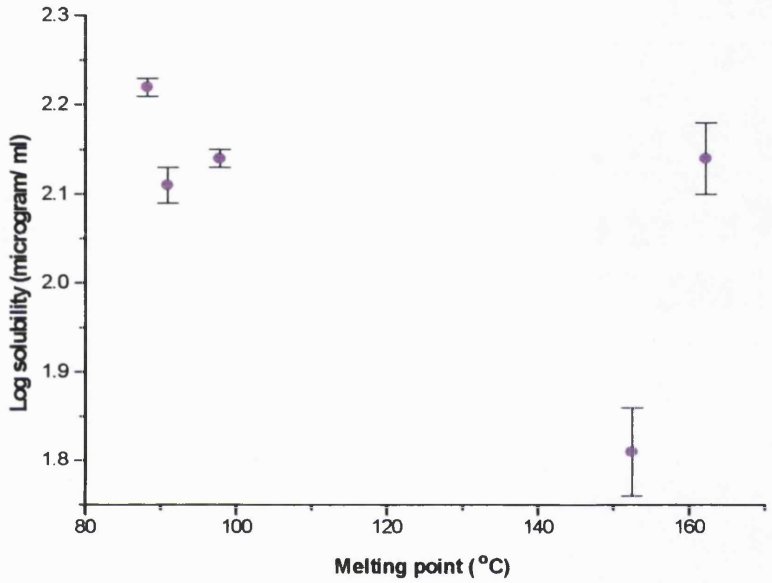

Figure 6.17 *The solubility of crystalline terfenadine and its salts in acetate buffer at pH 6 as a function of the melting points.*

6.2.1.2 SOLUBILITY OF THE AMORPHOUS FORMS:

Tables 6.8- 6.12 show the solubility results of the amorphous form of terfenadine as well as those of the amorphous forms of the four terfenadine salts as obtained in the acetate buffer at pH = 6 and analyzed by HPLC. The amorphous forms are prepared by melting and slow cooling of the melt (as explained in Section 3.2.1.1).

Table 6.8 Solubility results of amorphous terfenadine in acetate buffer at pH = 6 and a temperature of 37 °C (n = 2-3).

Time (minutes)	Concentration in solution (µg/ ml), (S.D.)
5	119.3 (0.6)
10	119.6 (3.2)
15	135.6 (0.07)
30	174.7 (12.5)
45	216.9 (0.2)
60	246.1 (5.5)
120	336.4 (12.2)
180	358.6 (8.7)
300	370.1 (27.5)

Table 6.9 Solubility results of amorphous terfenadine oxalate in acetate buffer at pH = 6 and a temperature of 37 °C (n = 2 -3).

Time (minutes)	Concentration in solution (µg/ ml), (S.D.)
5	248.7 (7.5)
10	296.4 (8.4)
15	281.2 (3.5)
30	345.7 (9.1)
45	374.3 (3.0)
60	452.3 (15.7)
120	409.3 (17.9)
180	205.2 (15.8)
360	186.9 (6.8)
480	185.9 (0.1)

Table 6.10 Solubility results of amorphous terfenadine succinate in acetate buffer at pH = 6 and a temperature of 37 °C (n = 3).

Time (minutes)	Concentration in solution (µg/ ml), (S.D.)
5	108.7 (4.7)
10	125.7 (10.4)
15	140.2 (6.0)
30	163.2 (12.0)
45	180.9 (5.1)
60	205.4 (7.5)
120	205.0 (6.8)
240	160.5 (8.0)
360	144.5 (0.9)

Table 6.11 Solubility results of amorphous terfenadine glutarate in acetate buffer at pH = 6 and a temperature of 37 °C (n = 2).

Time (minutes)	Concentration in solution (µg/ ml), (S.D.)
5	101.9 (8.3)
10	126.6 (5.6)
15	135.7 (0.4)
30	178.2 (0.1)
45	208.3 (2.1)
60	229.3 (3.0)
120	261.8 (7.2)
240	254.8 (6.5)
360	185.7 (3.0)

Table 6.12 Solubility results of amorphous terfenadine adipate in acetate buffer at pH = 6 and a temperature of 37 °C (n = 2 - 3).

Time (minutes)	Concentration in solution (µg/ ml), (S.D.)
5	61.4 (5.0)
10	77.6 (7.1)
15	72.2 (3.1)
30	86.0 (4.1)
45	118.4 (5.0)
60	146.8 (2.4)
120	207.0 (3.4)
240	152.3 (2.2)
360	151.0 (3.5)

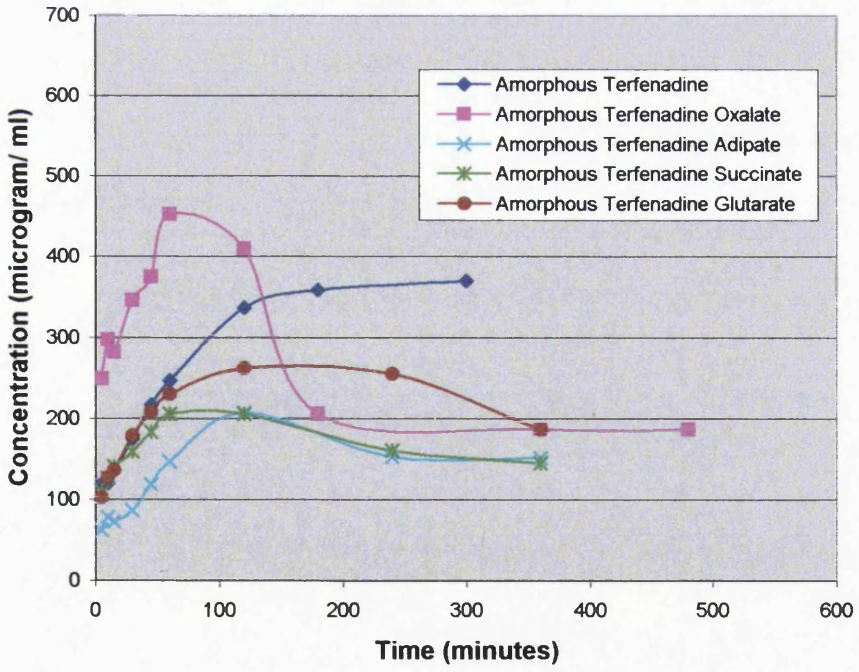

Figure 6.18 *Solubility profiles of the amorphous forms of terfenadine and the four salts at pH =6 in acetate buffer and 37 °C as tested by HPLC.*

Figure 6.18 shows the solubility profiles of amorphous terfenadine and its amorphous salts in acetate buffer (pH = 6). Amorphous terfenadine oxalate shows the highest average peak solubility value among the group (452 μg/ ml at 60 minutes). This value decreased only slightly reaching a concentration of 409 μg/ ml after 2 hours. This initial slight drop in solubility of amorphous terfenadine oxalate was then followed by a fast and sharp drop in solubility to a lower average equilibrium solubility value of ca. 193 μg/ ml. This drop in solubility is due to crystallization of amorphous terfenadine oxalate as indicated by Figure 6.20 where the solubility of the amorphous form shows a drop with the amorphous curve approaching that of the crystalline at equilibrium. A similar, yet shallower drop in solubility was noted with the other terfenadine salts (succinate, glutarate and adipate) as a consequence of crystallization of the amorphous forms. It is observed in Figure 6.18 that these three salts reach a peak solubility value followed by a more gradual fall in solubility with less difference between their peak and plateau solubilities than that observed in the case of amorphous terfenadine oxalate. Figure 6.18 demonstrates that both terfenadine succinate and terfenadine adipate had comparable solubility profiles but with an initial faster dissolution rate noted for terfenadine succinate. At the same time, amorphous terfenadine succinate and terfenadine adipate had similar plateau solubilities indicating similar apparent equilibrium solubility values for their crystalline forms. This is in agreement with the average equilibrium solubility results reported in Table 6.6 for the crystalline forms of these two salts. Amorphous terfenadine glutarate seems to have higher peak solubility than the amorphous forms of the succinate and the adipate salts with the most delayed onset of crystallization among the amorphous salts (the fall in solubility started after around 3 hours in contrast with 2 hours for the other 3 salts). Amorphous terfenadine seems to have the best solubility profile among the group with almost a plateau in solubility reached after around 2 hours. Amorphous terfenadine seems to be very stable at this pH and does not show any signs of crystallization within the time scale of the experiment (as indicated by the lack of drop in the solubility of the amorphous form). Figures 6.19 – 6.23 show a comparison of the solubility profiles of the crystalline and amorphous forms of terfenadine and its salts in the acetate buffer at 37 °C. It is clear from these graphs that complete crystallization of the amorphous forms is achieved in case of terfenadine succinate, terfenadine glutarate, and terfenadine adipate (Figures 6.21 – 6.23) by the end of the experiment. On the other hand, no signs of crystallization were seen in case of amorphous terfenadine (Figure 6.19) making this compound the most stable in the

acetate buffer among the group. Amorphous terfenadine oxalate showed fast yet incomplete crystallization during the time scale of the experiment (Figure 6.120).

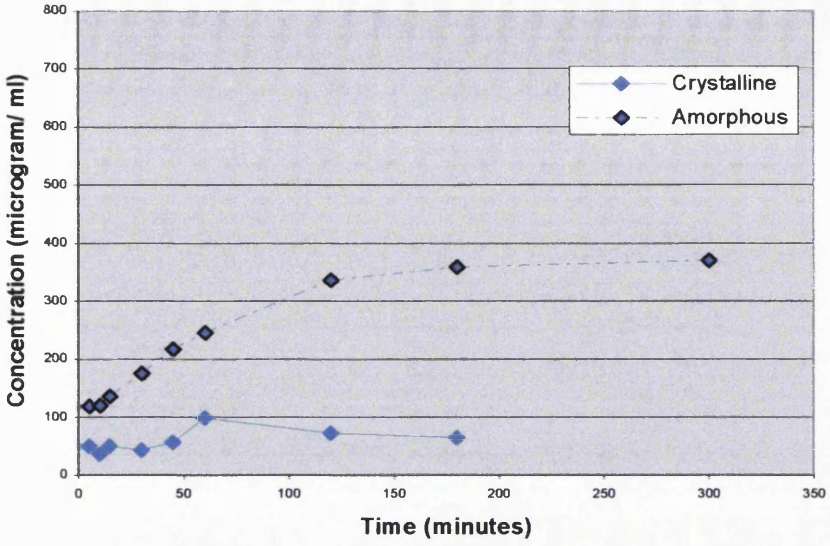

Figure 6.19 *Solubility profiles of the amorphous and crystalline forms of terfenadine at pH =6 in acetate buffer and 37 °C showing the high stability of the amorphous form.*

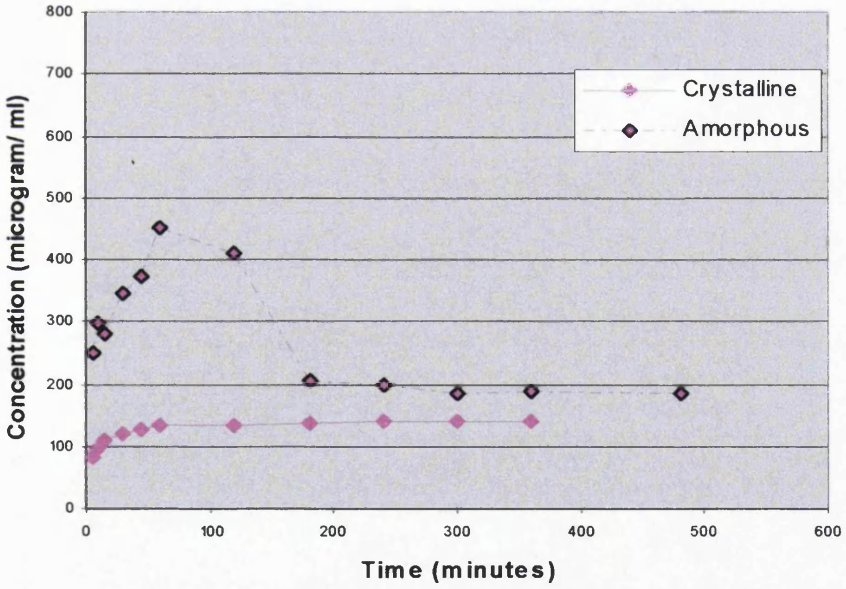

Figure 6.20 *Solubility profiles of the amorphous and crystalline forms of terfenadine oxalate at pH =6 in acetate buffer and 37 °C.*

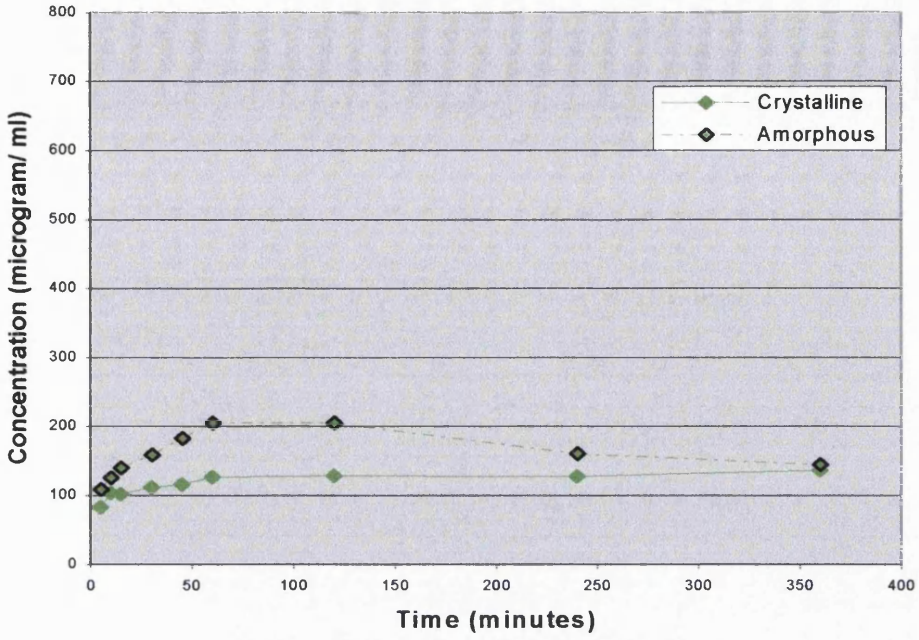

Figure 6.21 *Solubility profiles of the amorphous and crystalline forms of terfenadine succinate at pH =6 in acetate buffer and 37 °C.*

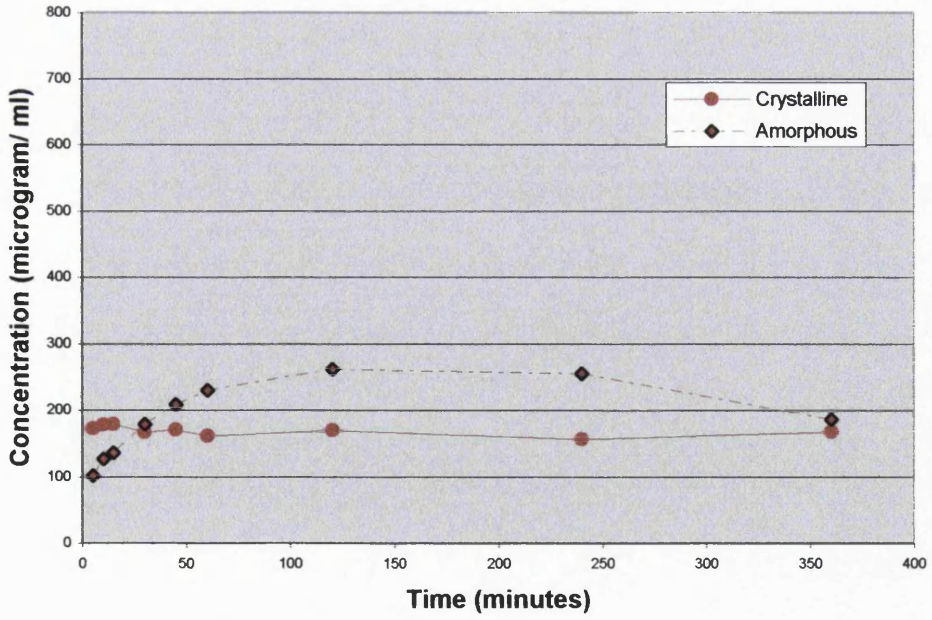

Figure 6.22 *Solubility profiles of the amorphous and crystalline forms of terfenadine glutarate at pH =6 in acetate buffer and 37 °C.*

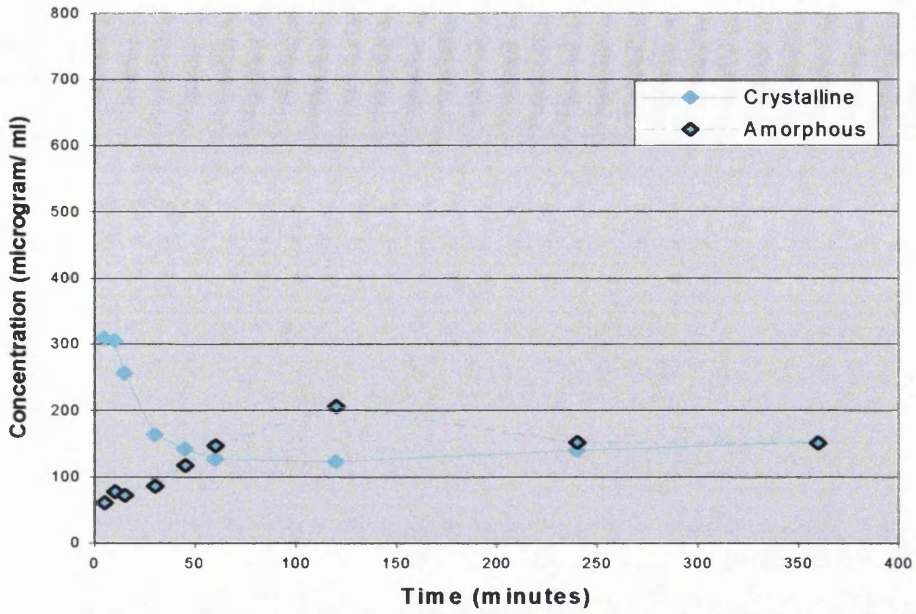

Figure 6.23 *Solubility profiles of the amorphous and crystalline forms of terfenadine adipate at pH =6 in acetate buffer and 37 °C.*

Similar observations of crystallization from the amorphous state of drugs in the dissolution medium during a solubility study were reported by Moustafa et al. (1971), Chiou and Kyle (1979) for sulphamethoxydiazene and for digoxin and digitoxin respectively.

From Figures 6.19 – 6.23, it can be noted that the amorphous forms have higher solubility values than the crystalline counterparts. This is in agreement with the expectation that the higher mobility of the amorphous form can lead to higher peak solubility in comparison with the crystalline one.

Table 6.13 Solubility ratios of amorphous relative to the crystalline counterpart and of the amorphous form relative to amorphous terfenadine in acetate buffer (pH = 6).

Compound	Solubility			Tg , Tm	
	Sp_a (µg/ ml)	(Sp_a/S_{aT})	(Sp_a/S_c)	Tg (°C)	Tm/Tg (K/K)
Terfenadine	355	1.0	5.5	58.5	1.28
Terfenadine oxalate	452	1.3	3.3	89.8	1.02
Terfenadine succinate	205	0.6	1.6	82.7	1.02
Terfenadine glutarate	258	0.7	1.6	79.9	1.02
Terfenadine adipate	207	0.6	1.5	71.7	1.26

Sp_a: peak solubility of amorphous form
Sp_a/S_{aT}: solubility ratios of amorphous form relative to amorphous terfenadine
Sp_a/S_c: solubility ratios of amorphous relative to the crystalline form

Table 6.13 shows a comparison of solubilities in the form of solubility ratios of the amorphous relative to the crystalline forms and of the amorphous forms of the salts relative to that of amorphous terfenadine. Solubility was taken as the peak value for the amorphous forms since equilibrium could not be always achieved in the amorphous state due to crystallization of the amorphous sample. In case of the crystalline solids, the apparent equilibrium solubility values were used (Table 6.6).

Table 6.13 also shows Tg values and Tm/ Tg ratios (calculated as ratios of temperatures in K degrees as reported in Table 5.12). It can be noted that terfenadine had the highest increase of 5 fold in solubility from the crystalline to the amorphous form. This can be explained as being due to the lowest Tg value of terfenadine making this compound of the highest mobility in the amorphous state among the group. The crystalline form on the other hand, is of relatively compact crystalline structure with stronger lattice bonds as indicated by a higher melting point (relative to terfenadine oxalate, succinate and glutarate). This combination may have resulted in a high increase in solubility of the

amorphous relative to the crystalline form of terfenadine. Amorphous terfenadine glutarate and terfenadine succinate had the closest Tg values among the group as seen in Table 6.13 as well as the closest melting points (Table 6.7). These two salts had similar solubility ratios of amorphous to crystalline forms with a 1.6 fold increase in the solubility of their amorphous forms relative to the crystalline ones. Terfenadine adipate showed the lowest increase in the solubility of the amorphous form relative to the crystalline one (though not far from the succinate and the glutarate salts). The adipate had the highest Tm among the group and a higher Tg than terfenadine making this salt less mobile in the amorphous state than terfenadine and the most closely packed in its crystalline form among the whole group. The net result was a salt that is less soluble in the amorphous form than terfenadine and with a negligible increase in the solubility from an average of 137 μg/ ml in its crystalline state to a peak of 207 μg/ ml in the amorphous state. The most interesting among the group is the oxalate salt with the highest Tg value making this salt potentially the most physically and chemically stable among its series while at the same time having a 3 fold increase in solubility in the amorphous form relative to the crystalline one. The problem with this salt is that it crystallizes sharply after 2 hours with a net increase in solubility of 1.4 times in the solubility of the amorphous relative to the crystalline counterpart (calculated based on the apparent equilibrium solubility of the amorphous form as an average value of 193 μg/ ml and that of the average equilibrium solubility of the crystalline form as 137 μg/ ml). Slade and Levine (1991) suggested that a high Tm/Tg value >> 1.5 indicates that a compound is readily crystallisable with low Tm/Tg ratios suggesting difficulty in crystallization. Based on this, terfenadine and terfenadine adipate should both crystallize readily from the amorphous state (relative to the other salts) with more difficulty in crystallizing the other three salts (Table 6.13). Terfenadine did not even start to crystallize in the experimental conditions and so did not follow the expectations based on its Tm/Tg ratio relative to the other salts. Terfenadine adipate followed the expectation and crystallized completely during the time scale of the experiment.

Another factor that has an impact on the achieved solubility values is the particle size of the solid. Buckton and Beezer (1992) explained that changes in particle size may affect the rate at which equilibrium is achieved in solution, yet such changes in particle size cannot alter the (time independent) equilibrium solubility value. In this study, the amorphous forms were prepared as beads of almost 3 mm in diameter while the crystalline forms were screened to a particle size range of 125 – 250 μm (oxalate,

succinate and glutarate terfenadine salts) and possessing a particle size below 75 μm (terfenadine and terfenadine adipate). This huge difference in particle sizes between the amorphous and the crystalline forms makes it more difficult to compare the extents of dissolution of the prepared compounds before equilibrium is reached. At the same time, a lower peak solubility value in the amorphous forms might be the one achieved (due to the large sizes of the amorphous beads) that the peak solubility value which could be obtained if the particle size of the amorphous forms were smaller and similar to the crystalline forms. Milling or crushing of the amorphous forms was avoided in order to rule out the possibility of crystallization taking place in the amorphous samples. This was evaluated by gentle crushing of terfenadine adipate with a spatula and testing on the DSC. The amorphous sample showed crystallization to be taking place in the sample as a result of this gentle crushing (result not shown).

6.2.1.2.1 RELATIONSHIP BETWEEN SOLUBILITY IN ACETATE BUFFER (pH 6) OF AMORPHOUS FORMS AND THE CARBON CHAIN LENGTH OF THE SIDE CHAIN:

Previous workers have related some physicochemical properties such as melting points or carbon chain length in a homologous series of compounds to solubility as mentioned earlier (Section 6.2.1.1.1) but the author is not aware of a study in which the physicochemical properties of a homologous series were studied and related to solubility of both the crystalline and the amorphous forms. Figure 6.24 shows the semi-logarithmic relationship between solubility of the amorphous form and the carbon chain length. From Table 6.14 and Figure 6.24, it can be seen that there is an increase in solubility going from the parent drug (terfenadine with zero carbons in the side chain) to the oxalate salt with one carbon in its side chain. This is followed by a decrease in the solubility of the amorphous forms as the carbon chain length is increased from 1 to 5 carbons in the side chain. Both the 3 C (Succinate) and the 5C (adipate) derivatives showed almost the same solubility values. It could be that the reduction in solubility with an increase in carbon chain length took an oscillatory fluctuation manner beyond the 3 C derivative but this would need higher derivatives to be tested in order to be verified.

Solubility had to be taken as peak value since the amorphous samples crystallized in the dissolution medium and the equilibrium solubility values in all cases reflected the

solubility of the crystalline form (except in terfenadine oxalate were incomplete crystallization of the sample in the dissolution medium was seen). It can be said that the solubility generally decreased with an increase in the carbon chain length from 1 to 5 carbons with the 3 C derivative (succinate) showing lower solubility than would be expected from the trend of the other salts. The increase in carbon chain length was related to a decrease in the glass transition temperatures of the amorphous solids (Figure 5.29). The only exception to the rule was terfenadine with the lowest Tg value among the group while possessing no carbons in the side chain.

Table 6.14 Peak solubilities in acetate buffer as related to carbon chain length in the dicarboxylic acid chain and glass transition temperatures (Tg) of terfenadine and its salts.

Compound	No. of carbons in side chain	Tg (°C)	Peak solubility (µg/ ml)	Log solubility (S.D.)
Terfenadine	0	58.5	355	2.6 (0.03)
Terfenadine oxalate	1	89.8	452	2.7 (0.02)
Terfenadine succinate	3	82.7	205	2.3 (0.01)
Terfenadine glutarate	4	79.9	258	2.4 (0.01)
Terfenadine adipate	5	71.7	207	2.3 (0.01)

It can be concluded from Table 6.14 that a decrease in solubility occurs with a decrease in the glass transition temperature of the series and with an increase in C chain length (Figure 6.24). However, the 3 C derivative shows lower solubility value than would be expected from the trend in the Tg values of the salts. Terfenadine with zero carbons in the side chain and with the lowest Tg value among the whole group was an exception to the rule with a higher solubility value than expected from the trend in the salts. It is postulated from Table 6.14 that solubility is related to the molecular arrangement in the amorphous structure as an increase in solubility with an increase in Tg is seen where terfenadine oxalate has the highest Tg and the highest peak solubility in the amorphous

form, terfenadine glutarate has an intermediate Tg value with an intermediate peak solubility while terfenadine adipate has the lowest Tg value among the salts and exhibits a lower peak solubility than either terfenadine oxalate or terfenadine glutarate. The only exception to the rule among the terfenadine salts was terfenadine succinate, which exhibited lower peak solubility than expected from the trend in the group of the salts (Table 6.14). Terfenadine behaved differently in the acetate buffer (pH = 6) in the amorphous form from its salts with higher peak solubility than the other salts (except for terfenadine oxalate). These results are not in agreement with the expectation that a higher mobility in the amorphous state potentially results in a higher solubility (lower Tg value suggesting higher mobility and expectedly higher solubility). This is a very interesting and potentially valuable observation as a higher stability (as suggested by a higher Tg value) coupled with a higher solubility might indicate the possibility of obtaining amorphous derivatives of a compound that exhibit higher solubility accompanied with higher stability in comparison with the other derivatives that are less soluble and are at the same time less stable in the amorphous state.

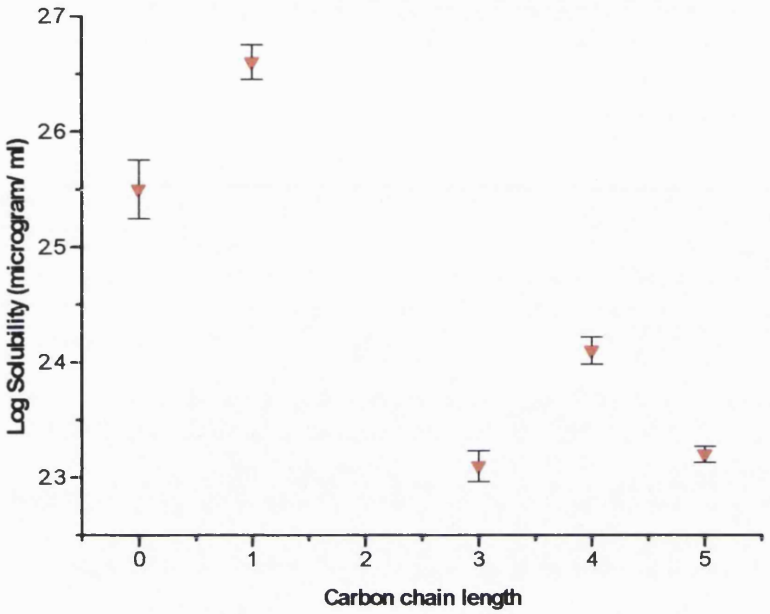

Figure 6.24 *The solubility of amorphous terfenadine and its salts in acetate buffer at pH 6 as a function of the number of carbon atoms in the dicarboxylic acid side chain.*

6.2.2 SOLUBILITY RESULTS OF TERFENADINE AND ITS SALTS AT pH 2:

This study was carried out by studying the solubility of terfenadine and its salts in a chloride buffer adjusted to pH = 2. The procedure followed for the preparation of the buffer solution was as described in Section 6.1.1. The solubility study of terfenadine and its salts was the one explained in Section 6.1.4. The HPLC method carried out for the analysis was as described in Section 6.1.5.

6.2.2.1 SOLUBILITY OF THE CRYSTALLINE FORM:

The solubility results of the crystalline form of terfenadine and that of its crystalline salts in the chloride buffer (pH = 2) in a water bath set at 37 °C and 40 rpm are presented in Tables 6.15- 6.18.

Table 6.15 Solubility results of crystalline terfenadine in chloride buffer at pH = 2 and a temperature of 37 °C (n = 2).

Time (minutes)	Concentration in solution (µg/ ml), (S.D.)
5	170.8 (0.3)
10	155.3 (1.5)
15	100.3 (0.7)
30	93.1 (4.4)
45	82.7 (1.1)
60	87.2 (3.1)
120	76.1 (2.7)
240	82.8 (1.5)

Table 6.16 Solubility results of crystalline terfenadine oxalate in chloride buffer at pH = 2 and a temperature of 37 °C (n = 2).

Time (minutes)	Concentration in solution (µg/ ml), (S.D.)
5	102.0 (3.9)
10	135.9 (8.0)
15	139.6 (11.9)
30	159.8 (8.6)
45	170.5 (0.9)
60	187.9 (5.0)
120	185.5 (0.2)
240	180.0 (10.4)
360	175.2 (0.7)

Table 6.17 Solubility results of crystalline terfenadine glutarate in chloride buffer at pH = 2 and a temperature of 37 °C (n = 2).

Time (minutes)	Concentration in solution (µg/ ml), (S.D.)
5	104.6 (3.5)
10	108.8 (7.1)
15	106.2 (0.3)
30	101.0 (0.8)
45	102.6 (3.3)
60	100.3 (3.8)
120	101.7 (1.1)
240	95.2 (1.6)
360	102.4 (3.9)

Table 6.18 Solubility results of crystalline terfenadine adipate in chloride buffer at pH = 2 and a temperature of 37 °C (n = 2).

Time (minutes)	Concentration in solution (µg/ ml), (S.D.)
5	339.4 (6.8)
10	238.4 (1.2)
15	230.2 (3.5)
30	179.3 (3.3)
45	175.5 (1.2)
60	165.3 (0.2)
120	163.2 (3.9)
240	162.8 (1.6)
360	163.6 (0.6)

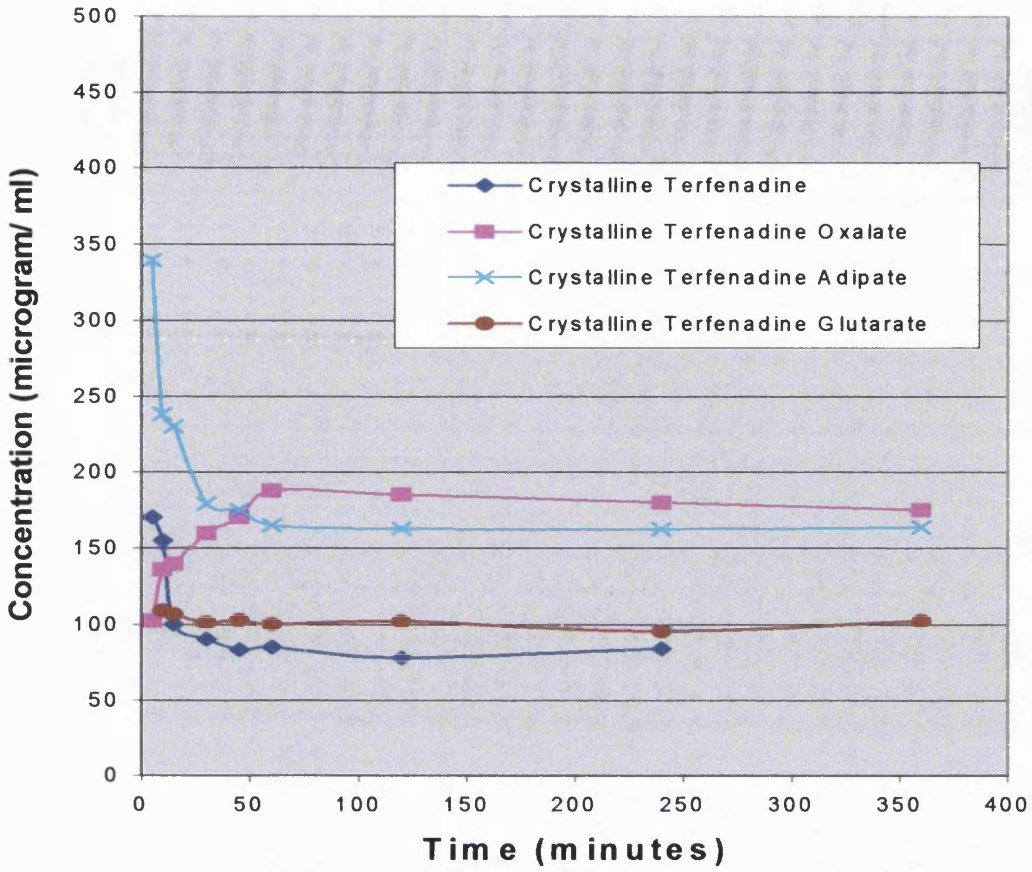

Figure 6.25 *Solubility profiles of the crystalline forms of terfenadine and three of its salts at pH =2 in chloride buffer and 37 °C as tested by HPLC.*

From Figure 6.25 and Table 6.19, it can be noticed that the three crystalline salts tested have a relatively higher solubility than crystalline terfenadine (as seen earlier for the same crystalline compounds in the acetate buffer in Section 6.2.1.1). Terfenadine oxalate and terfenadine adipate increased the solubility by approximately two fold while the glutarate exhibited a slight increase in solubility relative to terfenadine (1.3 folds) (Table 6.19). The fall in the concentration of the crystalline form of the drug in solution at the beginning of the solubility study in the case of both the terfenadine and the adipate salt (Figure 6.25) was thought to be due to sonication of the samples with 100 ml of chloride buffer (used in the solubility study) for 5 minutes prior to the start of the experiment. Both terfenadine and the adipate are fine powders (< 75 μm) and by sonication, de-agglomeration was achieved leading to a higher initial solubility than that which can be achieved at the conditions of the experiment. Agglomeration in aqueous solutions can be a problem in hydrophobic, sparingly soluble powders such as terfenadine. A similar observation was seen for crystalline terfenadine adipate in acetate

buffer at 37 °C and is explained in Section 6.2.1.1. It can thus be said that this observation is related to the crystalline form and is only seen in the two crystalline solids which were not screened for particle size prior to the solubility study (terfenadine and terfenadine adipate) and in which the powders are fine and cohesive. This is further confirmed by comparing the solubility profiles of the crystalline and amorphous forms of terfenadine at pH = 2 (Figure 6.28) and of terfenadine adipate at pH = 6 (Figure 6.23) and noting that the curve of the amorphous forms of terfenadine and terfenadine adipate tend to meet the crystalline curve at the plateau value. Chiou and Kyle (1979) used agitation of 200 rpm in an aqueous solubility study of digoxin and digitoxin. The authors mentioned that this high agitation rate was needed in order to overcome the effect of powder aggregation and agglomeration due to the hydrophobic nature of these cardiac glycosides. In contrast, only 40 rpm was used in the current study which might have been insufficient to prevent the aggregation and agglomeration of the two hydrophobic, fine powders namely terfenadine and terfenadine adipate while the force of sonication used succeeded in preventing aggregation prior to the start of the solubility study.

Table 6.19 Apparent equilibrium solubility ratios of the crystalline forms of terfenadine salts relative to terfenadine in chloride buffer (pH = 2) at 37 °C.

Compound	Average S_{eq} (µg/ ml)	Solubility ratios of compound relative to terfenadine
Terfenadine	82	1.0
Terfenadine oxalate	180	2.2
Terfenadine glutarate	103	1.3
Terfenadine adipate	164	2.0

As in the case of the solubility study carried out in the acetate buffer, no degradation was seen in terfenadine or any of the other three salts tested in the chloride buffer (pH = 2) during the time scale of the experiment as suggested by the absence of any additional peaks in the HPLC graph apart from the peak belonging to the drug and that belonging

to the internal standard (HPLC graphs in chloride buffer are not shown as they are similar to those in acetate buffer). Chen et al. (1986) stated that a low level of degradation (85 % of terfenadine remaining intact) is observed after 25 weeks of storage of terfenadine at pH = 1.5 using hydrochloric acid buffer solution. The general conclusion of their stability study was that terfenadine is quite stable in solution at pH range from 1.5 – 11.

6.2.2.1.1 RELATIONSHIP BETWEEN SOLUBILITY IN CHLORIDE BUFFER AND THE MELTING POINT OR CARBON CHAIN LENGTH OF THE SIDE CHAIN:

Figure 6.26 shows the semi-logarithmic relationship between the solubility (taken as average equilibrium solubility) of the crystalline forms of terfenadine and three of its dicarboxylic acids salts and the carbon chain length of the acidic chain in the compounds.

There is limited data to judge the exact trend of the solubility behaviour of terfenadine and its salts as related to carbon chain length in the chloride buffer. Yet, it can be observed from Figure 6.26 and Table 6.20 that initially there is a rise in solubility from terfenadine to the oxalate derivative with one carbon in its side chain. This is followed by a fall in solubility going from the oxalate with 1C to the glutarate with 4C in its side chain. A break is again seen at 5C where a rise in solubility is noticed for the adipate salt. It is clear from this limited data that the relationship between solubility of the crystalline forms and the carbon chain length differs in acetate buffer from that in the chloride buffer. From Table 6.20, it can be noticed that the solubility does not seem to depend on the breakage of the crystal lattice and thus the solubility in the chloride buffer cannot be predicted from melting point data (e.g, the oxalate exhibiting a higher melting point and a higher solubility in comparison with the glutarate and the adipate with the highest melting point showing a higher solubility than the other two salts (terfenadine oxalate and terfenadine glutarate). In this case, solubility seems to be limited by the dispersion of the solute molecules in the chloride buffer with higher hydrophobicity achieved by the sequentisal addition of methylene groups leading to lower solubility.

These findings are more in line with the findings of Foster et al. (1991) and Yalkowsky et al. (1972) where a fall in the aqueous solubility is generally seen as the carbon chain

length increases with a change in trend seen at the 5 C derivative. It has to be kept in mind though that the rise in the solubility of terfenadine adipate may be higher than what can be expected if all salts were hydrates or all were anhydrates (as explained in Section 6.2.1.1.1). This might be related to the fact that the adipate which is an anhydrous salt has a potentially higher aqueous solubility than the other tested salts which are hydrates (terfenadine oxalate and terfenadine glutarate).

Table 6.20 Apparent equilibrium solubilities in chloride buffer as related to carbon chain length in the dicarboxylic acid chain and to melting points of terfenadine and its salts.

Compound	No. of carbons in side chain	Tm (°C)	Average S_{eq} (µg/ ml)	Log S_{eq} (S.D.)
Terfenadine	0	152.4	82	1.91 (0.02)
Terfenadine oxalate	1	97.8	180	2.26 (0.02)
Terfenadine glutarate	4	88.2	103	2.01 (0.02)
Terfenadine adipate	5	162.2	164	2.21 (< 0.01)

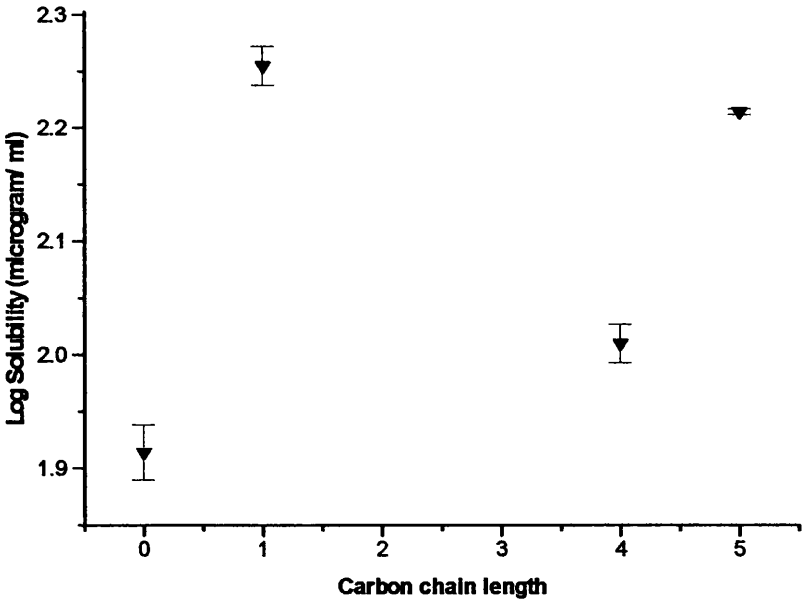

***Figure 6.26** The solubility of crystalline terfenadine and its salts in chloride buffer at pH 2 as a function of the number of carbon atoms in the dicarboxylic acid side chain.*

6.2.2.2 SOLUBILITY OF THE AMORPHOUS FORMS:

The HPLC solubility results of terfenadine, terfenadine oxalate and terfenadine glutarate in the amorphous form in the chloride buffer (pH = 2) at 37 °C are presented in Tables 6.21 – 6.23. Solubility was carried out in the same procedure as that for the crystalline form and described in Section 6.1.4. The HPLC method used was the one explained in Section 6.1.5

Table 6.21 Solubility results of amorphous terfenadine in chloride buffer at pH = 2 and a temperature of 37 °C (n = 2).

Time	Concentration in solution (µg/ ml), (S.D.)
5	26.7 (1.9)
10	30.0 (1.7)
15	35.8 (1.2)
30	35.6 (1.3)
45	41.7 (1.7)
60	56.3 (1.2)
120	79.2 (4.0)
240	78.2 (2.1)
360	60.6 (8.7)

Table 6.22 Solubility results of amorphous terfenadine oxalate in chloride buffer at pH = 2 and a temperature of 37 °C (n = 2 - 3).

Time	Concentration in solution (µg/ ml), (S.D.)
5	143.0 (9.6)
10	174.6 (0.1)
15	200.2 (1.1)
30	208.0 (9.7)
45	220.3 (6.5)
60	221.0 (8.8)
120	224.9 (0.1)
240	210.8 (12.2)
360	204.8 (0.3)

Table 6.23 Solubility results of amorphous terfenadine glutarate in chloride buffer at pH = 2 and a temperature of 37 °C (n = 2).

Time (minutes)	Concentration in solution (µg/ ml), (S.D.)
5	35.9 (3.2)
10	58.1 (0.3)
15	74.2 (0.8)
30	94.3 (3.8)
45	123.8 (3.9)
60	149.2 (2.2)
120	136.6 (0.8)
240	113.5 (0.7)

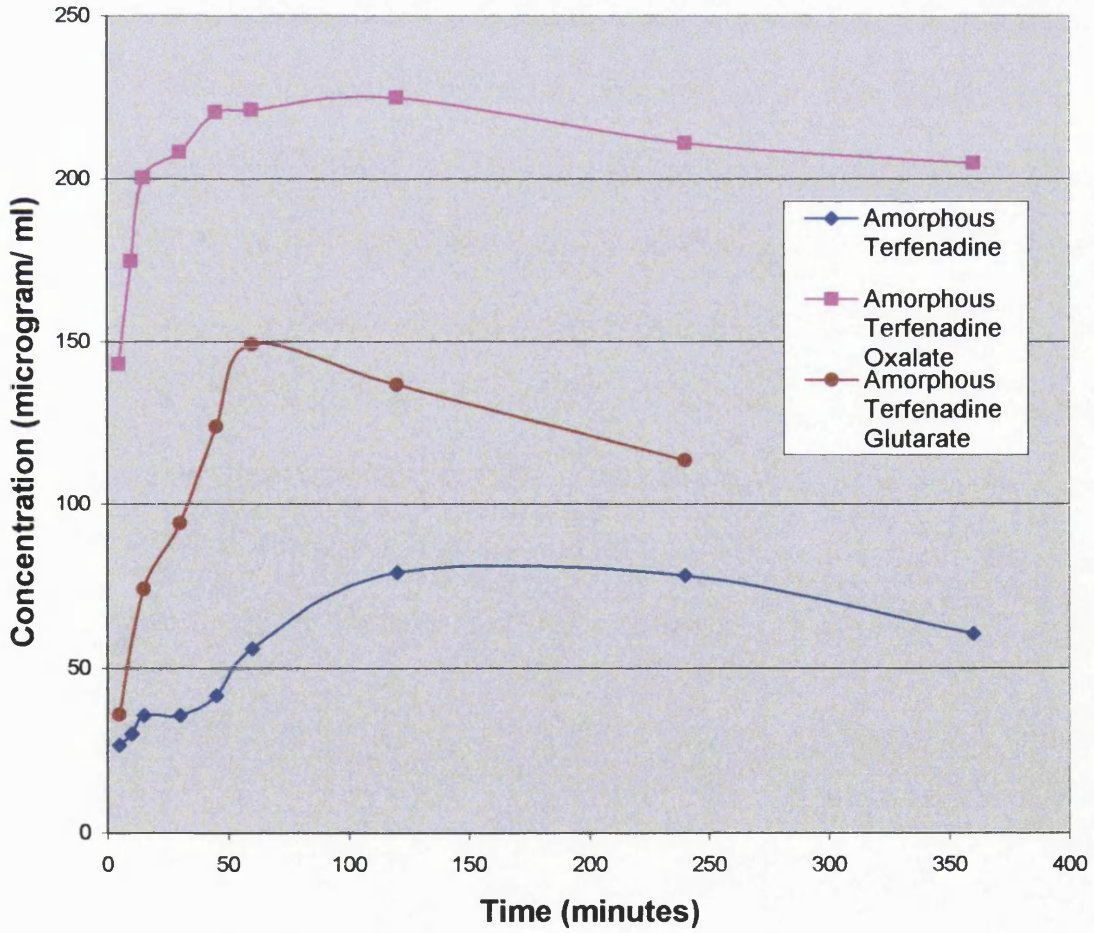

Figure 6.27 *Solubility profiles of the amorphous forms of terfenadine and two of its salts at pH =2 in chloride buffer and 37 °C as tested by HPLC.*

Figure 6.27 shows that the amorphous forms of both terfenadine glutarate and terfenadine oxalate have a higher solubility than terfenadine in the chloride buffer in the amorphous form. Amorphous terfenadine oxalate exhibited a 3-fold increase in solubility while amorphous terfenadine glutarate increased the solubility by 2 fold relative to amorphous terfenadine (Table 6.24). At the same time, terfenadine oxalate starts to crystallize after around 2 hours but crystalliztion is slow and incomplete in the chloride buffer media in the time scale of the experiment as indicated by a fall in the solubility at 2 hours while showing slow and gradual fall in the solubility without meeting the solubility of the crystalline form by the end of the experiment (Figure 6.29). Terfenadine oxalate has the additional advantage of possessing the highest Tg value among the salts, which might reflect higher physical and chemical stability of this compound in comparison with terfenadine and the rest of its prepared salts. A higher solubility in the amorphous state combined with a higher stability makes terfenadine oxalate a very favourable and interesting compound. A low Tm/Tg ratio suggests that a compound is more difficult to crystallize as explained by Slade and Levine (1991). Figures 6.28 – 6.30 show that terfenadine (with the highest Tm/Tg ratio as shown in Table 6.24) crystallized completely after 2 hours. Terfenadine oxalate and terfenadine glutarate have the same Tm/Tg ratios (Table 6.24) and while exhibiting some differences in their crystallization behaviour (Figures 6.29 and 6.30 respectively), both of these salts have higher apparent solubility than terfenadine with a potentially higher stability (as indicated by their higher Tg values relative to terfenadine). Terfenadine oxalate did not crystallize completely even after 6 hours (end of the experiment) and as judged by its rate of crystallization (Figure 6.29) it does not seem to be approaching complete crystallization in any measurable time. Terfenadine glutarate (Figure 6.30) seems to behave in an intermediate manner and approaches complete crystallization after 4 hours. It has to be noted that a slower dissolution was observed in the amorphous forms of terfenadine and terfenadine glutarate in chloride buffer in comparison with that of the crystalline form (Figures 6.28 and 6.30 respectively) as indicated by the lower initial solubility values for the amorphous forms. This was previously observed for terfenadine glutarate and terfenadine adipate in acetate buffer in Section 6.2.1.2 (Figures 6.22 and 6.23 respectively) and can be related to a particle size effect since the amorphous beads are much larger (ca. 3 mm in diameter) than the crystalline powders (125 – 250 μm for terfenadine glutarate and < 75 μm for terfenadine and terfenadine adipate).

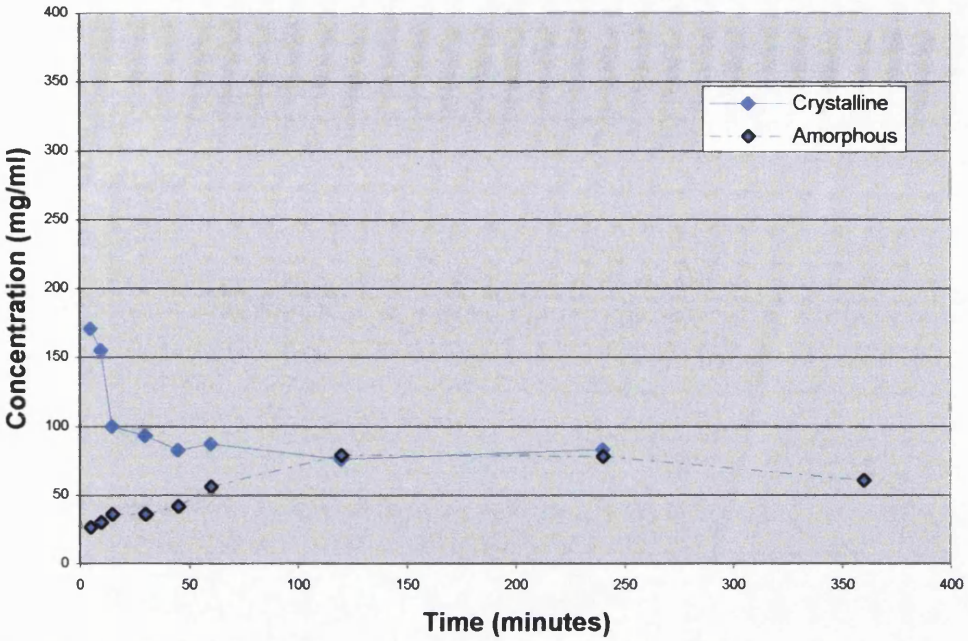

Figure 6.28 *Solubility profiles of the amorphous and crystalline forms of terfenadine at pH =2 in chloride buffer and 37 °C.*

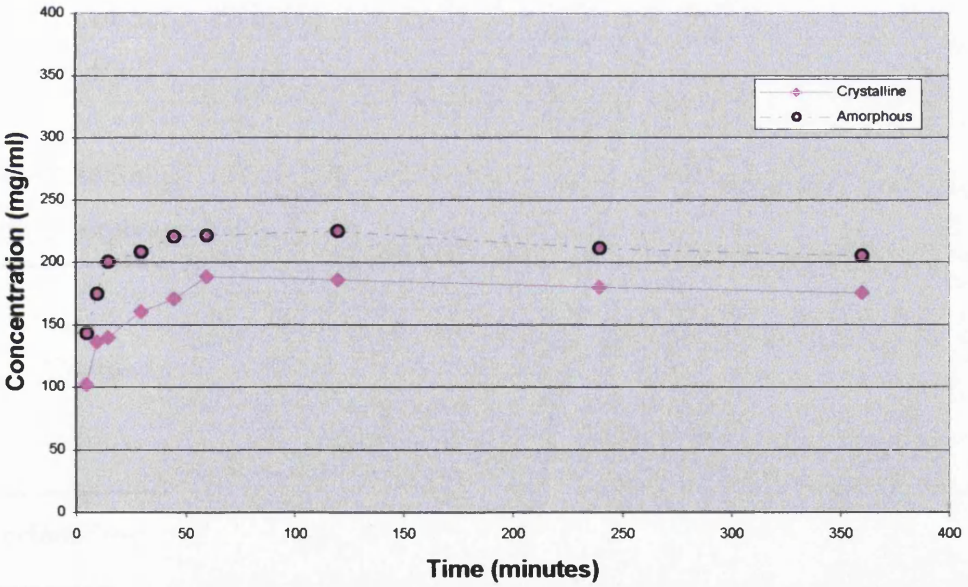

Figure 6.29 *Solubility profiles of the amorphous and crystalline forms of terfenadine oxalate at pH =2 in chloride buffer and 37 °C.*

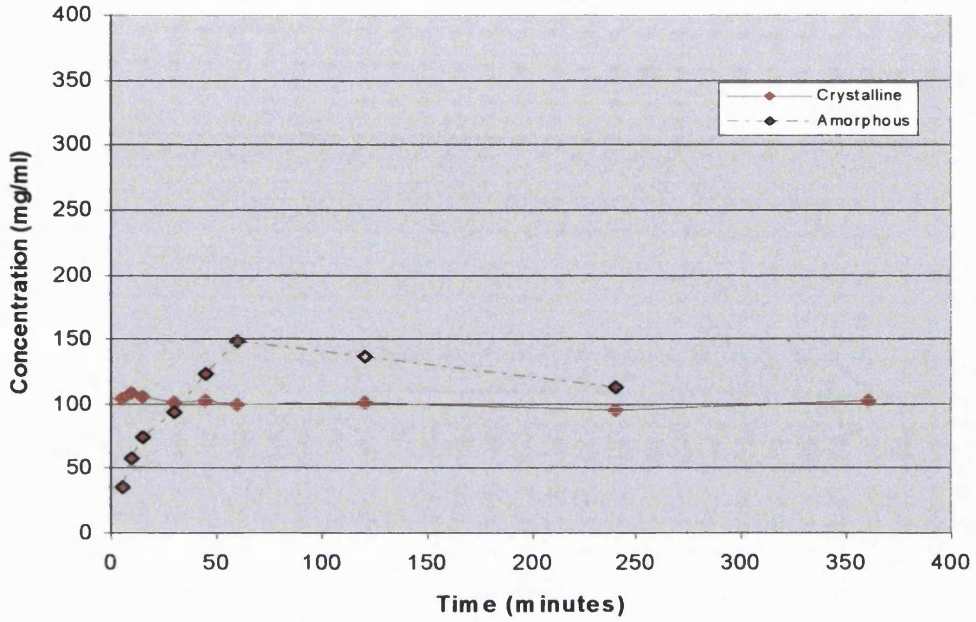

Figure 6.30 *Solubility profiles of the amorphous and crystalline forms of terfenadine glutarate at pH =2 in chloride buffer and 37 °C.*

Table 6.24 Solubility ratios of the amorphous relative to the crystalline counterpart and of the amorphous form relative to amorphous terfenadine in chloride buffer (pH = 2).

Compound	Solubility			Tg , Tm	
	Sp_a (µg/ ml)	(Sp_a/Sp_{aT})	(Sp_a/S_c)	Tg (°C)	Tm/Tg (K/K)
Terfenadine	79	1.0	1.0	58.5	1.28
Terfenadine oxalate	225	2.8	1.3	89.8	1.02
Terfenadine glutarate	149	1.9	1.4	79.9	1.02

Sp_a: peak solubility of amorphous form
Sp_a /Sp_{aT}: solubility ratios of amorphous form relative to amorphous terfenadine
Sp_a /S_c: solubility ratios of amorphous relative to the crystalline form

Table 6.24 shows the relationship between the solubility of the amorphous form and that of the crystalline one. The solubility of terfenadine remained almost the same with no advantage of the amorphous form over the crystalline one in the chloride buffer at pH 2. The solubility of both terfenadine oxalate and terfenadine glutarate increased slightly and to comparable levels (1.3 and 1.4 folds respectively) in the amorphous forms relative to their crystalline counterparts.

As in the case of the solubility study carried out in the acetate buffer, no degradation was seen in terfenadine or any of the other three salts tested in the chloride buffer (pH = 2) during the time scale of the experiment as suggested by the absence of any additional peaks in the HPLC graph apart from the peak belonging to the drug and that belonging to the internal standard (HPLC graphs in chloride buffer are not shown as they are similar to those in acetate buffer). Chen et al. (1986) stated that a low level of degradation (85 % of terfenadine remaining intact) is observed after 25 weeks of storage of terfenadine at pH = 1.5 using hydrochloric acid buffer solution. The general conclusion of the stability study that the authors conducted was that terfenadine is quite stable in solution at pH higher than 1.5 – and up to 11.

6.2.2.2.1 RELATIONSHIP BETWEEN SOLUBILITY IN CHLORIDE BUFFER OF AMORPHOUS FORMS AND THE CARBON CHAIN LENGTH OF THE SIDE CHAIN:

There is very limited data to talk about a trend or relationship between the carbon chain length in the amorphous forms of terfenadine and its salts (Figure 6.31); yet, from the data at hand (Table 6.25 and Figure 6.32), in the amorphous form, terfenadine seems to possess the lowest solubility though it is the most mobile in the amorphous state with the lowest Tg value. A jump in solubility is seen going from terfenadine to the oxalate salt while terfenadine oxalate is the least mobile among the group in the amorphous state (highest Tg among the group) with terfenadine glutarate possessing an intermediate Tg value with corresponding intermediate peak solubility in the amorphous state. It can thus be concluded that similar to the findings in the acetate buffer (Section 6.2.1.2.1), solubility in the chloride buffer at pH = 2 is related to molecular arrangement in the amorphous state. An increase in the solubility of the amorphous forms in the chloride buffer (pH = 2) was noted with an increase in the Tg value. This is contrary to the expectation that a higher mobility in the amorphous state can result in a higher

solubility. In the case of the chloride buffer, however solubilities of the two tested amorphous salts were higher than amorphous terfenadine itself. This was not the case in the acetate buffer (Section 6.2.1.2.1), where only terfenadine oxalate possessed a higher peak solubility than terfenadine in the amorphous state. This is a very interesting observation as a higher stability combined with a higher solubility might indicate the possibility of preparing amorphous derivatives of a compound that are more soluble and at the same time more stable than the parent compound in the amorphous state.

Table 6.25 Peak solubilities in chloride buffer as related to carbon chain length in the dicarboxylic acid chain and glass transition temperatures (Tg) of terfenadine and its salts.

Compound	No. of carbons in side chain	Tg (°C)	Peak solubility (µg/ ml)	Log solubility (S.D.)
Terfenadine	0	58.5	79	1.9 (0.02)
Terfenadine oxalate	1	89.8	225	2.4 (< 0.01)
Terfenadine glutarate	4	79.9	149	2.2 (0.01)

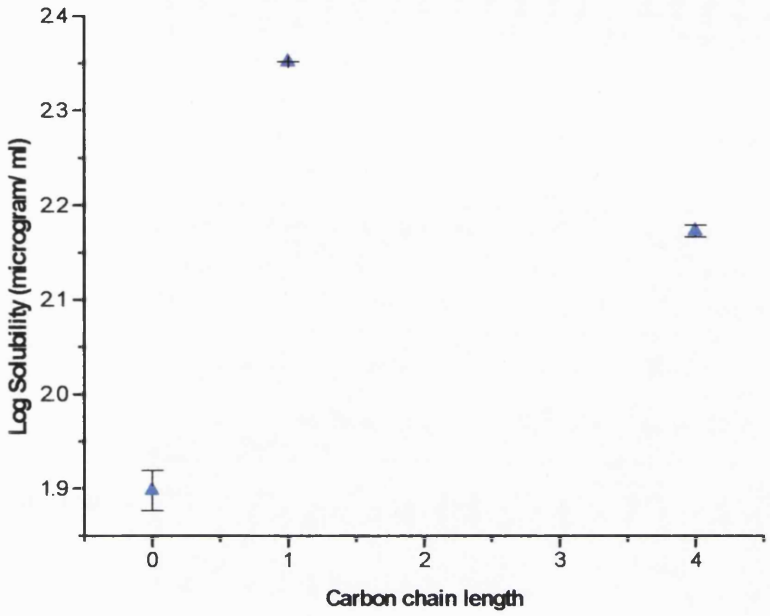

Figure 6.31 *The solubility of amorphous terfenadine and its salts in chloride buffer at pH 2 as a function of the number of carbon atoms in the dicarboxylic acid side chain.*

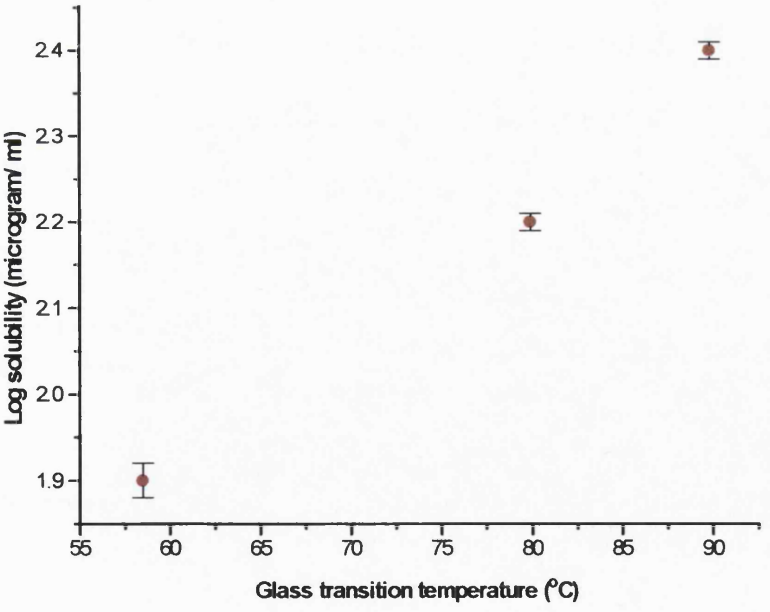

Figure 6.32 *The solubility of amorphous terfenadine and its salts in chloride buffer at pH 2 as a function of the glass transition temperature.*

6.2.3 COMPARISON OF SOLUBILITY RESULTS OF TERFENADINE AND ITS SALTS AT THE TWO pH values:

Table 6.26 demonstrates a comparison of the solubility of each compound (terfenadine and its salts) in both the amorphous and crystalline forms at the two pH values studied (pH 2 and pH 6).

Table 6.26 Solubility ratios of amorphous forms and those of the crystalline counterparts in acetate and chloride buffer at pH 6 and pH 2 respectively.

Compound	Solubility		Onset of crystallization (hours)	
	Sp_a2/Sp_a6	(S_{c2}/S_{c6})	pH 2	pH 6
Terfenadine	0.2	1.2	1	Not started
Terfenadine oxalate	0.5	1.3	2	1
Terfenadine glutarate	0.6	0.6	1	4
Terfenadine adipate	-	1.2	-	2

Sp_a2: peak solubility of amorphous form in chloride buffer at pH 2
Sp_a6: peak solubility of amorphous form in acetate buffer at pH 6
S_{c2}: average equilibrium solubility of the crystalline form at pH 2
S_{c6}: average equilibrium solubility of the crystalline form at pH 6

Table 6.26 shows that all crystalline compounds (with the exception of terfenadine glutarate) exhibited a higher solubility at the lower pH of two than the solubility seen at pH six. Terfenadine is a weakly basic drug that is expected to be more ionised at a lower pH value, which in turn can result in a higher aqueous solubility of the compound.
It is noted though that in the case of the amorphous forms, the reverse is observed with higher peak solubility values noticed at the higher pH of 6 than the peak solubility seen

at pH 2. This higher solubility at the higher pH of 6 in the amorphous state is hard to be explained at this point.

6.3 DISCUSSION:

The solubility of terfenadine and its salts was determined at two pH values of 2 and 6 in chloride and acetate buffer respectively. The results showed higher solubility of all crystalline salts relative to terfenadine at the same pH for both pH values. Higher solubility of the amorphous relative to the crystalline forms was noted at the same pH and in both the chloride and the acetate buffers. Amorphous terfenadine came lowest in its solubility in chloride buffer relative to the other two amorphous salts (terfenadine oxalate and terfenadine glutarate). Amorphous terfenadine in acetate buffer showed a peculiar and interesting high solubility combined with stability (evidenced by the lack of crystallization of this amorphous form at the time scale of the experiment). All amorphous salts crystallized by the end of the experiments at both pH values, while terfenadine oxalate showed incomplete crystallization in both cases. Terfenadine oxalate had high peak solubility in acetate buffer but with sharp and fast crystallization following two hours of exposure to the dissolution medium and settling to a net increase of 1.4 fold in solubility of the amorphous form (taking the apparent equilibrium solubility of the amorphous form) relative to the solubility of the crystalline state. All crystalline compounds showed higher solubility in the chloride buffer than in the acetate buffer which is expected and is explained as being due to higher ionisation of the basic drug (terfenadine) and its salts at the lower pH value. The reverse was noted in the case of the amorphous forms where lower solubility was measured in the chloride buffer than in the acetate buffer. This is not as initially predicted and is difficult to explain. The relationship between the carbon chain length (dicarboxylic acid chain part of the compound) and the solubility of the crystalline and amorphous forms of terfenadine and the salts was investigated in both buffer media. In the acetate buffer, the solubility of the crystalline forms increased when going from terfenadine to terfenadine oxalate with similar solubility values for terfenadine oxalate and terfenadine succinate while terfenadine glutarate had a comparable but slightly higher solubility than the rest of the group. The solubility in the acetate buffer might be related to the melting points; with higher solubility observed for the derivative with lower melting point (terfenadine glutarate) and lower solubility for terfenadine with a higher melting point than the rest

of the salts (except for terfenadine adipate). Terfenadine adipate seems not to follow this trend and this can be related to the fact it is the only anhydrous salt which might have lead to a higher solubility than would be predicted from its melting point. Solubility of the crystalline forms in the chloride buffer did not depend on breakage of the crystal lattice and hence solubility did not correlate with melting points. Solubility in this case was thought to be limited by the dispersion of the hydrophobic solute in the dissolution medium with a break in trend and an increase in solubility seen at the 5 C derivative which is more in agreement with trends reported by other workers (Foster et al., 1991 and Yalkowsky et al., 1972). The relationship between the carbon chain length and the peak solubility of the amorphous forms was investigated (peak solubility was taken as the plateau solubility corresponded to that of the crystalline forms except in the case of terfenadine oxalate where incomplete crystallization was observed). In acetate buffer the solubility of the amorphous forms decreased as the chain length increased going from 1 to 5 C in the series with the 4 C derivative (succinate) showing lower solubility than would be expected from the trend in the group. Peak solubility in the acetate buffer was related to Tg values in the case of terfenadine salts with terfenadine oxalate possessing the highest Tg and the highest solubility value and terfenadine adipate possessing the lowest Tg value among the salts with the lowest solubility among the salts, terfenadine glutarate had an intermediate Tg with an intermediate solubility value. The only exception was terfenadine succinate which exhibited a lower solubility than that expected from the trend of the amorphous salts while the parent compound (terfenadine) showed unusually higher solubility than all the other salts in the amorphous state (except for terfenadine oxalate). Investigating the solubility of the amorphous forms in the chloride buffer and judging from the three compounds tested (terfenadine, terfenadine oxalate and terfenadine glutarate), it was seen that terfenadine oxalate with the highest Tg value had the highest solubility, whereas, terfenadine with the lowest Tg had the lowest solubility among the three compounds. Terfenadine glutarate with an intermediate Tg value showed an intermediate solubility in the amorphous state. These findings again suggest that the solubility is dependent on molecular arrangement in the amorphous state with higher solubility generally obtained at a higher Tg value. This is a very interesting and potentially valuable observation as a higher stability when coupled with a higher solubility might indicate the possibility of preparing amorphous derivatives of a compound that are more soluble while at the same time are more stable than the parent compound in the amorphous state.

Comparison of the aqueous solubility of crystalline terfenadine (0.001 g/ 100 ml) as reported by Badwan et al. (1990) with its solubility in both the acetate buffer (65 μg/ ml) and the chloride buffer (82 μg/ ml) as determined in this study, showed an increase of almost 7 and 8 folds (relative to its aqueous solubility) in acetate buffer and chloride buffer respectively.

CHAPTER SEVEN

GRAVIMETRIC CHARACTERIZATION OF AMORPHOUS FORMS OF TERFENADINE GLUTARATE AND TERFENADINE ADIPATE USING WATER AND ORGANIC VAPOUR IN DYNAMIC VAPOUR SORPTION

7 INTRODUCTION:

Dynamic vapour sorption (DVS) as a gravimetric method for sample analysis was introduced and used in Chapter four (Section 4 for the introducion).

The aims of this study were:

- To evaluate the potential for crystallization of two salts of terfenadine (terfenadine glutarate and terfenadine adipate) under the combined effect of humidity (75% RH) and an elevated temperature of 50 °C in the DVS.
- To investigate the use of non-aqueous vapours (ethanol) in the Dynamic Vapour Sorption apparatus (DVS) in an attempt to recrystallize amorphous forms of terfenadine adipate and terfenadine glutarate.
- To compare the potential for crystallization of these two amorphous salts with that of terfenadine in the DVS apparatus (studied in Chapter four, Section 4.2.2).

7.1 METHODS:

7.1.1 PREPARATION OF AMORPHOUS SAMPLES:

Preparation of amorphous samples of terfenadine salts (adipate and glutarate) was carried out by melting and slow cooling the melt as explained in Section 5.4.1.

7.1.2 DVS METHODS USED IN CHARACTERIZATION OF AMORPHOUS FORMS OF TERFENADINE GLUTARATE AND TERFENADINE ADIPATE:

The basic principles of the DVS were discussed in Section 2.1.1. Six beads of the amorphous forms of terfenadine glutarate and terfenadine adipate were placed in the sample side quartz pan of the DVS apparatus while the reference side quartz pan was kept empty. The system was conditioned and dried at 0% RH until an almost flat baseline with minimal noise was obtained prior to the start of any experiment. The following experimental conditions were used in the DVS.

1. In an attempt to trigger crystallization of the amorphous forms by a combined effect of humidity and temperature. Using a ramp method in the DVS, the amorphous forms of terfenadine glutarate and terfenadine adipate were equilibrated at 0% RH for 1 hour followed by 75% RH for 20 hours and ended

with a drying step at 0% RH for 1 hour. The temperature in the DVS was set to 50 °C.

2. Using ethanol instead of water in the DVS at 25 °C, the amorphous samples of terfenadine glutarate and terfenadine adipate were run with an initial equilibration step at 0% RH for 1 hour followed by exposure to 95% ethanol in the total gas flow (mixed with nitrogen gas) for 20 hours and ended with a one hour step at 0% RH.

7.2 RESULTS:

7.2.1 DVS STUDY OF AMORPHOUS TERFENADINE GLUTARATE AND TERFENADINE ADIPATE:

7.2.1.1 RESULTS OF AMORPHOUS TERFENADINE ADIPATE AND TERFENADINE GLUTARATE UPON EXPOSURE TO WATER VAPOUR:

Using water in the DVS, amorphous terfenadine adipate and terfenadine glutarate were tested separately in the DVS. The amorphous sample of either terfenadine glutarate or terfenadine adipate was placed in the DVS quartz sample pan (6 beads used). The amorphous forms were prepared by melting and slow cooling of the melt (as explained in Section 5.4.1). The amorphous samples were prepared two days prior to performing the DVS experiments. DVS experiments were carried out in the DVS as explained in Section 7.1.2 part 1. The aim of these experiments was to investigate the potential for crystallization of the amorphous forms of these two terfenadine salts (chosen as examples on the behaviour of terfenadine salts) under the effect of humidity. The DVS experiments were carried out in duplicate for terfenadine glutarate and in triplicate for terfenadine adipate. Typical DVS profiles of terfenadine adipate and terfenadine glutarate are shown in Figures 7.1 and 7.2 respectively.

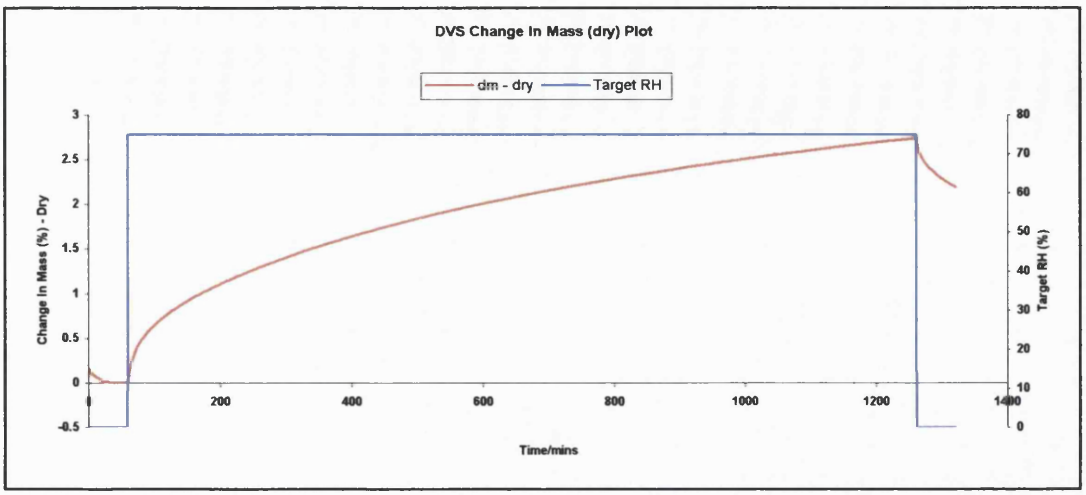

Figure 7.1 *Typical water sorption isotherm for amorphous terfenadine adipate exposed to 75% RH for 20 hours at 50 °C.*

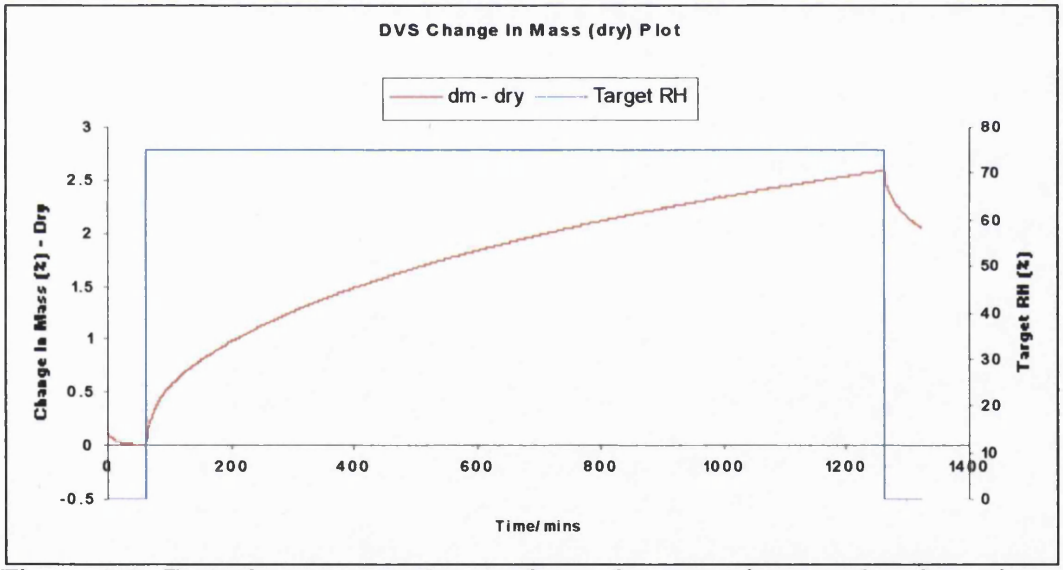

***Figure** 7.2 Typical water sorption isotherm for amorphous terfenadine glutarate exposed to 75% RH for 20 hours at 50 °C.*

From Figures 7.1 and 7.2, it can be seen that the amorphous samples of terfenadine adipate and terfenadine glutarate picked up moisture but without crystallizing under the effect of humidity. This is similar to the behaviour of terfenadine where the amorphous samples failed to crystallize under these same DVS conditions (Section 4.2.2.1.3). Low percentages of moisture were picked up by the amorphous samples of terfenadine adipate and terfenadine glutarate (ca. 2.7% for the adipate and ca. 2.5% for the glutarate salts of terfenadine).

Differential Scanning Calorimetry was carried out on the amorphous samples subsequent to exposure to humidity in the DVS at 75% RH for 20 hours and 50 °C. DSC was done to check if any depression in the Tg was noticed in the amorphous samples of these two salts of terfenadine and was performed within a heating range of 10 – 180 °C at 10 °C/min in hermetically sealed aluminium pans under nitrogen atmosphere. Both the adipate and the glutarate did not show any melting peaks and only a glass transition temperature was seen (traces not shown). The adipate had an average Tg of 68.1 °C (n = 2, S.D. = 0.7). This is in contrast to a Tg value of the slow cooled untreated amorphous form of ca. 72 °C (from Table 5.9). On the other hand, the glutarate had an average Tg of 62.8 °C (n = 4, S.D. = 1.8) in comparison with a Tg value of the original amorphous form of terfenadine glutarate of ca. 80 °C (from Table 5.9). Thus a slight depression was noted in the Tg values of both terfenadine glutarate and terfenadine adipate after exposure to 75% RH for 20 hours at 50 °C in the DVS. A depression that was still very far from the temperature of the experiment (T) of 50 °C. Hence, the depression in the Tg values was not sufficient to impart enough plasticization and molecular mobility and trigger crystallization of either terfenadine glutarate or terfenadine adipate.

7.2.1.2 RESULTS OF AMORPHOUS TERFENADINE ADIPATE AND TERFENADINE GLUTARATE UPON EXPOSURE TO ETHANOL VAPOUR:

Since crystallization of the amorphous forms of terfenadine glutarate and terfenadine adipate failed under the influence of humidity (75% RH) at 50 °C, another approach was attempted in order to evaluate the physical stability in terms of resistance to crystallization of these amorphous forms. Ethanol replaced water in the DVS and experiments were carried out as explained in Section 7.1.2 part 2. The percentage mass change by the end of the sorption step in the case of terfenadine adipate showed an average value of ca. 4.5% (n = 4, S.D. = 0.3) while that for terfenadine glutarate had an average value of ca. 25.5% (n =3, S.D. = 0.4). Typical DVS profiles of terfenadine adipate and terfenadine glutarate exposed to 95% ethanol (in the total gas flow) for 20 hours are shown in Figures 7.3 and 7.4 respectively. Figure 7.3 shows that terfenadine adipate crystallized in the DVS at these experimental conditions as indicated by the loss in weight in the DVS profile. Crystallization occurred as ethanol was sorbed into the amorphous terfenadine adipate beads causing plasticization of the amorphous sample,

which resulted in lowering of Tg below T, and triggered crystallization. The loss in weight almost reached a plateau at around 600 minutes indicating that no substantial crystallization was taking place beyond that time. It is worthwhile noting that crystallization occurred in different stages, an initial crystallization took place following almost 7.4% weight increase due to sorption of ethanol. This is followed by another crystallization starting at an inflection point at around 300 minutes where ca. 6.7% net weight increase was obtained before reaching a plateau at around 600 minutes with a net weight gain of ca. 4.6%. It is interesting to note that at the inflection point (ca. 6.7% weight gain), the mole ratio of ethanol to terfenadine adipate was approximately 1:1. A similar observation at an inflection point was reported by Buckton and Darcy (1996) and was linked to a 1:1 mole ratio of water to amorphous lactose. The difference between the two cases is that with Buckton and Darcy (1996) the inflection point was noted while the sample was gaining weight in a non crystallizing amorphous sample of lactose exposed to 40% RH whereas in this study, the inflection point was seen while the sample was crystallizing and losing weight on the DVS. Buckton and Darcy (1996) stated that no obvious explanation could be provided for the shape of the sorption data of the sample exposed to 40% RH.

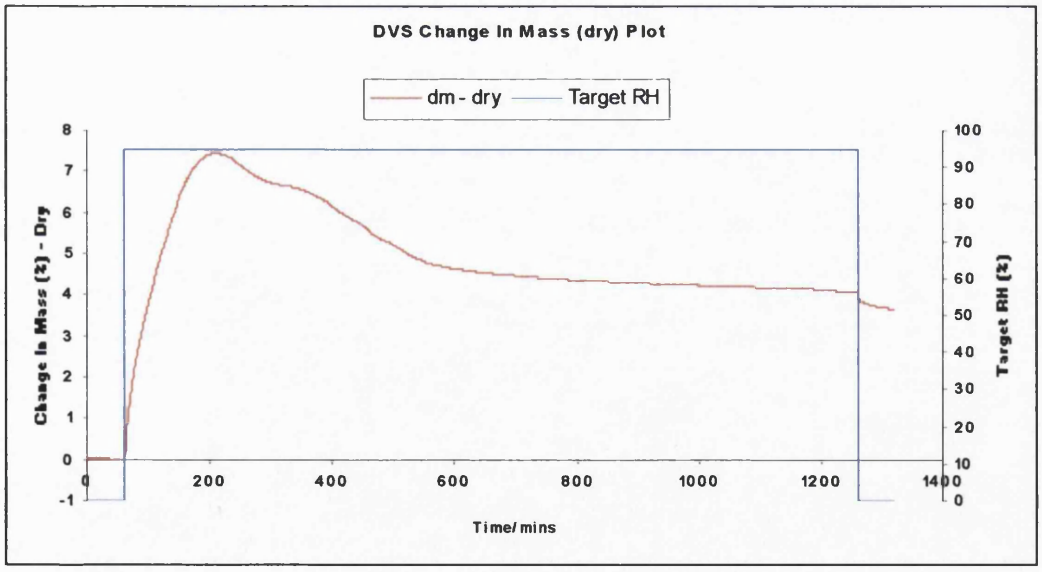

Figure 7.3 *A typical ethanol sorption isotherm for amorphous terfenadine adipate exposed to 95% ethanol (in the total gas flow) for 20 hours at 25 °C.*

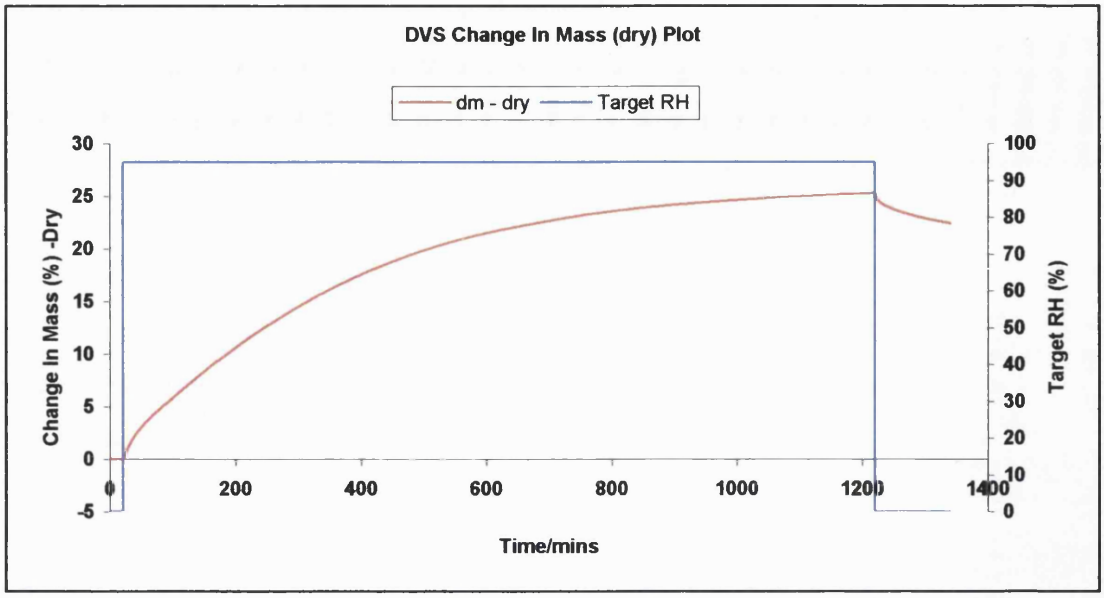

Figure 7.4 *A typical ethanol sorption isotherm for amorphous terfenadine glutarate exposed to 95% ethanol (in the total gas flow) for 20 hours at 25 °C.*

Figure 7.4 shows that terfenadine glutarate picked up a large amount of ethanol (average value of ca. 25.5%) while still failing to crystallize as no loss in weight was seen in the DVS.

Visual inspection of the beads of terfenadine adipate and terfenadine glutarate subsequent to exposure to 95% ethanol for 20 hours indicated the presence of a collapsed, opaque crystalline mass of terfenadine adipate and a soft gel material in the case of terfenadine glutarate. DSC was carried out on samples of terfenadine adipate and terfenadine glutarate after being exposed to 95% ethanol in the DVS. Differential scanning calorimetry was performed from 10 – 180 °C at 10 °C/ min in hermetically sealed aluminium pans in a nitrogen atmosphere. Terfenadine adipate did not show any glass transition and just a melt was seen with DSC trace identical to that of the original crystalline material. A typical DSC trace of the crystallized sample of terfenadine adipate is seen in Figure 7.5. The average melting point was 160.6 °C (n = 5, S.D. = 1.9). The average enthalpy of fusion (ΔH_f) was 74.9 J/g (n = 5, S.D. = 3.8). This is in contrast with an enthalpy of fusion of ca. 79 J/g of the original crystalline material (Table 5.1). Calculations of the percentage crystallinity based on the enthalpy of fusion as obtained from the DSC indicated that the terfenadine adipate sample that was exposed to ethanol in the DVS was ca. 95% crystalline. However TGA analysis was carried out on the crystallized sample of terfenadine adipate after exposure to 95%

ethanol in the DVS. TGA was done from ambient to 180 °C at 10 °C/ min in open aluminium pans under nitrogen atmosphere. An average weight loss of almost 1.8 % (n = 3, S.D. = 0.1) was noted between 110 – 180 °C, which superimposed with the melting point of terfenadine adipate. This suggests that the actual percentage crystallinity of terfenadine adipate might be slightly lower than the calculated ca. 95%. Whether ethanol is incorporated in the crystalline structure of terfenadine adipate, resulting partly in a monosolvate (since a weight increase of ca. 6.7 % corresponds to a monosolvate if ethanol were the solvent), or that ethanol is simply physically adsorbed onto the crystalline terfenadine adipate could not be known.

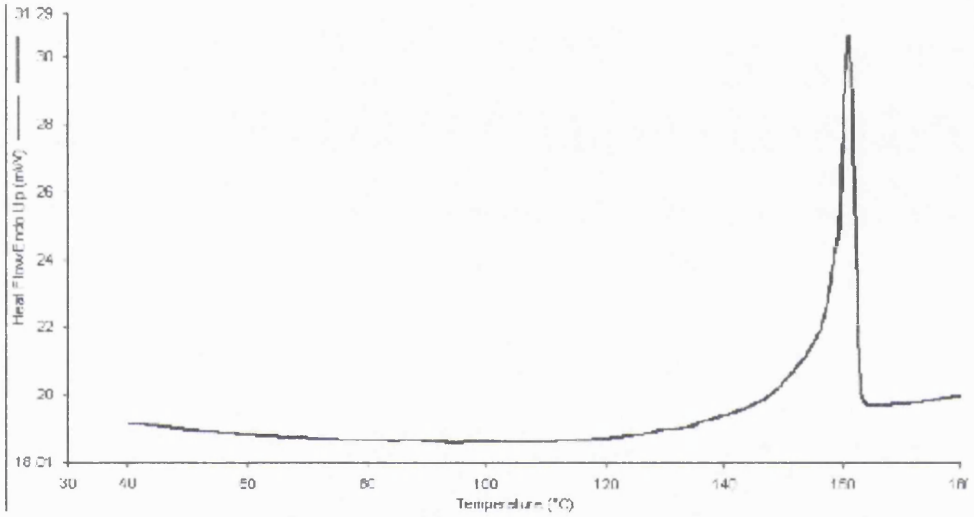

Figure 7.5 *A typical DSC trace of amorphous terfenadine adipate showing the melting peak after being exposed to 95% ethanol for 20 hours in the DVS at 25 °C.*

A typical DSC trace of terfenadine glutarate showing a Tg followed by the appearance of spiky peaks is seen in Figure 7.6. These peaks are due to ethanol evaporating from the gelled material (gelling occurred after exposure to 95% ethanol in the DVS). Due to this complicated DSC pattern, the Tg could not always be identified from the first run as the spiky peaks overlapped at times with the Tg of the glutarate and a second run was carried out from which the Tg values were reported. The results gave an average Tg value of 69.3 °C (n = 3, S.D. = 3.0). This is in comparison with a Tg value of ca. 80 °C for the original slow cooled amorphous terfenadine glutarate sample (Table 5.9). The Tg was still much higher than that of the temperature of the experiment (25 °C). Thus, the achieved plasticization was insufficient to lower Tg below T and trigger crystallization in the case of amorphous terfenadine glutarate exposed to 95% ethanol in the DVS. This

is in spite of the fact that the amorphous terfenadine glutarate sample showed a net weight gain of ca. 25.5% by the end of the sorption step in the DVS. The Tg value could be a bit lower than the one reported since loss of ethanol upon transfer of the sample from the DVS to the DSC might be fast resulting in less ethanol available to plasticize the sample. This possibility was checked by running TGA experiments on the gelled sample of terfenadine glutarate after exposure to 95% ethanol in the DVS. The sample was transferred immediately in closed wax paper from the DVS to the TGA. TGA experiments were carried out from ambient to 180 °C at 10 °C/min in open aluminium pans in an atmosphere of nitrogen. The samples showed an average weight loss of ca. 5.7% (n = 3, S.D. = 1.7) within a temperature range from the beginning until ca. 140 °C. This is a much lower percentage of weight loss than the net weight gained by the sample in the DVS due to sorption of ethanol which reached almost 23% at the end of the desorption step. This suggested that some loss of ethanol was actually encountered during handling and transfer from the DVS to the TGA and hence a higher Tg value might have been obtained on the DSC than the real value reached by taking up ca. 25.5% ethanol on the DVS.

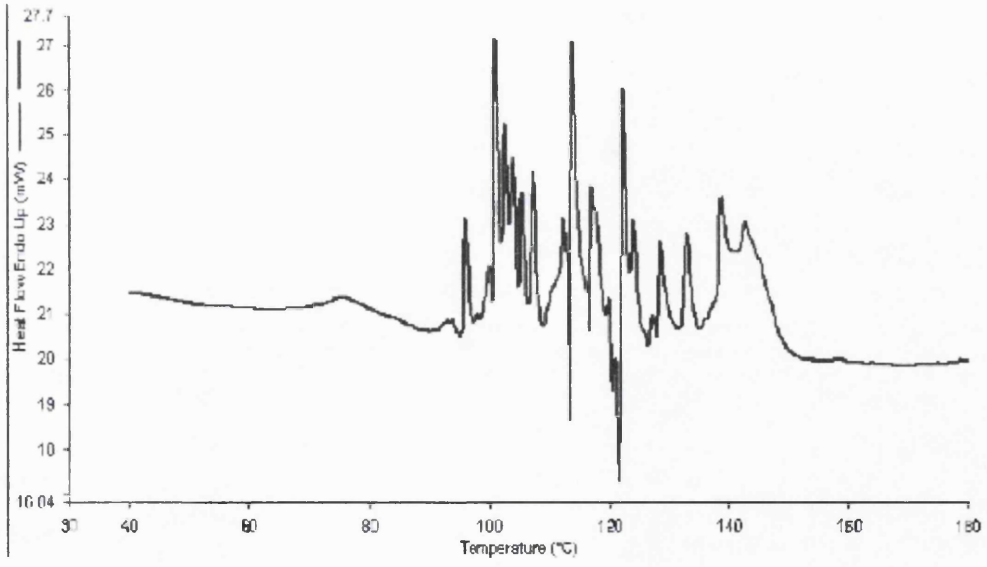

Figure 7.6 *A typical DSC trace of amorphous terfenadine glutarate showing a Tg followed by the appearance of complicated spiky peaks after being exposed to 95% ethanol for 20 hours in the DVS at 25 °C.*

7.2.2 COMPARISON IN THE POTENTIAL FOR CRYSTALLIZATION OF TERFENADINE AND ITS TWO SALTS AFTER EXPOSURE TO 95% ETHANOL IN THE DVS:

Figure 7.7 shows a comparison in the DVS profiles of terfenadine, terfenadine adipate and terfenadine glutarate. All the DVS profiles were for freshly prepared amorphous samples. The DVS profile of terfenadine is taken from the results in Section 4.2.2.2.2 and Figure 4.32.

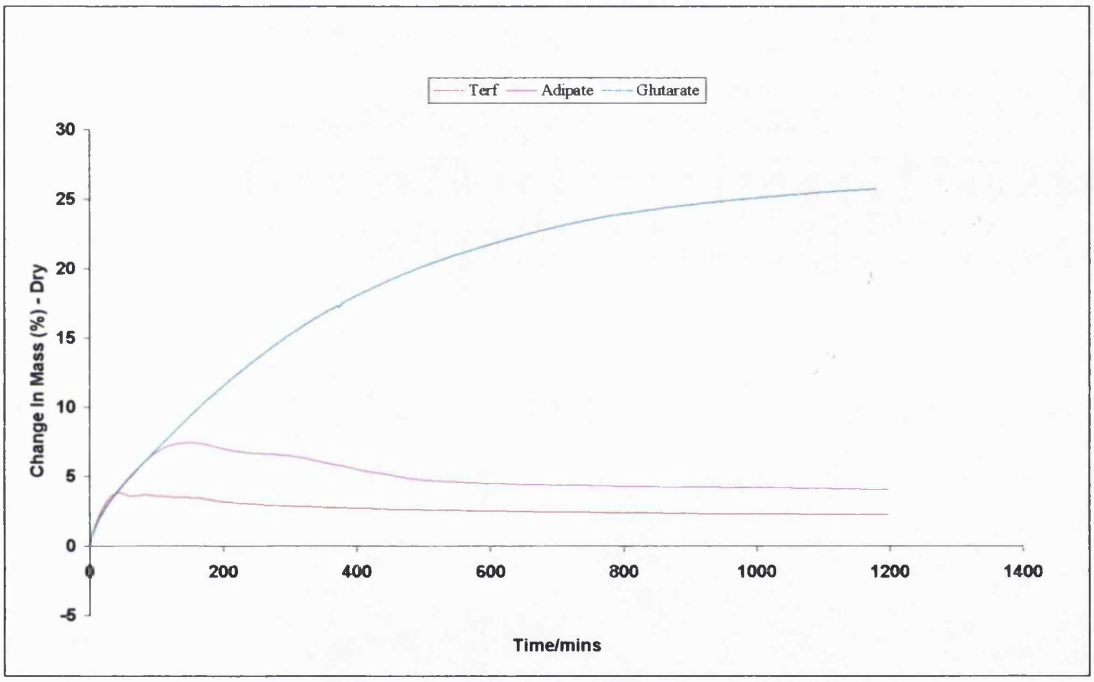

***Figure** 7.7 Ethanol sorption isotherm for initially amorphous forms of terfenadine, terfenadine adipate and terfenadine glutarate. Samples exposed to 95% ethanol (in the total gas flow) for 20 hours at 25 °C.*

Table 5.12 showed Tm/Tg ratios of terfenadine and its salts. By relating the Tg values (Table 5.9) and Tm/Tg ratios to the crystallization results of the amorphous forms for the three tested compounds (terfenadine, terfenadine adipate and terfenadine glutarate) which were exposed to 95% ethanol in the DVS for 20 hours at 25 °C, it can be concluded that terfenadine having the lowest Tg value was the fastest and most completely to crystallize among the three compounds. This is expected, as it would be easier to plasticize terfenadine and lower Tg below T and promote crystallization since terfenadine has the lowest Tg among the group (ca. 59 °C as seen in Table 3.4). The

glutarate derivative formed a soft gel yet failed to crystallize. The gel theory is one of the ways used to explain the mechanisms through which plasticizers work. It is assumed that the presence of a plasticizer will weaken intermolecular attractions in the solid resulting in gel formation and facilitating crystallization (Carraher, 1996). The glutarate has the highest Tg (ca. 80 °C as seen in Table 5.9) and did not crystallize although gelling took place. It seems that although a high level of ethanol was taken up by the gluatarate sample (average of 25.5%), it was insufficient to lower Tg below T and cause crystallization.

The adipate derivative came in between the two with incomplete crystallization taking place and an intermediate value of Tg (ca. 72 °C as seen in Table 5.9). The Tm/Tg ratios are higher and almost the same for both terfenadine and terfenadine adipate having values of 1.28 and 1.26 respectively in comparison with the low Tm/Tg ratio of the glutarate derivative (1.02). Polymers with high Tm/Tg ratio (>> 1.5) are considered to be readily crystallizable whereas a low Tm/Tg ratio reflects higher free volume requirement and lower viscosity in the glassy state with Tg falling close to Tm (difference less than 100 °C) (Slade and Levine, 1991). Based on the values of Tm/Tg ratios it can be concluded that terfenadine and terfenadine adipate are relatively more readily crystallizable than the glutarate derivative which has a Tm/Tg value that is even lower than that quoted by Slade and Levine (1991).

7.3 DISCUSSION:

The amorphous forms of two salts of terfenadine (terfenadine adipate and terfenadine glutarate) failed to crystallize under the influence of humidity at 75% RH for 20 hours at an elevated temperature of 50 °C in the Dynamic Vapour Sorption (DVS). Since crystallization of terfenadine adipate and terfenadine glutarate failed under the influence of humidity (75% RH) even at an elevated temperature of 50 °C, water was replaced by ethanol in the DVS instrument. Using ethanol in Dynamic Vapour Sorption proved to be an efficient method for triggering crystallization of hydrophobic amorphous materials that are resistant to change in physical form under normal and elevated conditions of relative humidity and temperature. Exposure of the amorphous forms of terfenadine adipate and terfenadine glutarate to 95% ethanol (in the total gas flow) for 20 hours at 25 °C and comparing the results with those obtained for amorphous

terfenadine exposed to DVS in the same conditions (studied earlier in Section 4.2.2.2.2) indicated that terfenadine was the most readily crystallizable among the series. The glutarate derivative proved to be highly resistant to crystallization as the amorphous beads of terfenadine glutarate gelled while picking up a large percentage of ethanol (ca. 25.5% of the total mass) without crystallizing. Terfenadine adipate fell in between the two showing close to complete crystallization (ca. 95% crystalline though this value is not exact as it superimposes with 1.8 % loss of ethanol) under the same conditions in the DVS. The above observations are in keeping with the potential for crystallization based on Tg values, Tm/Tg ratios and the difference between Tg and Tm (Slade and Levine, 1991) in the studied series.

General Conclusions:

This thesis showed the high resistance of the amorphous form of the hydrophobic drug terfenadine (used as a hydrophobic amorphous model) to crystallization under different humidity values. This high stability however is accompanied with low aqueous solubility, which lead to the idea of preparing a homologous series of terfenadine salts through reacting basic terfenadine with a homologous series of dicarboxylic acids. Such work was pursued in an attempt to enhance the solubility of the amorphous form of terfenadine since the reaction with oxalic acid can produce a salt that is more polar with higher ability to bind with water than terfenadine itself. At the same time, being more polar meant more rigidity of the molecule in the amorphous state suggesting a higher stability of the oxalate salt as indicated by its higher Tg value in comparison with terfenadine. The sequential addition of methylene groups through reacting terfenadine with the other series of dicarboxylic acids (succinic, glutaric and adipic acids) resulted in salts with higher mobility in the amorphous state than terfenadine oxalate but lower than terfenadine itself. In this piece of work, the carbon chain length was correlated (for the first time in the literature) with Tg values of the amorphous forms. The results showed a decrease in Tg values with an increase in carbon chain length going from the oxalate with 1C to the adipate with 5C in their side chains while terfenadine with no carbons in its side chain possessed the lowest Tg value. This meant (together with the Tm/Tg ratios) that the ammonium salts had a potentially higher stability than terfenadine in the amorphous form. A solubility study was carried out at two pH values (2 and 6). The results showed an increase in peak solubility of the amorphous salts with an increase in stability. Terfenadine oxalate possessed the highest stability and the highest solubility; the adipate showed the lowest stability coupled with the lowest solubility of the salts while terfenadine glutarate showed both an intermediate stability and peak solubility values in acetate buffer at pH 6. The solubility study in chloride buffer at pH 2 showed higher peak solubility values of the amorphous forms accompanied with a higher stability. Terfenadine oxalate possessed the highest solubility and stability, terfenadine showed the lowest stability and solubility while the glutarate possessed intermediate stability and solubility values. This was a very valuable observation in terms of the possibility of preparing amorphous forms that are more stable and at the same time possessing higher aqueous solubility than the parent hydrophobic molecule.

Plans For Future Work:

- Studying another basic drug similar or different in chemical structure to terfenadine and preparation and characterization of derivatives of the drug by using the same dicarboxylic acids and the same method used for the preparation of the terfenadine salts. Comparison of the behaviour of this drug and its derivatives to that of terfenadine and its salts can then be done in both the crystalline and the amorphous forms.

- Preparation of terfenadine salts from higher dicarboxylic acids than adipic acid (having more methylene groups in the dicarboxylic acid chain) in order to study the behaviour of their crystalline forms and to determine the melting point pattern beyond the adipate salt of terfenadine. To determine whether these higher derivatives of terfenadine crystallize and if so whether as hydrates or anhydrates. To study the pattern in the Tg values of the amorphous forms of the same higher salts of terfenadine (beyond the adipate salt) and to explain whether the Tg values of the higher salts keep on dropping beyond the adipate derivative.

- Preparation of amorphous forms of terfenadine and its salts by spray drying from an organic solvent (such as ethanol) and characterization of the spray dried amorphous forms in terms of their water uptake pattern in the DVS and the isothermal microcalorimeter as well as their potential for crystallization under these conditions. The amorphous powder obtained by spray drying is easy to handle with uniform particle size and can be studied in different analytical techniques much more easily than the large beads used in this study.

- A dynamic solubility study can be performed using similar particle sizes for both the crystalline and the spray dried amorphous forms whereby a better comparison of the solubility profiles in the crystalline and the amorphous forms can be obtained. A higher peak solubility value might be obtained from the smaller sized spray dried amorphous forms (compared with the large beads of ca. 3 mm in diameter of the slow cooled forms used in this

study). This in turn might lead to a larger difference in the apparent solubility of both the amorphous, and the crystalline forms.

- Pycnometry can be done to the spray dried amorphous powders and the true density of these amorphous forms can be determined. True density can then be used in order to calculate the expected drop in Tg (based on Gordon-Taylor equation) due to water uptake by the sample. Based on the same Gordon-Taylor equation and once true density is known, the amount of water that is needed in order to reduce Tg below T (which promotes crystallization) can be calculated and compared for terfenadine and its derivatives.

- Single crystal crystallography can be carried out in order to determine the exact number and positions of water molecules that are involved in the crystalline structures of the hydrous forms (terfenadine oxalate, terfenadine succinate and terfenadine glutarate).

- The solubility of terfenadine and its salts should be studied at other temperatures than the 37 °C used in this study. This will allow the computation of the parameters that govern the solubility behaviour of terfenadine and its salts through the application of the Van't Hoff equation.

- Solubility as well as stability of terfenadine and its salts in the crystalline and the amorphous forms can be studied in buffer solutions at pH values below 2 and above 6.

REFERENCES

- Ahlneck, C., Zografi, G., "The molecular basis of moisture effects on the physical and chemical stability of drugs in the solid state", Int. J. Pharm., 1990, Vol. 62, 87-95.
- Ahmed, H., Buckton, G., Rawlins, D. A.,"Crystallisation of partially amorphous griseofulvin in water vapour: determination of kinetic parameters using isothermal heat conduction microcalorimetry ", Int. J. Pharm., 1998, Vol. 167, 139-145.
- Ahmed, H., Buckton, G., Rawlins, D. A.,"The use of isothermal microcalorimetry in the study of small degrees of amorphous content of a hydrophobic drug ", Int. J. Pharm., 1996, Vol. 130, 195-201.
- Allcock, H. R., Lampe, F. W., Contemporary Polymer Science, 2nd edn., 1990, Prentice-Hall, New Jersey.
- Andronis, V., Yoshioka, M., Zografi, G.,"Effects of Sorbed Water on the Crystallization of Indomethacin from the Amorphous State", J. Pharm. Sci., 1997, Vol. 86, No. 3, 346-351.
- Andronis, V., Zografi, G., "The Molecular Mobility of Supercooled Amorphous Indomethacin as a Function of temperature and Relative Humidity", Pharm. Res., 1998, Vol. 15, No. 6, 835- 842.
- Angberg, M., " Lactose and thermal analysis with special emphasis on microcalorimetry", Thermochimica Acta, 1995, Vol. 248, 161-176.
- Angberg, M., Nystrom, C., Castensson, S., "Evaluation of heat-conduction microcalorimetry in pharmaceutical stability studies. V. A new approach for continuous measurements in abundant water vapour", Int. J. Pharm., 1992a, Vol. 81, 153-167.
- Angberg, M., Nystrom, C., Castensson, S., "Evaluation of heat-conduction microcalorimetry in pharmaceutical stability studies.VI. Continuous monitoring of the interaction of water vapour with powders and powder mixtures at various relative humidities", Int. J. Pharm., 1992b, Vol. 83, 11-23.
- Arafat, T., Kaddoumi, A., "Determination of Terfenadine in Pharmaceutical Dosage Forms by Spectrofluorimetry and High Performance Liquid Chromatography (HPLC)", Alex. J. Pharm. Sci, 1995, Vol. 9, 113-116.
- Aulton, M. D., Pharmaceutics The science of Dosage Form Design, 1998, Churchill Livingstone, Edinburgh.
- Badwan, A., Saleh, M., Owais, L., Al Kaysi, H., Arafat, T., Analytical Profiles of Drug Substances, 1990, Vol. 19, 627, 662.
- Briggner, Lars-Erik, Buckton, G., Bystrom, K., Darcy, P., "The use of isothermal microcalorimetry in the study of changes in crystallinity induced during the processing of powders", Int. J. Pharm., 1994, Vol. 105, 125-135.
- Buckton, G., " Applications of isothermal microcalorimetry in the pharmaceutical sciences", Thermochimica Acta, 1995b, Vol. 248, 117-129.
- Buckton, G., Beezer, A. E., "The applications of microcalorimetry in the field of physical pharmacy", Int. J. Pharm., 1991, Vol. 72, 181-191.

- Buckton, G., Beezer, A. E., "The relationship between particle size and solubility", Int. J. Pharm., 1992, Vol. 82, R7-R10.
- Buckton, G., Beezer, A., Denyer, S. P., Russell, S. J., "Observations on the biopharmaceutical importance of chain length in chemically related compounds", Int. J. Pharm., 1991, Vol. 73, 1-7.
- Buckton, G., Choularton, A., Beezer, A. E., Chatham, S. M., "The effect of comminution technique on the surface energy of a powder", Int. J. Pharm., 1988, Vol. 47, 121-128.
- Buckton, G., Darcy, P., "Assessment of disorder in crystalline powders-a review of analytical techniques and their application", Int. J. Pharm., 1999, Vol. 179, 141-158.
- Buckton, G., Darcy, P., "The influence of additives on the recrystallisation of amorphous spray dried lactose", Int. J. Pharm., 1995a, Vol. 121, 81-87.
- Buckton, G., Darcy, P., "The influence of heating/drying on the crystallisation of amorphous lactose after structural collapse", Int. J. Pharm., 1997, Vol. 158, 157-164.
- Buckton, G., Darcy, P., "The use of gravimetric studies to assess the degree of crystallinity of predominantly crystalline powders", Int. J. Pharm., 1995b, Vol. 123, 265-271.
- Buckton, G., Darcy, P., "Water mobility in amorphous lactose below and close to the glass transition temperature", Int. J. Pharm., 1996, Vol. 136, 141-146.
- Buckton, G., Darcy, P., Greenleaf, D., Holbrook, P., "The use of isothermal microcalorimetry in the study of changes in crystallinity of spray-dried salbutamol sulphate", Int. J. Pharm., 1995b, Vol. 116, 113-118.
- Buckton, G., Darcy, P., Mackellar, A., Holbrook, P., "The use of isothermal microcalorimetry in the study of small degrees of amorphous content of powders", Int. J. Pharm., 1995a, Vol. 117, 253-256.
- Buckton, G., Interfacial Phenomena in Drug Delivery and Targeting, 1995a, Harwood Academic Publishers GmbH, Switzerland.
- Byrn, S. R., Solid-State Chemistry of Drugs, 1982, Academic Press Inc., U.K..
- Carstensen, J., T., Pharmaceutical Principles of Solid Dosage Forms, 1993, Technomic Publishing Inc.,Pennsylvania, U.S.A.
- Chen, T. M., Sill, A. D., Housmyer, C. L., "Solution stability study of terfenadine by high-performance liquid chromatography", Journal of Pharmaceutical & Biomedical Analysis, 1986, Vol. 4, No. 4, 533-539.
- Chidavaenzi, O. C., Buckton, G., Koosha, F., Pathak, R., "The use of thermal techniques to assess the impact of feed concentration on the amorphous content and polymorphic forms present in spray dried lactose", Int. J. Pharm., 1997, Vol. 159, 67-74.
- Chiou, Win L., "Differential Thermal, Solubility, and Aging Studies on Various Sources of Digoxin and Digitoxin powder: Biopharmaceutical Implications", J. Pharm. Sci., 1979, Vol. 68, No. 10, 1224-1229.
- Ediger, M. D., Angell, C. A., Nagel, S. R., "Supercooled Liquids and Glasses", J. Phys. Chem., 1996, 100, 13200-13212.

- Elamin, A. A., Ahlneck, C., Alderborn, G., Nystrom, C., "Increased metastable solubility of milled griseofulvin, depending on the formation of a disordered surface structure", Int. J. Pharm., 1994a, Vol. 111, 159-170.
- Elamin, A. A., Alderborn, G., Ahlneck, C., "The effect of pre-compaction processing and storage conditions on powder and compaction properties of some crystalline materials", Int. J. Pharm., 1994b, Vol. 108, 213-224.
- Elias, Hans-Georg, An Introduction to Polymer Science, 1st edn., 1997, VCH, Weinheim.
- Flink, J. M., Physical Properties of Foods, Peleg, M., Bagley, E.B., AVI: Westport, 1983, 473-521.
- Florence, A. T., Attwood, D., Physicochemical Principles of Pharmacy, 3rd edn., 1998, Macmillan press Ltd., U.K.
- Florence, A. T., Salole, E. G.,"Changes in Crystallinity and solubility on Comminution of Digoxin and Observations on Spironolactone and Oestradiol", J. Pharm. Pharm., 1976, 28, 637-642.
- Foster, S., Buckton, G., Beezer, A., "The importance of chain length on the wettability and solubility of organic homologs", Int. J. Pharm., 1991, Vol. 72, 29-34.
- Giron, D., Remy, P., Thomas, S., Vilette, E., "Quantitation of amorphicity by microcalorimetry", Journal of Thermal Analysis, 1997, Vol. 48, 465-472.
- Guo, Y., Byrn, S., Zografi, G., "Effects of Lyophilization on the Physical Characteristics and Chemical Stability of Amorphous Quinapril Hydrochloride", Pharm. Res., 2000, Vol. 17, No. 8, 930- 935.
- Hancock, B. C., Dalton, C. R., Pikal, M. J., Shamblin, S. L., "A Pragmatic test of a simple Calorimetric Method for Determining the Fragility of Some Amorphous Pharmaceutical Materials", Pharm. Res., 1998, Vol. 15, No. 5, 762- 767.
- Hancock, B. C., Parks, M., "What is the True Solubility Advantage for Amorphous Pharmaceuticals", Pharm. Res., 2000, Vol. 17, No. 4, 397- 404.
- Hancock, B. C., Shamblin, S. L., Zografi, G., "Molecular Mobility of Amorphous Pharmaceutical Solids Below Their Glass Transition Temperatures", Pharm. Res., 1995, Vol. 12, No. 6, 799- 806.
- Hancock, B. C., Zografi, G., "Effects of Solid-State Processing on Water Vapor Sorption by Aspirin", J. Pharm. Sci., 1996, Vol. 85, No. 2, 246-248.
- Hancock, B. C., Zografi, G., "The Relationship Between the Glass transition Temperature and the Water Content of Amorphous Pharmaceutical Solids", Pharm. Res., 1994, Vol. 11, No. 4, 471- 477.
- Hancock, B. C., Zografi, G., "The Use of Solution Theories for Predicting Water vapor Absorption by Amorphous Pharmaceitical Solids: A Test of the Flory-huggins and Vrentas Models", Pharm. Res., 1993, Vol. 10, No. 9, 1262- 1267.
- Hancock, B.C., Zografi, G.,"Characteristics and Significance of the Amorphous State in Pharmaceutical Systems", J. Pharm. Sci., 1997, Vol. 86, No. 1, 1-12.

- Hatakeyama, T., Quinn, F. X., Thermal Analysis Fundementals and Applications to Polymer science, 2nd edn., 1999, Wiley and sons Ltd., West Sussex, England.
- Hendriksen, B. A., "Characterization of calcium fenoprofen", Int. J. Pharm., 1990, Vol. 60, 243-252.
- Her, Lih-Min, Deras, M., Nail, S. L., "Electrolyte-Induced Changes in Glass Transition Temperatures of Freeze-Concentrated Solutes", Pharm. Res., 1995, Vol. 12, No. 5, 768- 772.
- Hill, V. L., Craig, D. Q. M., Feely, L. C.,"Characterisation of spray-dried lactose using modulated differential scanning calorimetry", Int. J. Pharm., 1998, Vol. 161, 95-107.
- Hofer, K., Astl, G., mayer, E., "Vitrified Dilute Aqueous Solutions. Effects of Electrolytes and polyhydric Alcohols on the Glass transition Features of Hyperquenched Aqueous Solutions", J. Phys. Chem., 1991, 95, 10777-10781.
- Hogan, S. E., Buckton, G., "The Application of Near Infrared Spectroscopy and Dynamic Vapor Sorption to Quantify Low Amorphous Contents of Crystalline Lactose", Pharm. Res., 2001b, Vol. 18, No. 1, 112- 116.
- Hogan, S. E., Buckton, G., "Water sorption/desorption- near IR and calorimetric study of crystalline and amorphous raffinose", Int. J. Pharm., 2001a, Vol. 227, 57-69.
- Homan, R. E., Desantis, F., "The thermal characterization of terfenadine polymorphs in a suspension", Drug Development and Industrial Pharmacy, 1992, Vol. 18 (8), 861-868.
- Huttenrauch, R., Fricke, S., Zielke, P., "Mechanical Activation of Pharmaceutical Systems", Pham. Res., 1985, Vol. 2, 302-306.
- Kajiwara, K., Franks, F., "Crystalline and amorphous phases in the binary system water-raffinose", J. Chem. Soc., Faraday Trans., 1997, Vol. 93 (9), 1779- 1783.
- Kajiwara, K., Franks, F., Echlin, P., Greer, A. L., "Structural and Dynamic Properties of Crystalline and Amorphous Phases in Raffinose-Water Mixtures", Pharm. Res., 1999, Vol. 16, No. 9, 1441- 1448.
- Kordikowski, A., Shekunov, T., York, P., "Polymorph Control of Sulfathiazole in Supercritical CO2", Pharm. Res., 2001, Vol. 18, No. 5, 682- 688.
- Kuhnert-Brandstatter, M., Pure appl. Chem., 1965, 10, 133.
- Lachman, L., Lieberman, H. A., Kanig, J. L., The Theory and Practice of Industrial Pharmacy, 3rd edn., 1996, Lea & Febiger, Philadelphia, U.S.A.
- Lane, R. A., Buckton, G., "The novel combination of dynamic vapour sorption gravimetric analysis and near infra-red spectroscopy as a hyphenated technique", Int. J. Pharm., 2001, Vol. 207, 49-56.
- Larsen, M. J., Hemming, D. J. B., Bergstrom, R. G., Wood, R. W., Hansen, L. D., "Water-catalyzed crystallization of amorphous acadesine", Int. J. Pharm., 1997, Vol. 154, 103-107.
- Lehto, V. P., Laine, E., "A Kinetic Study on Crystallization of an Amorphous Lubricant", Pharm. Res., 1997, Vol. 14, No. 7, 899- 904.

- Lin, Song-Ling, "Preformulation Investigation:Dissolution Kinetics and Thermodynamic Parameters of Polymorphs of an Experimental Antihypertensive", J. Pharm. Sci., 1972, Vol. 61, No. 9, 1423-1430.
- Lu, Q., Zografi, G., "Phase Behaviour of Binary and Ternary Amorphous Mixtures Containing Indomethacin, Citric Acid, and PVP", Pharm. Res., 1998, Vol. 15, No. 8, 1202- 1206.
- Martin, A., Physical Pharmacy, 4th edn., 1993, Williams and Wilkins., Maryland, U.S.A.
- Matsumoto, T., Zografi, G., "Physical Properties of Solid Molecular Dispersions of Indomethacin with Poly(vinylpyrrolidone) and Poly(vinylpyrrolidone-co-vinyl-acetate) in Relation to Indomethacin Crystallization", Pharm. Res., 1999, Vol. 16, No. 11, 1722-1728.
- Moustafa, M. A., Ebian, A. R., Khalil, S. A., Motawi, M. M., "Sulphamethoxydiazine Crystal Forms", J. Pharm. Pharm., 1971, 23, 868-874.
- Moynihan, C. T., Easteal, A. J., Wilder, J., "Dependence of the Glass Transition Temperature on Heating and Cooling rate", The Journal of Physical Chemistry, 1974, Vol. 78, o. 26, 2673-2677.
- Mullin, J. W., Crystallization, 3rd edn., 1997. Butterworth-Heinmann, Oxford.
- Nyqvist, H., "Saturated salt solutions for maintaining specific relative humidities", Int. J. Pharm. Technol. Prod. Mfr., 1983, Vol 4, 47 - 48.
- Oberholtzer, E. R., Brenner, G. S., Zografi, G.,"Cefoxitin Sodium: Solution and Solid-State Chemical Stability Studies", J. Pharm. Sci., 1979, Vol. 68, No. 7, 863-866.
- Oksanen, C. A., Zografi, G., "Molecular Mobility in Mixtures of Absorbed Water and Solid Poly(vinylpyrrolidone)", Pharm. Res., 1993, Vol. 10, No. 6, 791- 799.
- Otsuka, M., Kaneniwa, N., "Effect of grinding on the crystallinity and chemical stability in the solid state of cephalothin sodium", Int. J. Pharm., 1990, Vol. 62, 65-73.
- Pikal, M. J., Grant, D. J. W., "A theoretical treatment of changes in energy and entropy of solids caused by additives or impurities in solid solution", Int. J. Pharm., 1987, Vol. 39, 243-253.
- Pikal, M. J., Lukes, A. L., Lang, J. E., "Thermal Decomposition of Amorphous B-Lactam Antibacterials", J. Pharm. Sci., 1977, Vol. 66, No. 9, 1312-1316.
- Pikal, M. J., Lukes, A. L., Lang, J. E., Gaines, K.,"Quantitative Crystallinity Determinations for B-Lactam Antibiotics by Solution Calorimetry: Correlations with Stability", J. Pharm. Sci., 1978, Vol. 67, No. 6, 767-773.
- Pikal, M. J., Rigsbee, D. R., "The Stability of Insulin in Crystalline and Amorphous Solids: Observation of Greater Stabiliy for the Amorphous Form", Pharm. Res., 1997, Vol. 14, No. 10, 1379- 1387.
- Roos, Y., "Melting and glass transitions of low molecular weight carbohydrates", Carbohydrates Research, Elsevier Science Publishers, 1993, Vol. 238, 39-48.
- Saleki-Gerhardt, A., Ahlneck, C., Zografi, G., "Assessment of disorder in crystalline solids", Int. J. Pharm., 1994b, Vol. 101, 237-247.

- Saleki-Gerhardt, A., Stowell, J. G., Byrn, S. R., Zografi, G., "Hydration and Dehydration of Crystalline and amorphous Forms of Raffinose", J. Pharm. Sci., 1995, Vol. 84, No. 3, 318-323.
- Saleki-Gerhardt, A., Zografi, G., "Non-Isothermal Crystallization of Sucrose from the Amorphous State", Pharm. Res., 1994a, Vol. 11, No. 8, 1166- 1173.
- Schmitt, E., Davis, C. W., Long, S. T.,"Moisture-Dependent Crystallization of Amorphous Lomotrigine Mesylate", J. Pharm. Sci., 1996, Vol. 85, No. 11, 1215-1219.
- Sebhatu, T., Angberg, M., Ahlneck, C., "Assessment of the degree of disorder in crystalline solids by isothermal microcalorimetry", Int. J. Pharm., 1994a, Vol. 104, 135-144.
- Sebhatu, T., Elamin, A. A., Ahlneck, C., "Effect of Moisture Sorption on Tabletting Characteristics of Spray dried (15 % Amorphous) Lactose", Pham. Res., 1994b, Vol. 11, 1233-1238.
- Seymour, R. B., Carraher, C. E., Polymer Chemistry, 4th edn., 1996, Marcel Dekker, New York.
- Shalaev, E. Y., Lu, Q., Shalaeva, M., Zografi, G., "Acid-Catalyzed Inversion of Sucrose in the Amorphous State at Very Low Levels of Residual Water", Pharm. Res., 2000, Vol. 17, No. 3, 366- 370.
- Shamblin, S. L., Zografi, G., "The Effects Of Absorbed Water on the Properties of Amorphous Mixtures Containing Sucrose", Pharm. Res., 1999, Vol. 16, No. 7, 1119-1124.
- Shamblin, S. L.., Zografi, G., "Enthalpy relaxation in Binary Amorphous Mixtures Containing Sucrose", Pharm. Res., 1998, Vol. 15, No. 12, 1828- 1834.
- Sheridan, P. L., Buckton, G., Storey, D. E., "Development of a Flow Microcalorimetry Method for the Assessment of Surface Properties of Powders ", Pharm. Res., 1995, Vol. 12, No. 7, 1025-1030.
- Skoog, D. A. Holler, F. J., Nieman, T. A., Principles of Instrumental Analysis, 5th edn., 1998, Saunders college publishing.
- Slade, L., Levine, H., "Mono and Disaccharides: selected physicochemical and functional aspects", Food science and technology, 1996, 41- 157, Marcel Dekker Inc.
- Slade, L., Levine, H., Critical Reviews in Food Science and Nutrition, 1991, Vol 30, 115-360.
- Stubberud, L., Arwidsson, H. G., Larsson, A., Graffner, C., "Water solid interactions. Effect of moisture sorption and glass transition temperature on compactibility of microcrystalline cellulose alone or in binary mixtures with polyvinyl pyrrolidone", Int. J. Pharm., 1996, Vol. 134, 79-88.
- Stubberud, L., Forbes, R. T., "The use of gravimetry for the study of the effect of additives on the moisture-induced recrystallization of amorphous lactose", Int. J. Pharm., 1998, Vol. 163, 145-156.

- Taylor, L. S., Williams, A. C., York, P., "Particle Size Dependent Molecular Rearrangements During the Dehydration of Trehalose Dihydrate- In Situ FT-Raman Spectroscopy ", Pharm. Res., 1998, Vol. 15, No. 8, 1207-1214.
- Taylor, L. S., Zografi, G., "Spectroscopic Characterization of Interactions Between PVP and Indomethacin in Amorphous Molecular Dispersions", Pharm. Res., 1997, Vol. 14, No. 12, 1691- 1698.
- Taylor, L. S., Zografi, G., "Sugar-Polymer Hydrogen Bond Interactions in Lyophilized Amorphous Mixtures", J. Pharm. Sci., 1998, Vol. 87, No. 12, 1615-1621.
- To, E. C., Flink, J. M., "Collapse, a structural transition in freeze dried carbohydrates, Effect of solute composition" J. Fd. Technol., 1978b, 13, 567-581.
- To, E. C., Flink, J. M., "Collapse, a structural transition in freeze dried carbohydrates, Evaluation of analytical methods" J. Fd. Technol., 1978a, 13, 551-565.
- To, E. C., Flink, J. M., "Collapse, a structural transition in freeze dried carbohydrates, Prerequisite of recrystallisation" J. Fd. Technol., 1978c, 13, 583-594.
- Tong, P., Zografi, G., "Solid-State Characteristics of Amorphous Sodium Indomethacin Relative to its Free Acid ", Pharm. Res., 1999, Vol. 16, No. 8, 1186-1192.
- Tsourouflis, S., Flink, J. M., Karel, M., "Loss of Structure of Freeze-dried Carbohydrates Slutions:Effect of temperature, Moisture Content and Composition", J. Sci. Fd. Agri., 1976, 27, 509-519.
- Villiers, M. M., Wurster, D. E., Watt, J. G., Ketkar, A.,"X-Ray powder diffraction determination of the relative amount of crystalline acetaminophen in solid dispersions with polyvinylpyrrolidone", Int. J. Pharm., 1998, Vol. 163, 219-224.
- Wadso, I., "Isothermal microcalorimetry near ambient temperature: An overview and discussion", Thermochimica Acta, 1997, Vol. 294, 1-11.
- Ward, G. H., Schultz, R. K., "Process-Induced Crystallinity Changes in Albuterol Sulfate and its Effect on Powder Physical Stability", Pham. Res., 1995, Vol. 12, 773-779.
- Watson, D. G., Pharmaceutical Analysis, A textboob for pharmacy students and pharmaceutical chemists, 1st edn., 1999, Churchill Livingstone.
- Yalkowsky, S. H., Flynn, G. L., Slunick, T. G., "Importance of chain length on physicochemical and crystalline properties of organic homologs", J. Pharm. Sci., 1972, Vol. 61, No. 6, 852-857.
- Yonemochi, E., Inoue, Y., Buckton, G., Moffat, A., Oguchi, T., Yamamoto, K., "Differences in Crystallization Behavior Between Quenched and Ground Amorphous Ursodeoxycholic Acid", Pharm. Res., 1999, Vol. 16, No. 6, 835- 840.
- Yonemochi, E., Inoue, Y., Buckton, G., Moffat, A., Oguchi, T., Yamamoto, K., "Differences in Crystallization Behaviour Between Quenched and Ground Amorphous Ursodeoxycholic Acid", Pharm. Res., 1999, Vol. 16, No. 6, 835- 840.
- York, P., "Solid-state properties of powders in the formulation and processing of solid dosage forms", Int. J. Pharm., 1983, Vol. 14, 1-28.

- Yoshioka, M., Hancock, B. C., Byrn, Zografi, G., "Inhibition of Indomethacin Crystallization in Poly(vinylpyrrolidone) Coprecipitates", J. Pharm. Sci., 1995, Vol. 84, No. 8, 983-986.
- Yoshioka, M., Hancock, B. C., Zografi, G.,"Crystallization of Indomethacin from the Amorphous State below and above its Glass Transition temperature", J. Pharm. Sci., 1994, Vol. 83, No. 12, 1700-1705.
- Zografi, G., "States of Water Associated with Solids", Drug Dev. Ind. Pharm., 1988, 14, 1905-1926.
- Zografi, G., Hancock, B. C., Topics in Pharmaceutical Sciences, Crommelin, D.J.A., Midha, K.K., Nagai, T., (eds.), Medpharm Scientific Publishers: Stuggart, 1994, 405-419.